

University of Trento
University of Brescia
University of Padova
University of Trieste
University of Udine
Università IUAV di Venezia

Enrico Mazzarolo

ANALYSIS AND DEVELOPMENT OF AN INNOVATIVE PREFABRICATED BEAM-TO-COLUMN JOINT

Advisor:
Prof. Enzo Siviero
Università IUAV di Venezia, Venice, Italy

Co-Advisors:
Prof. Airong Chen, Prof. Tobia Zordan
Tongji University, Shanghai, China
Prof. Bruno Briseghella
Fuzhou University, Fuzhou, China

UNIVERSITY OF TRENTO

Civil and Mechanical Structural Systems Engineering

Ph. D. Head's: Prof. Davide Bigoni

24 / April / 2012

Board of Examiners

Prof. Enzo Siviero	(Università IUAV di Venezia)
Prof. Antonio Tralli	(Università degli Studi di Ferrara)
Prof. Marina Fumo	(Università degli Studi di Napoli Federico II)

SUMMARY

The use of pre-fabricated concrete components and their related coupling systems in seismic engineering constitutes a subject of wide and deep interest among researchers, practitioners and manufacturers all over the world, as demonstrated by a large number of studies conducted, among other Countries, especially in Japan, New Zealand and United States since the early '80s and, in relatively more recent times, in Italy. A key issue is given by the possibility to apply the typical benefits of the pre-fabrication not only to low rise industrial/commercial structures, but also to multi-storey frames for public and strategic buildings such as schools, hospitals and many others, as well as to high-rise residential premises built in areas characterized by a medium to high seismic intensity. On the basis of what stated above, an original structural system made by prefabricated composite steel truss-concrete beams and centrifuged high-strength concrete columns is presented in the following. Specifically designed joints are provided to couple the different structural components in order to guarantee an overall ease of construction with reduced tolerance problems and self-bearing capacity during temporary erection phases, with a consequent reduction in schedule and costs. The use of high performance concrete for columns allows for a high bearing capacity with limited overall dimensions and the consequent maximization of the commercial or saleable space. The original layout of the system proposed has led to the need to perform an intensive theoretical and experimental research activity. The finite element model of the structural system was calibrated upon both static and cyclic testing evidence carried out on full scale samples built in Italy and tested at the Tongji University-Shanghai, China. On the basis of the data collected, the tuned model was used to carry out further analyses and to deepen the specific knowledge on several further aspects, as specified in the following. Firstly, an estimation of the joint's strength domain, suitable for everyday's design was carried out based on a component-approach. Then, a structural optimization on the component used to guarantee hogging and sagging bending moment resistance to the joint, was carried out in order to achieve the minimization of the construction material employed. Furthermore, the estimation of the seismic performance of the joint, based on the evaluation of a purposely defined vulnerability parameter, supplied encouraging results with reference to the applicability of the investigated technology over most of the National territory. Finally an improved layout of the joint, with reference to confined concrete and the related possibility to achieve a suitable seismic response also at edge joints, is presented.

SOMMARIO

La possibilità di impiego in ambito sismico di singole componenti strutturali prefabbricate e dei relativi accoppiamenti è una tematica che ha da tempo suscitato un forte interesse a livello internazionale, come provato dai numerosi studi condotti in Giappone, Nuova Zelanda e Stati Uniti a partire dagli anni '80 e, in periodi più recenti, in Italia. L'obiettivo rimane quello di unire ai vantaggi tipici della prefabbricazione, la possibilità di realizzare non solo strutture ad esclusivo utilizzo industriale o commerciale, ma anche telai multipiano per edifici pubblici e strategici come scuole, ospedali e molti altri, nonché edifici residenziali in aree caratterizzate da media ed elevata intensità sismica. Sulla base di quanto detto, nel seguito viene presentato un originale sistema strutturale prefabbricato costituito da travi tralicciate composte, realizzate cioè da tralicci metallici conglobati in getti di calcestruzzo, e pilastri in calcestruzzo centrifugato ad alta resistenza. Particolari nodi in struttura metallica, appositamente progettati, vengono impiegati per accoppiare le diverse componenti strutturali, così da garantire facilità di montaggio, minimizzando al contempo i problemi di tolleranza e assicurando una considerevole capacità di carico in fase transitoria, con una conseguente riduzione di tempi e costi di costruzione. L'impiego di calcestruzzo ad alte prestazioni per gli elementi verticali permette una elevata resistenza degli stessi, pur con ingombri della sezione trasversale estremamente ridotti. Ciò consente di massimizzare la superficie commerciale. Il layout originale del sistema proposto ha richiesto una intensa fase di ricerca teorica e sperimentale. Il modello numerico ad elementi finiti è stato calibrato sulla base dei risultati delle prove statiche e dinamiche condotte presso il College of Civil Engineering della Tongji University di Shanghai, Cina. Sulla base dei dati raccolti, il modello sviluppato è stato impiegato per ulteriori analisi e approfondimenti legati ad aspetti specifici, come di seguito specificato. Innanzitutto la stima del dominio di resistenza del nodo, ottenuto per mezzo di un approccio per componenti. In secondo luogo, un'ottimizzazione strutturale delle singole componenti utilizzate per garantire resistenza flessionale al nodo, in modo da minimizzare il materiale strutturale impiegato. Sono state in seguito valutate le prestazioni sismiche del nodo, sulla base di uno specifico parametro di vulnerabilità appositamente definito, che ha restituito risultati incoraggianti circa l'applicabilità del sistema prefabbricato sulla maggior parte del territorio nazionale. Infine una proposta migliorativa del nodo, basata su un più efficace effetto di confinamento del calcestruzzo, così da ottenere una risposta sismica adeguata anche nelle zone di bordo di un edificio, dove l'azione confinante del solaio è generalmente limitata.

DEDICATION

to Giorgia, Nives, Gianpietro

ACKNOWLEDGEMENTS

First and foremost, I would like to express sincere gratitude to my advisor Prof. Enzo Siviero for the support to my Ph.D study and research. His knowledge and expertise have been a precious reference during these three years.

I can not find words to express thankfulness to my co-tutors Prof. Bruno Briseghella and Prof. Tobia Zordan. They have been a source of friendships as well as enriching and stimulating collaboration. This thesis would have not been possible unless their precious contribution.

Thanks to Dr. Eng. Lan Cheng, irreplaceable workfellow during writing of many papers.

The research has been jointly supported by IUAV and Tecnostrutture S.R.L., that has provided the test structures. This support is gratefully acknowledged.

Assistance for experimental studies from State Key Laboratory for Disaster Reduction in Civil Engineering (SLDRCE) in Tongji University has been also appreciated.

In the end I would like to thank all those persons I collaborated with during these years. Among the others I am indebted with Prof. Roberto Scotta, Prof.ssa Anna Saetta, Eng. Luisa Berto and Prof. Luigi Fenu. Thanks for help and encouragement

CONTENT

CHAPTER 1

<u>1. LITERATURE SURVEY</u>	1
<u>1.1. Introduction</u>	1
<u>1.2. Initial development of precast technology</u>	1
<u>1.3. Former precast earthquake resisting frames experiences</u>	5
<u>1.4. New Zealand approach to precast framing</u>	9
<u>1.4.1. The emulative approach</u>	9
<u>1.4.2. Precast system n°1</u>	11
<u>1.4.3. Precast system n°2</u>	16
<u>1.4.4. Precast system n°3</u>	19
<u>1.4.5. Precast system n°4</u>	20
<u>1.4.6. Benefits and drawbacks of emulative approach</u>	23
<u>1.5. United States approach to precast framing</u>	24
<u>1.5.1. The dry connection approach</u>	24
<u>1.5.2. Non linear elastic systems</u>	25
<u>1.5.3. Tension-compression yielding systems</u>	29
<u>1.5.4. Energy dissipating systems</u>	33
<u>1.5.5. Hybrid frame system</u>	35
<u>1.5.6. Benefits and drawbacks of dry-connection approach</u>	40
<u>1.6. Italian approach to precast framing</u>	40
<u>1.6.1. The precast CSTC beam technology</u>	40
<u>1.6.2. CSTC beam specifications</u>	43
<u>1.6.3. Experimental testing on CSTC beam</u>	44
<u>1.6.4. Code design provisions for CSTC beam</u>	49
<u>1.6.5. Beam-to-column joint testing</u>	50
<u>1.6.6. Current CSTC beam application on framing system</u>	58

CHAPTER 2

<u>2. PROPOSED PRECAST JOINT LAYOUT</u>	61
---	----

CHAPTER 3

<u>3. EXPERIMENTAL TESTING</u>	69
--------------------------------	----

<u>3.1. Introduction</u>	69
<u>3.2. Material properties</u>	69
<u>3.2.1. Concrete</u>	69
<u>3.2.2. Steel</u>	71
<u>3.3. Static testing</u>	73
<u>3.3.1. Specimens description and test setup</u>	73
<u>3.3.2. Force vs. displacement curves</u>	76
<u>3.3.3. Horizontal strain sensor on column concrete</u>	78
<u>3.3.4. Vertical strain sensor on concrete</u>	79
<u>3.3.5. Strain sensor on lower horizontal steel plate</u>	82
<u>3.3.6. Vertical strain sensors on vertical steel plate</u>	83
<u>3.3.7. Conclusions</u>	85
<u>3.4. Cyclic testing</u>	86
<u>3.4.1. Specimens description and test setup</u>	86
<u>3.4.2. Force vs. displacement curves</u>	92
<u>3.4.3. Strain gauges on CSTC beam's truss</u>	97
<u>3.4.4. Strain gauges on truss girder</u>	98
<u>3.4.5. Strain gauges on vertical plate</u>	100
<u>3.4.6. Displacement gauges on outer beam surface</u>	102
<u>3.4.7. Conclusions</u>	103
<u>CHAPTER 4</u>	
<u>4. CONCRETE MODELLING</u>	105
<u>4.1. Introduction</u>	105
<u>4.2. Compression models</u>	106
<u>4.2.1. Mander model (1988)</u>	107
<u>4.2.2. Nagashima Model (1992)</u>	112
<u>4.2.3. Cusson and Paultre Model (1995)</u>	113
<u>4.2.4. Razvi model (1999)</u>	116
<u>4.2.5. Legeron model (2003)</u>	119
<u>4.2.6. Cusson model (2008)</u>	121
<u>4.2.7. Cui and Sheick model (2010)</u>	123
<u>4.2.8. Provisions for concrete ductility</u>	124
<u>4.2.9. Provisions for concrete strength</u>	125
<u>4.2.10. Models' validation</u>	127
<u>4.3. Numerical implementation of concrete models</u>	132
<u>4.3.1. Tensile behaviour</u>	132
<u>4.3.2. Compressive behaviour</u>	135

CHAPTER 5

<u>5. LATTICE GIRDERS' PARAMETRIC OPTIMIZATION</u>	137
<u>5.1. Introduction</u>	137
<u>5.2. Numerical parametric pull-out tests</u>	139
<u>5.3. Bending strength</u>	149
<u>5.4. Conclusion</u>	153

CHAPTER 6

<u>6. COMPOSITE-COLUMN'S FE MODEL CALIBRATION</u>	155
<u>6.1. Introduction</u>	155
<u>6.2. FE model</u>	155
<u>6.3. Experimental vs. numerical response</u>	157
<u>6.4. Conclusions</u>	166

CHAPTER 7

<u>7. OPTIMIZATION OF COMPOSITE-COLUMNS</u>	169
<u>7.1. Introduction</u>	169
<u>7.2. HSC column numerical analyses</u>	170
<u>7.3. Core-joint numerical analyses</u>	172
<u>7.4. Column-joint connected with welded flanges</u>	175
<u>7.5. Column plus bolt-connection (4 bolts)</u>	179
<u>7.6. Column plus bolts-connection (6 bolts)</u>	183
<u>7.7. Conclusion</u>	186

CHAPTER 8

<u>8. ROTATIONAL STIFFNESS OF COLUMNS' COUPLING SYSTEMS</u>	189
<u>8.1. Introduction</u>	189
<u>8.2. Reverse component approach</u>	190
<u>8.3. Analytical component approach</u>	191
<u>8.4. Rotational stiffness of column-to-joint interface</u>	193
<u>8.5. Column-to-joint interface classification</u>	194
<u>8.6. Conclusions</u>	197

CHAPTER 9

<u>9. ANALYTICAL STUDY OF COMPOSITE-COLUMNS</u>	199
<u>9.1. Introduction</u>	199
<u>9.2. Provisions for HSC column bending strength</u>	199

<u>9.3. Analytical modeling of composite-column</u>	202
<u>9.3.1. MATLAB subroutine</u>	202
<u>9.3.2. HSC column</u>	204
<u>9.3.3. Composite-core-joint</u>	205
<u>9.3.4. Bolted connection</u>	206
<u>9.4. Design domain for composite-column</u>	207
<u>9.5. Conclusions</u>	211
<u>CHAPTER 10</u>	
<u>10. NUMERICAL JOINT CYCLIC PERFORMANCE</u>	213
<u>10.1. Introduction</u>	213
<u>10.2. Numerical model</u>	214
<u>10.3. Implementation of experimental static test</u>	216
<u>10.4. Expected cyclic behaviour for precast joint</u>	218
<u>10.5. Conclusion</u>	223
<u>CHAPTER 11</u>	
<u>11. ESTIMATION OF SEISMIC VULNERABILITY</u>	225
<u>11.1. Introduction</u>	225
<u>11.2. Plastic hinges' reference theory</u>	226
<u>11.3. Beams' plastic hinges</u>	230
<u>11.3.1. Adopted formulations</u>	230
<u>11.3.2. Computed plastic hinges</u>	231
<u>11.4. Columns' plastic hinges</u>	234
<u>11.4.1. Adopted formulations</u>	234
<u>11.4.2. Lateral confining steel</u>	235
<u>11.4.3. Column plastic hinge</u>	237
<u>11.5. Vulnerability-based approach</u>	241
<u>11.5.1. Frame models</u>	241
<u>11.5.2. Reference seismic action</u>	243
<u>11.5.3. Verification procedure</u>	245
<u>11.6. Seismic analyses results</u>	252
<u>11.6.1. Layout A frames</u>	252
<u>11.6.2. Layout B frames</u>	256
<u>11.6.3. Layout C frames</u>	258
<u>11.6.4. Layout D frames</u>	261
<u>11.7. Reduction factor identification</u>	263
<u>11.8. Conclusions</u>	264

<u>CHAPTER 12</u>	
<u>12. PRACTICAL DESIGN PROVISIONS</u>	267
<u>12.1.Introduction</u>	267
<u>12.2.Continuity lattice girder design</u>	268
<u>12.2.1. Design for bending</u>	268
<u>12.2.2. Design for shear</u>	269
<u>12.2.3. Shear-connection design</u>	271
<u>12.3.CSTC beam design</u>	272
<u>12.4.HSC column axial and bending strength</u>	273
<u>12.4.1. Flexural strength for seismic design</u>	273
<u>12.4.2. Shear strength design and minimum confinement</u>	274
<u>12.4.3. Lateral reinforcement to provide confinement</u>	276
<u>12.5.Bolted connection</u>	277
<u>12.5.1. Bending strength</u>	277
<u>12.5.2. Shear strength</u>	277
<u>12.6.Core-joint M-N domain strength</u>	278
<u>12.7.Core-joint shear strength</u>	278
<u>12.7.1. Design for shear</u>	279
<u>12.7.2. Design for confinement</u>	285
<u>12.8.Improved layout for exterior joints</u>	286
<u>CHAPTER 13</u>	
<u>13. REAL CASE-STUDY APPLICATION</u>	289
<u>CONCLUSION</u>	291
<u>BYBLOGRAPHY</u>	299

1. LITERATURE SURVEY

1.1. Introduction

Presented in this chapter is a detailed literature survey about implementation of precast framing technologies in seismic area, which deal with the topic of this thesis. Introducing the different solutions developed through the years in different geographical areas helps not only to deepen the knowledge on the subject and to recognize past and actual building trends, but mainly to emphasize advantages and disadvantages of previous experiences, so to give researchers space for further improvements.

To provide a unitary framework, an historical overview is presented. In the first part is reported a rapid introduction on preliminary worldwide precast technology development since the '50s. In the second part, attention is focused on the evolution of precast moment resisting frame structures through two main chapters, as many as the countries characterized by major progress on this topic. These are New Zealand, where the monolithic emulative approach developed since the '80 and Unites States which promoted the dry connection approach since the '90s. Finally, the Italian trend is considered, characterized by an emulative approach, reinterpreted through a patented hybrid truss beam born in the '60 and topical still nowadays.

1.2. Initial development of precast technology

The introduction of precast elements in building constructions started nearly contemporary in different countries in the second half of 20th century, mainly due to the economic boom after the Second World War. During this period the need for cost competitive and rapid to assembly infrastructures and both industrial and social

buildings increased. The high cost of structural steel promoted the adoption of reinforced concrete as base material, with a cost advantage 1 to 10 when resisting compressive columns are considered (Griffis, 1992). The need for reducing construction costs, led to moving out from site-construction long time spending casting and scaffolding operations. More conveniently, these could be brought off into factory plants, where monolithic, easy to transport and assemble modular RC element started being produced.

In Canada structural precast concrete construction started in the 1950's with a number of notable buildings. Early examples include a 10000 m² one-storey structure, with column and girder framing system and double tee roof members in Edmonton in 1955 and eight storey precast frames building built in Winnipeg in 1960. Contemporarily the use of precast concrete in flooring systems (prestressed hollow core sections) was becoming commonplace also in Japan and New Zealand, in the 60's leaving cast-in place floor construction generally uncommon in these countries (Park, 2002).

Based on the concept that maximum economy is achieved with maximum repetition and mass production, development of standard products was one of the major activities through the 1950s and the 1960s in United States. Initial applications dealt with pre-tensioned precast units such as single or double T section and hollow core section. Afterward long-line beds for precasting/prestressing (Fig. 1), high strength concrete and steam curing were also introduced.

Early in the 1960s, the US government sponsored the so-called research program "Operation Breakthrough" that led to the introduction of different high-rise precast building prototypes for housing (Precast Concrete Industry (PCI), 2007). As part of this program, a significant testing program was conducted by the Portland Cement Association to establish design principles for precasting and defining the typical precast gravity load resisting frame layout, which relies mainly on simply supported beams, statically determined structural scheme and dry contact joint. Inverted tee ledger and rectangular beam were used for structural framing to support deck members. Square or rectangular columns, with or without corbels, became an integral part of the column-beam-deck framing solution that makes rapid, all-weather erection possible (Fig. 1 to Fig. 3).



Fig. 1: Long-line prestressed double tee casting bed



Fig. 2: Example of typical precast frame layout

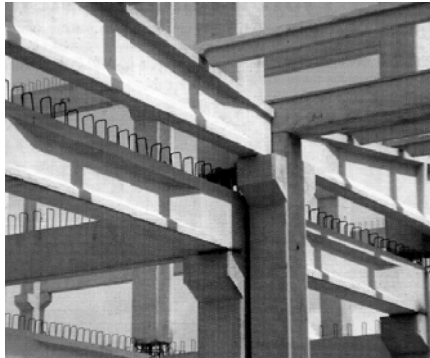


Fig. 3: Dry joints for precast frames



Fig. 4: Load-bearing wall structure

In Italy particularly successful was the development of precasters between the 1950's and the 1970's. The introduction of prestressing, the growth of manpower costs and the high demand for industrial building of all kinds turned construction rapidly towards precast concrete solution (CEB-FIP, 2003). Precast technology based on gravity load resisting skeleton structures in combination with shear resisting walls (either precast or cast-in-place) became popular not only for low-storey commercial (storehouses, markets, malls) and industrial buildings, but also for multi-storey parking garage, municipal facilities (schools, hospitals, etc) and residential building, thank to the development of prefabricated composite steel truss-concrete beams, patented in the late '60s by Salvatore Leone (cf.ch. 1.6). In parallel also load-bearing precast wall-panels appeared (Fig. 4) even if these systems, due to their functional rigidity, have been no longer widely used.

Conversely this solution became rather popular in East Europe and former Soviet Union Republics for urban residential buildings, usually five to ten stories high (Fig. 5), to provide low-income housing for the growing urban population (Brzev & Perez, 1990). Alternatively, structural systems combining load-bearing precast panel and precast column appeared (Fig. 6).

Analysis and development of an innovative prefabricated beam-to-column joint

Another solution employed in Eastern Europe since the 60's was the so-called "IMS technology", consisting in cantilever floor slabs (totally replacing beams and girders), directly post-tensioned against column (Fig. 7) and coupled with shear walls to withstand seismic induced solicitations.

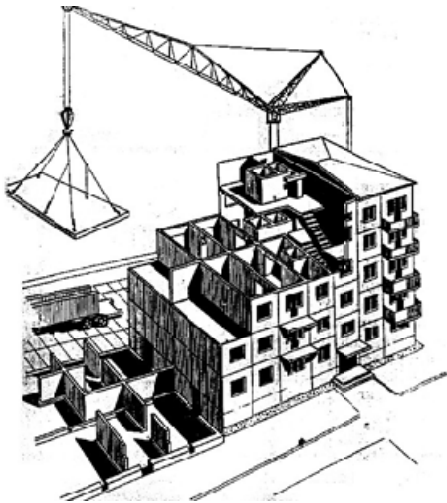


Fig. 5: Seria 135 precast system, Brzev & Perez, 1990

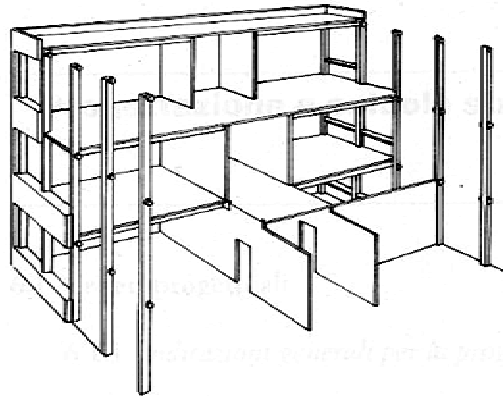


Fig. 6: Precast frame system of Seria IIS-04, Brzev & Perez, 1990

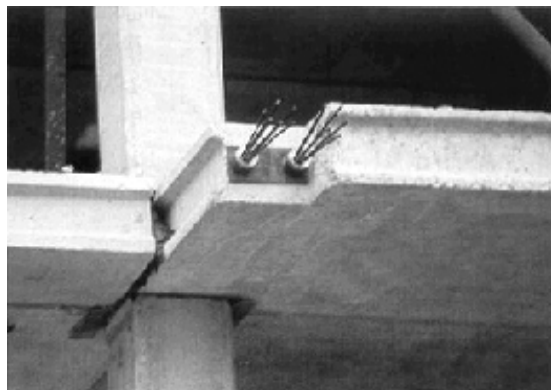


Fig. 7: IMS precast frame technology: post-tensioning of floor slab

1.3. Former precast earthquake resisting frames experiences

The adoption of precast moment resisting frames was limited until the 80's. Precast framing technology was mainly employed as gravity resistant skeleton structure, in combination with shear panel or load-bearing panels, both precast or cast-in-place, to provide strength against seismic action. An example is the Bromley Palace apartment building in Calgary, a 31 storey building, completed in 1985, which still represent the tallest total precast building in Canada .

Some exceptions are however revisable in the worldwide panorama.

In New Zealand and Japan, for example, in the 1960's and 1970's precast elements post-tensioned together to form continuous moment resisting frames were sometimes used (Fig. 8, Fig. 9). Experimental research on this precast solution was conducted by Park & Blakeley, 1971 (see par 1.5.2), but potentiality was not fully comprehended until the beginning of the '90s, when United States first interested on this topic (Cheek & Lew, 1991).

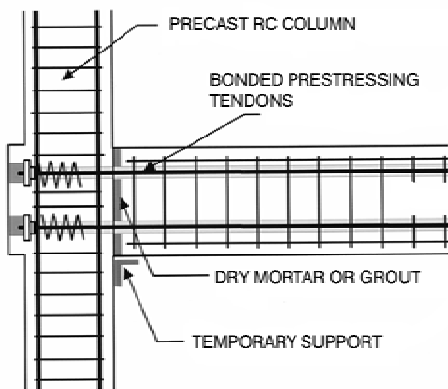


Fig. 8: General reinforcing details of post-tensioned system



Fig. 9: Building constructed in New Zealand with post-tensioned system

Since the 60's in Mexico a limited number of building with moment resisting frames incorporating precast concrete elements have been constructed, despite limited design provision covering this aspect. Precast concrete frame were mainly assembled with multi-level columns with voids in the beam-column joint regions ("windowed columns"). Beam's through joint connection was provided by welding of longitudinal reinforcement and by subsequent concrete casting to restore structural continuity in the joint region. Just in 1976, Mexico City Building Code introduced for the first time some provisions for moment resisting precast structures, basically suggesting the emulation concept (emulation of cast-in-place frames). The use of

welding for connections in precast elements was common practice in Mexico until designers were aware of failures of welded connections during the 1994 Northridge earthquake in California. Alternative methods were used more recently for connecting precast elements in frames (par. 1.4.2).

An appreciable development of moment resisting frame technology is revisable in Soviet Union Republics. In particular the “Seria 106 system”, developed in Kyrgyzstan in 1975, represented one of the former system adopting cruciform precast beam-to-column sub-assembly (Fig. 10a). The frame was constructed using two main modular elements: the cruciform element and a linear beam element (Fig. 10b). The precast elements were joined by welding the reinforcement bars at midspan and casting the concrete in place.

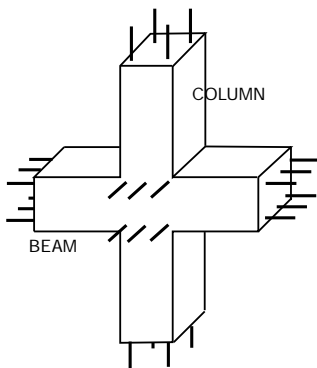


Fig. 10: a) Cruciform precast units “Seria 106”; b) building example with highlighted cruciform and transversal beam elements

Moment resisting frames with beams substituted by concrete slab, were implemented in the last decade of the Soviet Union (1980-1989). This type of precast construction is known as “Seria KUB”. Frames were usually 5 to 12 storeys high, with multi-level precast columns, normally two storeys long (Fig. 11). Precast square slab elements were used as flooring system. Some of these slabs presented a central hole with dimension 680 by 680 mm that was used to thread the slab along the column, from the top down to the joint level. Here some longitudinal rebars in the upper and lower face of the slab were welded to assure continuity of longitudinal rebars and self-bearing capabilities. The other slabs were placed beneath the central one and welded together. Cast-in-site concrete at connections was completing the structure. “Seria111” technology was similar, with the main difference that floor slabs were larger panels casted on the ground and then lifted and erected to the final position.

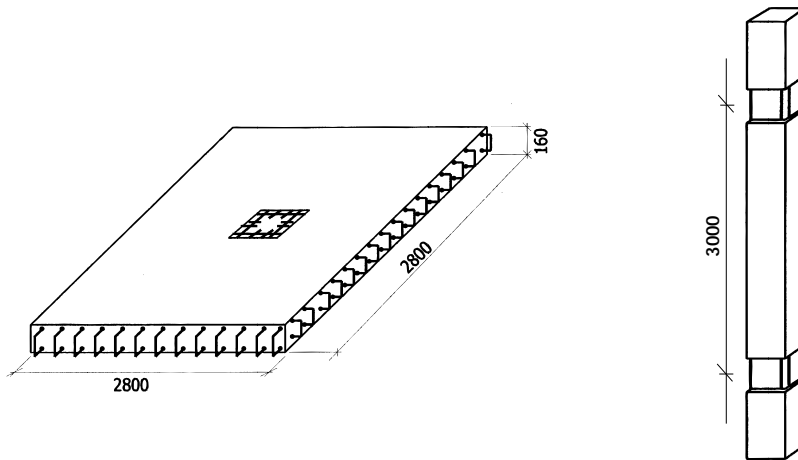


Fig. 11: Flooring element and column of "Seria KUD" precast system

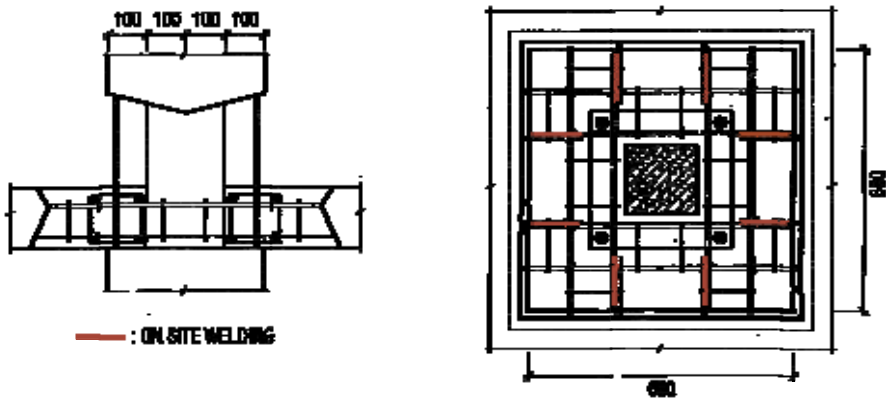


Fig. 12: "Seria KUD" joint assembling



Fig. 13: Seria KUD frame under construction in Kyrgyzstan

Hence, a certain evolution in precast framing technology is revisable in the considered period, especially in the Asian region. Despite these progresses, limited

knowledge about seismic design and required details to prevent unexpected failures, jointed to low quality of adopted materials and construction control, led to catastrophic consequences during several earthquake events.

Chinese earthquake in 1976 at Tangshan caused the collapse of many precast frame buildings (Fig. 14). In the same year in Russia, many large-panel buildings were damaged in the second Gazly earthquake of 1976 (Magnitude 7.3, Fig. 15).

Several precast concrete frames collapsed during the 1977 Vrancea (Romania) Earthquake (Magnitude 7.2), as well as in the 1988 Armenian Earthquake (Magnitude 7.5). In the latter case, collapsed frames were generally 9-storey, built with precast frame systems “Seria 111” (Fig. 11 to Fig. 13) with floor diaphragms poorly connected to the frame elements and columns detailed with inadequate confinement (2003).



Fig. 14: Tangshan (China) Earthquake in 1976 Fig. 15: Gazli (Russia) Earthquake in 1976



Fig. 16: Armenian (Turkey) Earthquake in 1988

Based on these evidences, there was a general concern among the engineering community, regarding the seismic performances of precast constructions. It is a matter of fact that “bad news” are more widely publicized than “good news.” For example, the poor performances of precast frame systems “Seria 111” in the 1988 Armenian Earthquake were well known. Conversely, few engineers were aware of

the good seismic performance of several large-panel buildings under construction in the same site (background buildings in Fig. 16).

Fintel, 1986 reports that after Mexico City Earthquake (1985) only 5 of 265 buildings that either collapsed or were severely damaged, used precast concrete elements. Besides, many of the precast buildings and multi-storey parking garage in Mexico City survived the severe ground shaking without damage or distress.

Nevertheless, the bad feeling raised around precast systems caused the use of precast concrete in earthquake-resisting structures to be view with suspicion in several countries as for example United States and Chile for many years. In this latter in particular, still nowadays precast concrete elements are being used mainly in gravity load resisting skeleton systems, just in combination with cast-in-place reinforced concrete walls. Even the use of precast concrete in flooring systems is seldom used, preferring using cast-in-place floors solution (2003).

1.4. New Zealand approach to precast framing

1.4.1. *The emulative approach*

Since the '60s in New Zealand there was a steady increase in the use of precast concrete in buildings, in particular for flooring system (hollow core slab) and non-structural cladding. On the contrary, the adoption of totally precast frames in such a high seismicity region was still uncommon at the beginning of the '80s for two main motivations: the bad feeling about the poor seismic performances of poorly designed precast buildings in the Russian and Asian regions and the absence of specific seismic provisions for precast structures. A significant growth in use of precast concrete in moment resisting frames and structural walls took place during the boom-years of building construction in the mid-to-late 1980s.

The main input was given by economical motivations. Incorporation of precast concrete elements had several advantages like high quality control, reduction of in site formwork and site labour and increased speed of construction. High interest rates and demand for new building space in the mid '80s, highlighted the benefits of precast technology over cast solutions. Contractors readily adapted to precast concrete and the new construction techniques resulting from off-site fabrication of building components (Park, 2002).

Beside economical motivation, development of *capacity design approach* (Paulay & Priestley, 1992) gave the designer the confidence that adequate ductility (i.e.

adequate seismic performance) may be achieved in precast frame structures. Until mid 1970s, it was customary in the seismic design of structures to use linear elastic structural analysis to determine internal force and design the members to be at least strong enough to resist those actions. As a result, when structures was subjected to a severe earthquake, the manner of post-elastic behaviour was totally unpredictable. Flexural yielding of structural members could occur at any of the regions of maximum bending moment (either beams or column's ends) and shear failures could also occur, depending on where the flexural and shear strength of members and joints were first reached.

The capacity design method was first introduced by a discussion group of the New Zealand Nation Society for Earthquake Engineering in the 1970s. It was later recommended by the New Zealand Loading Standards (NZS 4203:1976) and definitively formulated in the New Zealand Concrete Design Standard in 1982 (NZS 3101:1982). For moment resisting frame buildings, the best way to achieve ductile post-elastic deformations is by flexural yielding at selected plastic hinge location. The preferred mechanism is the beam-sidesway (Fig. 17). Column sidesway mechanism should be prevented since the possibility to get a soft storey response preclude development of any ductile response. In addition, specific detailing in critical regions is required against brittle failures, due to shear mechanisms.

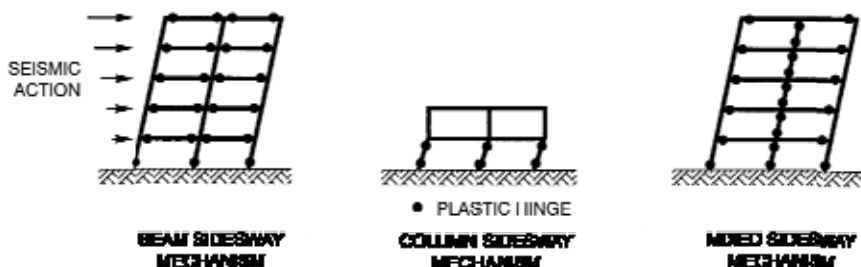


Fig. 17: Post-elastic deformation mechanisms for framed structures

Confidence in the use precast concrete in moment resisting frames and structural wall required the development of satisfactory method for connecting the precast elements together. Being current design code mainly devoted to cast-in-place buildings provisions (NZS 3101:1982), the design methods introduced for the connections between precast elements aimed to achieve behaviour as for a monolithic concrete structure. This is called *cast-in-place emulation technology* and consist on capacity design approach applied to precast structures. The challenge was to find economical and practical means of connecting the precast elements together to ensure adequate stiffness, strength ductility and stability (Park, 2002).

A Study Group of the New Zealand Concrete Society, the New Zealand National Society for Earthquake Engineering and the Centre for Advanced Engineering of the University of Canterbury was formed in 1988 to summarize and present data on precast concrete design and construction, to identify special concerns and to indicate recommended practices (Restrepo et al., 1989). The outcome of the deliberations of the Study Group was the publication of a manual entitled "Guidelines for the Use of Structural Precast Concrete in Buildings," which was first printed in August 1991. A second edition incorporating experimental research evidences undertaken in the first half of the '90s in Japan by Kurose et al., 1991 and New Zealand by Restrepo et al., 1995a was published in 1999. Two main connections categories are identified: strong and ductile. Strong connections of limited ductility are designed to be sufficiently strong, so that the connection remain in the elastic range, when the building is satisfying the ductility demand imposed by earthquake (Ghosh et al., 1997). Ductile connections of equivalent monolithic system are designed for the required strength and with longitudinal bars, grouted post-tensioned tendons or mechanical connections located in the regions that are expected to enter the post-elastic range in a severe earthquake (Park, 2002). Depending on the arrangement of precast concrete members forming moment resisting frames, 4 different approaches may be identified as suggested by "*Guidelines for the Use of Structural Precast Concrete in Buildings (1999)*":

- System 1, precast beam units between columns;
- System 2, precast beam units through columns;
- System 3, cruciform elements;
- System 4, pretensioned precast U-beam units between columns.

This approaches represent even today a reference in the field of emulative precasting. In the following, a brief description of each system is reported together with most recent experimental researches.

1.4.2. *Precast system n°1*

Layout of this system is shown in Fig. 19. The arrangement involves the adoption of precast reinforced members to form the lower part of the beams. These are placed between column and seated on the cover concrete of the previously cast-in-place or precast column (Fig. 21). Propped erection is usually required (Fig. 19 right).

The column bars are spliced above the joint using grouted steel sleeve or by grouting them into corrugated steel ducts embedded in the column above (Fig. 18).

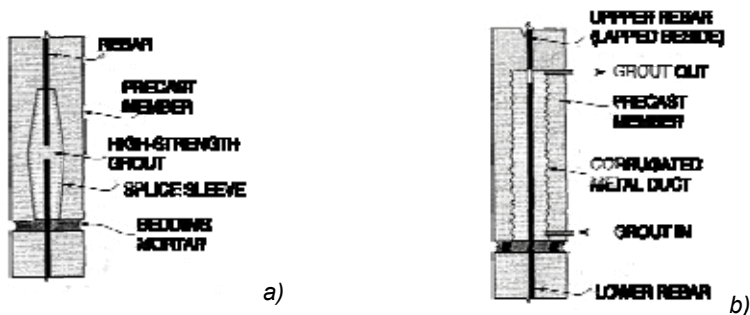


Fig. 18: Vertical rebar splice systems; a) grouted steel sleeve; b) corrugated steel ducts

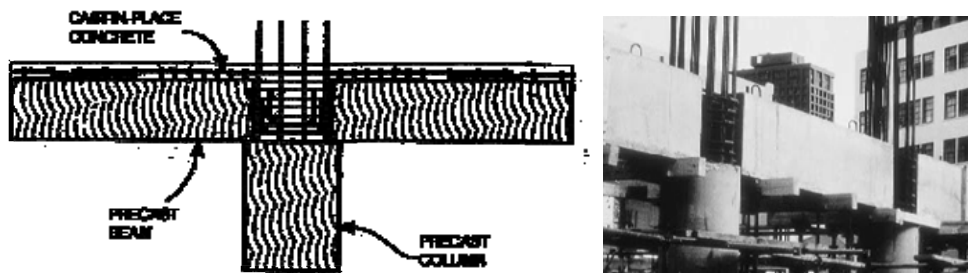


Fig. 19: Precast system n°1 layout

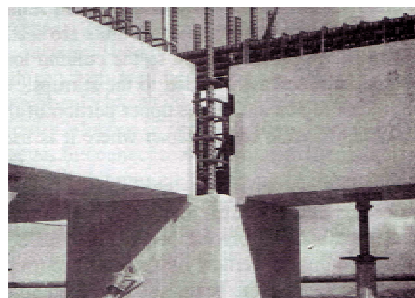
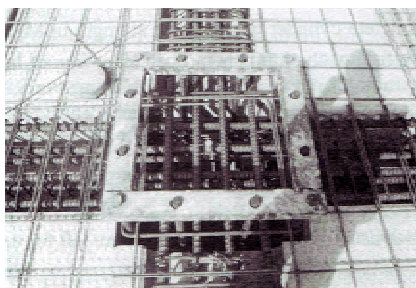


Fig. 20: Joint's reinforcement for system n°1 Fig. 21: System n°1 before casting

Lower longitudinal reinforcement is spliced in the joint core using 90-degree hooks at the far face of the cast-in-place joint. Hence the column dimensions need to be reasonably large to accommodate the required development length and to reduce congestion caused by hooked rebars (Fig. 20). Reinforcement is then placed in the top of the beams, over the precast floor and in the beam-column joint core. The topping slab over the precast floor system and the cast of the joint core complete the system. To assure a ductile frame behaviour the column connection should be oversized, leaving the beams' end to behave in a ductile manner (ductile connection) as required by the capacity design approach.

Full-scale laboratory tests reported by Restrepo et al., 1989 and Restrepo et al., 1995b evidence excellent energy dissipation capabilities similar to those expected from cast-in-place-members (Fig. 22).

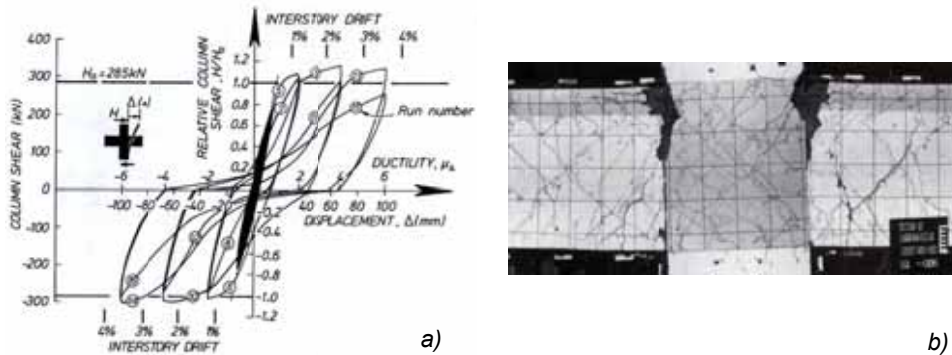


Fig. 22: Experimental tests on precast system n°1: a) hysteresis cycle; b) Crack pattern at the end of tests, Restrepo et al., 1995b

Main drawback of this precast system is related to construction tolerances. Beam units slightly longer than anticipated could restrict the placement of joint hoops, as usually very small tolerances are left for this purpose.

Dimensioning detail can be found in Restrepo et al., 1989, Restrepo et al., 1995a.

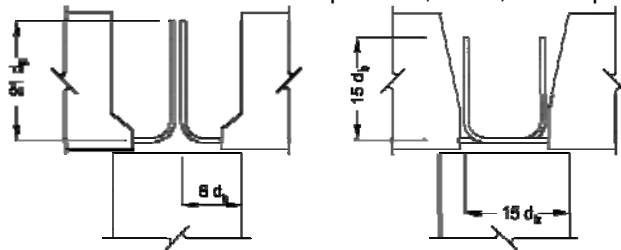


Fig. 23: Lap splicing design detail (Restrepo et al., 1989)

A slightly modified version of this system is being widely adopted in the last decade in Mexico. It replaces the practice of in-site beam longitudinal rebars welding, after the numerous failures of fully welded moment connections during the 1994 Northridge and 1995 Kobe earthquakes. Single-storey columns used for the original layout of precast system n°1, are replaced with multi-level “window type” columns in order to increase mounting speed, and reduce time required for concrete strengthening. To overcome the issue related to construction tolerances, it is common practice in Mexico to hook bottom beams’ longitudinal reinforcement in the column voids, to provide structural continuity. This solution is adopted in particular when limited column dimension does not comply with the Code provisions for

anchorage length, despite this approach is not explicitly allowed neither in the ACI Building Code (ACI 318-08), nor in the Mexico City Building Code (MCBC-93). Experimental cyclic tests on real-scale beam-to-column joint (Fig. 24) performed by Alcocer et al. (2002) do not provide encouraging results. Energy dissipation capability is good for drift level lower than 3% but strength is only 80% of the expected level from equivalent monolithic sample. Premature bending flexibility of hoops used to achieve continuity, as well as pullout of beam bottom bars, contributed to initial joint damage. Joint mechanisms of resistance were impaired by further beam rotation inside the joint (Fig. 25). Further tests on a half scale two storey performed by Rodriguez & Blandon, 2005 confirmed that the continuity hoops in the hooked bars could not provide the required continuity for these bars.

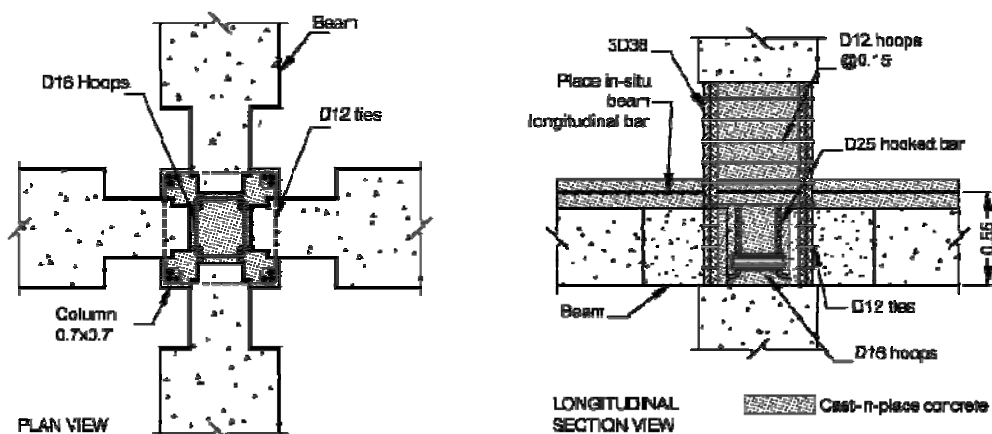


Fig. 24: Reinforcing details of a window-type beam-to-column connection, Alcocer et al., 2002

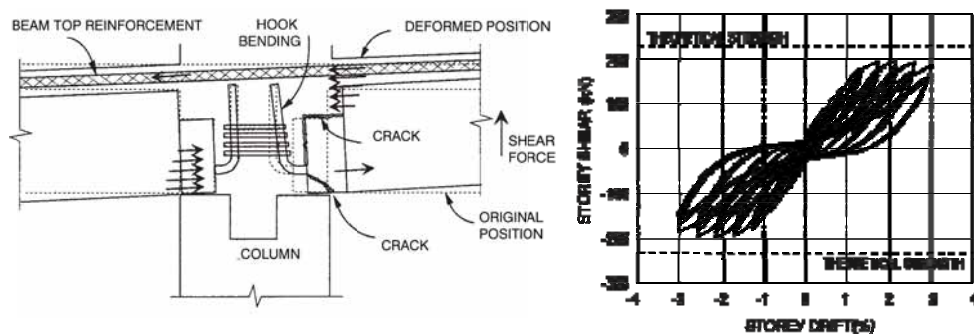


Fig. 25: a) plastic mechanism at failure; b) experimental cyclic loops (Alcocer et al., 2002)

This issue could be overcome adopting precast system n°1 for moment resisting frames subjected only to gravity loads. Rahman et al., 2008 investigated this aspect testing two samples, the first representative of the precast frame, the second

corresponding to an equivalent monolithic cast-in-place frame with continuous upper and lower rebar through the joint. No specific confinement or hooking reinforcement was placed at core-joint level. Experimental evidence from monotonic curve response in Fig. 27 indicates comparable or higher performance of precast specimen with respect to cast-in-place specimen. Crack pattern at failure points out limited damage in compression of the precast frame, probably due to the effect of the corbel. Splitting failure of compressive concrete took place in monolithic frame. Moreover force deflection curve allows to estimate stiffness of the precast connection. There are several studies investigating the effect of precast connections in reducing global framed structure stiffness, like those presented by Elliott et al., 2004 and Ferreira et al., 2011. In the considered case experimental evidence suggests to classify the solution proposed by Rahman et al., 2008 like a totally rigid connection.

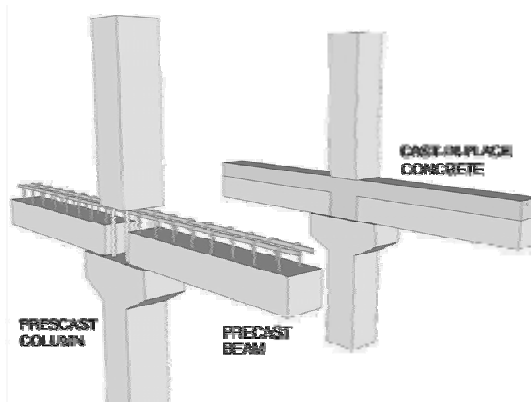


Fig. 26: Beam-to-column joint samples tested by Rahman et al., 2008

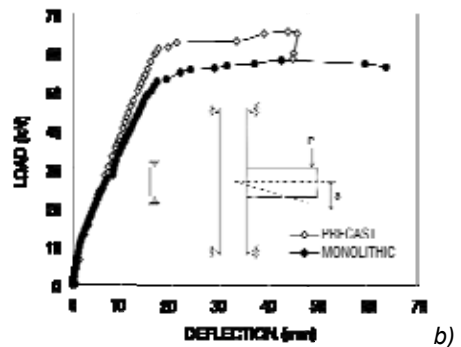


Fig. 27: Experimental results by Rahman et al. (2008); a) crack pattern of precast specimen at ultimate load; b) load-deflection curve

1.4.3. Precast system n°2

Precast system n°2 takes more extensive use of precast and avoids the placing of cast-in-place concrete in the congested beam-column joint Fig. 28. The precast portion of the beam extends from midspan to midspan and hence, it includes within the precast element over the column the complex arrangement of joint core hoop reinforcement. The success of the system depends on smaller than normal tolerances, due to the fact that precast or cast-in-place columns need to occupy the clear height between beams without gaps. The vertical column bars below the joint protrude up through vertical corrugated steel duct located in the precast beam unit, where they are grouted and passed into the column above. To help this operation, plastic tubes are placed over the bars (Fig. 29a) and then removed, once the beam has been placed over the column.

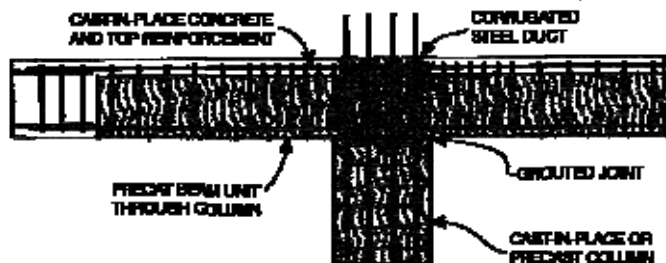
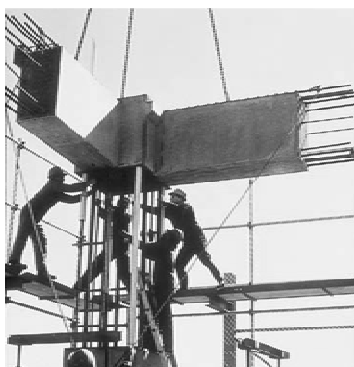


Fig. 28: Precast system n°2 layout



a)



b)

Fig. 29: Precast system n°2; a) mounting phase; b) column bars after joint grouting

To complete the frame system, connections have to be created at the mid-span of the beam. Design information on a variety of beam-to-beam connections are provided by literature (Restrepo et al., 1995a). A review of most commonly implemented connection techniques is reported from Fig. 30 to Fig. 32:

- Straight and double-straight bar laps

- Drop-in double hooked bars
- Welded connections
- Mechanical coupler

Some examples about construction in New Zealand adopting system n°2 are reported in Fig. 34.

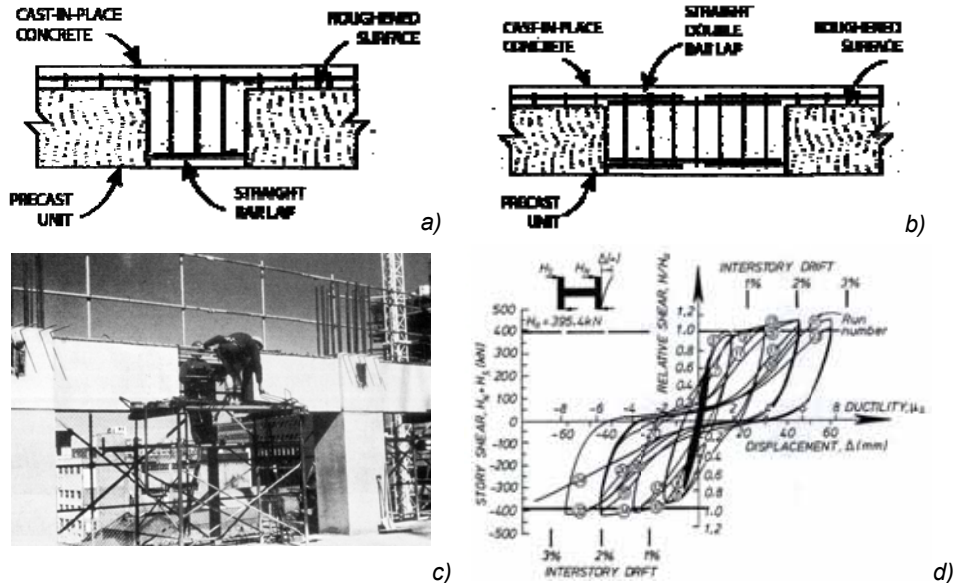


Fig. 30: a) Beam-to-beam connection using straight bar laps; b) double straight bar laps; c) example of connection using double-straight bar laps; d) experimental results from cyclic test from Restrepo et al., 1995b

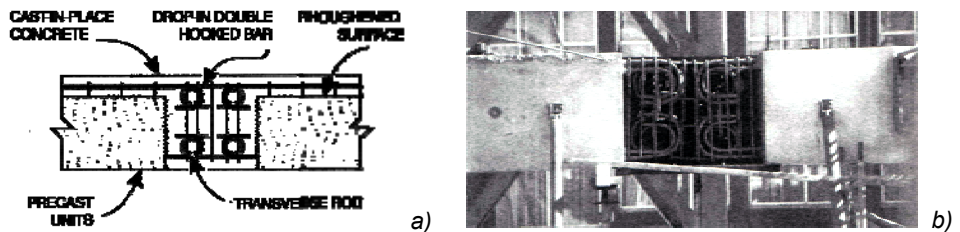


Fig. 31: Beam-to-beam connection using drop-in double hooked bars, 2003

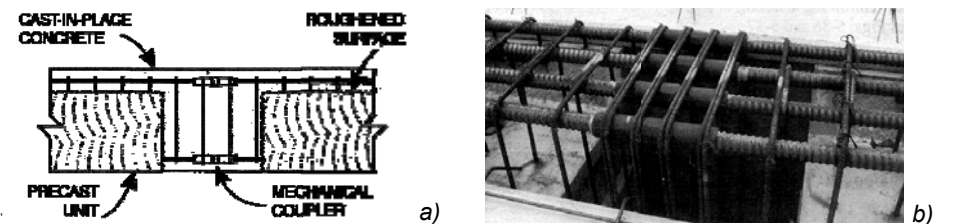


Fig. 32: a) Beam-to-beam connection using mechanical coupler, 2003

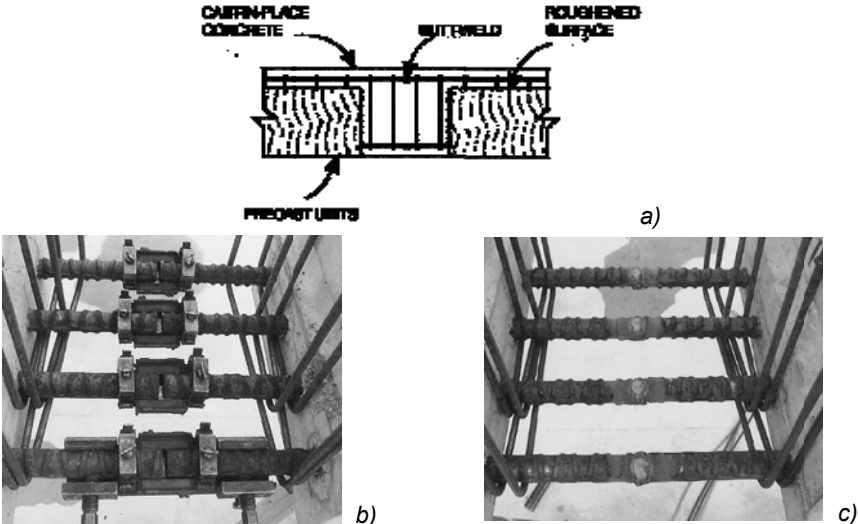


Fig. 33: a) Beam-to-beam connection using welded bars; b)welding operation set-up; c) welded rebars, 2003



Fig. 34: a) 22-storey Prince Waterhouse-Cooper building in Christchurch (NZ); b) 152 m tall ANZ Tower in Auckland (NZ), Park, 2002

1.4.4. Precast system n°3

Precast system n°3 is given by an arrangement incorporating T-shaped, H-shaped, cruciform or multi-storey cruciform units, depending on precaster's solution (Fig. 35). It appears as an update of original "Seria 106" technology (Fig. 10).

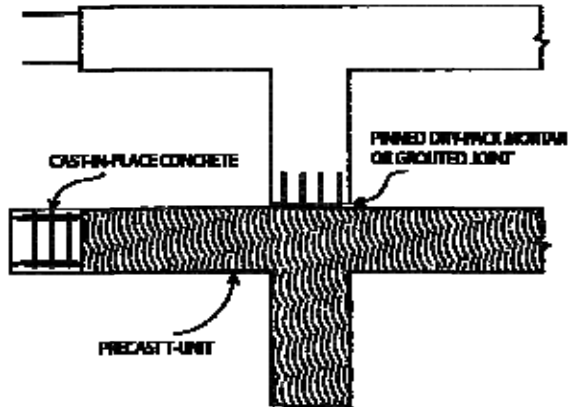


Fig. 35: Precast system n°3: precast T-shaped element, 2003



Fig. 36: 13-story Unisys House in Wellington (NZ), Park, 2002

Vertical column bars in the precast units are connected using grouted steel sleeve or grouting them into corrugated steel ducts, at core-joint or mid-span level (Fig.

18). Cast in place beams connection are identical to those employed for System 2 (Fig. 30 to Fig. 32). Main benefits of system n°3 are the extensive use of precast concrete and the elimination of complex reinforcing details on construction site. Mounting ease, on the contrary, might be sensibly affected by dimensions of precast elements, in particular when provided in multi-level layout, resulting those heavy and bulky and difficult to manage.

1.4.5. Precast system n°4

In this precast system, widely adopted in New Zealand, the precast concrete beam has U-shaped cross section (U-shell). In the construction site, the U-shell beams are seated on the column. Longitudinal rebars are placed inside the U-shell and concrete is cast monolithically in the beam core and the beam-column connection. In the early development by Park & Bull, 1986, the precast concrete shell is used as the formwork for core concrete in the temporary construction phase, and only the core concrete enclosed by the stirrups is used for structural purpose Fig. 38 (left),. Cyclic experimental tests performed by Park & Bull, 1986 evidenced that, during severe seismic loading, there was a tendency for the plastic hinging to spread along the cast-in-place reinforced concrete core within the precast U-beam due to breakdown of bond. This had a negative impact on energy dissipation capability of this precast system.

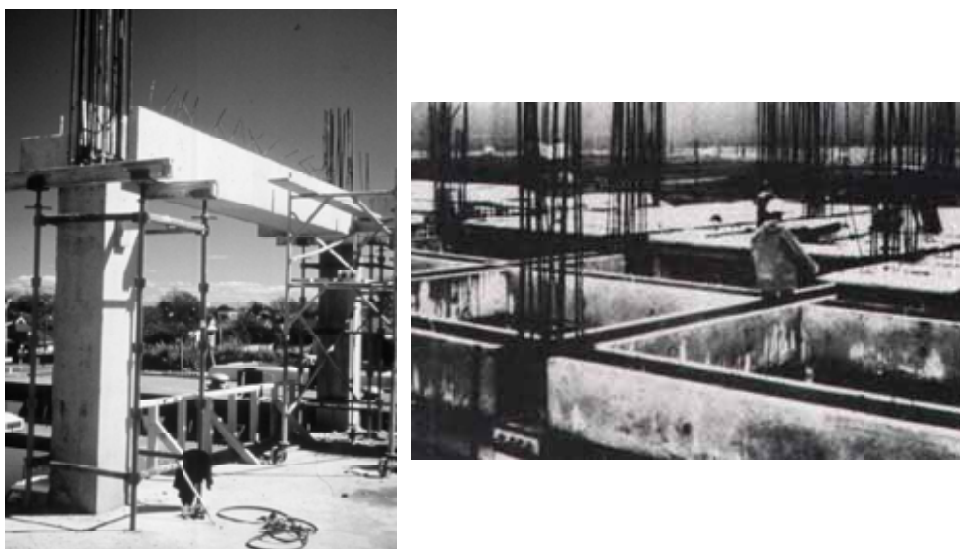


Fig. 37: Precast system n°4, Park and Bull (1986)

Lee et al., 2004 developed an updated version of the U-shaped shell. Stirrups placed in the precast concrete are connected to the cast-in-place core concrete, to favor a full-section strength (Fig. 38). To enhance the mounting speed of the precast frame, one-piece multi-level columns are adopted. The beam-column joint is filled with cast-in-place concrete. Longitudinal bottom bars are placed inside the U-shell after the two continuous beams are seated on the column voids. Despite improved layout, experimental tests exhibited poor energy dissipation capacity, with severe pinching.

A recent experimental campaign performed by Park et al., 2008 further investigated this aspect. 5 different specimens were arranged with different reinforcement and confinement details to improve the joint performance in terms of stiffness, strength and energy dissipation capability. The specimens show good load-carrying capacity and deformation capacity, which were comparable to those of conventional monolithic reinforced concrete specimen. On the contrary, energy dissipation capacity and stiffness of the specimens are significantly lower than those of the cast-in-place specimen. This is mainly due to the diagonal shear cracks and the slippage of rebars occurred at the beam-column connection.

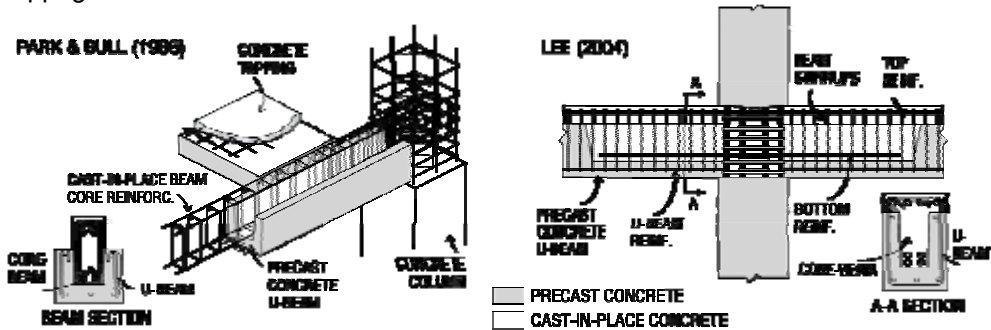


Fig. 38: U-shell joint layout developed by Park & Bull, 1986 (left) and updated by Lee et al., 2004 (right)

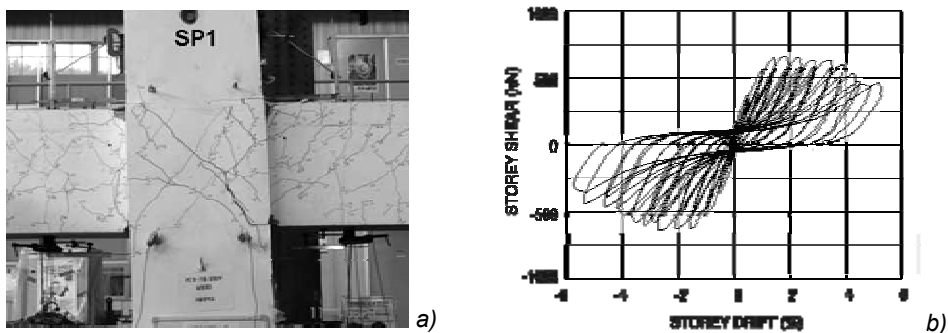


Fig. 39: Cyclic behaviour of U-shell joint (specimen SP1); a) crack pattern at 2,5% drift; b) cyclic hysteresis loops, Park et al., 2008

A similar beam to column joint was developed recently in Italy under the patented name “APE system”. U-shell beam acts as scaffolding for cast-in-place concrete and additional rebars are placed in the joint to assure beam-to-column connection. Experimental tests performed at University of Bologna by Mazzotti et al., 2011 both on interior (Fig. 40) and exterior joints indicate as the samples behave well in terms of strength and ductility (Fig. 41b), but bond failure of rebars inside the joint under cyclic loading cause an appreciable “pinching” effect. This is further confirmed by the absence of smeared cracks inside beam-to-column joint (Fig. 41a).

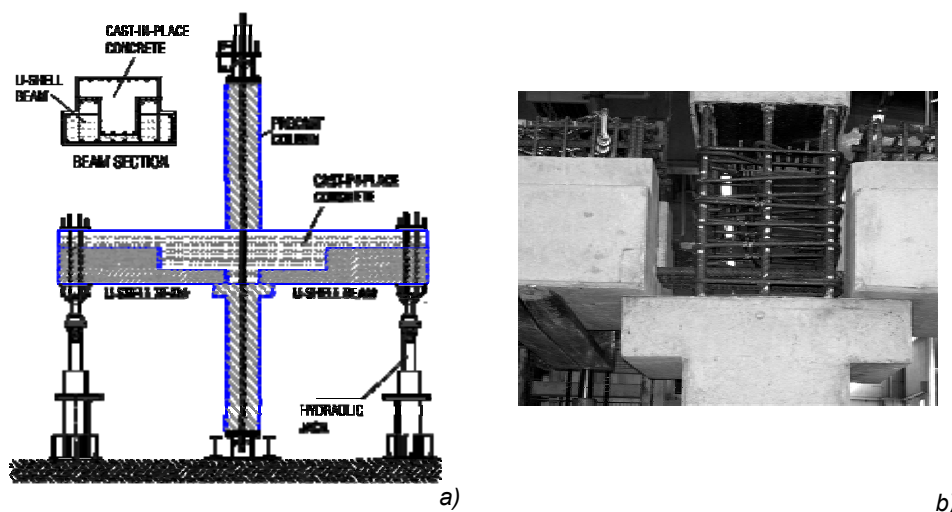


Fig. 40: a) cyclic tests configuration for U-shell joint from APE system; b) details of joint assembly, Mazzotti et al., 2011

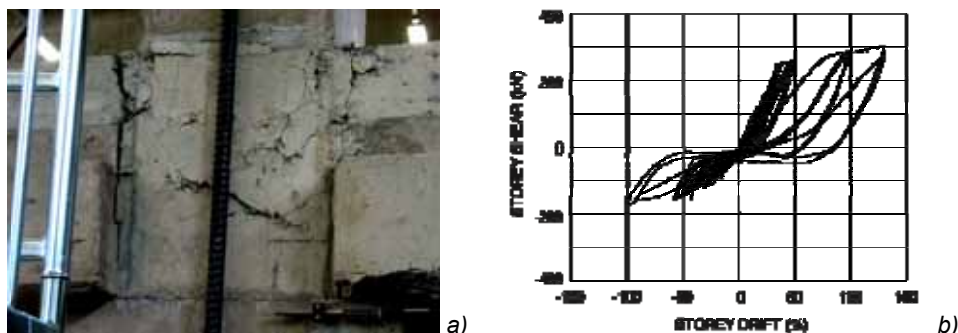


Fig. 41: Cyclic behaviour of U-shell joint from APE system; a) crack pattern at failure; b)cyclic hysteresis loops, Mazzotti et al., 2011

A further confirmation of the rebar debonding phenomena under cyclic loading for this kind of precast solution is given by third party tests, performed by Lignola et al., 2010. Both interior and exterior U-shell joint were tested. The experimental activity

evidenced that un-proper detailing may lead to a dramatically worst joint's performance compared to an equivalent cast-in-place monolithic solution (Fig. 42). To reduce the pinching effect resulting from the first test series, both cast-in-place concrete grade is increased to improve bond and the U-shell thickness is reduced, as suggested by Park et al., 2008. These improvements led to a considerable increase of joint performance in term of energy dissipation, despite joint's strength was about 5% and 10% lower than the equivalent cast-in-place sample, respectively for interior and exterior joints.

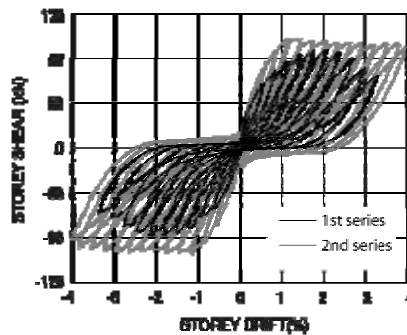


Fig. 42: Cyclic behaviour of interior U-shell joint, Lignola et al., 2010

1.4.6. Benefits and drawbacks of emulative approach

A general positive aspect for emulative monolithic systems is related to their long tradition. Since the 80's they demonstrated to perform well under seismic action, if properly detailed. Their design is reasonably simple, being required to fulfil provisions usually adopted for cast-in-place constructions. This guarantee in general the restoring of adequate strength and ductility level, analogous to classical RC frames, with the exception of system n°4, suffering considerable rebars' debonding during cyclic loading.

Further aspects to consider to check effectiveness of a precast solution should be the ease of assembly and mounting speed. Considered emulative precast solutions generally deal with self bearing capacity, thus not requiring for temporary scaffoldings during construction. Nevertheless considerable amount of cast-in-place concrete is necessary to provide global structural strength and stability. This limit sensibly the erection speed of frames, being required enough time for concrete strengthening after each casting. An accurate planning of construction phase is then necessary not to slow down excessively the rising of the building.

To improve this issue, multi-level precast columns may be adopted. In this way, up to 3-4 storeys can be assembled contemporarily. Limitation in the maximum storey number is given by the dimension of the precast elements, which might become bulky and difficult to transport and manage.

1.5. United States approach to precast framing

1.5.1. *The dry connection approach*

Differently from other countries like New Zealand, Mexico and Japan, where the monolithic-emulative precast technology has been widely adopted since the middle of the 80's (par. 1.4), in the United States this solution didn't find the approval of precasters and contractors (Stone et al., 1995).

Main motivation was that mixing of precast concrete and cast-in-place concrete could result in scheduling conflicts between construction phases when the cast-in-place concrete is required for structural stability of the system, with increased construction time and with economical impact on construction costs (Saqan, 1995). As a result, during the 80s and the whole 90s, the implementation of precast construction in high-seismicity area was seldom used (Stone et al., 1995).

Beyond practical application, even the American research community opposed strictly to emulative approach for precast system. As reported by Stanton et al., 1997, this approach was perceived like "*a limitation that inhibits innovation without considering peculiarities and potentialities of precast system*". The basic idea that marked US research during the whole 90s was that of moving inelastic response from members to connections. These are detailed to be weaker than the precast elements, and are intended like locations of inelastic deformations. As a consequence, the precast members should not be detailed for ductility and should remain elastic during seismic action.

Two multi-year multi-phase research programs were arranged with the aim of investigating this topic: the National Institute for Standards and Technology (NIST) program (1987-1995) and PRESSS (Precast Seismic Structural System) program (1991-1999) (Sritharan et al., 2000).

During this research phase, a new typology of moment resisting precast frames was defined, characterized by the adoption of "jointed" or "dry" connections to connect precast members together. They are also mentioned as "jointed system", since they are composed by monolithic beam and column elements, jointed together by "dry"

connections, in contrast to the “wet” connections typical of cast-in-place monolithic emulative systems.

Developed “jointed systems” may be grouped into three main categories (Fig. 43), namely:

- Post-tensioned/pre-tensioned connection (NLE);
- Tension-compression-yielding (TCY) and energy dissipating connection;
- Hybrid connections;

NLE solution consists substantially in a rocking system, characterized by a prestressed central tendon. The typical behaviour of this connection is non linear elastic. The second connection type use yielding of rebar or other devices to dissipate energy and emulate cast-in-place behaviour.

Hybrid system is a third category which merge together characteristics of two mentioned systems. It consists in post-tensioned connection with mild steel or other devices to dissipate energy

Further details on these technologies, their past development and actual trends are reported in next chapters.

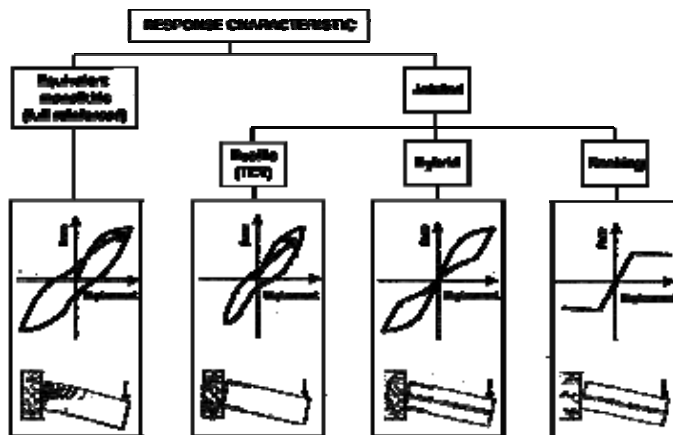


Fig. 43: Precast joint classification (2003)

1.5.2. Non linear elastic systems

For this connection type, nonlinear behavior is achieved through crack opening and closing at the interface between beams and adjoining columns. This nonlinearity is related to geometrical rather than material nonlinearity. Beams used in this connection type are prestressed with cables passing through the beam length and

the column. Cracks or joints at the column face open when bending moments produce flexural stresses large enough to exceed the precompression stresses at the face of the column.

Early study on this type of connection were conducted by Park & Blakeley, 1971. The authors observed that yielding of the cables occurred at column face, tending to spread into the beam as a consequence of debonding. Prior to crushing of concrete, energy dissipation was minimal. Progressive debonding of the cable passing through the column caused a reduction of bending resistance.

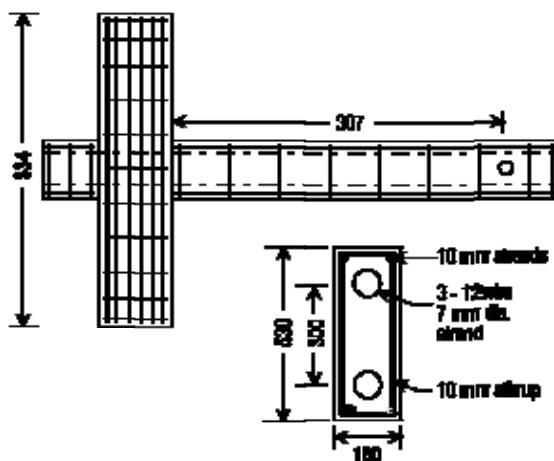
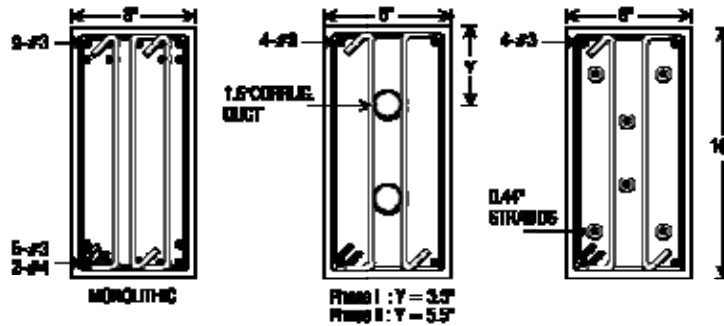


Fig. 44: Connections tested at University of Canterbury, Park & Blakeley, 1971

Further investigations on similar specimens were carried out during NIST research program (Cheok & Lew, 1993, Cheok & Stone, 1993)

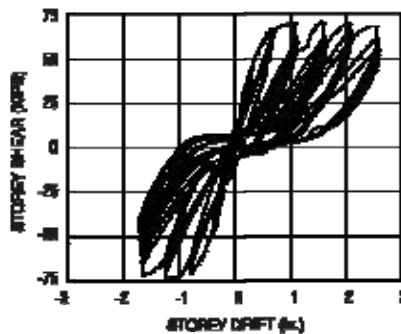
The tested sub-assemblages were 1/3 scale models of planar interior beam-column connections and consisted of one precast column and two precast beams connected in a cruciform shape. Connection between members was given by a dry joint with post-tensioned fully bonded cables passing through column and the beam with different arrangements (Fig. 45).



Note: 1in. = 25.4mm

Fig. 45: Beam cross-sections for connections tested at NIST, Saqan, 1995

It was concluded that post-tensioned bonded precast concrete beam-column connections could perform as well than equivalent monolithic specimens in terms of connection strength. However these subassemblages suffered excessive stiffness degradation (Fig. 46).



Note: 1in. = 25.4mm 1kip = 4.44kN

Fig. 46: Hysteresis curve from a precast prestressed beam-column joint tested at NIST, Cheek & Lew, 1991

A considerable contribute to full understanding of results obtained at NIST was given by Priestley & Tao, 1993. The solution proposed by the authors to improve performances was to use partially debonded tendons through the joint, with following advantages:

- prestressing steel should not yield if it is unbonded over an adequate length;
- the global response of frame building should be elastic, even if non linear;
- Small residual drifts are expected.

As a result, this connection is described as “self-righting” or “rocking” system.

Limited dissipation capabilities should be expected by this technology, with equivalent damping factor ξ usually comprised between 5 and 10%. Typical force vs. drift expected response is reported in Fig. 47

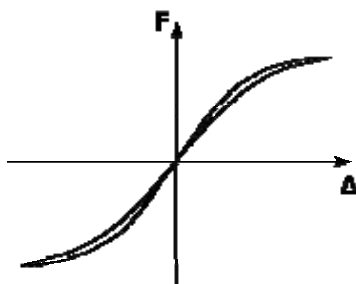


Fig. 47: Typical prestressed precast system force-drift response (Priestley, 1996)

Based on above reported experiences, University of Texas at Austin (Saqan, 1995) and University of Minnesota (Palmieri, 1996; Palmieri et al., 1996) proposed different prestressed (NLE) precast system layouts. The first frame uses multi-bay beams and single-story columns (Fig. 48 and Fig. 50). The second multi-story columns and single-bay beams. Post-tensioning cables are located in lateral dogbone to simplify reinforcement arrangement (Fig. 49 and Fig. 50). Both prototype follow similar provisions and adopt partially unbonded post-tensioning cables in central position. Also the experimental evidence is similar for storey drift level lower than 2%. Self-centering capabilities are revisable in both specimens.

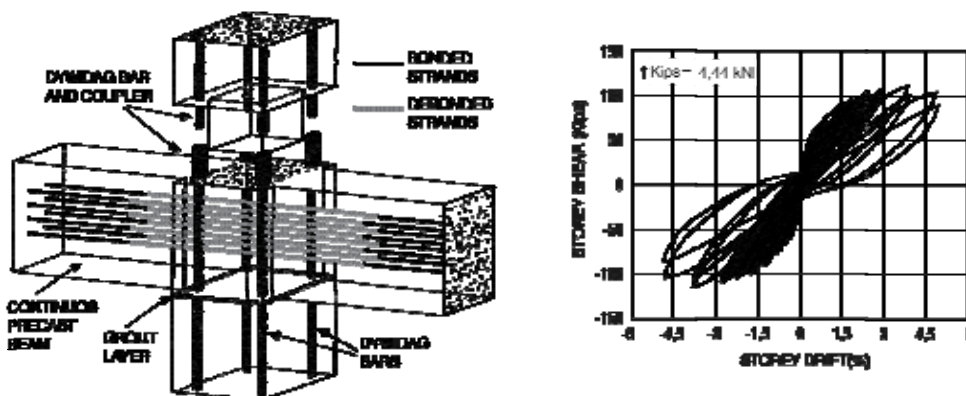


Fig. 48: Pretensioned system; University of Texas at Austin (Saqan, 1995)

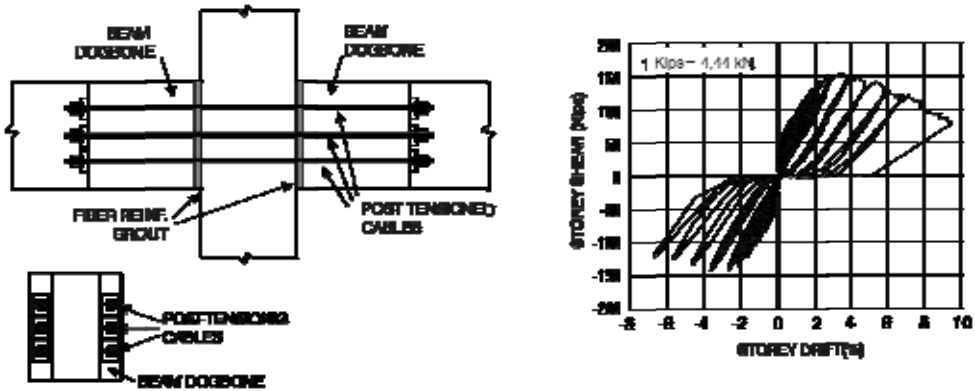


Fig. 49: Pretensioned system; University of Minnesota (Palmieri et al., 1996)

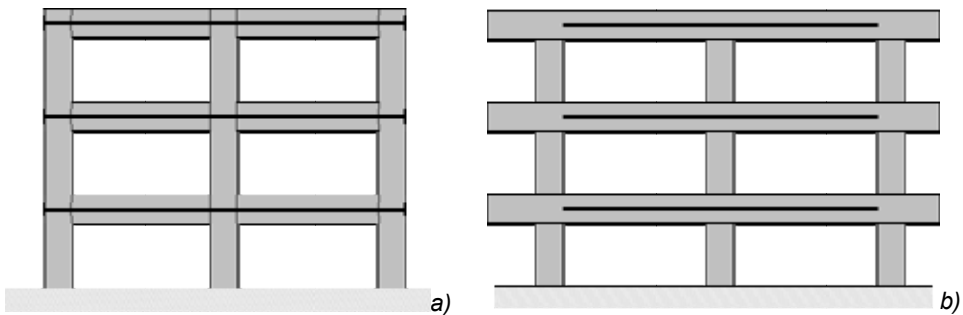


Fig. 50: Possible arrangement of pretensioned connection in frame buildings; a) beam between columns; b) beam through columns

1.5.3. Tension-compression yielding systems

In this kind of precast joint connection, energy is dissipated through yielding of the connecting elements. These are allowed to yield in both tension and compression, hence the name tension/compression yielding.

The basic idea is that of simulating the non-linear behavior of monolithic connection (i.e. high energy dissipation capabilities, $\xi=25-35\%$), concentrating contemporary damage effect in the joint section, without spread it along the beam (avoiding then beam plastic hinging).

Major efforts in the development of this kind of connection were done during initial phases of PRESSS program. Solutions proposed by Texas University at Austin (Sagan, 1995) and Minnesota University (Palmieri et al., 1996) are reported in Fig. 51 and Fig. 52.

The first one adopt vertical dogbone and mechanical coupler to guarantee longitudinal continuity of rebars. Ducts that contained the high-strength threadbars

were grouted after threadbars were snug tightened . Even if connection behaviour was reasonably acceptable until 1% storey drift, some local concrete crushing around connection system caused an anticipated failure of specimen.

The prototype proposed by Palmieri et al., 1996 appears simpler than the previous, even if is revisable a considerable use of cast-in place concrete to fill block-out regions were rebar are located. The specimen performed very good with high energy dissipation capability during the whole test and for drift level bigger than 4% (usually lower than 2% in the design practice).

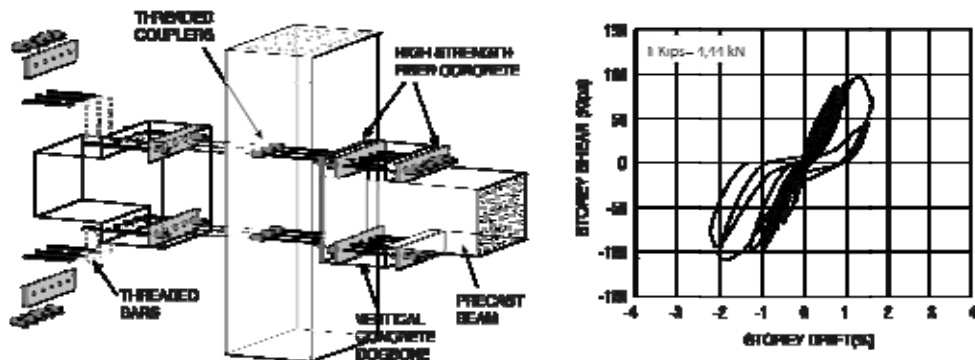


Fig. 51: TCY system with vertical “dogbones”; University of Texas at Austin (Saqa, 1995)

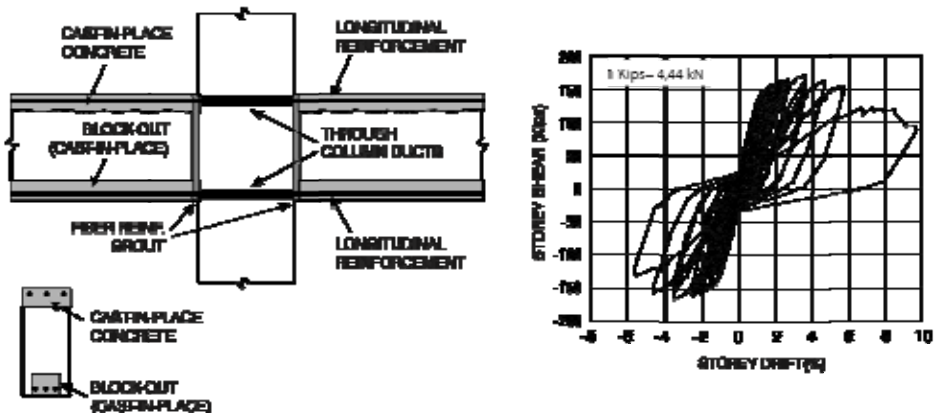


Fig. 52: TCY system; University of Minnesota (Palmieri et al., 1996)

The TCY concept has been furtherly improved by PRESSS research program (Fig. 53). The solution appears similar to the one proposed by Palmieri et al., 1996, even if the adoption of corrugated steel duct instead of block-out to locate mild steel rebars reduce drastically cast-in-place operations. Furthermore to avoid inelastic strain concentration, rebars are wrapped for a limited length near the column interface.

Details about the test arrangement and results are reported in par. 0.

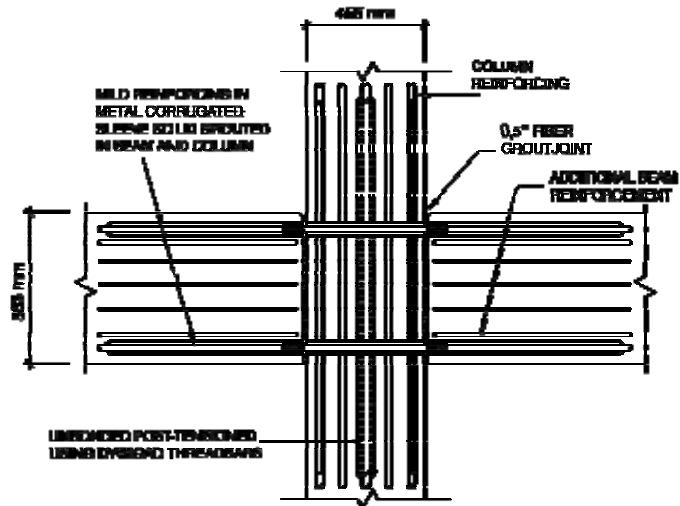


Fig. 53: Layout for TCY joint tested at PRESS (Sritharan et al., 2000)

A further evolution of TCY system found an interesting application during construction of Paramount tower (Fig. 65) as connection system in a limited number of single bay beams. Normally in plastic hinges the high concrete strains imposed on the unconfined cover of the beam are exacerbated by the tendency of the once overstrained reinforcing bars to buckle outward when subjected to compression loads.

The adopted solution in DDR system is to move the yielding element out of the frame beam and into the column where high confinement is possible. This relocation is made possible through the development of a forged ductile rod which could be placed in the precast column. A high strength bar would then be screwed into the end of the ductile rod (Fig. 54). A preliminary version of this technology was proposed to connect single span beams in the Paramount Tower (Englekirk, 1995; Englekirk, 2002). Particular attention has been devoted to dimension shear resistance mechanism and assure adequate confining (Fig. 55). Inside the joint specific strut-and-tie model has been identified for this purpose (Fig. 56). Shear transfer between beam and joint is assured by bolt pretensioning and associated friction mechanisms. Differently from other regulations, ACI 318-08 allows to consider friction as resisting mechanism for shear transfer. Recently the solution has been updated and specific formulations for design have been provided (Englekirk & Wang, 2008). Experimental tests performed by Chang et al., 2008 confirmed high seismic performance from this technology with equivalent damping ratio between 16% and 22% and maximum storey drift between 5,47% and 7,07% depending on reinforcement arrangement.

Despite encouraging structural performances, some important limiting factors could be recognised: the high rebars congestion in the core-joint zone and the high precision required for assembling process between beam and columns.

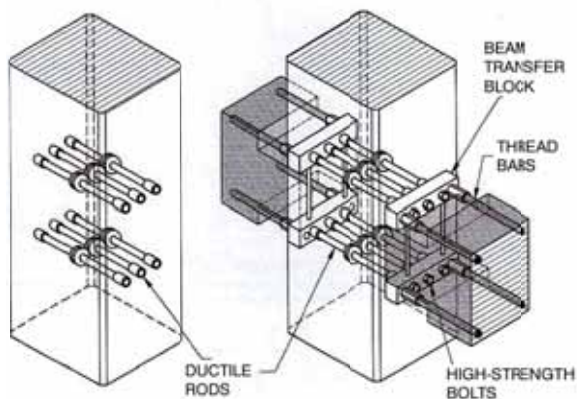


Fig. 54: DDB precast system

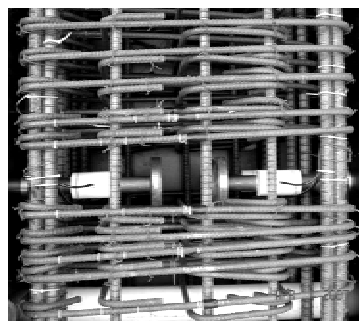


Fig. 55: DDB joint details

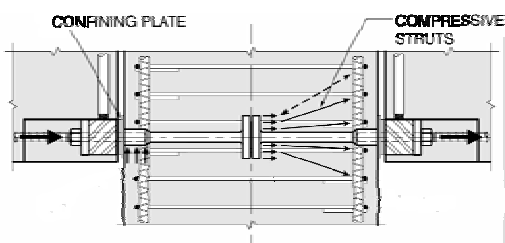


Fig. 56: DDB strut-and-tie model; top view

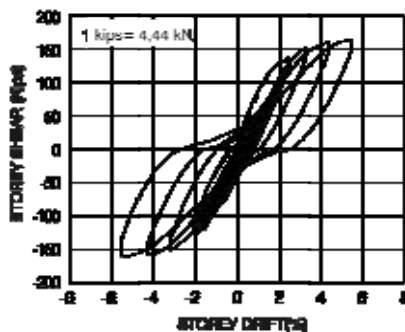


Fig. 57: Load-deflection relationship

Metelli & Riva, 2008 have recently proposed a dry joint prototype based on TCY system. Main characteristic of the connection is a Z-shaped plates interface that should increase shear resistance of connection (Fig. 58). The joint assembly should results easy and damage should concentrate at interface without spreads inside precast elements. Specific high-strength ($\phi 24$) rebars should yield at beam-column interface, both in tension and compression. Specific embedded connection inside column should guarantee force transfer from beam. The idea is that of transfer tensile force through steel studs embedded inside concrete as originally proposed by Roeder & Hawkins, 1981 and recently investigated by Zanchettin et al., 2011

The experimental results on a full-scale specimen show a good performance of the joint, in term of moment versus curvature response, characterized by a stable behaviour up to 2.0% drift. Concerning higher drift values, the joint has shown a

limited dissipative capacity because of the early collapsed, reached during the cycle at 2.5% drift, due to the brittle failure of the connection on the column side with the pull-out of a conical fracture surface radiating from the anchored end.

Further development of the joint detail on the column side is required in order to obtain an effective bar anchorage system allowing the bar yield which should provide the ductility and dissipative capacity of the joint, even in case of a high earthquake intensity

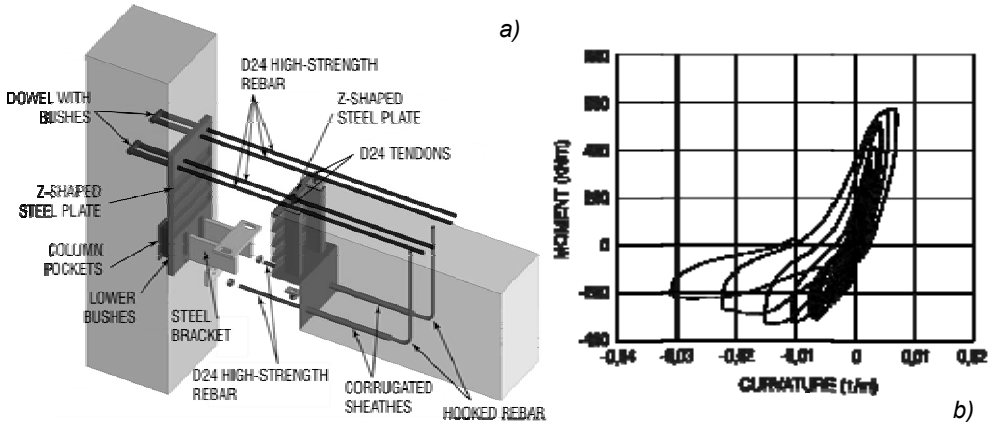


Fig. 58: Dry joint developed at University of Brescia: a) joint layout; b) Experimental cyclic behaviour

1.5.4. Energy dissipating systems

In this connection type, energy is dissipated through friction when slip occurs between connecting elements. Special material can be used to enhance the slip behavior. The advantage of this connection type is that reinforcing steel does not yield, resulting in cracking in the precast members that is relatively small even at large displacement levels. The same concept can be used as in the tension/compression connections where slip occurs on one side of the beam while the other side permits only rotation. Then a gap must be provided to allow the slip to occur in both directions (Fig. 59). Very high energy dissipation is evidenced by experimental tests ($\xi > 35\%$)

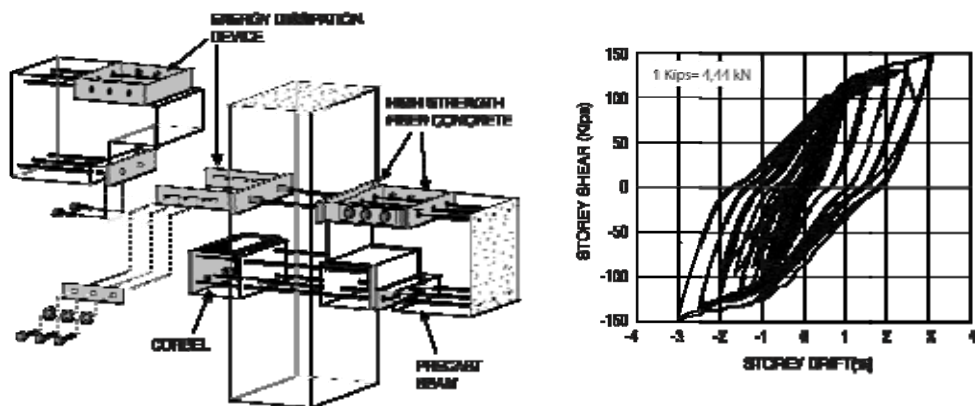


Fig. 59: Friction connection; University of Texas at Austin (Sagan, 1995)

A similar energy dissipation concept though friction can be implemented in shear connection at beam mid-span. A main advantage of this system above the others is that connection can be easily repaired or substituted after earthquake event. Disadvantages of energy dissipation systems are related to limited self recentering capability. This is probably the reason why this kind of connections based on friction and energy dissipation have been limited considered in PRESSS program.

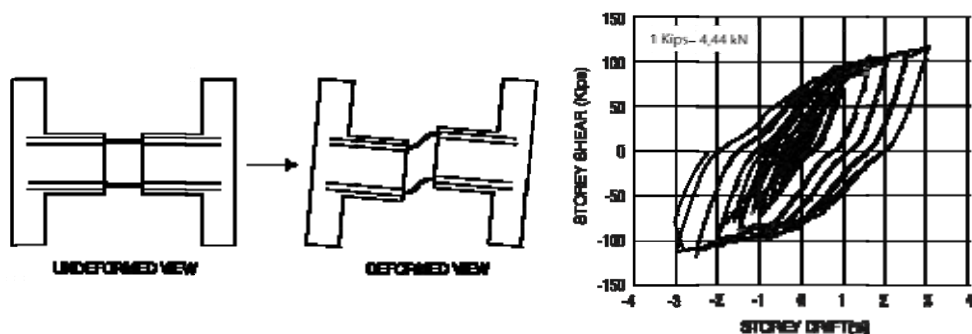


Fig. 60: Friction connection, University of Texas at Austin; Sagan, 1995

Recently an energy dissipation system has been developed by Marinini et al., 2011 to improve seismic performance of a typology of skeleton precast structures, usually one to three storey height, widely adopted in Italy mainly for industrial and commercial building. The energy dissipation devices consist in a friction mechanism used to connect the beam to the column elements. Through the relative sliding between these two monolithic element during seismic event a certain amount of input energy get dissipated, thus reducing frame's total drift and solicitations on columns' base.

1.5.5. Hybrid frame system

The basic idea in this system is to combine two different technology: NLE system that can provide self-centering capabilities and TCY system, that can provide energy dissipation capability.

The hybrid joint technology was mainly developed during the last phase of NIST program between 1992 and 1994 (Stanton et al., 1997).

In developed specimens energy dissipation capability was slightly lower than equivalent monolithic specimen and failure was achieved with bar fracture (at drift level bigger than 2%). However limited damage in concrete and self recentering capability were demonstrated. Similar results were also obtained by Priestley & MacRae, 1996.

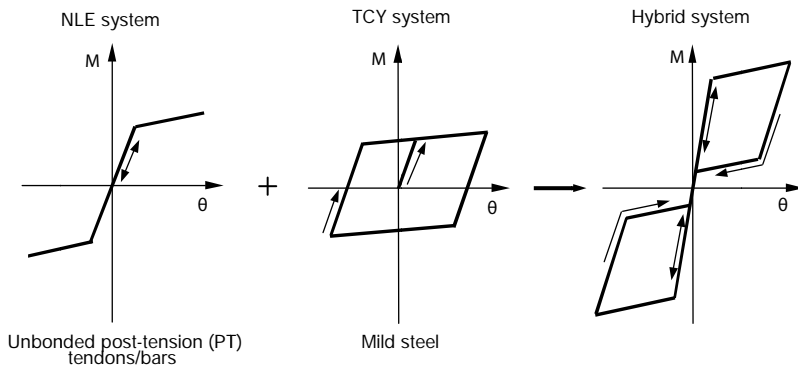


Fig. 61: Typical NLE system force-drift response

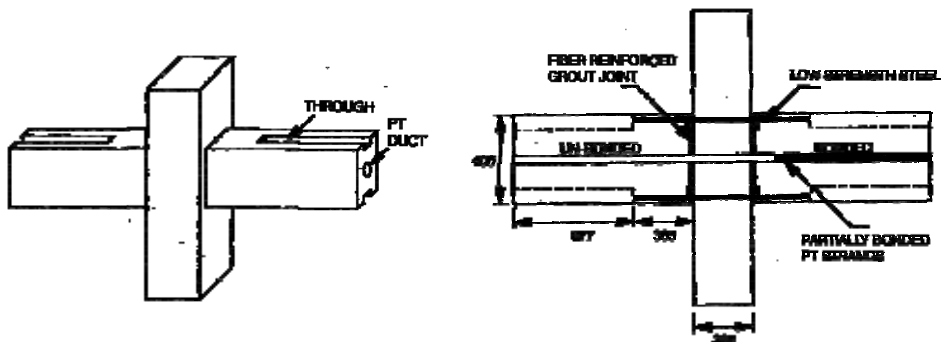


Fig. 62: Hybrid connection developed at NIST; Stone et al., 1995

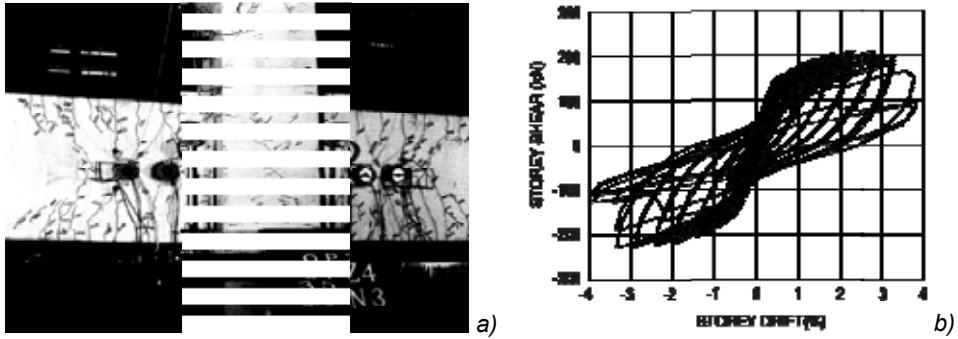


Fig. 63: Experimental performance of hybrid specimen OPZ4; a) crack pattern at the end of cyclic load test; b) hysteresis curve; Stone et al., 1995

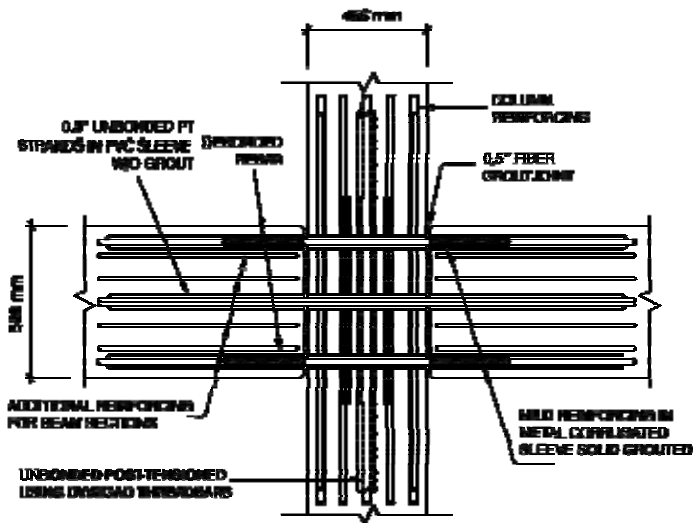


Fig. 64: Layout for hybrid joint tested during PRESS program; Sritharan et al., 2000

A slightly modified version of the NIST hybrid system, was further developed in the PRESS program (Fig. 64), improving self recentering capabilities. A similar joint layout was adopted for the 39 storey Paramount tower (Englekirk, 2002). Additional testing was required to develop a performance based design criterion for the Hybrid System (Fig. 66), and this effort was undertaken at the University of Washington (Day, 1999; Kim, 2000).

Paramount tower superstructure build-up started on March 2001 and was completed in 16 month. Actually it represents the highest precast building in high seismicity area.



Fig. 65: Paramount tower in San Francisco CA (Englekirk, 2002)

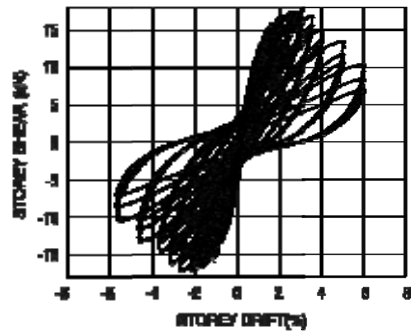


Fig. 66: Hysteretic behaviour of hybrid precast system (Day, 1999)

Together with experimental and in site validation of hybrid precast technology, also specific code regulation were approved in the ACI T1.2-03 (ACI Committee 318, 2008). With this publication, the technology transfer process for hybrid connections, of the type developed by NIST and Pankow, was complete. Actually this solution is widely used in the US region, in particular for high-storey building for commercial or social use. The Park Plaza in Daly City (California) is a example of this trend.

Beside the original hybrid frame layout constituted by mild-steel rebars and post-tensioned cables, new solutions have been recently proposed to further improve performances.

Morgen & Kurama, 2004 developed a typology of hybrid connection (Fig. 67), where mild steel reinforcement is replaced by external friction damper devices. Displacements at the beam-to-column interface result in slip displacements at the friction surfaces between the beam and column damper components, thus dissipating energy. The proposed damper system utilizes relatively simple connections to the beam and column members. In addition to the simpler installation, the use of the proposed dampers may offer other benefits, such as:

- close-to-rectangular force-displacement response with large energy dissipation per cycle;
- post-earthquake inspections and repairing (if needed) of the beam-to-column joints can be easily completed since the dampers are placed external to the joint;
- the dampers can act as corbels to support the beams during construction, until the post-tensioning force is applied;
- dampers contribute to the transfer of shear forces at the beam-to-column interfaces.

Specimens performed well during experimental tests (Fig. 68), evidencing both self recentering capability and dissipation capabilities ($\xi=15-25\%$).

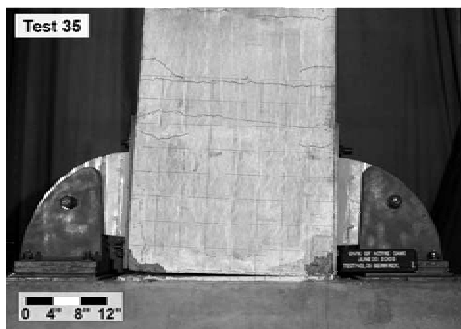


Fig. 67: Experimental sample tested by Morgen & Kurama, 2004

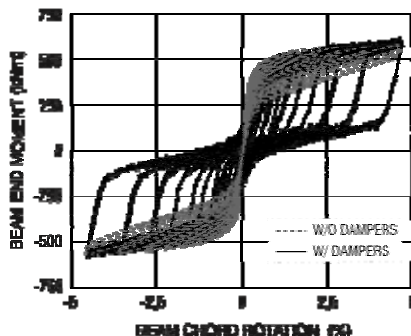


Fig. 68: Experimental hysteretic behaviour, Morgen & Kurama, 2004

A further layout for hybrid frames was proposed by Pampanin, 2005. In this precast system continuous post-tensioned tendons, anchored at the exterior columns of the frame, supply, through an appropriate parabolic longitudinal profile, the desired moment resistance. Furthermore inclined cables are effective in transferring shear load to the adjoining columns. Longitudinal beam are then suspended by the cable and this recall the suspended bridge category (Brookling Bridge). Hence the name of the patent, Brookling Systems. This solution, initially developed for static loading, was improved to sustain also lateral seismic forces. The joint was developed as hybrid solution, with external devices used to dissipate energy. To solve the problem of shear transfer in the temporary phase a specific bracket was designed. This system is actually adopted in low storey buildings, being maximum number of storeys limited by to the maximum dimension of precast columns (2 to 3 storeys).

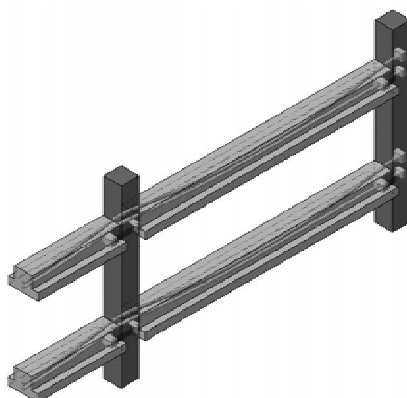


Fig. 69: Brookling system (Pampanin, 2005)

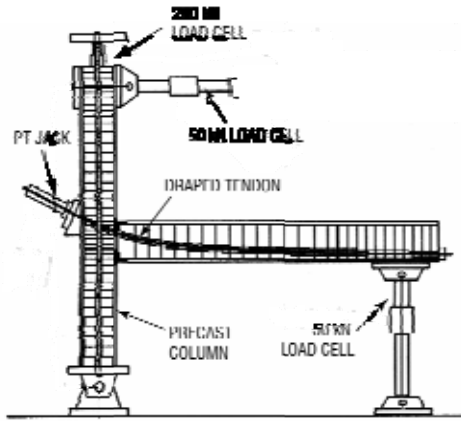


Fig. 70: Experimental tests set-up of Brookling system (Pampanin, 2005)

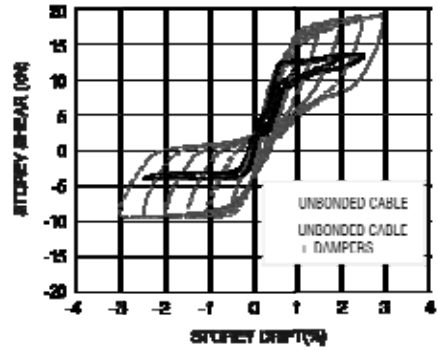


Fig. 71: Experimental hysteresis loops of Brookling system joint



Fig. 72: Hidden steel bracket



Fig. 73: Application of Brookling system with external dampers



Fig. 74: Brookling system application for low storey building

1.5.6. Benefits and drawbacks of dry-connection approach

Dry connection between members, unpropped erection and favorable scheduling of frame mounting process, are the main benefits provided by jointed systems.

This solution is particularly favourable when a limited storey number is considered. Increasing the number of storey would require the introduction of strong connection between columns borrowed from emulative approach, thus reducing partially the benefits of the “jointed” approach.

Further positive aspect is the possibility to control the damaged level on the structure during seismic action, much more than in emulative solutions.

Jointed systems like TCY ones, localize damage at beam-to-column interface, while residual deformations are expected to be analogous to cast-in-place jointed solutions. Pre-tensioned or post-tensioned systems have demonstrated to reduce drastically residual deformations, even if energy dissipation is limited. Finally, hybrid jointed systems are a sort of compromise between previous solutions, that allow to control both residual deformations and damage level, through an accurate design of mild and post-tensioning steel inside joint.

Accounting for these parameters allows a building not only to sustain seismic action, but also to be immediately operative after seismic event (Pampanin, 2005). The benefits provided by this opportunity appear evident especially in case of strategical buildings (i.e. hospitals, fire departments...), even if post-earthquake inspection and repairing appear not trivial operations and thus they are still open issues. A compromise could be the adoption of external damping devices replacing mild steel rebars (Fig. 73). In this case maintenance costs should be considered.

Further aspect to account about jointed system are mounting tolerances, that are sensibly lower than those generally required for emulative precast solutions (Hawkins & Ghosh, 2004) (Fig. 54). Higher precision level might have a negative impact on precast manufacturing costs.

1.6. Italian approach to precast framing

1.6.1. The precast CSTC beam technology

Italy has a long tradition in the field of precast industry. Right from the start of its large employment, at the beginning of the 1950's, the great demand for reinforced

concrete precast structures was mainly targeted for industrial and commercial buildings. The typical precast skeleton structures was adopted, consisting in a one to two (seldom even three) storey gravity-resisting frames composed of monolithic columns fixed at the base and free at the top, with pinned beams on corbels, strengthened with shear panel (either precast or cast-in-place) to provide additional seismic resistance when necessary. This same solution is still widely adopted at present (Bellotti et al., 2008). A considerable research effort has been devoted recently in Europe on investigation of seismic performance of those kind of industrial buildings as testified by the project PRECAST STRUCTURES EC8, concluded in early 2007 after 4 years of activity, and the project SAFECAST (<http://www.safecastproject.eu/>) aiming to the design of dry connections between members and to study their contribution to the structure's global behaviour (Colombo et al., 2008; Kramar et al., 2008). To the same branch of research belong recent applications consisting in beam-to-column connection through energy dissipation devices (Metelli & Riva, 2008, cf. ch.1.5.3 and Marinini et al., 2011, cf. ch.1.5.4).

Besides classical precast technology based on RC monolithic elements dry coupled together for low rise industrial/commercial buildings, an alternative solution was developed in Italy during the '60, from an idea of Eng. Salvatore Leone. At that period he was dealing with a yard in Pescara where classical steel-concrete composite beams were required. Given delivery times of approximately 6 months for such beams, he faced the problem of how to implement them in the workshop in the most simple way. He verified that the web and top flanges of the steel beam were unnecessary. So he replaced them with a truss girder and a longitudinal top rebar respectively, welding them together and to the bottom steel flange. With this shape the steel beam was strength enough to bear concrete floor slab without temporary scaffolding. Furthermore bottom steel plate could be used to house directly floor slab, before cast-in-place concrete grout. This solution was patented in 1967 and production rules and assessment methods were deposited to the Italian Superior Council of Public Works. The concrete doesn't had any other longitudinal or web transverse reinforcement. The hybrid truss beam, also called Composite Steel Truss Concrete Beam (CSTCB) was born. The original brand name that is an acronym standing for Rapidity, Efficiency, Practicalness (REP beams) resumes the main advantages of proposed technology.

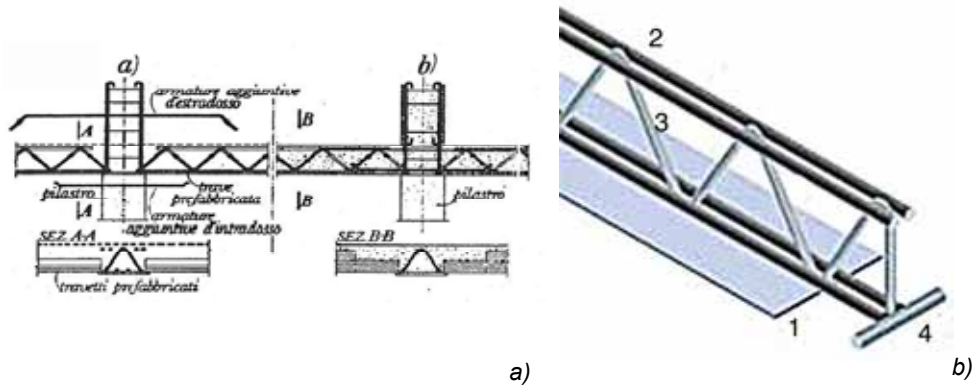


Fig. 75: a) Original drawing from of Hybrid beam patent; b) Original layout of hybrid beam

Rapidly the layout of this beam changed, with the addition of more vertical steel truss layers and upper longitudinal rebars, to increase bearing capacity, especially during the temporary phase.

The typical assembly layout evolved then in a steel plate as bottom chord, two or more straight bars as top chord and one or more sequences of curved bars to form the diagonal truss members. These last diagonal bars are usually convergent in the top chord in such a way to give the truss a typical triangle section to provide it with stiffness against the torsion and the out-of-plane buckling. This solution found immediately a wide range of application, not only in industrial and commercial buildings but also office and social building like hospital and schools.

At the end of 70's, beside the bottom steel plate layout, the concrete base was introduced, with the advantage of increasing fire-resistance capacity. In this case the diagonal bars were welded to some lower straight bars embedded in a prefabricated reinforced concrete base, that could also be prestressed. Other solutions were provided with a lower clay tile that constituted the bottom finish of the beam or with larger concrete base, to form a slab, The firsts are particularly suited for residential applications, the latter are designed for bridge, car park and high bearing applications.

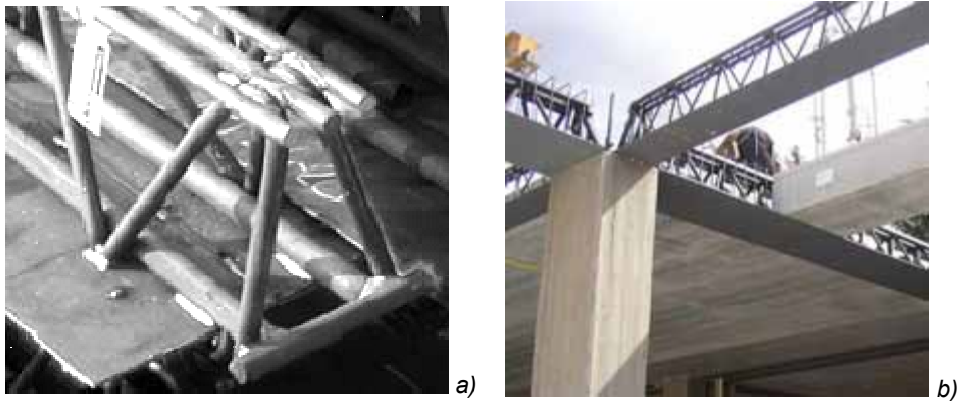


Fig. 76: Typical layout of CSTC beam with bottom steel plate

Since the global behaviour of these beam typology is similar, they should be comprised in the composite steel truss and concrete beam (CSTCB) category. The name can be justified seeing that the skeleton of the truss is made by steel in all the cases. Initial application of CSTC beam deal manly with simply supported static scheme and gravity load resisting frames, also several storey high, leaving to additional shear resistant walls the role to withstand seismic induced action. Nevertheless a notable improvement in the development of this technology for earthquake-resisting frame took place in the last decade. Further details are reported in chapter 1.6.5.

1.6.2. CSTC beam specifications

The main feature of CSTC beam is the capacity of prefabricated truss to bear its own weight, the slab and the concrete cast. Contemporarily beam's base can be used as formwork for the concrete cast. Any other provisional support is required necessary for the temporary phase. The most efficient application of the CSTC beams is in pair with prefabricated self bearing slabs.

Moreover all the delicate constructive processes, as the steel cut and welding, are finalized in prefabrication plants. Because of previous reasons, the need of manpower is considerably reduced and the construction speed can notably increase.

A composite steel truss and concrete element necessitates of an considerable welding amount. For this reason original trusses were made by structural steel (usually S355). The later apparition of weldable reinforcing steel even ribbed let the choice of the steel material.

The benefit of having ribbed bars is the better bond between the steel bar and the concrete, even if some considerations are necessary. The fabrication of the truss needs to bend the diagonal members and their integrity should be verified through a restriction for the minimum bending diameter depending on the bar diameter. The production rules for CSTC beams deposited at the Italian Superior Council of Public Works, prescribes the adoption of structural steel (S355) and a minimum bending diameters equal of four times the bar diameter. On the contrary Code Provision in Italy and Europe for reinforcing steel (grade B450A/C) requires minimum bending diameters to be limited as follows:

bar diameter	Italian Code	Eurocode 2
$\phi < 12 \text{ mm}$	4 ϕ	4 ϕ
$12 \leq \phi \leq 16 \text{ mm}$	5 ϕ	4 ϕ
$16 < \phi \leq 25 \text{ mm}$	8 ϕ	7 ϕ
$25 < \phi \leq 40 \text{ mm}$	10 ϕ	7 ϕ

Table 1: Minimum rebar bent diameter

If a medium size rebar should respect such limitations, the subsequent eccentricities of the resulting joints in the truss girder could become very disadvantageous for the design of such components.

Another consideration is that layout of the inclined trusses make possible a deep interaction with the surrounding concrete. This fact reduces the importance of increasing the bond resistance adopting threaded rebars and justify the adoption of plain rebars for the CSTC beam typology. In general this dowel action of the steel truss beared against concrete, is able to guarantee full interaction only if the steel truss is stiff enough. Several experimental tests have been performed to capture and highlight this effect. A numerical implementation by Sassone & Bigaran, 2007 using 1-D elements evidence how bending resistance of CSCT beam could be compromised if not enough stiffness of web truss is assured.

1.6.3. Experimental testing on CSTC beam

Over the years, numerous investigations have been carried out both experimental and analytical, for the evaluation of behavior, global or local, of CSTC beams. Several publications, mainly at national level, dealt with different topics, primarily

related to technological issues and possible improvement of the original proposed solution.

From the experimental research point of view, available data is however still limited, as limited and not easy to find are the publications of experimental results on the subject. This comes both from the tendency of most manufacturers not to provide results to the scientific community, and from lack of a coordinated, continuous and comprehensive scientific research plan (Sorgon, 2009). Therefore the state-of-the-art on the subject is given by a sparse set of experimental and analytical results, respectable, but not always incorporated into a comprehensive and homogeneous framework.

Schematically three main research topics can be identified:

- Evaluation of bending strength
- Evaluation of shear strength
- Evaluation of stress transfer (bond) and interaction given by embedded steel truss

The first topic, studied mainly during the 80's and the 90's is related to the issue of evaluation of ductile capability of the beam, both in temporary and final phase.

In earlier experimental studies (Giordano & Spadea, 1983; Giordano et al., 1987; Giordano et al., 1988), authors observed that beam ductility increase as the area of compressed reinforcement steel increase, as long as adequate connection is provided by inclined truss girder. It was evidenced then as still low ductility level, compressed reinforcement could undergo buckling phenomena is not enough restraining was provided by inclined truss (i.e. truss is not enough stiff).

Recently other author have gone deeper into these issues, in particular to assess the ductile performance of CSTC beam with reference to seismic design.

A wide experimental campaign has been performed by University of Padova on different typology on simple supported beam, tested both in temporary and final phase (Tesser & Scotta, 2008; Tesser, 2009).

In the first case, in beams with steel plate base, failure is attained at buckling of compressed reinforcement (Fig. 77a). This failure mechanism is unrelated to the scheme of a perfect truss and the cause is the eccentricity at the nodes created by the bent bars. In fact, at the beginning of the loading process, the truss bars are subjected not only to axial force but also to bending moment. In particular the eccentricity between the two tensile-compressive diagonal bars creates the bending of the top chord. When the top chord yields, the rotational stiffness of the node decays and the critical length of the converging compressed bars increases leading to the bars buckling.

In beam with prestressed concrete base, tested in temporary phase a similar behaviour is recognized, but in this case the bending diameter of inclined truss was so small (one diameter), that top chord was subject to a brittle failure (Fig. 77b).

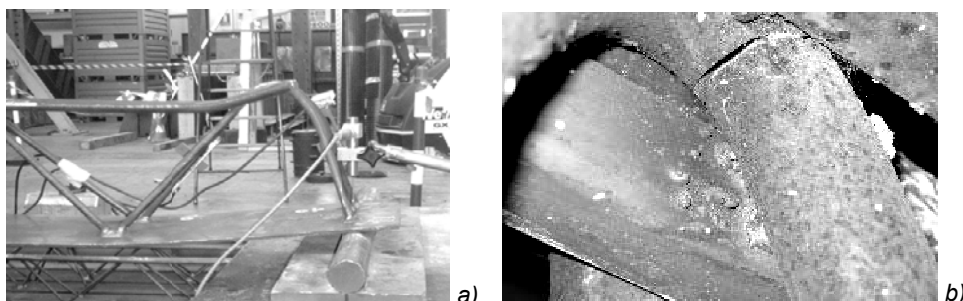


Fig. 77: Failure mode of CSTC beam in temporary phase (Tesser, 2009)

When the bending test is performed on the beam with concrete grout (final layout), the failure mechanism is the compressed concrete crushing at midspan, due to the absence of confining stirrups, even if a global ductile behaviour was observed.

The same behaviour is observed in four-point bending test on simply supported beam performed by Borri & Grazini, 2007 on CSTC beams with steel plate base completed with concrete grout. Two category of steel were tested, structural (S355) and reinforcing (B450). In both cases failure was achieved at crushing of concrete after satisfactory global ductile behaviour.

After these tests some general considerations on the global behaviour of the CSTC beams are possible. The resistance of the nude truss is demonstrated to be conditioned by local failure like buckling and bar fracture. Particular attention should be paid to the assembly of the steel truss by limiting the eccentricities as much as possible. These must be considered explicitly in design of the temporary phase.

For what concerns the composite behaviour, a good ductile behaviour can be obtained by an adequate design of the steel truss: when it is sufficiently stiff and adequate interaction with the surrounding concrete is provided, expected strength is analogous to the one of an equivalent RC section. Higher ductile performance could be achieved by considering higher amount of compressed longitudinal steel or by inserting confining stirrups in critical regions.

Concerning shear strength investigation, a limited number of experimental tests were performed in the past. For example between 1987 and 1990 a precasters' association investigated this aspect. Analysis coming from that data evidenced higher shear resistance than expected from classical r.c. theory (Sorgon, 2009).

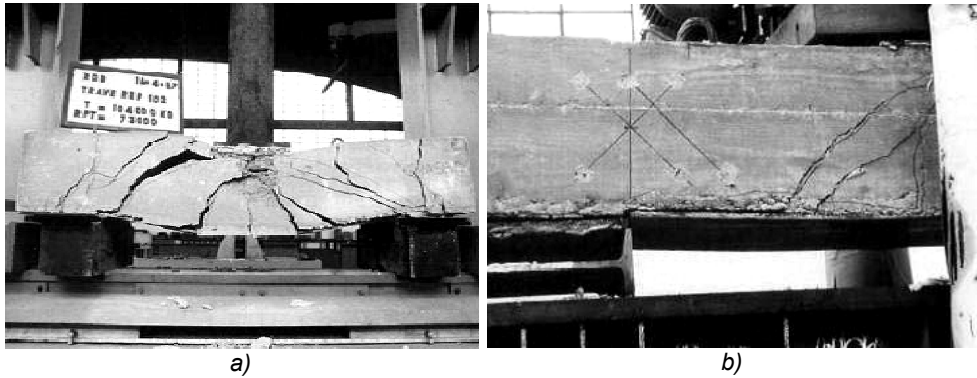


Fig. 78: Shear tests on CSCT beam in late '90s (Sorgon, 2009)

Recently shear test have been performed by Tesser, 2009. Also in this case experimental shear strength appeared just slightly bigger than theoretical one (7 to 14%) and however comparable to scatter of material strengths.

The fact that the truss diagonal bars are not homogeneously distributed, but rather disposed with a certain step, suggests that a Ritter-Mörsch shear mechanism could be established after primary concrete cracking (Fig. 79). Referring to this static scheme a new composite truss can be considered in which: the truss bottom chord is in tension, the top chord is composed by the compressed concrete section and steel top bars, the diagonal members are alternated in tension and in compression and are respectively constituted by only steel bars or by composite steel bars and concrete. The adequacy of this resistance mechanism is conformed by the crack pattern at failure that evidence the compressed concrete strut starting in correspondence to the lower truss node that offers preferential support. Similar crack pattern is also reported by Borri & Grazini, 2007. The separation of the inferior plate from the concrete section revisable in Fig. 78b and Fig. 80a corroborates the absence of dowel action coming from the steel plate base.

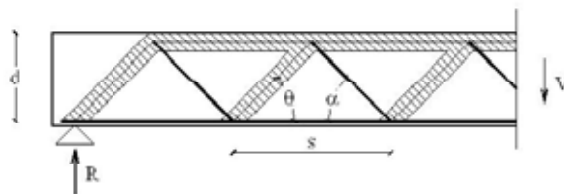


Fig. 79: Ritter-Mörsch shear mechanism shear mechanism on CSCT beam

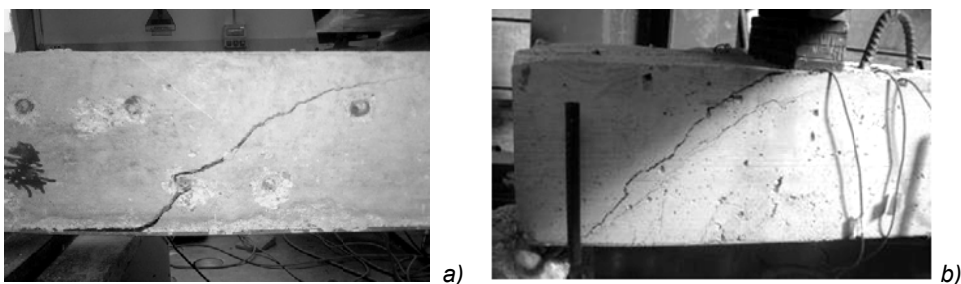


Fig. 80: Shear tests on CSTC beam after failure; a) Tesser & Scotta, 2008; b) Borri & Grazini, 2007

The third topic revisable in current state of art with reference to CSTC beam is the investigation of stress transfer mechanism between concrete and reinforcement or steel plate. In other word the dowel effect played by the inclined truss against concrete.

Preliminary experimental tests were performed by Puhali & Smotlack, 1980. Recently test have been performed by other authors, adopting a similar test set-up: Tullini et al., 2006; Badalamenti et al., 2008 (see Fig. 81); Aiello, 2008; Aiello et al., 2009.

These authors have identified three different failure mechanism:

- Failure of diagonal truss with ductile behaviour
- Concrete crushing or splitting
- Local failure of bottom steel plate, due to concentrate force transmitted by diagonal rebars

An analytical model to describe experimental evidences has been recently introduced by Colajanni et al., 2011 even if a considerable scatter of results is still revisable.

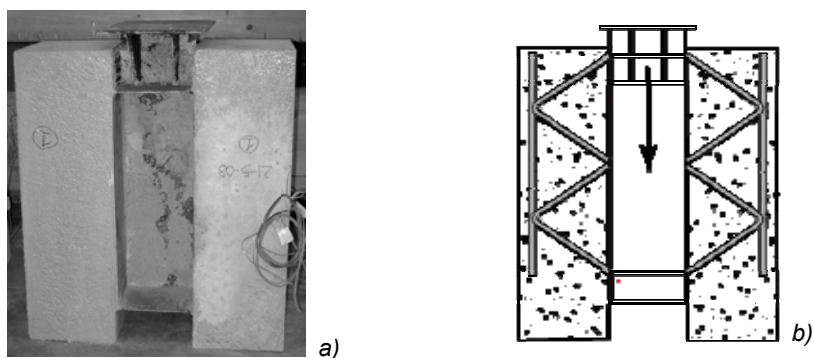


Fig. 81: pull-out test on CSTC beam; a) picture of specimen tested; b) schematic representation of the test (Badalamenti et al., 2008)

1.6.4. Code design provisions for CSTC beam

The recent Italian Code NTC 2008 (Ministero delle Infrastrutture, 2008) mentions the composite steel truss and concrete structures under “other material constructions”. It establishes that the use of this typology requires the authorization of the Italian Superior Council of Public Works and it doesn’t contain any other specification.

To withstand this issue, a National Committee with the task to deal with the CSTC beam was created by the Italian National Research Council. This committee led to the publication of “*Guidelines for the use of steel lattice girders embedded in concrete and procedures for the authorized use*” (Consiglio Superiore dei Lavori Pubblici, 2009). In this document three different classes are identified to comprehend CSTC beam, depending on the peculiarity of each producers’ structural typology:

- Steel-concrete composite structures
- RC or RC prestressed structures
- Other structures

With reference to the first category a definition is given at point 4.3 in NTC 2008: “*the composite structures are formed by structural steel parts and by reinforced concrete ones (ordinary or pre-stressed) made collaborating by means of a connection system accurately designed*”.

The design connection system is defined as “*the device suitable for the transmission of the tangential forces*”.

Similar concept can be found in UNI EN 1994-1:2005 (European Committee for Standardization, 2005c), where a composite structures is defined as: “*a structural member with components of concrete and of structural steel or cold-formed steel, interconnected by shear connection so as to limit the longitudinal slip between concrete and steel and the separation of one component from the other*”; and the shear connection as: “*an interconnection between the concrete and the steel components of a composite member that has sufficient strength and stiffness to enable the two components to be designed as parts of a single structural member*”.

Belonging to the second class requires instead that load bearing capacity in 2nd phase be guarantee by the only concrete and reinforcement or prestressed steel. In this case if structural steel is used to bear load during the first phase (temporary), it will be totally disregarded for second phase members’ design.

If neither of previous category is adequate to describe the considered structural typology (others structures), specific experimental tests must be performed to verify material property and member performance following prescriptions reported in EN

1990 Appendix D (“Design supported by experimental tests”). The member will be tested under different force combinations (for both serviceability and ultimate load conditions) and an adequate number of tests will be performed.

From the classification above reported it appear clear that CSCT beams have to make reference to composite beam design provisions. This has several consequences in particular with reference to shear design. The concrete effect have to be disregarded and the only steel lattice girder embedded into concrete have to withstand the entire shear force. This means that Morsch-Ritter mechanism should not be adopted to design CSTC beam.

Secondary the inclined truss girder is now considered as shear connection between longitudinal steel and concrete, similarly to steel studs in classical steel-concrete composite beams. This justify the experimental effort made to investigate this aspect and the trial to define some analytical model for design procedure (Colajanni et al., 2011). As stated above this aspect is still far to be fully comprehended and further research is still required on this aspect.

Finally, during the 1st phase the beam, if it is made only by steel, has to be considered as steel construction and can be designed according with the corresponding rules. If a concrete base is used, provision to avoid buckling of compressed trusses are still to be considered, adopting provisions for steel structures.

1.6.5. Beam-to-column joint testing

Original applications adopting CSTC beam technology, dealt mainly with gravity resisting framed structure. This is related to limited confidence generally shown by Italian designs with seismic performance of precast structures, in some measure justified by the lack of indications in the seismic Code, until the beginning of 2000 (Bellotti et al., 2008) On the other hand adoption of CSTC in continuous framed structures appears to be an effective tool to make a structure resistant against earthquake loading. This requires a detailed knowledge of the behaviour of beam edge zone and of beam-column joint both in the linear and nonlinear field (in particular under cyclic loading) While the knowledge of joint behaviour in reinforced concrete framed structures is consolidated, having been the object of many theoretical and experimental investigations to date, research on the behaviour of steel-concrete composite beam to RC column joint is more recent (Kuramoto & Nishiyama 2004) and just a few papers have looked at the behaviour of hybrid steel truss-RC beam joints (Sanpaolesi et al., 1988; Mele et al., 1993). In the last decade

there has been new interest in this field, related in particular to the increasing number of real case application of CSTC beam in seismic resistant frames, despite still limited experimental research on the topic (Fig. 95, Fig. 96). Different solutions have been proposed to overcome the issue.

A common approach is the introduction of pieces of reinforcing bars across the joints to restore the beam continuity within the joint region. The joint becomes kind of reinforced concrete structure while the beams remain kind of composite structure. This possibility is recognisable still in earlier drawing made by Eng. Salvatore Leone, even if he probably dealt more with the problem to achieve a beam continuity scheme for static loading, than achieve a monolithic beam-to-column joint to withstand seismic action. With this same purpose, some monotonic tests were even conducted by “Consorzio Produttori Travi REP” in the early ‘90s (Fig. 82). Failure was achieved by concrete crushing due to inadequate confinement in joint region.

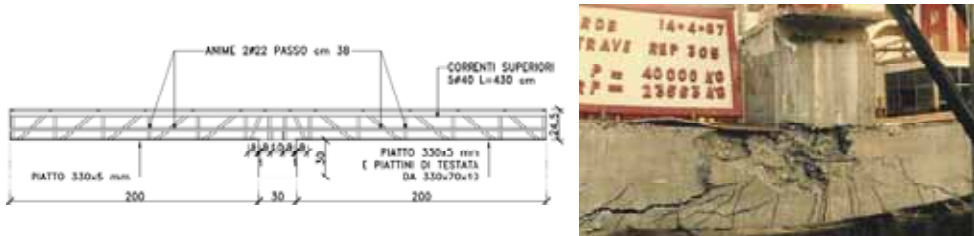


Fig. 82: Earlier experimental study on CSTC beam continuity (Sorgon, 2009)

Earlier studies conducted by Sanpaolesi et al., 1988, evidenced poor performance of such a joint typology under cyclic tests, with rapid degradation of stiffness and energy dissipation capabilities. Such performances were mainly due to absence of confinement stirrups inside joints and reinforcement to withstand shear forces. Progressive rapid degradation of bond between longitudinal rebar and concrete was also observed.

Mele et al., 1993 tested a joint characterized by a steel jacketed column and a truss bottom steel plate welded on it. Continuous rebars were placed on upper side on the beam to assure reinforcement continuity.

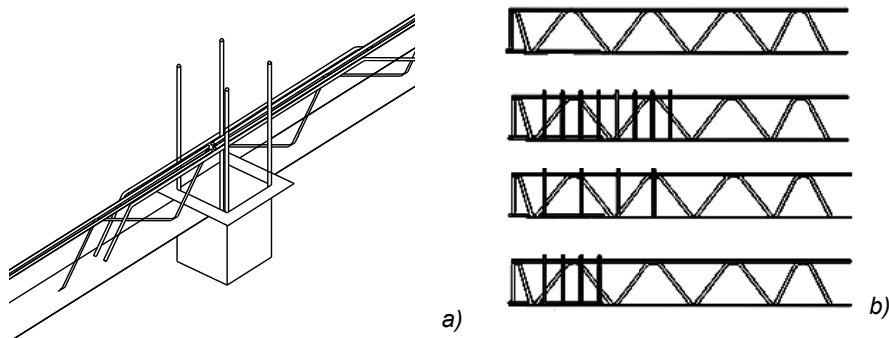


Fig. 83: a) Beam-to-column connection reported in Mele et al., 1993; b) Different typologies of precast truss beam investigated by Mele & Sassone, 2002

The tests showed several failure mechanisms occurring at the beam-column connection with the final formation of a hinge effect, as result of detachment of the bottom plate flange from the column and from the beam concrete core. These phenomena were attributed to the degradation of bond strength given by insufficient anchorage of the additional upper reinforcement, together with inadequate dowel action against concrete of inclined truss and insufficient shear strength of the lattice. In a subsequent research program performed by Mele & Sassone, 2002 analogous specimens were tested. Investigated aspects were the influence of geometry of the lattice and the role played by stirrups in the beam end. In addition a further connection system was added to each sample, consisting of studs welded to the bottom plate. These tests evidenced as connection deformability depends significantly on the amount of connectors used, resulting maximum for beams without connectors. In such condition stress transfer is guarantee mainly by mere truss web. However deformability of the connection seems to play more relevant effect on the stiffness of the system rather than on its resistance.

Recently full scale joint prototypes, constituted by two-span continuous beams and prestressed column stubs 20 centimetres long, were tested under monotonic (Badalamenti et al., 2008) and cyclic loading (Amato et al., 2010). Stirrups along column provide confinement inside the joint (Fig. 84). Both positive and negative monotonic bending tests suggested that if no specific anchorage devices is provided to lattice elements in tension, only additional reinforcement stubs contributes to develop section resistance at beam to column interface. On the country beam's lattice elements gave a certain contribute in transferring compression force, increasing global ductility capabilities. This is reasonably due to dowel action of inclined trusses and bearing of longitudinal steel plate and longitudinal rebars against concrete at joint interface. Such a contribute in compression, tend to decrease when cyclic tests are considered. In general then only additional longitudinal reinforcement should be fully considered as effective

both in positive and negative bending moment joint design. Bottom steel plate results effective in tension as much as distance from the joint increase, confirming the shear stress transfer among concrete and bottom plate due to inclined trusses. During cyclic tests nearly the same strength level was attained than provided by monotonic loading. Furthermore stable load cycle are revisable under positive bending, while pinching effect affects load-displacement curves under negative bending, probably due to progressive rebar debonding.

Even if final joint failure is attained by crushing of concrete at joint interface, both monotonic and cyclic testes demonstrated that an adequate amount of compressive reinforcement allows to attain good ductility performance.

Resuming eventually experimental evidences about the possibility to restore beam continuity across joint by adding longitudinal rebars, it is evidenced that despite strength and reasonably ductility, slippage of rebar inside a joint is still a limiting factor. It should be observed that a similar drawback was revised in beam to column joint prototype tested Park & Bull, 1986 consisting in threaded rebars settled inside U-shell beams. Similar layout was furtherly updated and tested by other authors (Lee et al., 2004; Park et al., 2008; Lignola et al., 2010). Despite limited differences, all tests showed good load-carrying capacity and deformation capacity, which were comparable to those of conventional monolithic r.c. joint. However, the energy dissipation capacity and stiffness of the specimens were significantly less than those of the cast-in-place specimen due to slippage of rebars occurred at the beam-column connection, as suggested by severely pinched hysteresis curves.

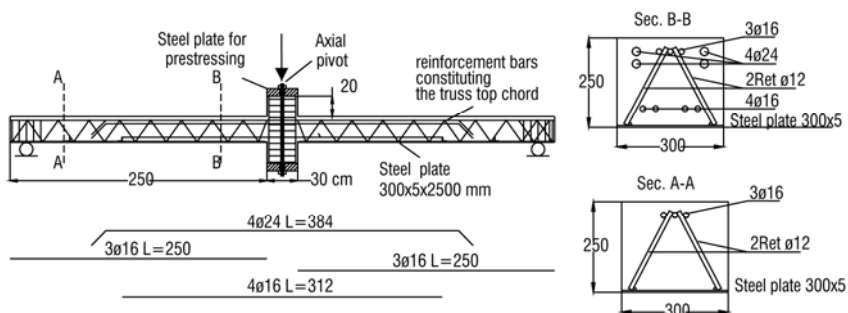


Fig. 84: Beam to column connection tested by Badalamenti et al., 2008

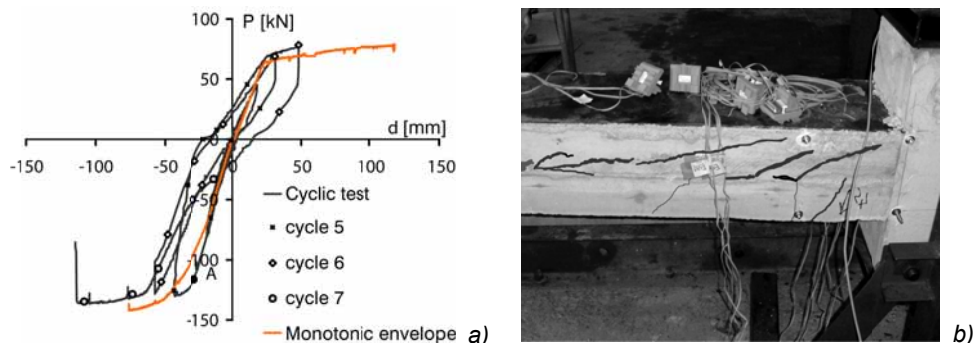


Fig. 85: a) Force vs. displacement comparison between static and dynamic tests (Amato et al., 2010); b) crack opening under negative bending

To resolve this issue Di Marco, 1995 proposed an alternative approach consisting in overlapping of beam lattice girder across the joint (Fig. 86). This solution requires a particular layout consisting in non symmetric lattice girder or adjacent lattice girder with shifted longitudinal axes. In this case the joint type is the same as the beam one and the continuation of the trusses within the joint increases both the bending moment and the shear strength. The problem of the confinement of the compressed concrete still arises. Moreover the transmission of the stresses between the extensions of the beam trusses can still be critical

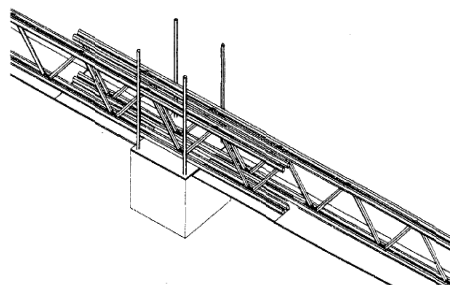


Fig. 86: Beam to column connection proposed by Di Marco, 1995

A further alternative solution is the overlapping of an additional truss across the joint. It consists in a new prefabricated steel truss that can be placed over the common beam trusses across the joint. Its shape must take into account the beam truss presence and the longitudinal column bar obstacle.

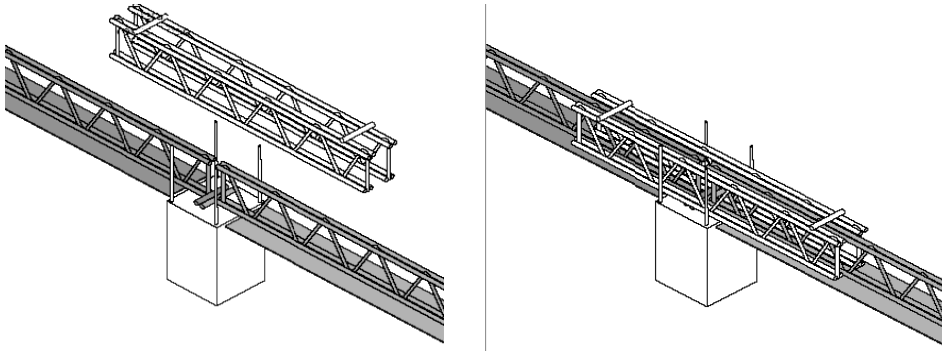


Fig. 87: Additional truss girder to provide beams' continuity across the joint (Tesser, 2009)

Early investigations on this kind of joint connection are reported by Borri & Grazini, 2007, where superior performance of lattice girder (test 4) over straight rebars (test 3) are evidenced. This solution was furtherly analytically investigated by Tesser, 2009, that considered CSTC beam with both steel plate and concrete base. He recognised that integrative truss, when properly designed, could improve core-joint confinement, and even provide adequate shear strength inside core-joint and at beam-to-core joint interface. Furthermore solution seem to be particularly suited for precast solutions, being in-situ positioning of additional reinforcement rapid and accurate.

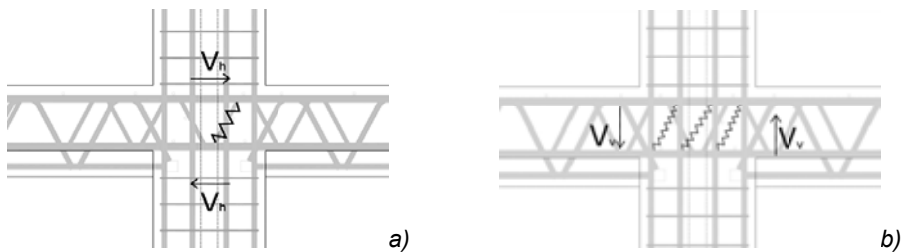


Fig. 88: Joint truss mechanism resisting the horizontal shear force (Tesser, 2009)

Even a prototype consisting in cruciform truss was developed and tested. It consists in a prefabricated trussed cross which penetrates into both the end of beams and columns. This joint typology has been tested by Scotta & Tesser, 2011 under cyclic loading and compared to equivalent monolithic joint, designed under design code prescription to withstand seismic action. Experimental tests suggests that both stiffness, strength and ductility of composite truss joint are analogous to the one of cast-in-place joint designed for high-ductility. Generally lateral girder solutions performed better than cross truss joints: in the latter plastic hinge was located inside the joint, causing a slight maximum drift reduction. Good confinement effect are actually provided by lateral trusses during the whole tests, even if in some cases a

local buckling failure with consequent concrete pull-out is observed. Such experimental evidences provide a sound-basis to justify the adoption of truss in place of mere longitudinal reinforcement to provide beam continuity across the joint.

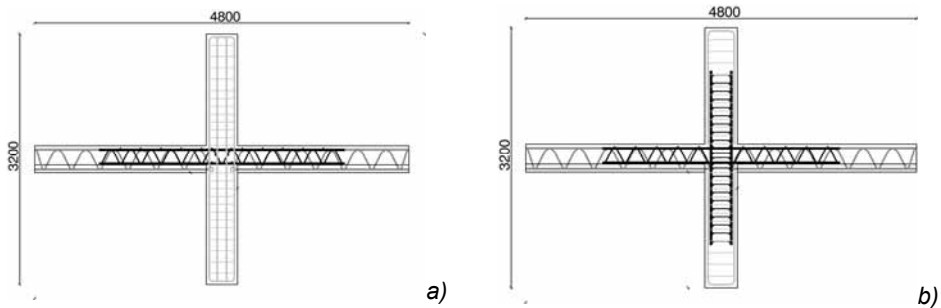


Fig. 89: Beam-to-column joint samples tested by Scotta & Tesser, 2011

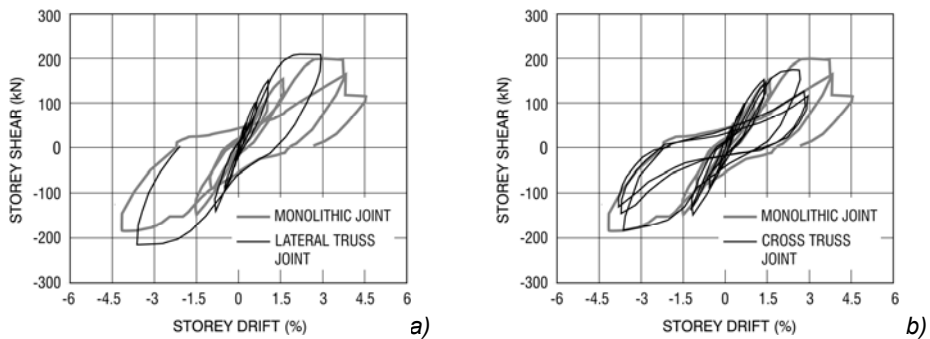


Fig. 90: Force vs. storey drift from different samples tested by Scotta & Tesser, 2011

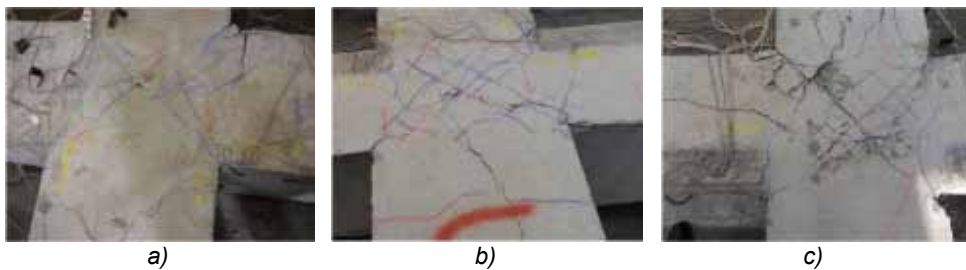


Fig. 91: Core joint cracking from different samples tested by Scotta & Tesser, 2011: a) monolithic joint; b) joint with single truss; c) joint with cross truss

With the aim to provide still more effective and advantageous way to restore beam-to-column joint monolithic behaviour, even further alternatives have been recently developed by Italian universities. At present, they are just prototypes, with no real-case applications, but confirms the liveliness of the investigated subject in the thesis.

Sorgon, 2009 and Petrovich, 2009 (University of Trieste) suggest to emulate a monolithic cast-in-place joint, through standardized components that can be used both for beams and columns.

A new typology of CSTC component is presented, characterized by angular steel profiles, connected by steel girder made up with truss. The beam is furnished with precast concrete base to guarantee self bearing capability in the temporary phase. For the column an analogous assembly is proposed.

Connection between the two elements is provided by an in-site welded steel plates. Even column to column connection is restored through welding.

Experimental tests evidences high dissipation capability of the proposed system with limited damage pattern. Failure was reached far from the node due to shear failure with buckling of lower angular steel profile.

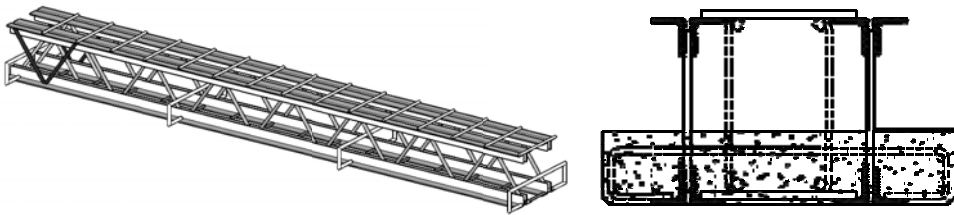


Fig. 92: Beam prototype developed at Trieste University (Sorgon, 2009)

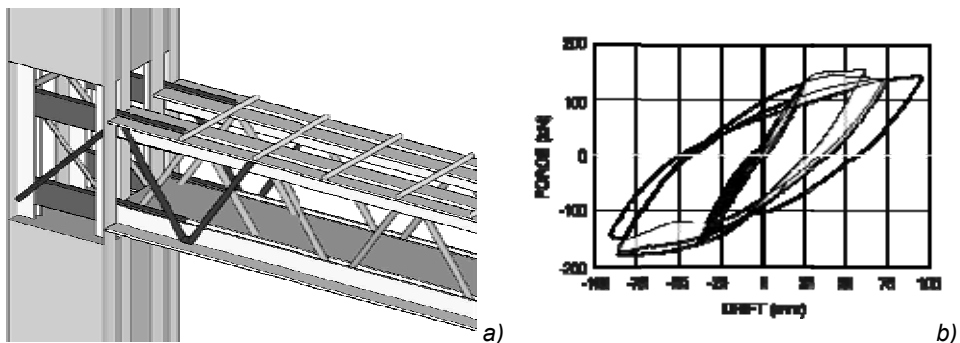


Fig. 93: a) Beam-to-column joint prototype developed at Trieste University; b) experimental hysteretic behaviour (Sorgon, 2009)

The proposal made by University of Padova adopts a CSFT column for bearing vertical load. In the past, connection of this column typology with steel beams required a considerable amount of in-site welding. At the same time the numerous failures of fully welded moment connections during the 1994 Northridge and 1995 Kobe earthquakes indicated that conventional fully welded moment connections had several inherent drawbacks, whereas bolted and riveted connections had performed well in past earthquakes.

For this reason in new developed connection system, welding has been limited as more as possible, and is-site welding has been completely eliminated.

To restore the continuity of the upper longitudinal beam bars a new element composed by four bars is inserted through the joint. Manpower operations needed in site are relatively limited and easy enough to ensure a good construction speed and accuracy.

Preliminary FE analysis indicated good capability of this kind of connection in term of strength and energy dissipation capabilities if compared to an equivalent monolithic cast-in-place joint.

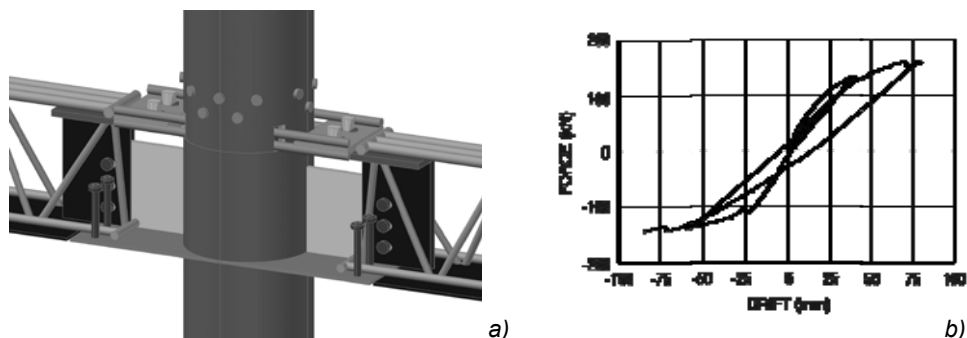


Fig. 94: a) beam-to-column joint prototype developed at Padova University; b) numerical hysteretic behaviour (Tesser, 2009)

1.6.6. Current CSTC beam application on framing system

Despite the experimental study phase on performances of beam-to-column joint adopting CSTC beam solution is still not concluded, real case applications are being adopted even more and more in Italy in the recent years, both in seismic and non-seismic regions. Two principal solutions are recognisable in the National panorama:

- Frames adopting precast concrete columns
- Frames adopting Concrete Filled Steel Tubes (CFST)

The first solution is borrowed from monolithic emulative precast technology and consists in a modified version of precast system n°4 (see par. 0), with precast beams substituted with CSCT ones. Multilevel precast RC columns presents voids at each floor level that are used to accommodate the longitudinal beam. Columns structural continuity is provided by rebars overlapping or by grouted steel sleeve

and ducts or mechanical couplers at mid-span or core-joint level (Fig. 18). Beam continuity is provided by lattice girders or additional longitudinal rebars.

This solution is suited for low cost frames with limited storey number. Column are normally provided in a 2 to 3 storey layout (Fig. 95a) to reduce transportation and managing issues.

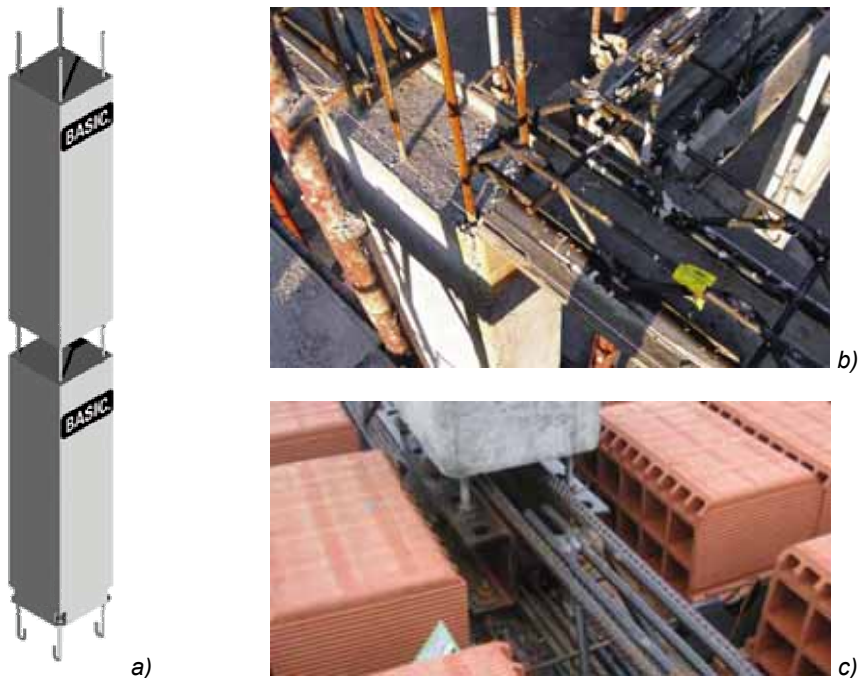


Fig. 95: Example of CSTC beam coupled with RC precast column

Alternative to this approach is the adoption of Concrete Filled Steel Tubes (CFST) technology combined with CSCT beams. Specific steel brackets need to be welded on tube outer face to provide temporary support for beams. Main benefits adopting this solution is related to high-axial load bearing capacity of the columns, with limited section dimension, thanks to the steel tube and to the confining action it provides on in-filled concrete. Higher structural performance compared to RC structures is counterbalance by higher cost of the structure, due to the large amount of required steel. Welding operations to provide columns structural continuity should be substituted by bolted connections to prevent further costs' growth. Even assembling process may result un-economic. Despite columns self-bearing capacity, maximum number of storeys risen-up at the same time is limited by buckling load of the steel tube section. Being required concrete cast to provide adequate column strength, construction phases need to be accurately scheduled, not to slow down excessively the mounting process.



Fig. 96: CSTC beams resting on steel corbel of CFST columns



Fig. 97: Example of CSTC beams coupled with CFST columns

2. PROPOSED PRECAST JOINT LAYOUT

As pointed out in the state of the art concerning the precast framing technologies, a wide number of solutions and prototypes have been developed at present, with the general goal to extend the typical benefits of prefabrication, from low rise industrial/commercial structures to seismic-resistant multi-storey frames suitable for social and residential use. Based on this topic, an innovative precast technology is presented in this thesis, capable of both high static and seismic performance, reduced construction time and production cost.

The horizontal structural element of the proposed joint is constituted by a Steel Truss Concrete (CSCT) beam with concrete base. Such a precast solution was introduced in Italy in the '70s, where nowadays it is widely adopted and it is having a rapid spread even outside the Italian borders. Moreover, the Italian Superior Work Council has recently released specific instructions for design of these components, that are fully compared to steel-concrete composite elements, removing any limitations for their employment in seismic regions (Consiglio Superiore dei Lavori Pubblici, 2009). Among the benefits provided by CSTC beam technology some are here recalled: high bearing capacity, high mounting speed thanks to unpropped erection, limited costs owing to high prefabrication level. Furthermore, being a concrete base section adopted for CSTC beam, good fire-strength is also provided. Adopting CSTC beam technology implies an emulative monolithic approach (cf. ch.1.4.1), because implementing a “dry-joint” to couple them to the adjoining columns would result excessively cumbersome.

A major advantage of “dry-jointed” connection systems, over monolithic ones, is the reduction of scheduling conflicts between construction phases related to in-place concrete casting and strengthening (cf. ch.1.5.1). This is just a finishing phase, not required to get structural strength and stability during assembly process. Hence, challenge faced during design phase of the new precast system, consisted in making assembling process less dependent from construction phases than usual emulative precast technologies, taking inspiration from dry-jointed system approach, without renouncing to assembly ease and structural performance.

The best solution was found in the adoption of single or double-storey “window-type” columns (see Fig. 98g), with voids at storey level to rest beams in the temporary phase and with a bolted connection pre-arranged at both column’s ends, to provide structural continuity. Column’s section is ovoid, with section dimensions 330 by 550 millimeters. These columns assure several benefits over multi-level one, since shorter elements are easier to transport, handle and rising. Therefore, modularity of the precast components allows to assemble a low-storey frame with the same ease than taller one. Maximum number of storeys may be just limited by columns’ bucking issue. In this case, a concrete grouting at lower storey levels may be required to provide adequate lateral restraining. Nevertheless, only limited concrete strengthening is necessary in order to exert such an effect, sensibly reducing this way construction phases’ clashing. A further peculiarity is the adoption of High Strength Concrete (HSC) C75/90 as base material for RC columns, casted through a centrifuged process, leading to the typical ovoid section of columns. This material assures high-bearing capacity (almost 15000kN) with limited overall section dimensions for maximizing the amount of living, commercial or sealable space, thus taking aspects typical of steel or CFST frames into a RC one.

To decrease costs of the proposed solution, though maintaining high quality materials, precast manufacturing process, schematized in Fig. 98, is highly standardized and automated. As a first step the single-storey column-skeleton is assembled by welding two end-flanges (steel grade S355) at both ends on 8 longitudinal rebars (steel grade B450) (Fig. 98a-d) and coiling up of $\phi 6$ stirrups to complete the reinforcement cage (Fig. 98e). Afterwards the upper “windowed” steel-core-joint is assembled (Fig. 98f) by welding two 40 millimetres thick vertical steel plates on the top (steel grade S355). Specifically designed steel-core-joint should be considered the pivot element of the whole precast joint, since it restore structural continuity between different columns’ segments, it acts as corbel for CSTC beams and it guarantees an adequate level of axial load capacity, still in the temporary phase (almost 6000kN). To provide a double-storey column layout, another column-skeleton is welded on the top of the previous one. Finally an horizontal flange get welded on the top of this assembly (Fig. 98f), to complete the skeleton-column layout. All necessary welding operations are performed in factory, guaranteeing quality, limited geometric tolerances and limited costs. To accommodate bolts for member-to-member vertical joining, four holes are pre-arranged on the lower and upper horizontal flanges (Fig. 98g-h). Corresponding to each holes, particular steel casings are welded on the lower flange to provide housing for bolts after concrete casting. Besides, all horizontal flanges present a central hole (120 millimetres diameter) designed for the HSC centrifuged casting process, this latter performed on formwork specifically designed for this purpose (Fig. 100).

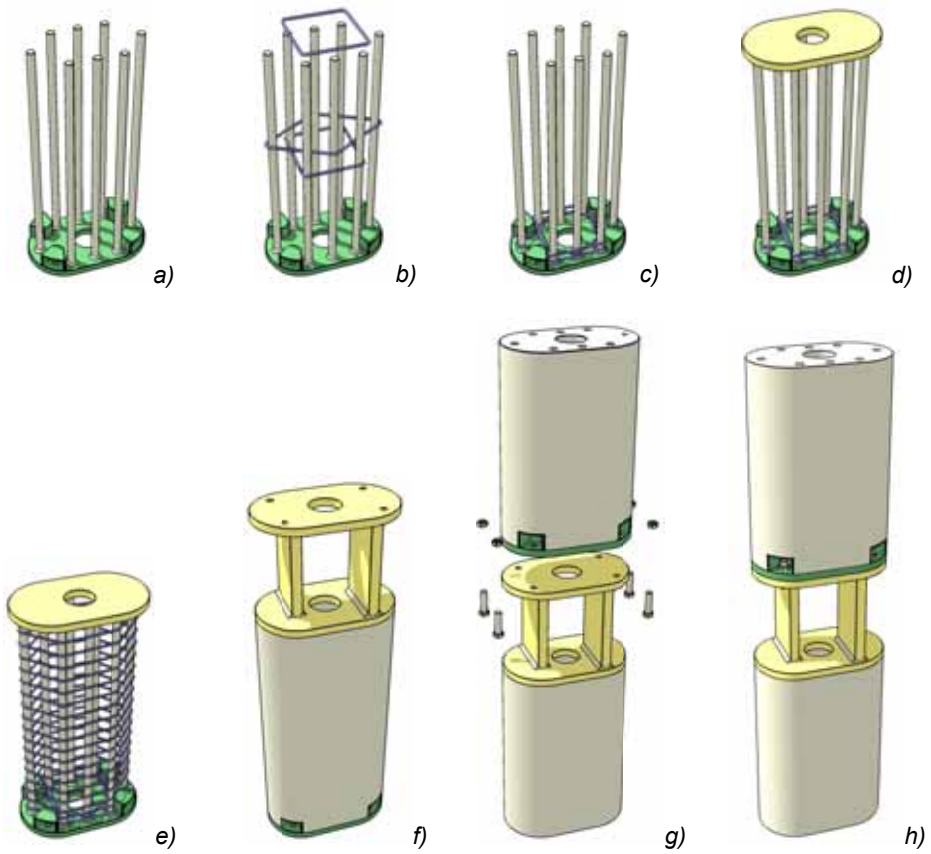


Fig. 98: Manufacturing process of composite-column (single-storey layout)

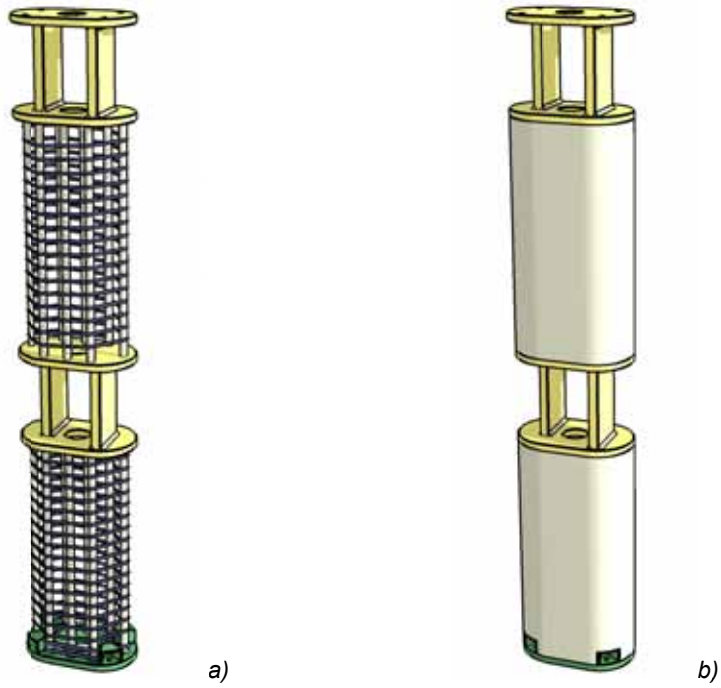


Fig. 99: Double-storey composite column; a) skeleton column; b) final layout



Fig. 100: Skeleton column manufacturing process



Fig. 101: Composite-column after HS concrete casting

In-site columns' assembling is straightforward, as well as CSCT beams placement: the asymmetrical layout of vertical steel plates belonging to steel-core-joint enables a convenient beams accommodation (Fig. 103), reducing drastically construction tolerance issues and increasing construction speed. During the temporary phase, CSCT beams rest in simple support scheme without requiring for temporary scaffolding (Fig. 104a).

To complete the framed structure and make it able to withstand seismic induced forces, beams' continuity is restored through lattice girders made by plain rebars in structural steel S355 (Fig. 104b). Experimental tests suggest as this solution provides an adequate strength level, with a slower section stiffness degradation and limited debonding phenomena under cyclic loading (cf. ch.1.6.5). Beside these benefits, in-site positioning of lattice girder is more rapid than single rebars, thus positively contributing to mounting ease.

The proposed joint layout appears extremely tidy, avoiding reinforcement congestion typical of reinforced concrete frames or other precast solutions (Fig. 20, Fig. 24). After placement of the floor slabs (Fig. 104c), a cast-in-place concrete grout is required to make the assembly monolithic (Fig. 104d).

Total self bearing capacity and mounting ease of proposed solution, make rapid all-weather erection possible even by unskilled labours, contributing to reduce final costs. Quality of adopted materials and smartness of final joint layout make this solution suited not only for multi-storey industrial/commercial structures and multi-storey parking garages, but also for multi-storey frames for municipal facilities and strategical building like schools, hospitals and many others, high-rise residential structures in areas of medium to high seismic intensity. Despite high quality of base materials, the final cost is comparable to those of an equivalent RC structures,

thank to high automation level during manufacturing precast process and thank to in-site mounting ease.

Among the others, the following appear to be the most relevant benefits of proposed precast technology (Mazzarolo et al., 2010):

- Modular components easy to transport and manage
- High bearing capacity
- Mounting ease
- Reduced tolerance issue
- No in-site welding required
- Un-propped erection
- Reduced scheduling conflicts between construction phases
- Fire strength
- Reduced costs

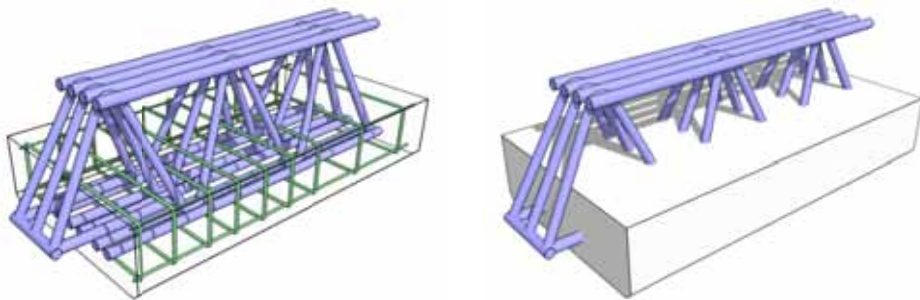


Fig. 102: Typical CSTC beam layout

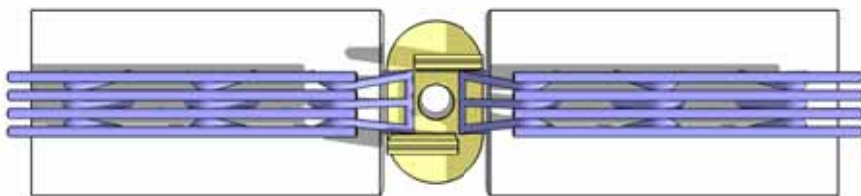


Fig. 103: Positioning of CSTC beam over steel-core joint

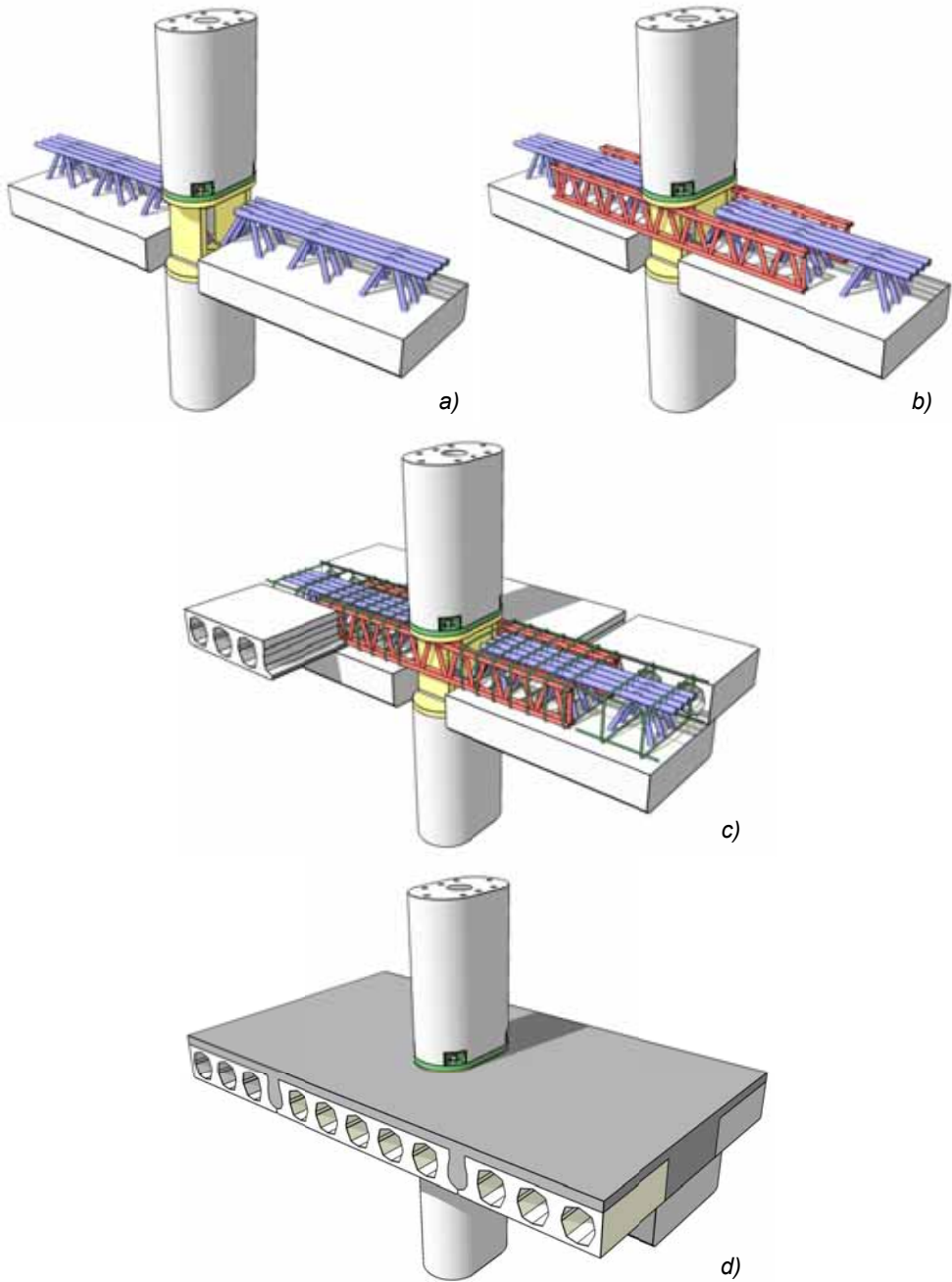


Fig. 104: Beam-to-column joint assembling operations

3. EXPERIMENTAL TESTING

3.1. Introduction

The innovative layout and lack of similar reference experiences in literature, revealed the need for experimental testing to check on mechanics and resisting mechanisms of proposed precast joint system.

Toward this aim two sets of lab tests were designed. The first focused on axial load bearing capacity of the composite-column, and investigated the influence of steel-core-joint geometry on static performances.

The latter investigated the performance of the joint under lateral loading and the capability of beams to develop plastic hinging at column interface.

The experimental campaign was conducted at State Key Laboratory for Disaster Reduction in Civil Engineering (SLDRCE) in Tongji University in January 2010

In this chapter collected results are reported and commented.

3.2. Material properties

In this section mechanical material properties are reported. Just in-site grouted concrete (class C25/30) was tested in laboratory. For missing material data, reference is made to current design codes, as indicated by the supplier of precast components.

3.2.1. Concrete

For concrete class C25/30, both compressive strength (R_c) and elastic modulus (E_c) are measured in laboratory, by testing concrete cube with edge dimension 150mm.

Elastic modulus is evaluated measuring secant stiffness after 5 time loading-unloading procedure at 50% of maximum strength. Cylindrical strength (f_c) is estimated as $0,83R_c$. Totally, three samples are tested.

According to JTG E30-2005 (China Traffic Ministry, 2005) samples' curing is made at controlled temperature of $20^{\circ}\text{C} \pm 3^{\circ}\text{C}$ and relative humidity higher than 90 percent for 28 days. Loading speed during testing is limited to 0,3 MPa/s.

Sample	R_c (MPa)	f_c (MPa)	E_c (MPa)
1	37.4	31,0	3.07e4
2	35.0	29,0	3.35e4
3	31.7	26,3	3.24e4
average	34.7	28,7	3.22e4

Table 2: Experimental material properties for grouted concrete C25/30

For precast concrete classes C30/37 and C75/90, characteristic compressive strength f_{ck} is assumed as a reference value (30 and 75 MPa, respectively). Missing parameters are estimated adopting EN 1992-1-1 (European Committee for Standardization, 2005a) provisions:

$$f_{cm} = f_{ck} + 8MPa \quad 1)$$

where f_{cm} =average compressive strength

$$E_{cm} = 22000 \left(\frac{f_{cm}}{10} \right)^{0,3} \quad 2)$$

where E_{cm} =average elastic modulus

$$f_{ctm} = 0,3(f_{cm})^{2/3} \quad 3)$$

where f_{ctm} =average concrete tensile strength

$$\varepsilon_{c,0} = 2,0 + 0,085(f_{cm} - 50)^{0,53} \geq 2\text{‰} \quad 4)$$

where $\varepsilon_{c,0}$ =unconfined concrete strain at peak stress f_{cm}

$$\varepsilon_{c,50} = 2,8 + 27[(98 - f_{cm}) / 100]^4 \leq 3,5\text{‰} \quad 5)$$

where $\varepsilon_{c,50}$ =unconfined concrete strain at 50% f_{cm} residual strength

$$\nu = 0,2 \quad 6)$$

where ν =Poisson's coefficient for concrete in elastic phase

Validity of expressions 4 and 5 is checked in chapter 4.2.8. For fracture energy value, reference is made to CEB-FIB Model Code 2010 (International Federation for Structural Concrete (FIB), 2010) formulation:

$$G_f = 73(f_{cm})^{0,18} \quad 7)$$

Table 3 summarizes the main mechanical parameters for adopted concrete classes:

Grade	f_{cm} (MPa)	f_{ctm} (MPa)	E_{cm} (MPa)	$\varepsilon_{c,0}$ (‰)	$\varepsilon_{c,0}$ (‰)	G_f (N/mm)	ν
C25/30	28.7	2,8	32.2e3	2	3.5	133	0,2
C30/37	38	3,3	32.8e3	2	3.5	140	0,2
C75/90	83	5,7	41.5e3	2,8	2.8	161	0,2

Table 3: Concrete mechanical properties

Complete stress-strain relationship for concrete is defined adopting the Légeron & Paultre, 2003 model, introduced in chapters 4.2.5 and 4.2.6 and validated in chapter 4.2.10.

3.2.2. Steel

Different components are adopted in the proposed beam-to-column joint, each characterized by specific material grades. Components are listed below, together with their corresponding steel grade and chosen reference code:

- Lattice girders, steel-core-joint and CSCT beam truss; steel S355J0; EN 10025:European Committee for Standardization, 1995;
- Column reinforcements and stirrups; steel B450C: EN 1993-1-1:2005 Appendix C (European Committee for Standardization, 2005b);
- Bolts; steel grade 10.9; ISO 898-1:1999 (International Standard, 1999).

Estimation of yield (Lüders) plateau length in the σ - ε curve and the corresponding strain limit ε_L (Fig. 105), is estimated through a formulation reported in SINTAP BS/23 (British Steel, 1998):

$$\varepsilon_L = 0,0375 \left(1 - \frac{f_y}{1000} \right) \quad 8)$$

Estimated steel mechanical properties are listed in Table 4.

Grade	tk (mm)	f_y (MPa)	f_t (MPa)	ϵ_y (%)	ϵ_L (%)	ϵ_u (%)	E (MPa)	E_{pl} (MPa)	ν
S355	>16 ≤40	345	500	0,2	2,4	22	2e6	3e3	0,3
S355	>40	335	490	0,2	2,5	22	2e6	3e3	0,3
B450C	-	450	540	0,2	1,8	7,5	2e6	3e3	0,3
10.9	-	900	1000	0,2	-	9	2e6	3e3	0,3

Table 4: Steel mechanical properties

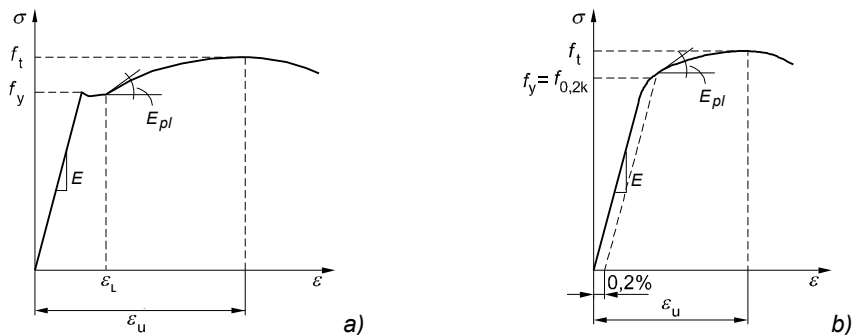


Fig. 105: Stress-strain relationship for steel: a) S355 and B450C; b) 10.9 grade

To define the complete stress vs. strain relationship, the Briseghella, 1988 model is assumed:

$$\begin{aligned}
 \sigma(\epsilon) &= E \cdot \epsilon & \epsilon &\leq \epsilon_y \\
 \sigma(\epsilon) &= f_y & \epsilon_y < \epsilon &\leq \epsilon_L \\
 \sigma(\epsilon) &= f_u - (f_y - f_u) \left| \frac{\epsilon_u - \epsilon}{\epsilon_u - \epsilon_y} \right|^P & \epsilon_L < \epsilon &\leq \epsilon_u
 \end{aligned}
 \tag{9)$$

with: $P = E_{pl} \frac{\epsilon_u - \epsilon_L}{\sigma_u - \sigma_y}$

3.3. Static testing

3.3.1. Specimens description and test setup

Static experimental tests deal with real scale samples of composite-columns. The tested samples consist of inter-storey column assemblies, namely two column-stubs 780 millimeter long, connected together by the steel-core-joint (Fig. 107). The lower column is directly connected to steel-core-joint by welded longitudinal rebars. Upper column is connected by means of bolted connection (4 M24 10.9 bolts). Primary scope of static tests is evaluate the influence of flange thicknesses and column reinforcement on stiffness and strength capacity, deformation characteristic and failure mode, to find the best solution layout from both the mechanical and the economical points of view.

Towards this aim, six specimens were designed, each characterized by specific thicknesses of horizontal flanges and rebars' diameter (see Table 5). Samples "A" and "B" adopt $\phi 30$ and $\phi 20$ longitudinal rebars, respectively. After assemblage of the composite-column, the steel-core-joint and the hollow core of HSC column are filled with cast-in-place concrete.

Samples are positioned at the center of a rigid frame (Fig. 108) and axial load on top column is applied by an electro-hydraulic jack with maximum capacity equal to 20000kN. The imposed load steps are reported in Fig. 106. Several unloading and reloading among 3000 and 5000 kN are used to settle the composite-column and to reduce possible gap at connection interface. Load is finally increased until failure. Load speed application is limited to 5kN/s.

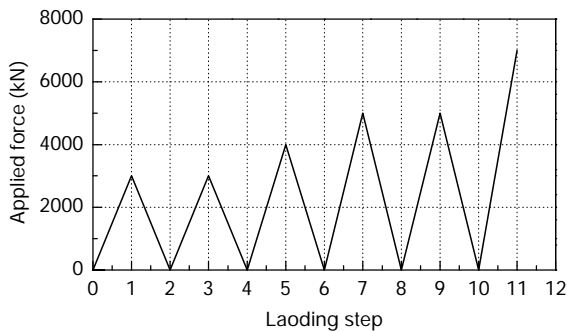


Fig. 106: Imposed load history at top column

Analysis and development of an innovative prefabricated beam-to-column joint

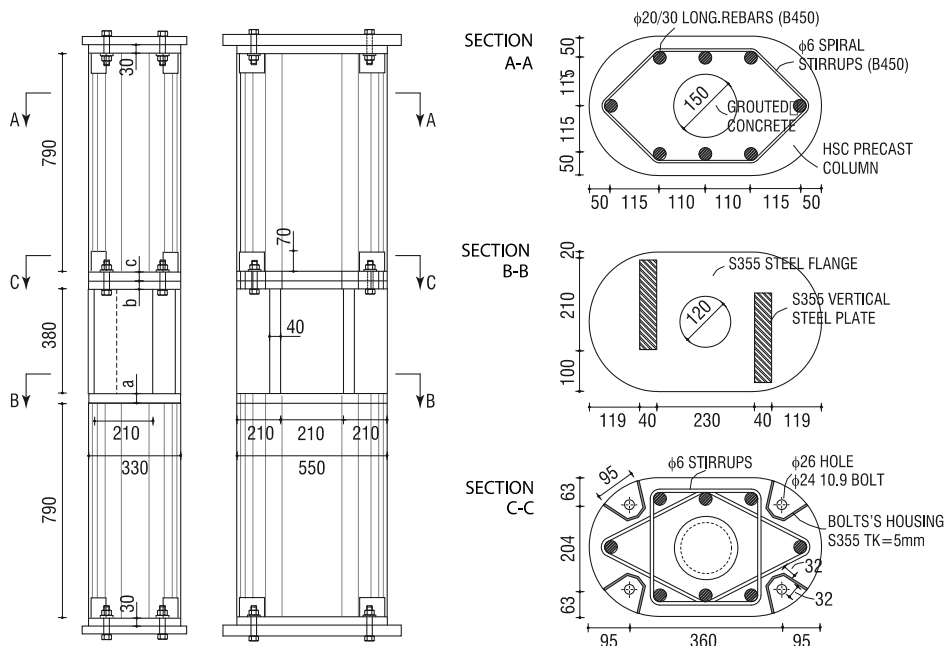


Fig. 107: Geometry of composite-column samples

Specimen	a (mm)	b (mm)	c (mm)	rebar diameter (mm)
A1	65	30	35	30
A2	45	25	30	30
A3	30	20	25	30
B1	50	25	30	20
B2	35	20	25	20
B3	25	15	20	20

Table 5: Geometrical properties of composite-column samples

Several sensors are positioned on specimens to capture strains during testing. 8 and 6 strain-gauges are placed on column surface 200 mm far from central joint, to record concrete strains in the axial and transversal direction, respectively (Fig. 109). 12 strain-gauges are stuck on the steel-core-joint, 8 of them to monitor axial strains on vertical steel plate, the remaining on lower steel flange to monitor in-plane strain (Fig. 111). Finally, to measure the axial deformation of the steel-core-joint, two LVDTs (Linear Variable Differential Transformers) on both column faces (Fig. 110): the first between top horizontal steel flange and top concrete column, the latter between the two concrete columns including the steel-joint. Deformations of this components are obtained from the average value of LDVT's Value(502)-2*Value(501) and Value(504)-2*Value(503).

To improve readability, experimental data have been filtered by removing initial settlement steps and leaving only last load cycle till failure.

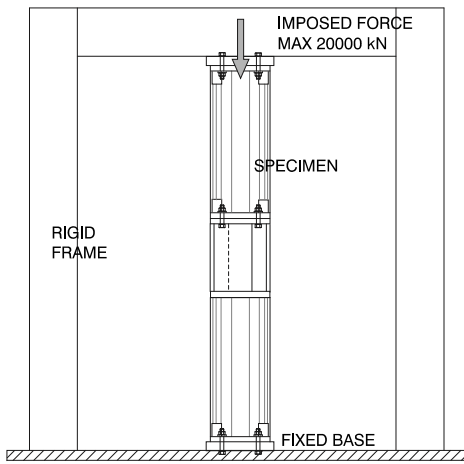


Fig. 108: Static test set-up

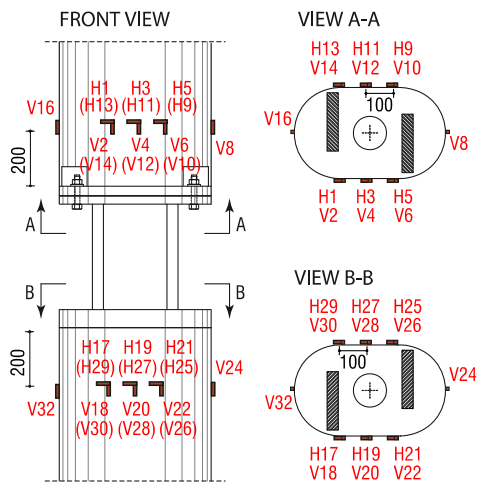


Fig. 109: Strain-gauges applied on column

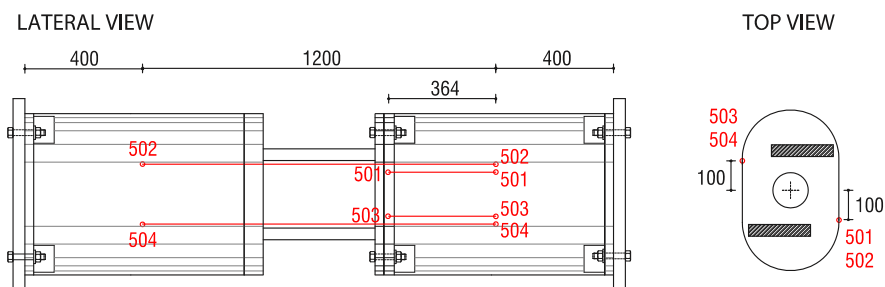


Fig. 110: Composite column displacement transducer

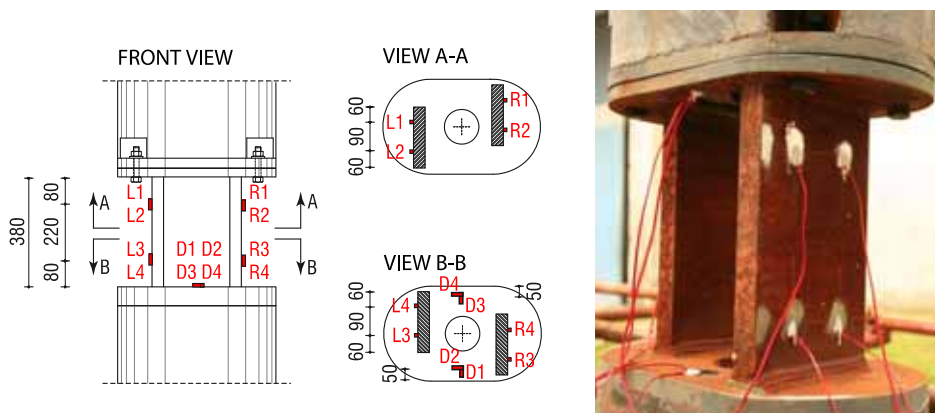


Fig. 111: Strain gauges applied on steel-core-joint

3.3.2. Force vs. displacement curves

Load vs. steel-core-joint deformation relationships are reported in Fig. 112. The result obtained from different samples is similar, despite the different geometry. In all cases splitting failure of grouted concrete at core-joint level take place during settlement phase, when active load attains 5000kN (Fig. 111a). Before failure all samples display an elasto-plastic due to yielding of vertical steel plates. Being core-concrete splitted-out, the naked steel-core-joint become the weak component of the assembly. The yielding force is calculated as the force level corresponding to a residual stiffness 15% lower than the initial one. Experimental values range between 5294 and 5933 kN, while corresponding yielding displacements range between 1,28 and 1,77 mm. Furthermore, the average yielding force equal to 5620 kN agrees well with analytical estimation of axial strength provided by vertical plates (eq. 74). All samples experience failure due to buckling of vertical steel plates after appreciable plastic deformation (Fig. 111b,c). Experimental evidence allows to conclude that a considerable reduction of horizontal flanges' thicknesses can be

performed without affecting composite-column structural performance, at least during temporary construction phase, before casting of concrete-core.

$$F_y = A_{steel} \cdot f_y = 210 \cdot 40 \cdot 2 \cdot 345 = 5796 \text{ kN} \quad 10)$$

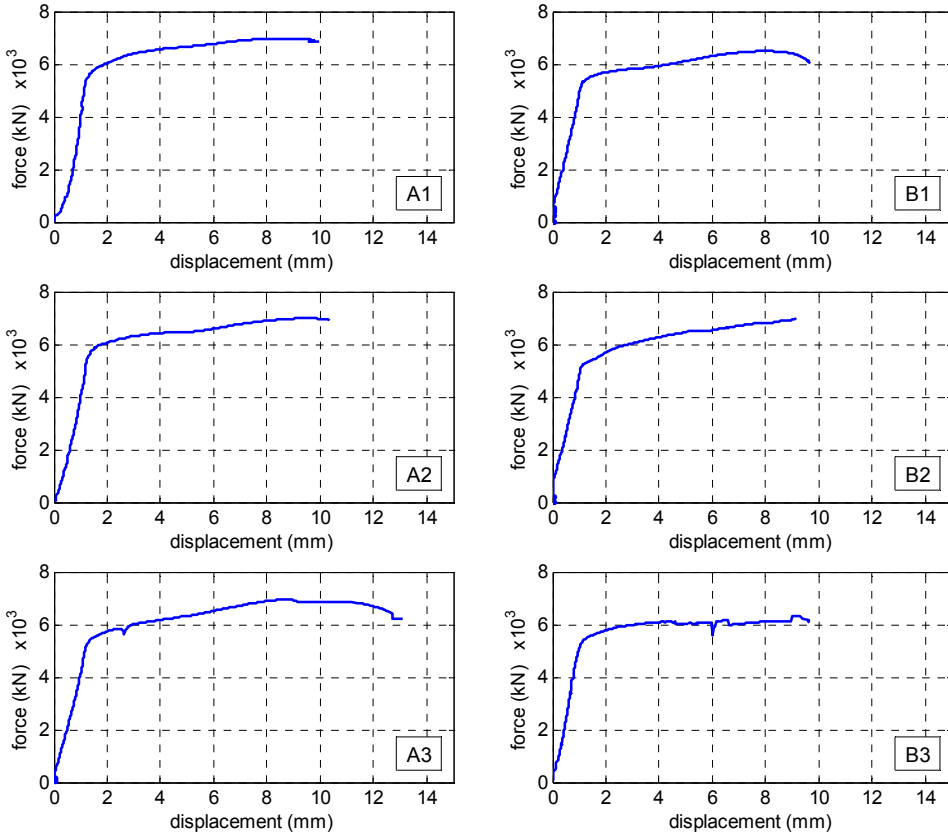


Fig. 112: Force vs. displacement relationship from static tests

Specimen	F_y (kN)	u_{Fy} (mm)	F_{MAX} (kN)	u_{MAX} (mm)
A1	5930	1,77	6960	9,96
A2	5933	1,55	6986	10.26
A3	5579	1,61	6954	13.08
B1	5424	1,28	6496	9.67
B2	5294	1,25	7004	9.16
B3	5557	1,41	6312	9.66
average	5620	1.48	6785	10.30

Table 6: Static performances for different samples tested

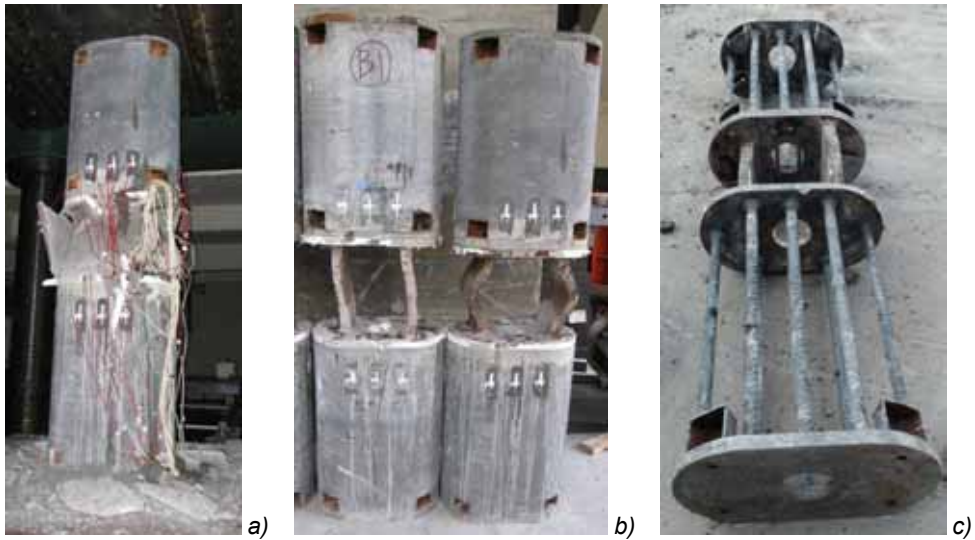
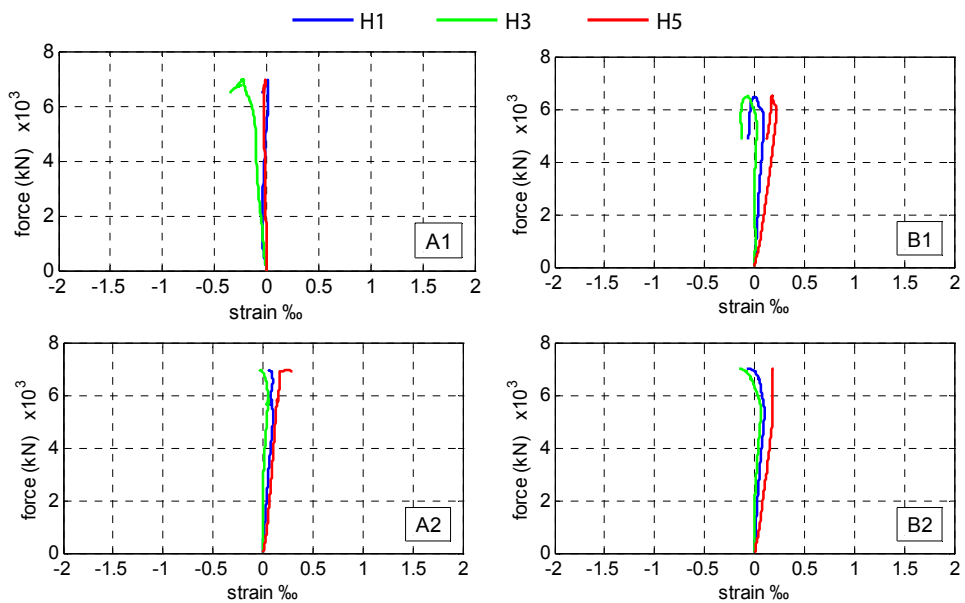


Fig. 113: Composite-columns after failure

3.3.3. Horizontal strain sensor on column concrete

Transverse strain gauges on the upper and lower column experience deformations always less than 300 μm , suggesting that concrete response in the transversal column direction remains elastic during the whole test.



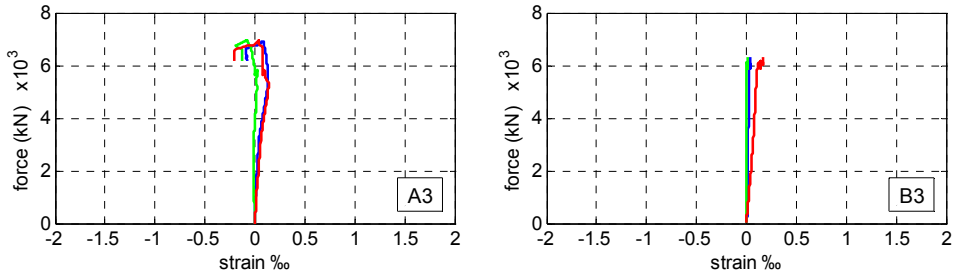


Fig. 114: Column horizontal strain sensors H1, H3, H5

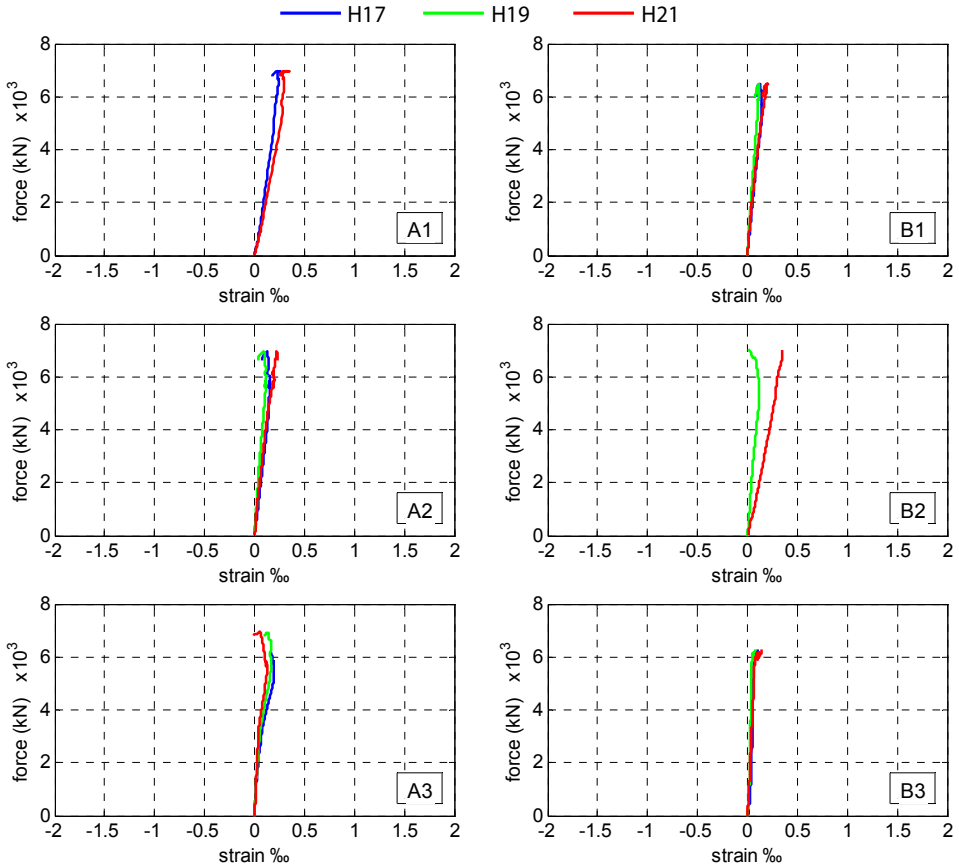


Fig. 115: Concrete strain-gauge location: sensor H17 H19 H21

3.3.4. Vertical strain sensor on concrete

Vertically oriented strain sensors stuck on the upper and lower column, 200mm far from steel-joint, registered a similar trend for all samples. Probably due to asymmetrical layout of the vertical steel plate in the steel-core-joint, both columns'

ends are characterized by non-uniform axial strain field over their section. Sensors V10 and V22 placed nearer to vertical steel plates, experience the highest compressive deformation, ranging between 1000 to 1650 μm . Concrete strains tend to diminish for adjoining sensors belonging to the same alignment. Axial strains at the center of column face range between 500 to 750 μm . Remaining gauges located in the arch-shaped side of column record still lower deformation, never exceeding 500 μm . Global force vs. strains trends appear nearly linear elastic for all sensors until failure. The highest recorded strain, equal to 1650 μm and well below the peak-strength-strain ϵ_{c0} (2800 μm in Table 3) means that HSC columns performed elastically during static testing, thus far from exploiting their maximum bearing capacity

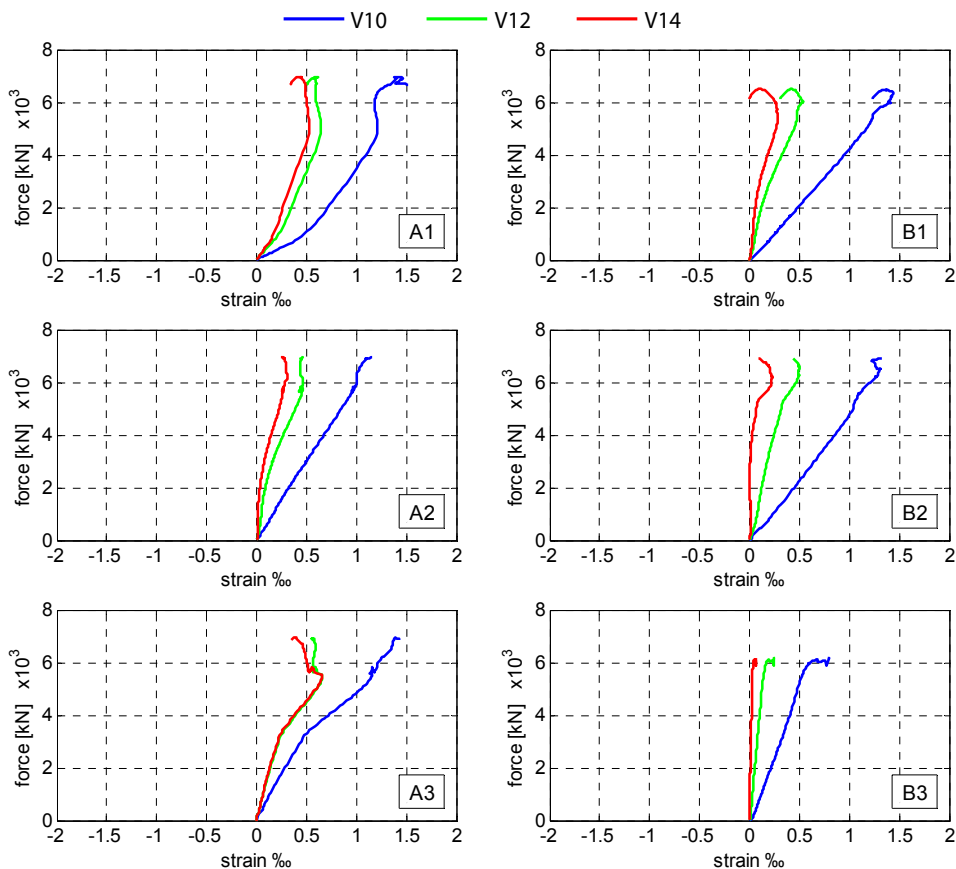


Fig. 116: Concrete strain-gauge location: sensor V10 V12 V14

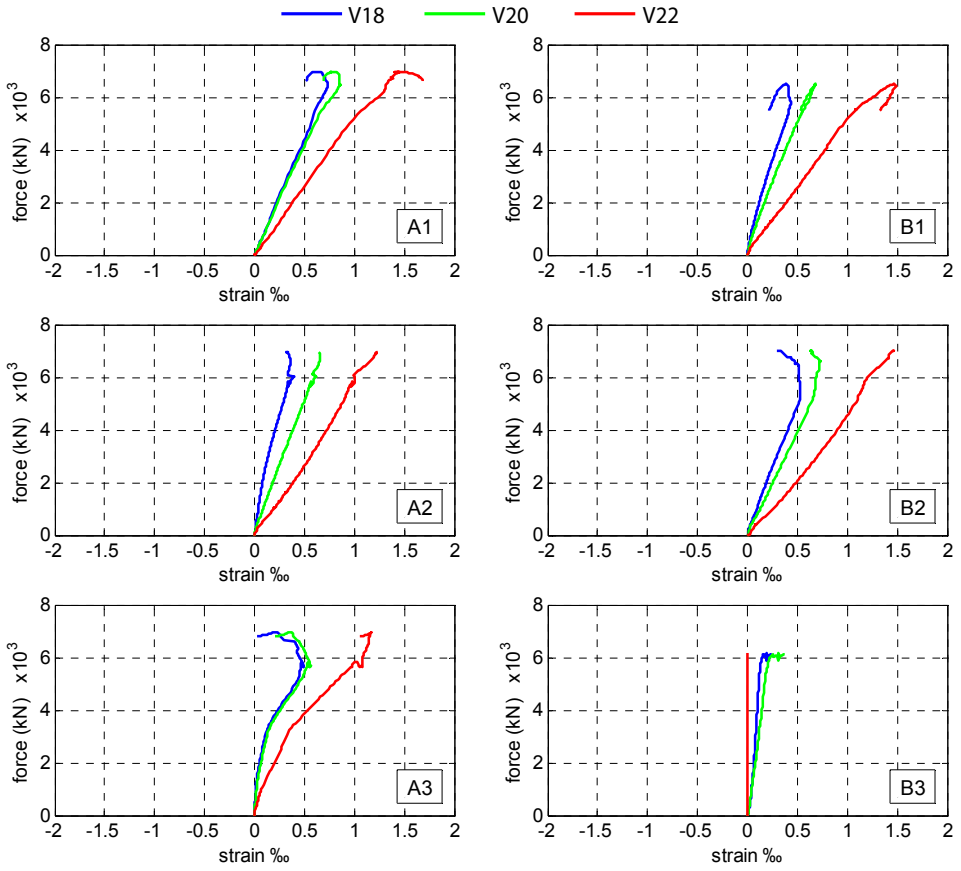
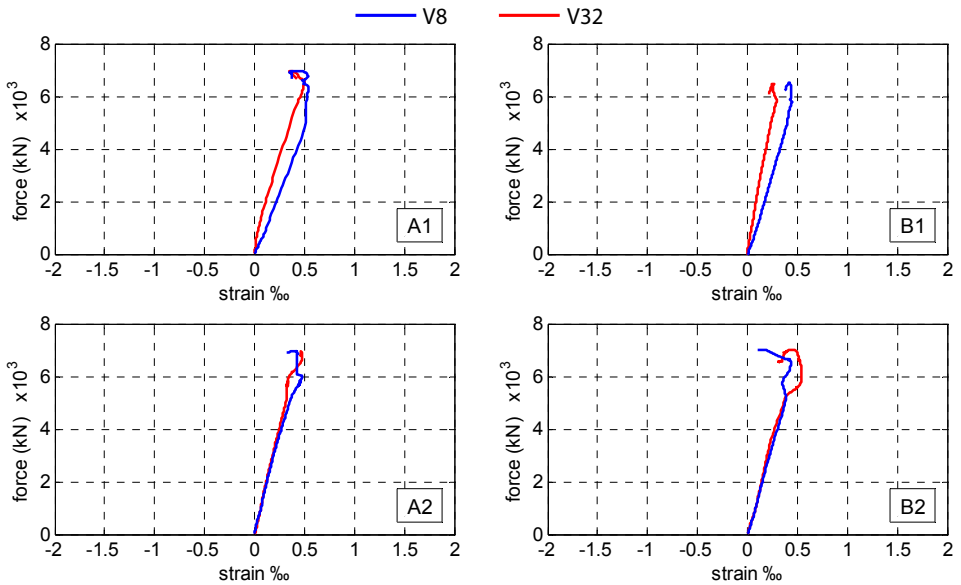


Fig. 117: Concrete strain-gauge location: sensor V18 V20 V22



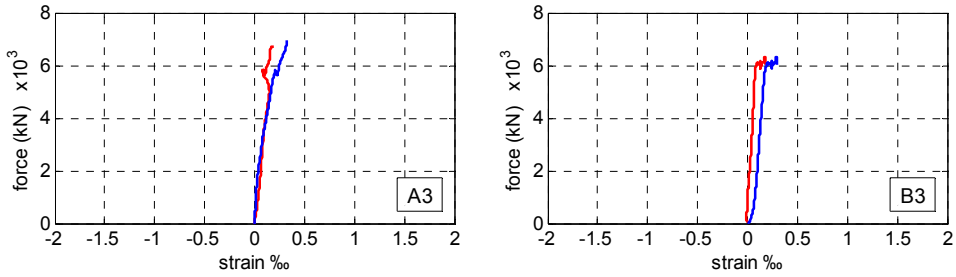
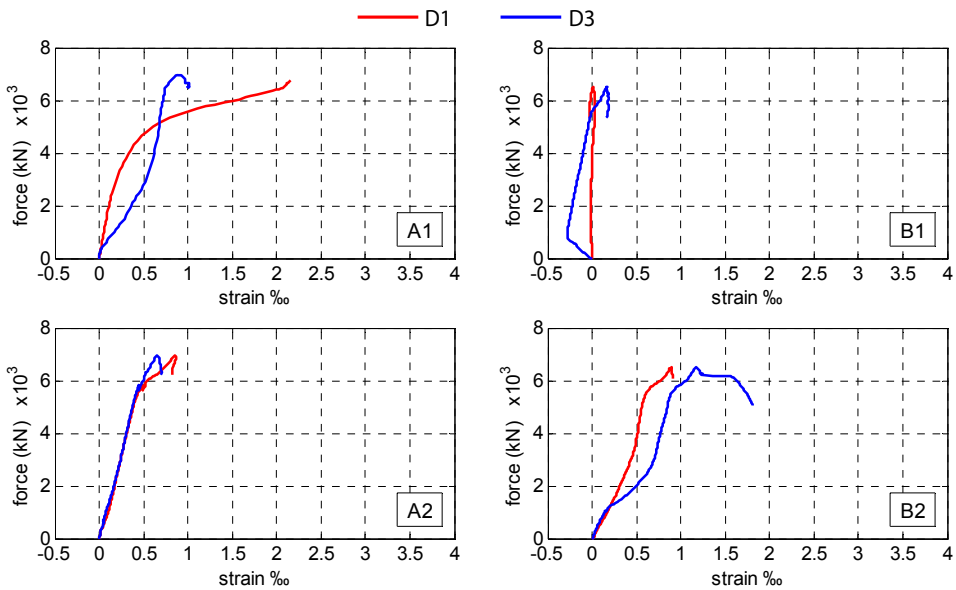


Fig. 118: Concrete strain-gauge location: sensor V8 V32

3.3.5. Strain sensor on lower horizontal steel plate

From all sensors located in the lower horizontal steel plate belonging to steel-core-joint, an elastic response was observed, being strain values always less than 2‰. Sensors D1, D3 oriented in the wider column edge direction, experienced negligible deformation, approaching 0,5 ‰ only in sample B1 (Fig. 119). Gauges D2, D4, oriented along the orthogonal direction, recorded higher strains, approaching the yielding limit. This indicates that bending solicitations acted on the lower plate along this direction (see Fig. 215).



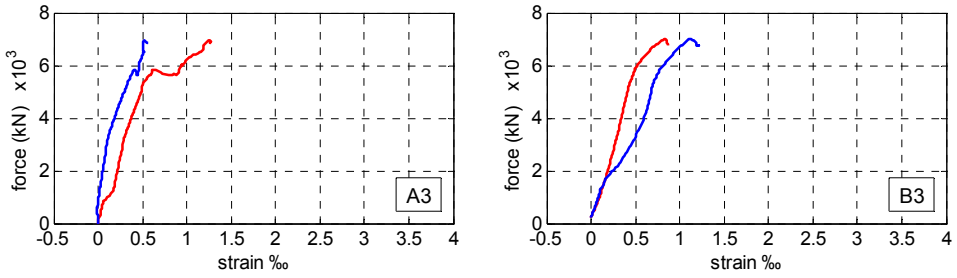


Fig. 119: Concrete strain-gauge location: sensor D1-D3

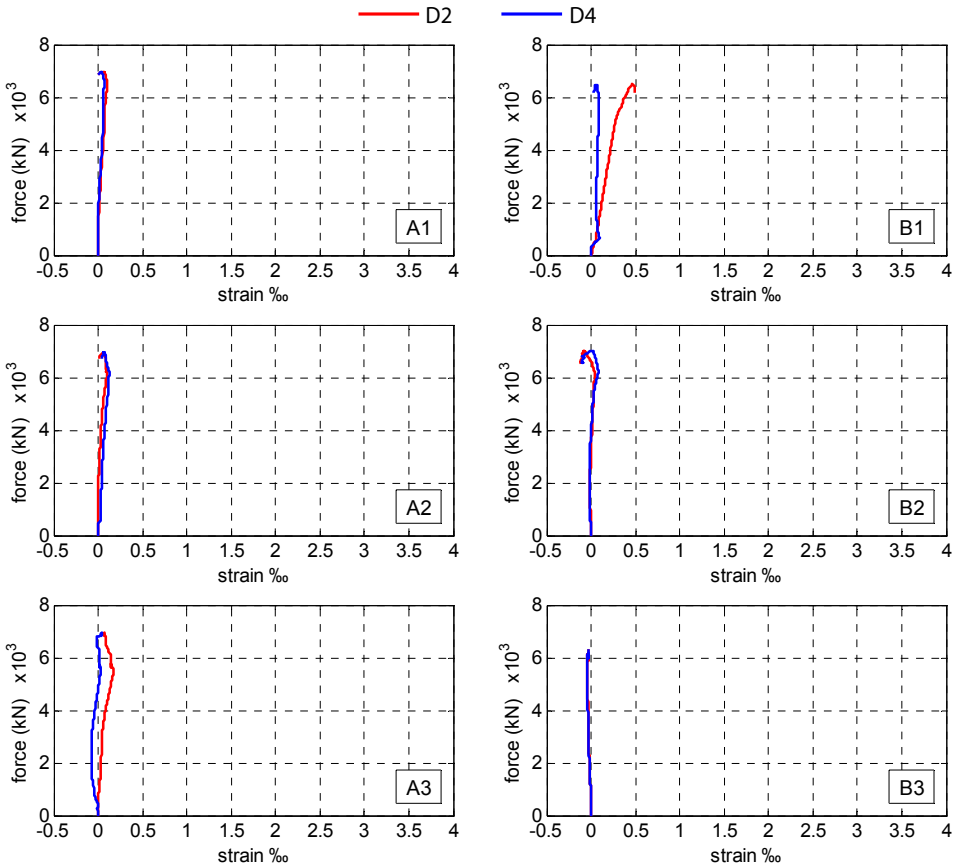


Fig. 120: Concrete strain-gauge location: sensor D2-D4

3.3.6. Vertical strain sensors on vertical steel plate

Considerable plastic deformation should be expected from these sensors, being vertical steel plates the weak component of the composite-column. Considering that

average deformation of steel-core-joint is nearly 10 mm (Table 15) and steel plate are 380mm long, the expected average steel plate strain at failure is almost 25‰. Some gauges record rather high deformation levels: 10‰ in sensor L4-A3, 6‰ in sensors L1-A2, L2-A2, L3-B2. Some other sensors just enter the yielding plateau. Attained deformation level is then well below expected one. This could be justified by two motivations. On the one hand, it resulted that some sensors were severely damaged after concrete splitting failure. The most evident case is provided by samples B3. For samples A3, B1, B2, respectively just two, two and one sensors worked continuously, while data provided by the others were clearly corrupted and thus disregarded. On the other hand, the buckling failure achieved by samples, might have favored a premature separation of several sensors from steel surfaces. (Fig. 113). Sample A1, for example, failed after reaching an active force level equal to 6950kN, while gauges stopped recording at 6000 kN. A similar behaviour is shown even by sensors applied to samples A2 and B1.

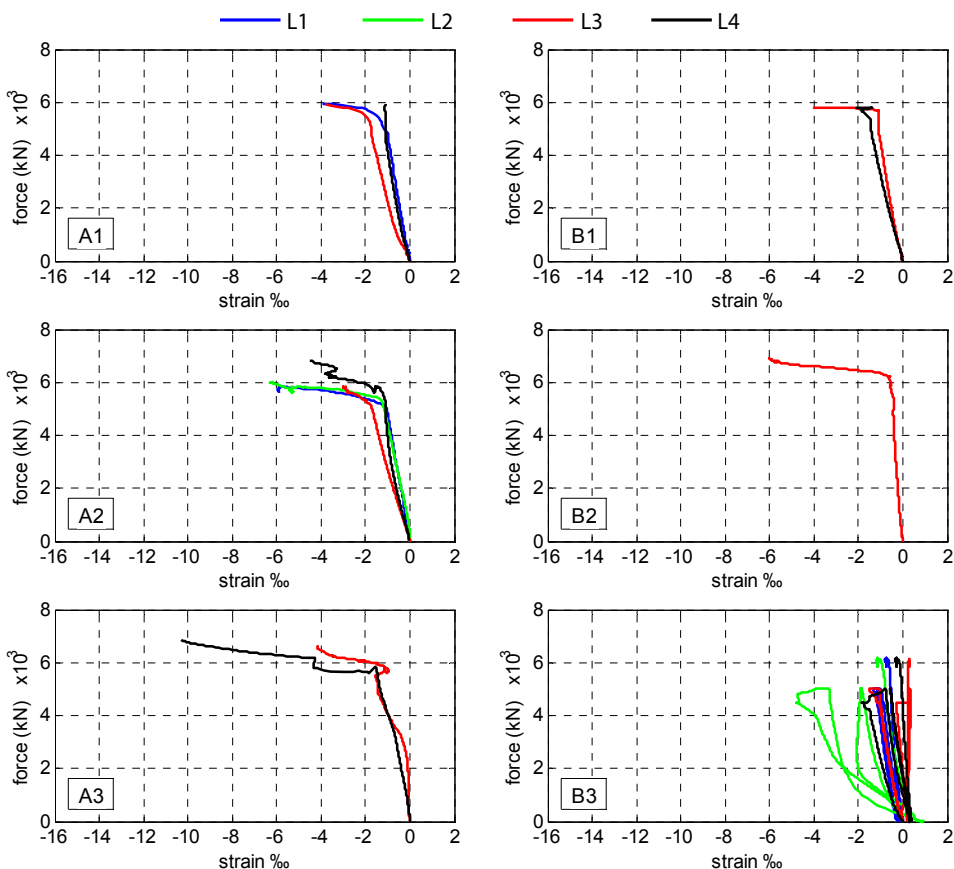


Fig. 121: Concrete strain-gauge location: sensor V8 V32

3.3.7. Conclusions

Static experimental tests allowed to clarify several issues about structural response of composite column under increasing axial load.

First of all it results that core-joint concrete is subject to splitting out failure as force attains almost 5000kN, leaving the naked steel-core-joint bearing the whole load. This means that vertical steel plates are not able to provide adequate confinement to core concrete at high axial load level. As a consequence, particular care in design phase should be taken for exterior joints, where confinement action provided by flooring system is limited (cf. ch.12.7.2).

Given that core-concrete splitted out, experimental tests permit to evaluate the ultimate load bearing capacity of the composite-column under temporary phase, before concrete cast. Assembly response is nearly elastic until vertical steel plates attain yielding. This limit should be assumed as reference for design (equation 74).

Good deformation capabilities are observed before failure, the latter achieved by buckling of vertical steel plates.

Structural response from different samples is rather similar, despite different geometry of steel-core-joint and reinforcement. This imply that reduced steel flange thickness could be adopted without compromising mechanical performance in the temporary phase. The issue about optimum flange thicknesses layout to get the best compromise from both the mechanical and the economical points of view is further investigated in chapters 7.4 to 7.6.

Finally it should be recalled as during static testing HSC column performed elastically, with maximum recorded compression strain well below the peak limit. This is a clue suggesting as expected mechanical performances for this component might be sensibly higher. An estimation of HSC column limit strength domain is reported in chapter 7.2.

3.4. Cyclic testing

3.4.1. Specimens description and test setup

Cyclic laboratory test deal with real scale samples of the proposed beam-to-column precast assembly. The vertical components of the joints are identical to those adopted for static testing: two HSC column stubs connected together by the specific designed steel connection. The joint layout is completed by two 1150 mm long CSTC beams. Two 1500 mm long lattice girders are used to restore beam continuity through the core-joint. A cast in place concrete grout make the assembly monolithic. The samples are approximately 2 meter high and 2,6 meter wide, mainly owing to the test-machinery space restriction.

Geometrical details of samples are reported in Fig. 122. Columns and steel-joint section geometries are reported in Fig. 107.

Capacity of the proposed joint-prototype to develop plastic hinge on beam and role played by lattice girder, represented the main issues to be investigated during cyclic testing. Towards this aim, six specimens are tested (Fig. 123), each of them characterized by a different thickness of horizontal steel flanges and longitudinal rebar diameter (see Table 7). Samples “C” are characterized by $\phi 30$ column longitudinal threaded rebars, while samples “D” are provided with $\phi 20$ longitudinal rebars. A schematic representation of test equipment is reported in Fig. 124. Prototype joint is positioned at the center of a rigid frame, with horizontal loading maximum capacity equal to 2000kN, and maximum displacement of horizontal actuator limited to ± 500 mm. Upper and lower column’s ends are hinged; beams’ ends are restrained by a steel box, hinged on the beam and connected to outer rigid frame by four tubular steel braces.

Tests are displacement controlled (Fig. 125), though an hydraulic rolling system acting on the lower column. Loading speed is limited to 0.02 mm/s.

Before cyclic loading started, an axial force equal to 2000 kN is imposed on column top, through an electro hydraulic servo loader, in order to simulate more realistic axial stress conditions inside composite-joint’s column.

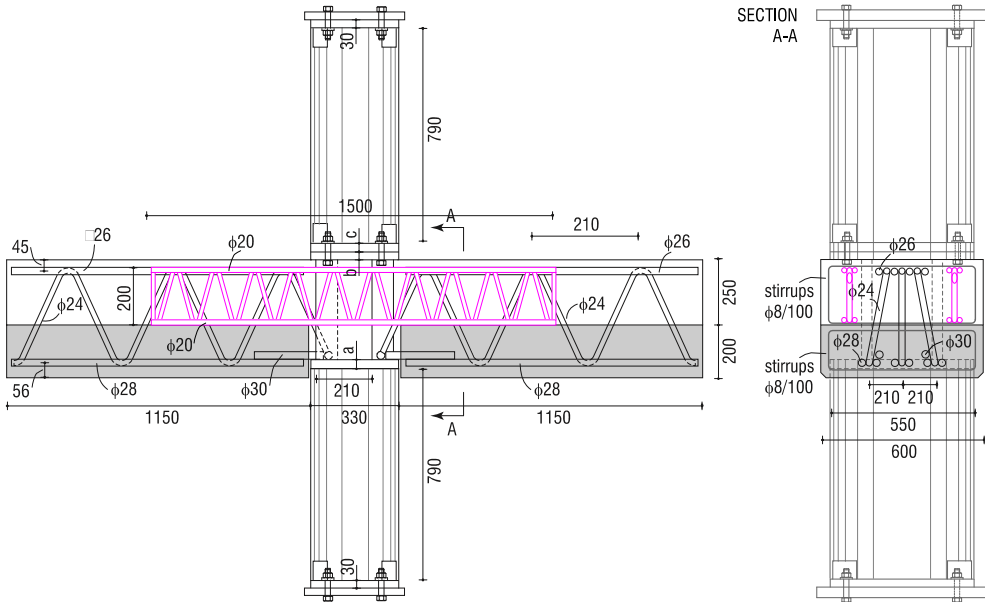


Fig. 122: Beam-to-column joint samples geometry



Fig. 123: Preparation of cyclic test samples

Specimen	a (kN)	b (mm)	c (mm)	rebar diameter (mm)
C1	65	30	35	30
C2	45	25	30	30
C3	30	20	25	30
D1	50	25	30	20
D2	35	20	25	20
D3	25	15	20	20

Table 7: Geometrical properties of composite beam-to-column joint samples

Analysis and development of an innovative prefabricated beam-to-column joint

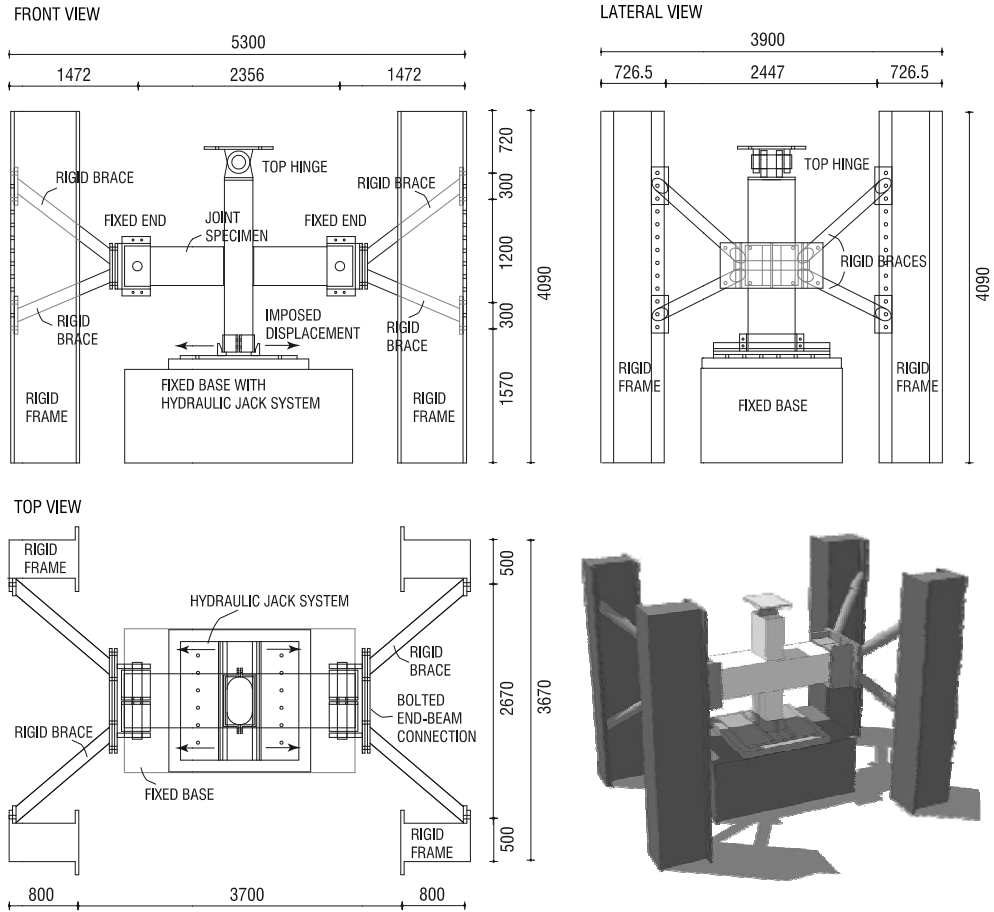


Fig. 124: Geometry of testing machinery

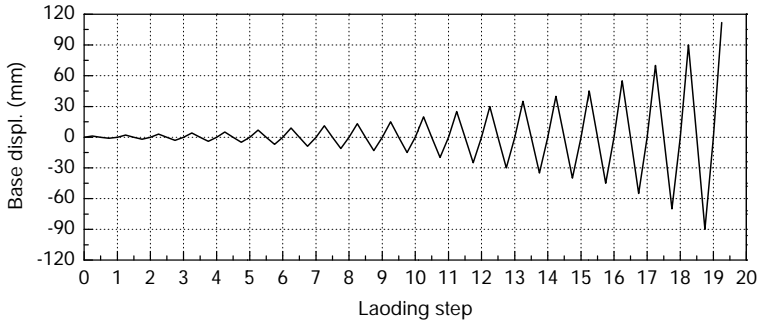


Fig. 125: Imposed base column displacement

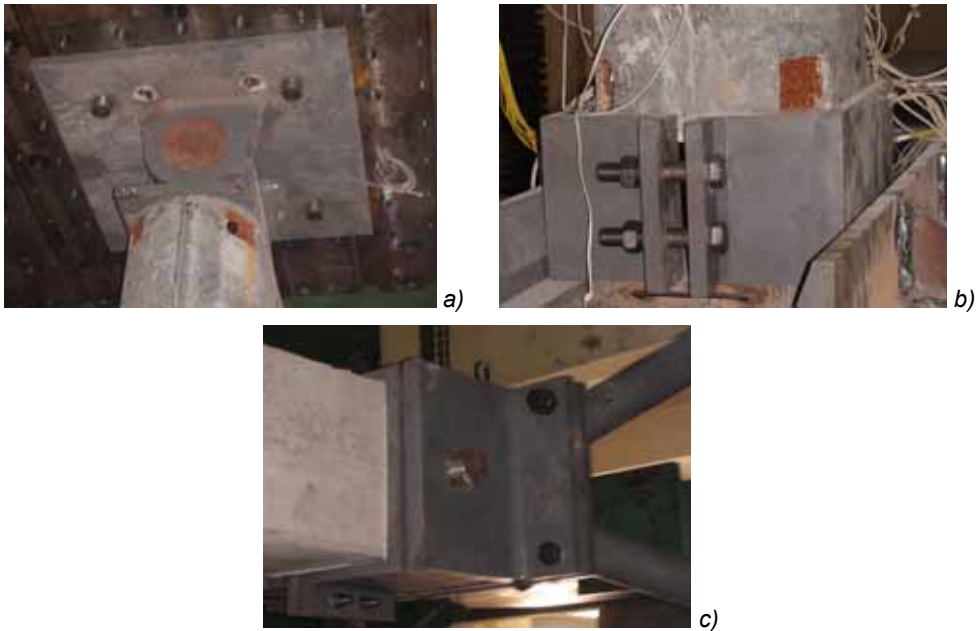


Fig. 126: Boundary conditions: a) top column, b) column base, c) beams' ends

During testing of sample D2, it was found that the concrete of bottom column near connection performed brittle failure at imposed drift displacement less than 30mm, while both the top column and beams still displayed elastic behaviour.

Such an behaviour is ascribed to unforeseen boundary conditions, different from that defined during test design. In particular beams' ends resulted fixed in term of horizontal displacements, while a roller support was supposed and also base column's rotation was restrained. This caused a solicitations' concentration along lower column, that lead to premature failure. Further details are provided below. Since it was not possible to modify test-set-up and test-equipment, it was decided to strength the bottom column of remaining samples by adopting FRP materials (Fig. 127), in order to promote a ductile behaviour. FRP plates (14x100 mm) were stuck on column to bear bending moment in the loading direction (Fig. 128, left). The column was then wrapped with four layers of CFRP fabric 0.167mm thick (Fig. 128, right) to improve confinement. Each layer was overlap at different positions, and the overlap length was 10cm. Furthermore base column's rotation was allowed.

Through FRP strengthening, the lateral force introduced in the composite-joint assembly was enough to guarantee plastic hinge formation along beam.

Analysis and development of an innovative prefabricated beam-to-column joint

Type	Model	Carbon fiber	Thickness (mm)	f_t (Mpa)	E (GPa)	ϵ_u (%)
Plate	CFC3-S1014	T700SC-12K	1.4	>2800	> 165	1.7
Fabric	CFC2-2	T700SC-12K	0.167	>3500	>220	1.8

Table 8: Mechanical properties of FRP materials

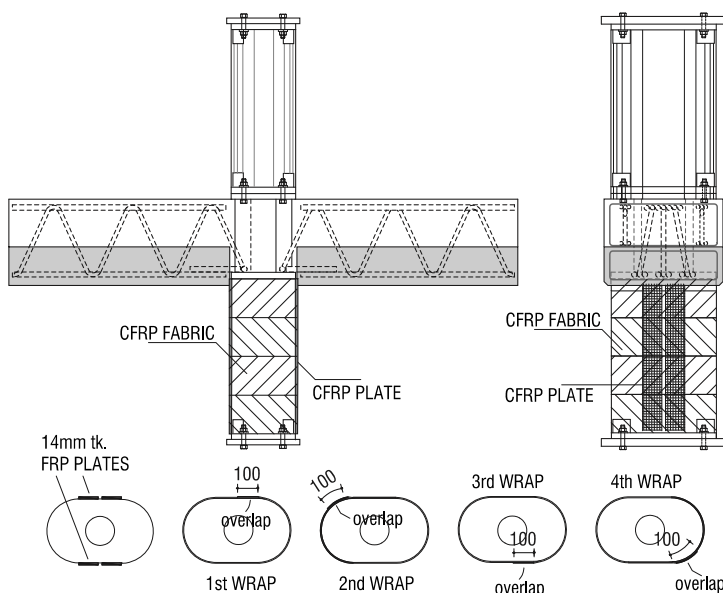


Fig. 127: The bottom column strengthened by CFRP materials



Fig. 128: Some images of the bottom column strengthening process with CFRP materials

To capture this effect, both CSCT beam's trusses (Fig. 129) and lattice girders (Fig. 130) get instrumented, 200 mm far from column faces, sticking strain gauges on longitudinal and inclined bars (Fig. 131). Further sensors are placed on vertical steel plates, to capture the steel-core-joint vertical deformations (Fig. 132). Finally

crack opening at beam-to-column interface get monitored by a displacement transducer positioned along the beams' bottom side (Fig. 133)

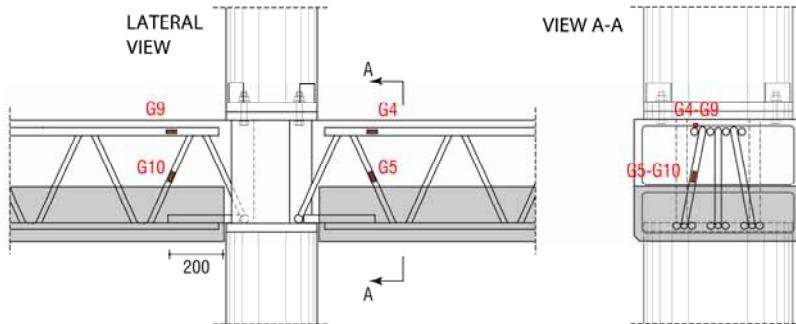


Fig. 129: Strain gauges on CSCT beam trusses

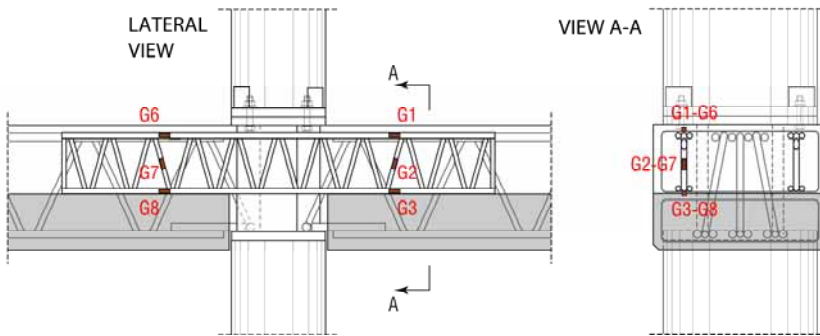


Fig. 130: Strain gauges on lattice girders providing beam's continuity



Fig. 131: Strain gauges applied on beam's reinforcement before grouted concrete finishing

Analysis and development of an innovative prefabricated beam-to-column joint

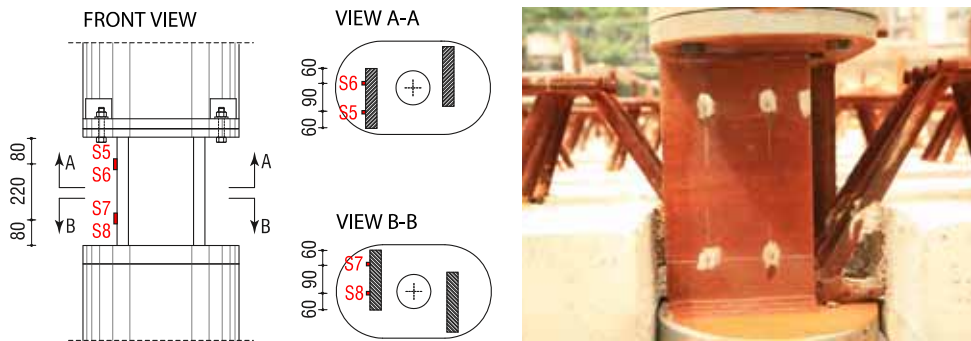


Fig. 132: Strain gauges on steel-core-joint vertical plates

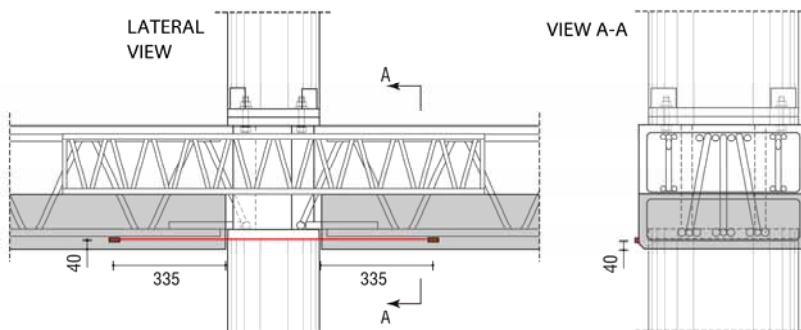


Fig. 133: Beam's displacement transducer

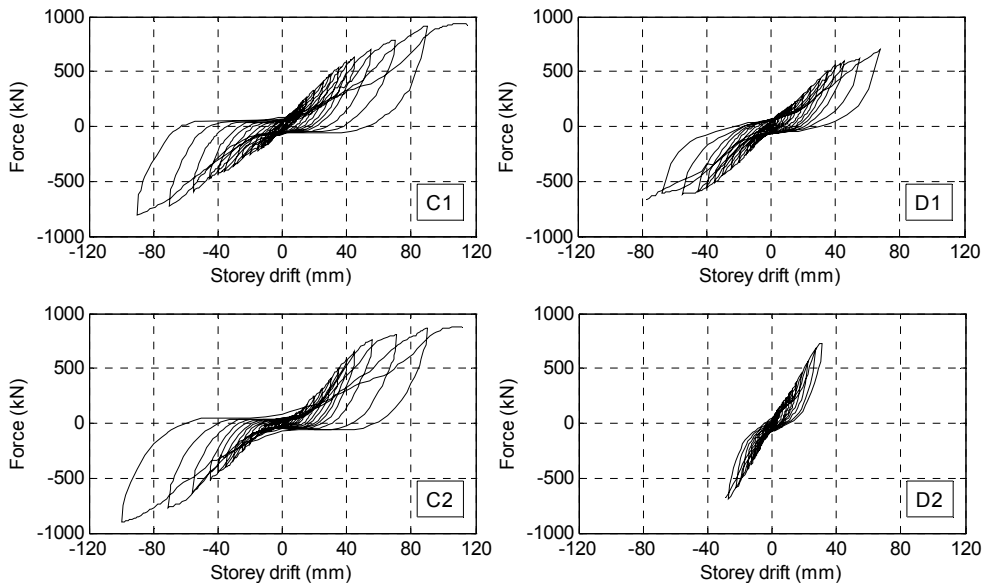
3.4.2. Force vs. displacement curves

During cyclic testing, sample D2 was subject to a premature deterioration due to brittle failure of bottom column concrete cover, while the remaining part of assembly (upper column and beams) displayed still an elastic behaviour. To identify the reason of such an event, attention should be stressed on boundaries conditions adopted for the experimental tests, in which beams' ends result partially restrained against horizontal movement and rotations (Fig. 124, Fig. 126c). In Fig. 137 is reported an illustrative representation of elastic bending moment distribution along joint components, depending on imposed boundary conditions. Restraining beam's translations affect considerably bending moment distribution, making it sensibly different from the distribution supposed in the test design phase (Fig. 137a). Bending moment, and consequently shear forces, acts mainly on the bottom column stub, while reduced bending moments stress the remaining elements of the assembly. This agree with experimental evidence. The fact that rotational degree of freedom at beams' ends is partially restrained during "D2" testing, contributed even

more to an unfavorable bending moment (and shear forces) distribution, leading to elastic beam performance.

The ultimate shear force attained from sample D2 is 728kN, corresponding to a bending moment at core-joint level equal to 431kNm (assuming a lever arm equal to $3/4 \times 0.79\text{m}$, where $3/4$ coefficient accounts for partial rotation fixity condition). Looking at formulations reported by NTC 2008 and EN 1992-1-1:2005 for shear strength calculations, the maximum expected strength provided by the bare stirrups is no more than 140 kN. Considering the column section as non-reinforced and accounting for secondary concrete shear resistant mechanisms, like the arch-tie one, the compressive chord one, the dowel action of the longitudinal steel, strength amounts to 470kN (considering an axial force level equal to 2000kN), which is lower than the maximum experienced shear force. At the same time, looking at M-N domain for column (Fig. 136), it appears that the maximum bending strength is slightly exceeded as well. For these reasons, brittle failure experienced by sample D2 is probably the result of a nearly contemporary exceeding of both bending and shear strength.

For all remaining samples, strengthening of bottom column stub with FRP materials and removing of rotational degree of freedom restraint at base column, allowed to withstand forces acting on it, achieving a global ductile behaviour. In these samples, development of plastic hinges along beams is confirmed by relevant vertical cracking at beam-to-column interface, in particular for samples “C” (Fig. 135).



Analysis and development of an innovative prefabricated beam-to-column joint

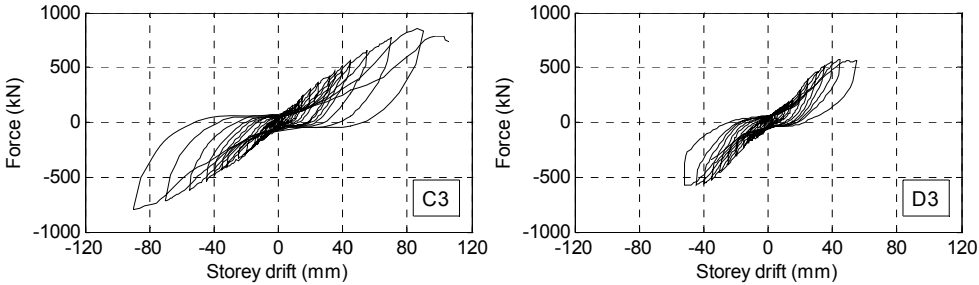


Fig. 134: Force vs. displacement curve from cyclic testing

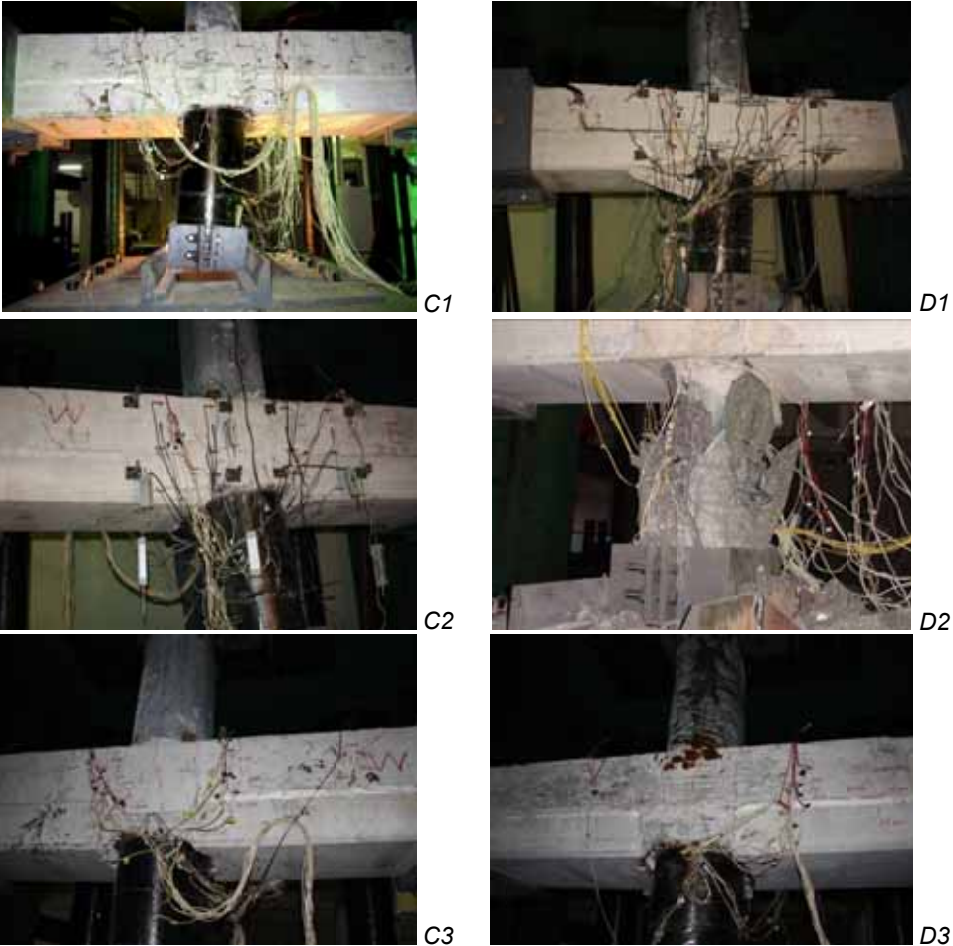


Fig. 135: Experimental samples at the end of cyclic test

Specimen	F_{max} (kN)	U_{max} (mm)	F_{min} (kN)	U_{min} (mm)
C1	930	115	-807	-90
C2	878	112	-902	-100
C3	828	105	-796	-90

Table 9: Cyclic strength and deformation capability for samples "C"

Specimen	F_{max} (kN)	U_{max} (mm)	F_{min} (kN)	U_{min} (mm)
D1	617	68	-617	-77
D2	728	28.5	-695	-31
D3	578	55	-574	-52

Table 10: Cyclic strength and deformation capability for samples "D"

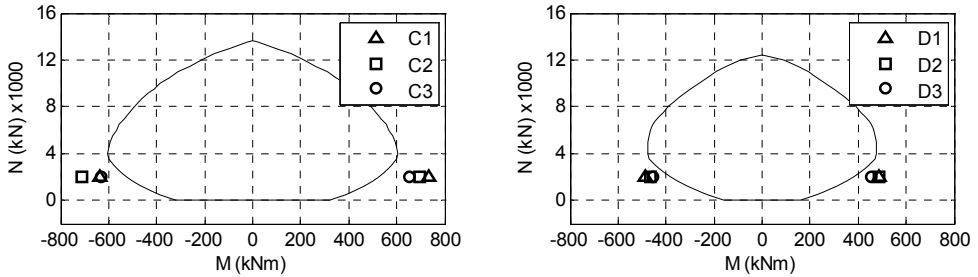


Fig. 136: M-N analytical domain and experimental results

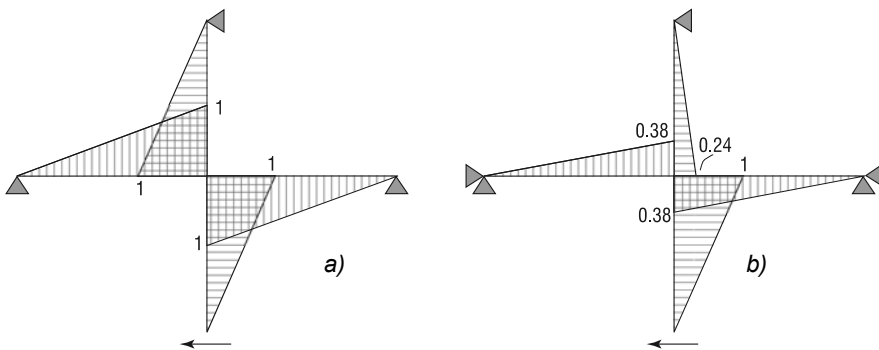


Fig. 137: Normalized bending moment elastic distribution depending on boundary conditions

Independently from attained strength level, force vs. displacement curves evidence a considerable pinching effect. When dealing with cyclic tests of monolithic emulative joints, this phenomena usually is a consequence of rebar's progressive debonding in the core-joint zone (cf.ch.0). In the tested joints this kind of

phenomena is highly unlikely for several reasons. Firstly, third party experimental tests prove the efficacy of lattice girder in assure adequate interaction with surrounding concrete and numerical simulations in chapter 5 confirm this evidence. Secondly, in the considered tests, solicitations acting on beams are limited and naked eyes observation confirms total absence of relative slipping between reinforcement and concrete. Finally, no debonding take place in column's reinforcement. The most likely way to explain the hysteresis cycles' shape is a rigid-body movement of the whole samples, due to supports' deformability. Experimental tests reported by Scotta & Tesser, 2011, confirm as correct filtering of recorded data accounting for supports' movement is usually required. This could explain the displacements with nearly zero reaction-force between unloading and subsequent reloading phases in recorded data. Besides, it justify a global stiffness of the samples lower than expected one. A tentative is done to filter out this contribute, acting on the recorded displacement time history, since acting on recorded forces would result excessively cumbersome. To partially remove the pinching effect from hysteresis cycles, the unloading branch get modified, replacing the linear trend with a parabolic one (Fig. 138). Subsequently the displacement is scaled, in order to filter out the fictitious stiffness effect, due to rigid body movement. A scale factor of 30% is assumed, looking at the fact that horizontal part of the unloading branch is almost 70% of the total (Fig. 139). Filtered curves are plotted in Fig. 140.

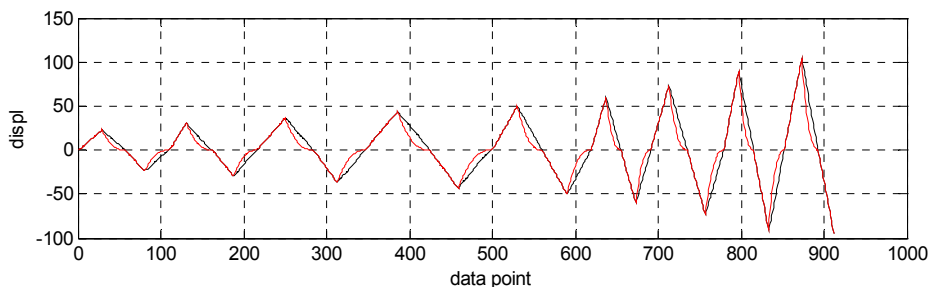


Fig. 138: Original (black) and filtered (red) displacement history

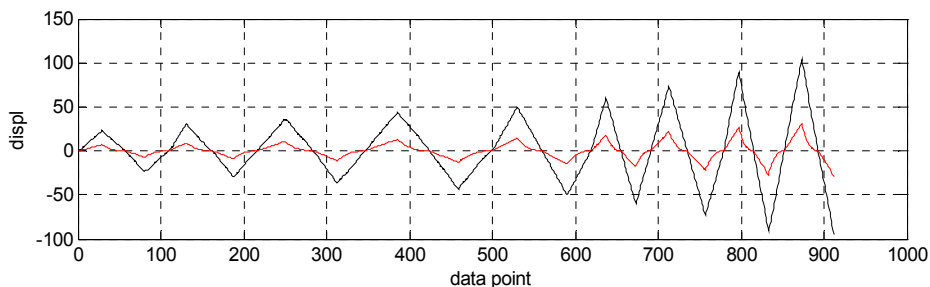


Fig. 139: Original (black) and filtered-scaled displacement history (red)

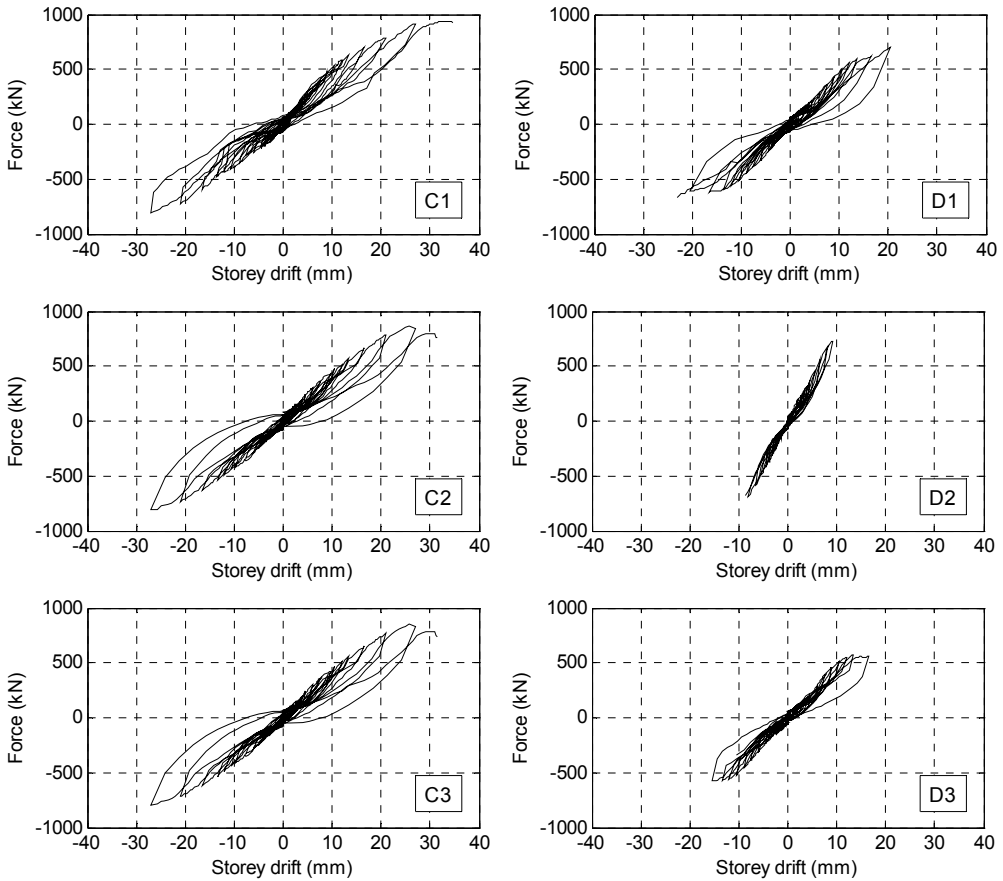


Fig. 140: Force vs. displacement filtered curves

3.4.3. Strain gauges on CSTC beam's truss

To investigate the role played by CSTC beam truss, results coming from samples C1 (strengthened) and D2 are directly compared. The remaining samples' experimental performances are analogous to the one recorded from specimen C1 and commenting each of them would be redundant.

Low strains on truss belonging to CSTC beams are recorded. Strains are considerably below the yielding limit, both for sample D2 and C1, despite this last is over-strengthened in order to favor plastic hinge development at beam ends.

This means that, CSTC beam does not provide any considerable strength contribute in the plastic hinge zone. Such a result confirms experimental evidences reported by Amato et al., 2010.

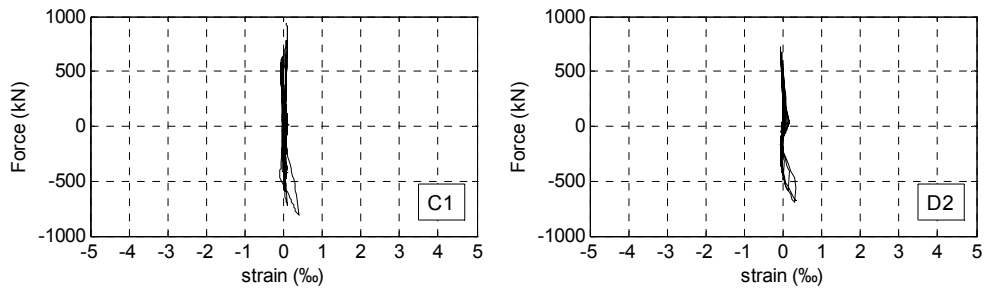


Fig. 141: Strain on CSTC beam trusses; longitudinal bar sensor G4

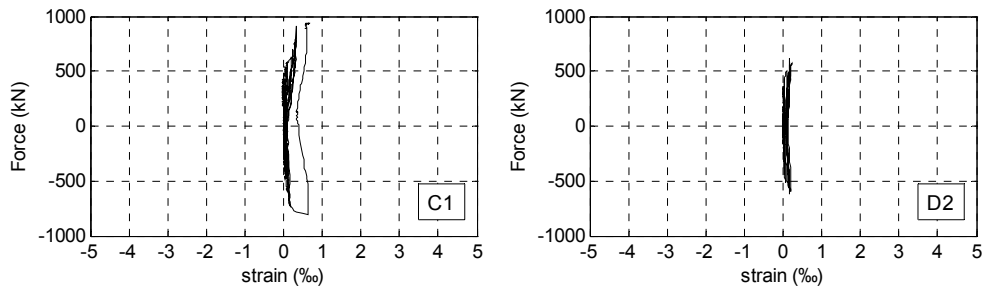


Fig. 142: Strain on CSTC beam truss; inclined bar sensor G5

3.4.4. Strain gauges on truss girder

As expected, reinforcement belonging to truss girders performed elastically in sample D2, due to premature failure of the column. Indeed, plastic deformations are recorded from specimen C1 confirming the effectiveness of the FRP column strengthening towards this aim. Upper (Fig. 143a) and lower (Fig. 145a) longitudinal bars yield in tension alternatively, under negative and positive bending respectively. Yielding penetration for lower bars is more than double the one experienced by upper bars. This is consistent with cracking spreading from the bottom side of the beam, very close to column face, that reduce progressively the effective beam's depth under positive bending. Only truss girder and surrounding concrete section is effective to bear bending in this condition. Conversely, previous crack tend to re-close under negative bending and effective section depth increase again, thus reducing stresses on the upper bars. A smeared cracking typify the upper beam side under this load condition. These evidences provide precious information about the effective section at beam-to-column interface to be considered for plastic hinge design: reinforcement provided by CSCT beam should be completely disregarded.

Only the reinforcement provided by lattice girder is strength-effective. Besides effective section depth to be considered is function of the bending sign.

Further information on the performance of lattice girder under cyclic loading are provided by the analysis of strain experienced by inclined bars (Fig. 144). Limited strains on these bar suggest limited bearing action against concrete and thus limited relative sliding between truss girder and surrounding concrete. It is a proof about possibility of this reinforcement typology to assure full interaction with concrete despite plain bars.

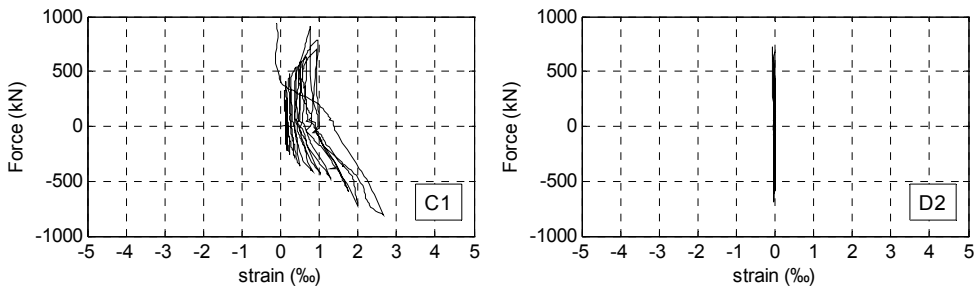


Fig. 143: Strain on lattice girder; upper longitudinal bars (sensor G1)

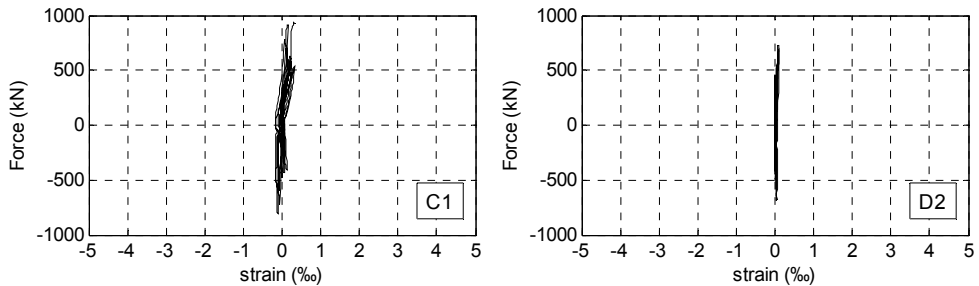


Fig. 144: Strain on lattice girder; inclined bar (sensor G2)

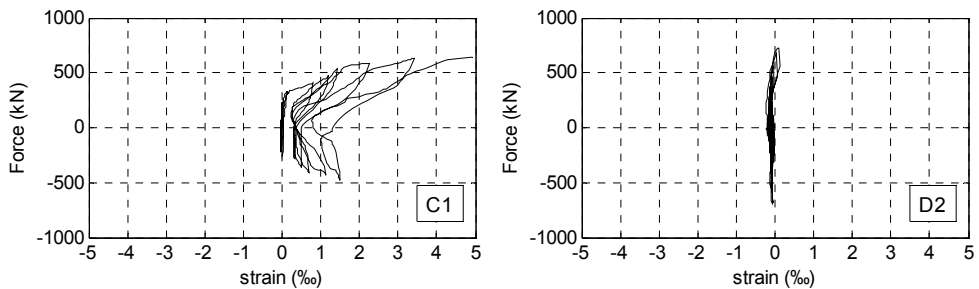
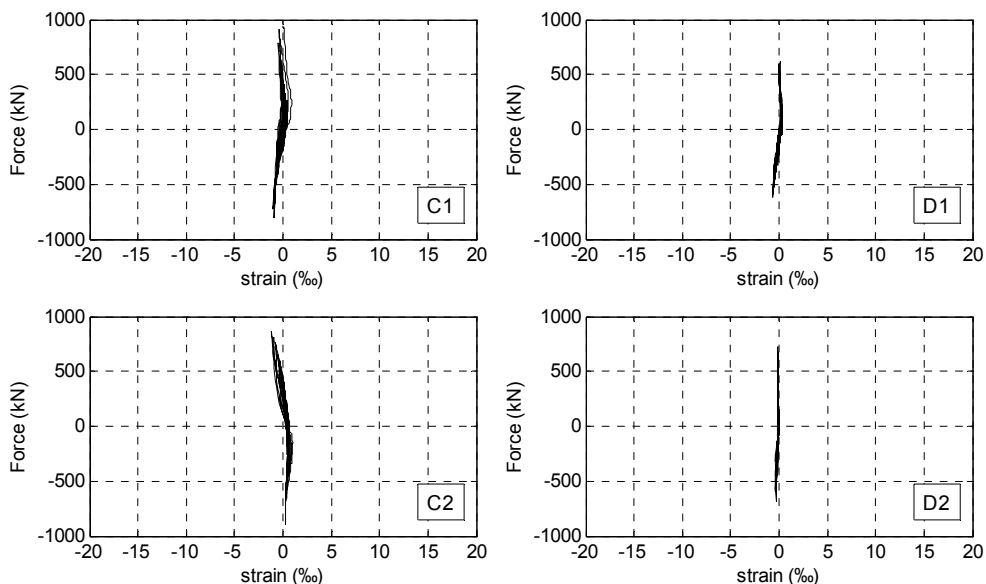


Fig. 145: Strain on lattice girder; lower longitudinal rebar (sensor G3)

3.4.5. Strain gauges on vertical plate

Interpretation of experimental data relative to steel joint vertical plates leads to two main remarks.

Firstly, they endorse the hypothesis about the role played by boundary conditions on cyclic tests' performances. Comparing strains coming from sensors S6 (higher joint's side, Fig. 146) and S7 (lower joint's side, Fig. 147), higher deformations are provided by sensor S7 for all samples. It indicates that a considerable bending moment is acting in the lower side of the steel joint, at column base and tends to reduce rapidly in the upward direction due to equilibrium conditions inside the core-joint. This trend is consistent with bending moment distribution reported in Fig. 137b, relative to boundary conditions with constrained beam-ends' horizontal translations. Secondly, from strain data coming from sensor S7 (lower joint side, Fig. 147), it is possible to notice that samples "C" reaches a consistent yielding, whereas samples "D" is characterized by a nearly elastic behavior, with just limited plasticization. Clearly, only in the first case, the bending strength of the core-joint is attained. This is confirmed by plotting experimental bending moment values at joint base for different samples, in the M-N strength domain estimated by analytical approach (Fig. 148). Bending moments are calculated as the horizontal reaction force multiplied by the lower column length, i.e. 790mm. Corresponding axial force level is assumed to be the one applied to samples prior to cyclic testing, namely 2000 kN. Samples "C" lies exactly on the edge of strength domain, while samples "D" lie inside it.



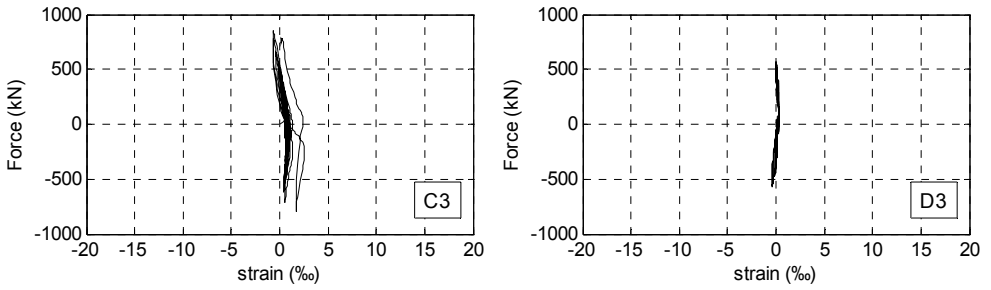


Fig. 146: Concrete strain-gauge location: sensor S6

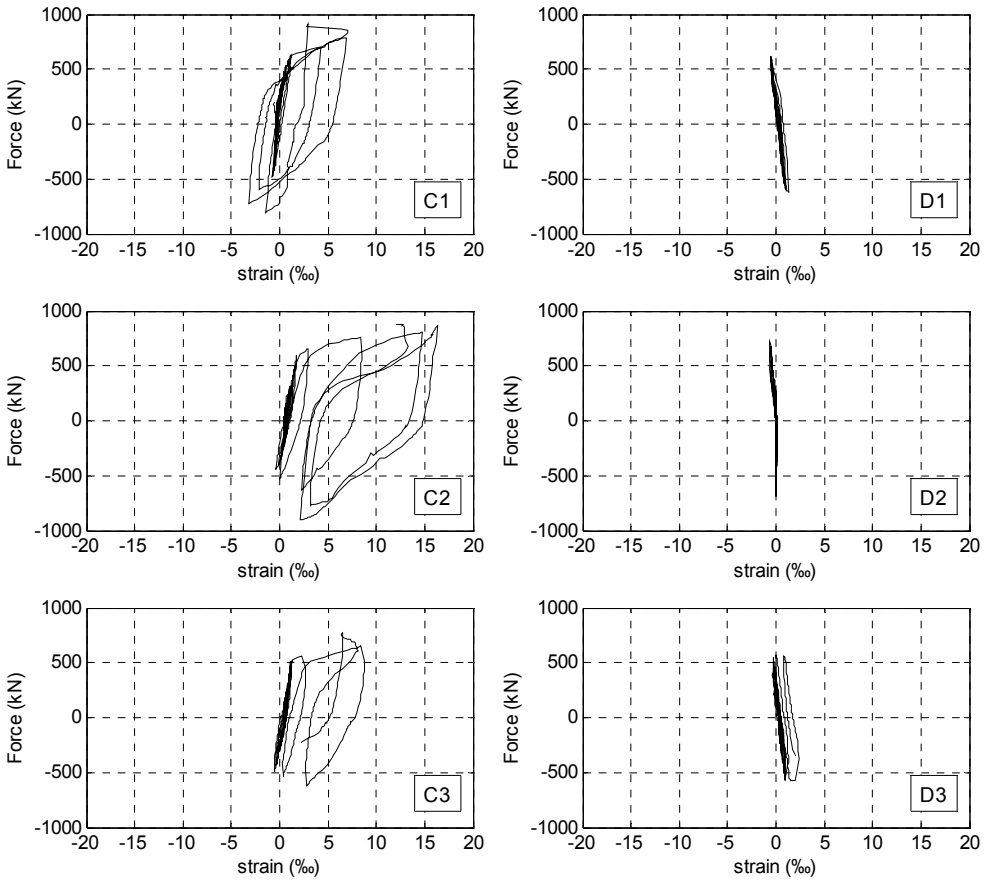


Fig. 147: Concrete strain-gauge location: sensor S7

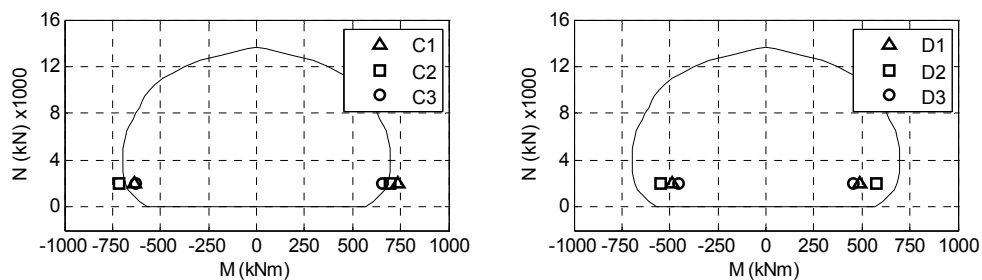


Fig. 148: M-N domain for concrete filled steel joint: analytical and experimental results

3.4.6. Displacement gauges on outer beam surface

The displacement transducer stuck on the outer beams' surface (Fig. 133) aims to measure the relative movement among the two beams, to capture inelastic effects like crack opening at beam to column interface, related to beams' plastic hinging. The ends of sensor are located 100 mm far from the lower beam edge and connect the two beam passing through the joint. In Fig. 149 data collected for samples C1 and D2 are reported. It is evident that in the second case the beam's end remained elastic, due to premature column failure. On the contrary, for sample C1, relevant relative displacement between beams was recorded, because of crack opening at beam-to-column interface. It is a further proof that strengthening of the lower column with FRP fabric led to formation of plastic hinge on beam. This is consistent with data related to plastic deformation of the truss girder recorded for the same sample (Fig. 143, Fig. 145).

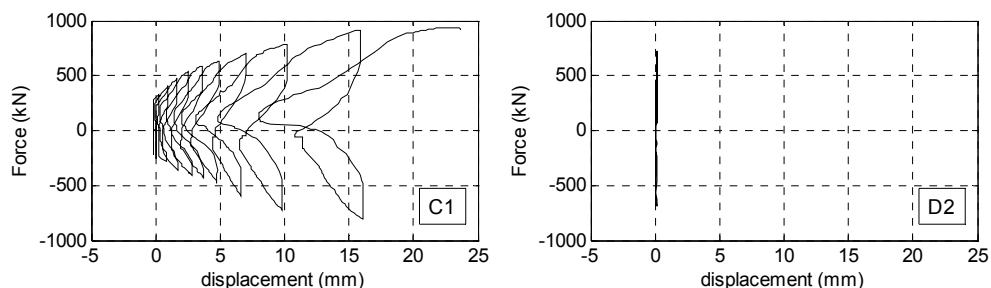


Fig. 149: Concrete strain-gauge location: sensor S7

3.4.7. Conclusions

Despite brittle unexpected failure characterized sample “D2”, due to unfavorable boundary conditions different from supposed ones, for all remaining sample FRP strengthening on lower column promoted a ductile behaviour.

This allowed to clarify the role played by truss girder and beam truss in the plastic hinge region, providing useful information for design.

Limited strains recorded from gauges applied on CSTC beam truss, in either sagging and hogging bending conditions, suggests that no resistance contribute is provided by this element in the plastic hinge zone. Such an evidence is consistent with experimental results reported by Amato et al., 2010.

On the contrary, active role played by lattice girder in the plastic hinge zone is remarked by consistent deformation of longitudinal rebars, with lower ones deformed more than double with respect to the upper ones. This suggests that beam’s effective depth changes during cyclic loading. In particular under sagging moment, missing longitudinal reinforcement passing through the joint in the lower beam’s side, cause a discrete cracking to spread progressively upwards until bare lattice girder result effective in providing bending strength. Under reversed loading, opened crack tend to re-close again, increasing the effective concrete section depth and thus reducing stresses (and strains) in the upper lattice girder longitudinal reinforcement. Data collected by displacements’ transducers along concrete beams and naked-eye-viewing of samples at the end of testing, confirm this trend.

Elastic response coming from inclined truss belonging to lattice girder suggests that bearing action against concrete is limited. As evidenced by Pushover FE analyses reported in chapter 5.2, limited strain and deformation on this component are always related to reduced relative slipping between lattice girder and surrounding concrete.

This means that when properly designed (cf. eq. 71) lattice girder is able to provide adequate strength and stiffness even under cyclic loading (Scotta & Tesser, 2011). From this point of view lattice girder appears rather more performant compared to usually adopted alternative to provide beam continuity, consisting in additional longitudinal reinforcement placed across the core joint (Amato et al., 2010).

Beside lattice girder issue, further considerations are even possible.

Owing to the column over-strength provided by FRP jacketing, a relevant bending is transferred inside the steel-core-joint. By comparison of analytical domain resistance estimated for composite core-joint with experimental data, a good agreement is found, leading then to a validation of analytical approach adopted to design this component.

Finally, it is important to highlight that under applied axial force level and during the whole cyclic testing, no concrete splitting phenomena took place. It means that a certain confinement level is provided by vertical steel plate on core concrete, despite lateral reinforcement is missing.

4. CONCRETE MODELLING

4.1. Introduction

Proper concrete modeling is a crucial issue when dealing with modeling of RC members. This is still more relevant in proposed beam-to-column precast joint, with different components made by different material: centrifuged High Strength Concrete (HSC) C75/90 for columns, Normal Strength Concrete (NSC) C30/37 for CSTC beams' base and NSC C25/30 cast concrete, required to provide a monolithic layout.

Since the 80's a considerable effort has been devoted to the definition of proper stress-strain relationships for concrete, both in tension (Hordijk et al., 1986) and compression (Sheikh & Uzumeri, 1980, Mander et al., 1984). Since the '90s, beneath NSC and mild steel reinforcement also performance of HSC ($f_c > 70\text{MPa}$) and high strength steel ($f_c > 600\text{MPa}$) started to be seriously investigated. Experimental tests evidenced in particular the less ductile compressive behaviour of HSC specimens compared to NSC ones (Fig. 150) and the need of minimum lateral reinforcement amount to provide adequate ductility. This caused even concern over the applicability of building code requirements for design and detailing of HSC columns, in particular for seismic regions (ACI 441-R96). Correct accounting of descending branch is a fundamental issue for proper simulation of RC elements' performance, especially when they undergo large plastic deformations. Adopted compression model should be able to account for different confinement conditions provided by lateral reinforcement and for a wide range of concrete grades. The main problem is that most of the empirical models proposed by different authors through the years result effective in interpreting only their own tests' results or selected data. In the following a review is presented about main compressive concrete models available from literature. Experimental tests on real scale columns under axial compression provided by Sharma et al., 2005 are used for a comparative study to highlight the most proper model. Also Nation and International code provisions are recalled to provide further details on the topic.

Finally a chapter is spent about numerical concrete modeling issue, both in tension and compression.

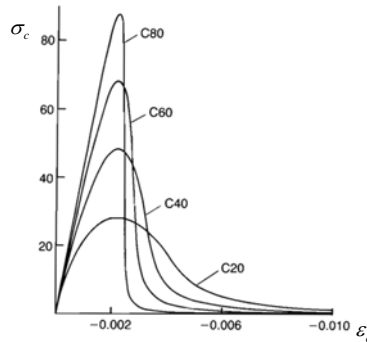


Fig. 150: Typical concrete compression response as reported in Model Code 90

4.2. Compression models

The main issue when dealing with analytical formulation of concrete behaviour under compression is the definition of proper softening branch able to account for different confinement pressure, depending on sample's reinforcement.

Two main approaches for experimental testing of concrete performances are recognizable in literature.

The first one consists of compressive tests on real scale columns' samples, with different stirrups geometry and material properties. Main parameters investigated are:

- volumetric ratio of lateral reinforcement
- stirrups spacing
- yield strength of transverse reinforcement
- longitudinal reinforcement ratio
- lateral steel configuration
- shape of cross section
- concrete compressive strength

Starting from available experimental data, lateral reinforcement arrangement is converted into equivalent analytical hydrostatic confining pressure. In general such pressure level is not constant and is dependent both from the lateral dilation of the

concrete under axial load and from the stress-strain relationship of the confining steel. In current survey, following concrete models are considered

- Mander & Priestley, 1988
- Nagashima et al., 1992
- Cusson & Paultre, 1995
- Razvi & Saatcioglu, 1999
- Légeron & Paultre, 2003
- Cusson (2008)

The second approach available from literature is the experimental testing of concrete in compression adopting confinement provided by fluid pressure. In general a more stiff response is evidenced in these testing's typology, cause initial shear cracks on specimens are prevented by active confining pressure. Attard & Setunge, 1996 suggest that, for low confining pressures, when the ratio of the confining stress to maximum axial stress is less than 0.15, there is little difference between the ultimate strength obtained using either active or passive confinement. In this paper the model proposed by Cui & Sheikh, 2010 is considered, which is an update of Attard & Setunge, 1996 model. Being necessary a prediction about equivalent effective confinement pressure, depending on lateral reinforcement's arrangement, formulation by Cusson & Paultre, 2008 is adopted.

4.2.1. *Mander model (1988)*

The model developed by Mander & Priestley, 1988 is considered for this survey, since it represents a famous and commonly used approach for modeling NSC in compression. Furthermore these authors contributed considerably in understanding of the role played by lateral steel in providing confinement. The analytical model they proposed, is valid still today and represents a sound basis in design of reinforced concrete members.

When unconfined concrete is subjected to compression stress level approaching the crushing strength, high lateral tensile strains develop as a result of the formation and propagation of longitudinal micro-cracks. This phenomena leads to instability of the compression zone, and subsequent failure. Close-spaced transverse reinforcement in conjunction with longitudinal rebars acts to restrain the lateral expansion of the concrete, enabling higher compression stresses and strains to be sustained by the compression zone before failure occurs. As originally suggested by Sheikh & Uzumeri, 1980, this effect take place cause transversal reinforcement

elements are placed in tension by the expanding concrete and an arching action is assumed to act on it, in the form of parabolas, with initial tangential slope of 45 degrees.

In this model it is supposed that yield limit is attained by transversal reinforcement. In the simplified case of compressed concrete encased in a steel tube with thickness t , equivalent confining action acting on the concrete is defined by equation 11, based on fluid hydrostatic analogy:

$$f_l = \frac{2f_h t}{d} \tag{11}$$

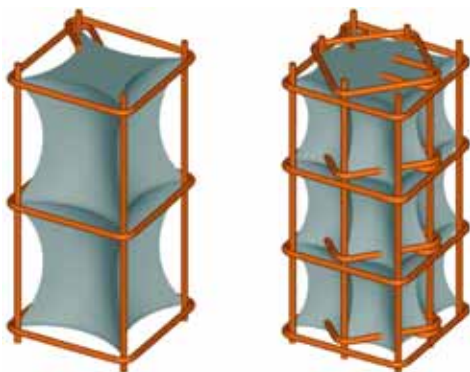


Fig. 151: Arching effect provided by lateral reinforcement (Légeron & Paultre, 2003)

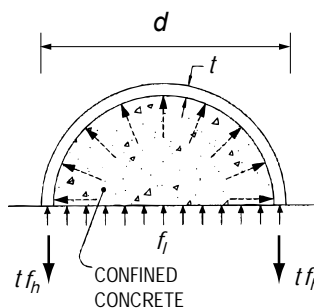


Fig. 152: Confinement provided by a steel tube

Similarly, by pure equilibrium consideration, the maximum lateral confining pressure provided by circular hoops is given by

$$f_l = \frac{f_{y, st} A_{st}}{d s} = \rho_{st} A_{st} \tag{12}$$

where $f_{y, st}$ =yield stress of the transverse steel reinforcement; A_{st} =total cross section area of the hoop in one direction; ρ_{st} =transverse steel ratio; d =hoop diameter; and s =center to center hoop spacing.

Square hoops, differently from circular ones, can apply full confining reactions only near the corner of the hoops, because the pressure of the concrete tend to bend the sides outward. For accounting this effects, square section should be transformed into equivalent circular tube (equivalent column concept, Légeron & Paultre, 2003) .The equivalent steel tube thickness is defined as:

$$t_{eq} = k_s \frac{A_{st,y}}{2s} \quad (13)$$

where k_s =coefficient of confinement efficiency for the considered section; $A_{st,y}$ =total cross section area of the hoop in y direction

and correspondent confining pressure as:

$$f_l = k_s \rho_{st} f_{y,st} \quad (14)$$

$$\rho_{st} = \frac{\sum_{i=1}^q (A_s \sin \alpha)_i}{sc} \quad (15)$$

where q =number of tie legs that cross the side of core concrete for which the average lateral pressure f_l is being computed and α =the inclination of considered tie.

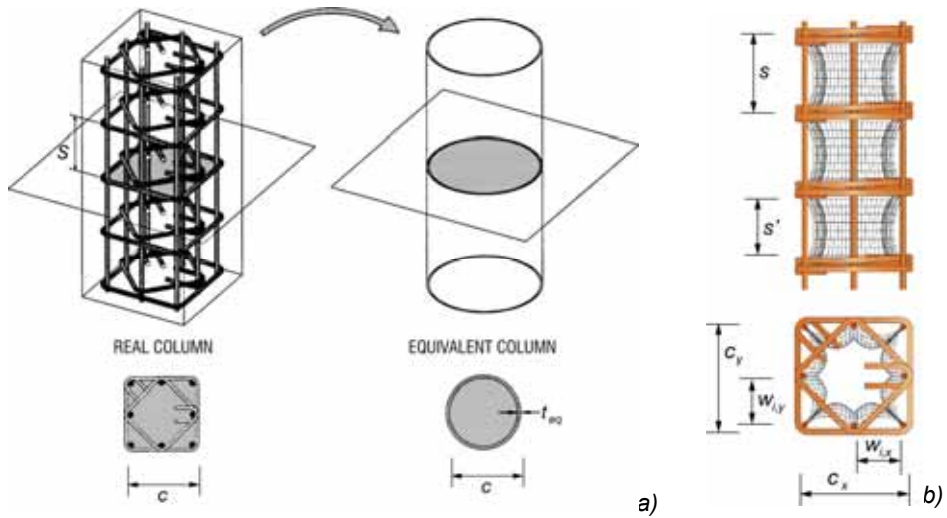


Fig. 153: a) Equivalent column concept for square section; b) main geometry parameters

Eq. 14 is based on the approach proposed by Sheikh & Uzumeri, 1980. The efficiency coefficient k_s for the confining transverse steel is given by Sheikh & Uzumeri, 1982 and Mander et al., 1984:

$$k_s = k_{es} k_v \quad (16)$$

where k_{es} =coefficient of horizontal efficiency defined as

$$k_{es} = \frac{1 - \sum (w_{xi}^2 + w_{yi}^2) / 6c_x c_y}{1 - \rho_{cc}} \quad k_{es} = 1 \text{ for circular cross section.} \quad (17)$$

and k_v is the coefficient of vertical efficiency defined as:

$$k_v = \frac{\left(1 - \frac{s'}{2d_s}\right)^2}{1 - \rho_{cc}} \quad \text{for circular columns confined with stirrups} \quad 18)$$

$$k_v = \frac{\left(1 - \frac{s'}{2d_s}\right)}{1 - \rho_{cc}} \quad \text{for circular columns confined with spirals} \quad 19)$$

$$k_v = \frac{(1 - s'/2x)(1 - s'/2y)}{1 - \rho_{cc}} \quad \text{for rectangular beam} \quad 20)$$

where c_x, c_y = the dimension of confined core to the centreline of the hoop; w_{xi}, w_{yi} =distances between two longitudinal bars along the two main directions in the cross section plane; ρ_{cc} =longitudinal steel ratio; d_s =diameter of the stirrups/spirals; and s' =net distance between two stirrups/spirals.

For a rectangular section two different confinement pressure values can be computed for the cross section in the x and y direction

An average lateral confining pressure value could be defined as

$$f_l = k_s \rho_{st} f_{y,st} \quad \rho_{st} = (\rho_{st,x} + \rho_{st,y}) / 2 \quad 21)$$

where ρ_{st} =effective transversal reinforcement ratio as define by Mander & Priestley, 1988.

Alternative to equation 21, the correct account of transversal confinement ratio ρ_{st} can defined as proposed by Richart & Brandtzaeg, 1928:

$$\rho_{st} = \frac{A_{st,x} + A_{st,y}}{s(c_x + c_y)} \quad 22)$$

The increased peak compressive stress resistance and corresponding strain due to confinement pressure f_l is defined as:

$$f_{cc} = f_{co} \left(-1.254 + 2.254 \sqrt{1 + \frac{7.94 f_l}{f_{co}}} - 2 \frac{f_l}{f_{co}} \right) \quad 23)$$

$$\varepsilon_{cc} = \varepsilon_c \left[1 + 5 \left(\frac{f_{cc}}{f_c} - 1 \right) \right] \quad 24)$$

where f_{cc} = max. confined concrete strength; f_{co} = max. unconfined concrete strength and ε_c = unconfined concrete strain at peak stress.

The strain at peak stress given by equation 24 does not represent the maximum useful strain for the design purposes, as high compression stresses can be maintained at strains several times larger, depending from the effective confinement conditions. Mander & Priestley, 1988 suggest that a useful limits occurs when transverse confining steel fractures. This strain level may be estimated by equating the strain energy capacity of the transverse steel at fracture to the increase in energy adsorbed by the concrete. A conservative estimate for ultimate compression strain is given by Paulay & Priestley, 1992:

$$\varepsilon_{ccu} = 0.004(= \varepsilon_{cu}) + 1.4\varepsilon_{su} \frac{\rho_{st} f_{y,st}}{f_{cc}} \quad \rho_{st} = \rho_{st,x} + \rho_{st,y} \quad 25)$$

where ε_{ccu} =confined concrete limit strain; ε_{cu} =unconfined concrete limit strain; ε_{su} =transversal steel limit strain (5% from Mander).

Panagiotakos & Fardis, 2001 making reference to a database of more than 1000 tests on specimens representative of various type of RC members (beams, columns and walls), propose a modification to estimate limit strain:

$$\varepsilon_{ccu} = 0.004(= \varepsilon_{cu}) + 0.6\varepsilon_{su} \frac{\rho_{st} f_{y,st}}{f_{cc}} \quad \rho_{st} = \rho_{st,x} + \rho_{st,y} \quad 26)$$

The stress-strain relationship for confined concrete illustrated in Fig. 154, based on formulation suggested by Popovics, 1973, covers both ascending a post-peak branch:

$$f_c = f_{cc} \left[\frac{k(\varepsilon/\varepsilon_{cc})}{k-1+(\varepsilon/\varepsilon_{cc})^k} \right] \quad k = \frac{E_c}{E_c - E_{sec}} \quad 27)$$

where f_{cc} =max. confined concrete strength, E_{sec} =secant modulus of elasticity of confined concrete (f_{cc}/ε_{cc}) and E_c =modulus of elasticity of unconfined concrete.

To define the stress-strain behavior of the cover concrete, the same formulation reported in eq. 27 is used, by substituting f_{cc} and ε_{cc} , respectively with the unconfined strength $f_{c,0}$ and corresponding peak strain $\varepsilon_{c,0}$. The part of the falling branch in the region where $\varepsilon > 2\varepsilon_{c,0}$ is assumed to be a straight line which reaches zero stress at the spalling strain, ε_{sp} (usually assumed to be 0.005).

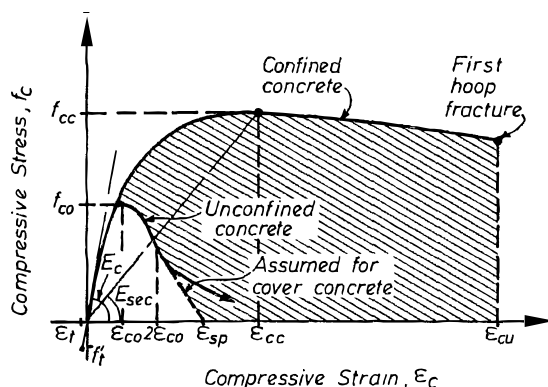


Fig. 154: Adopted stress-strain model from Mander & Priestley, 1988

4.2.2. Nagashima Model (1992)

Nagashima et al., 1992 propose a stress-strain relationship for HSC calibrated on 26 different square specimens (225x225x776mm) with compressive strength between 59 and 118 MPa, laterally reinforced with ties of yield strength 784 and 1374 MPa, tested under monotonic axial loading with different tie configurations.

Following formulation for confined compressive strength f_{cc} and corresponding strain ϵ_{cc} is found by regression fitting on available data from tests:

$$f_{cc} = f_c + 3.41 \sqrt{k_s \cdot \rho_{st} \cdot f_{y,st}} \quad (28)$$

$$\epsilon_{cc} = \epsilon_c \left[138 \left(\frac{k_s \rho_{st} f_{y,st}}{0.85 f_c} \right)^2 + 1 \right] \quad (29)$$

where k_s =confinement effectiveness factor (eq. 16), ρ_{st} =transverse steel ratio, $f_{y,st}$ =yield stress of the transverse steel reinforcement, ϵ_c =unconfined concrete strain at peak strength.

The shape of the stress-strain formulation in the post-peak branch is defined by the ϵ_{cc50} parameter, which is the strain corresponding to 50% of residual strength:

$$\epsilon_{cc50} = \epsilon_c + 0.193 \left(\frac{k_s \rho_{st} f_{y,st}}{0.85 f_c} \right) \quad (30)$$

This strain can be assumed like ultimate strain ϵ_{ccu} for confined concrete, as suggested by CEB-FIP Model Code 90 (International Federation for Structural Concrete (FIB), 1993). The shape of the constitutive model is defined by the

Popovics, 1973 model for the ascending branch and a linear descending segment for post-peak branch, respectively.

$$f_c = f_{cc} \left[\frac{k(\varepsilon/\varepsilon_{cc})}{k-1+(\varepsilon/\varepsilon_{cc})^k} \right] \quad k = \frac{E_c}{E_c - E_{sec}} \quad 0 \leq \varepsilon_c \leq \varepsilon_{cc} \quad (31)$$

$$f_c = f_{cc} \left[1 - 0.5 \frac{\varepsilon_c - \varepsilon_{cc}}{\varepsilon_{cc50} - \varepsilon_{cc}} \right] \geq 0.3 f_{cc} \quad \varepsilon_c \geq \varepsilon_{cc}$$

where f_{cc} =max. confined concrete strength, E_{sec} = secant modulus of elasticity of confined concrete calculated as stated in eq. 27 and E_c = modulus of elasticity of unconfined concrete

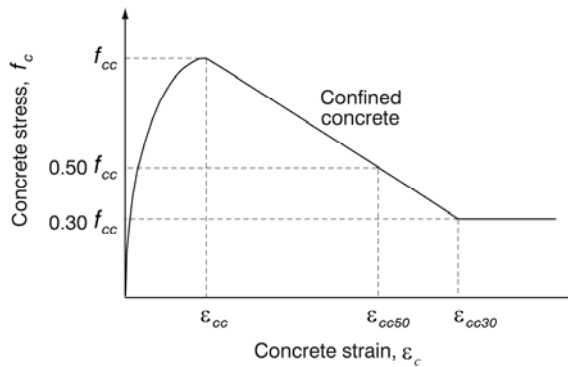


Fig. 155: Adopted stress-strain model for confined concrete (Nagashima et al., 1992)

4.2.3. *Cusson and Paultre Model (1995)*

Cusson & Paultre, 1995 propose a stress-strain relationship to model HSC, calibrated through the results provided 50 large-scale HSC tied columns tested under concentric loading; out of them, 30 HSC tied columns (235x235x1400 mm) were tested by the Cusson, 1994 and 20 HSC tied columns (225x225x715 mm) were the one tested by Nagashima et al., 1992. It is then interesting the approach of the authors of broadening the experimental data horizon, to make their proposal as general as possible.

The concrete compressive strengths of the samples ranged between 60 to 120 MPa. The proposed model takes into account tie yield strength, tie configuration, transverse reinforcement ratio, tie spacing, and longitudinal reinforcement ratio.

Proposed relationship aims to fit better the behaviour of such specimens that exhibits a less ductile behaviour than normal-strength concrete (NSC).

In equation 25 and 26 the confinement index $\rho_{st}f_{y,st}/f_{cc}$ is considered as an indicator of the confinement efficiency of reinforced concrete columns, based on the assumption that yielding of transversal reinforcement occurs.

However columns with various tie configurations or tie spacings may present very different responses, while having the same confinement index. Moreover, if the yield stress is not developed in the transverse reinforcement when the confined concrete reaches its maximum strength, the confinement index above defined could overestimate the real degree of confinement in the column. Observation of earlier experimental data provided by Sheikh & Uzumeri, 1980 shows that yield is not always reached, even with normal strength concrete columns.

Experimental studies conducted by Cusson, 1994 and Li et al., 1994 show that yield strength may not be reached at peak, especially with low confinement ratio or transverse reinforcement made of high-yield-strength steel ($f_y > 800\text{MPa}$).

To account the real confining condition provided by lateral steel, Cusson and Paultre (1995), re-arranging eq. 20 and 21, proposed to use the actual steel stress to compute the confinement pressure:

$$f_l' = k_s \rho_{st} f_{eff,st} \tag{32}$$

where f_l' =effective confinement pressure, $f_{eff,st}$ = effective stress state on lateral confining rebar and k_s = geometrical effectiveness factor (see equation 16 to 20).

The authors introduce the ‘*effective confinement index*’ as an indicator of confinement efficiency

$$I_e' = f_l' / f_c \tag{33}$$

Based on a regression fit on available data, following relationship were found to take into account confinement effect on concrete behaviour:

$$f_{cc} = f_c [1 + 2.1(I_e')] \tag{34}$$

$$\varepsilon_{cc} = \varepsilon_{c0} + 0.21(I_e')^{1.7} \tag{35}$$

Determine the I_e' value is not a trivial problem; in fact for determining the strain (and corresponding stress) in the confining steel, following expression must be solved:

$$\varepsilon_{eff,st} = \nu_{cc} \varepsilon_{cc} - \frac{(1 - \nu_{cc}) f_l'}{E_{cc}} \tag{36}$$

where $\varepsilon_{eff,st}$ =effective strain in confining steel, ν_{cc} =‘equivalent’ Poisson’s coefficient evaluated at peak stress (assumed value 0.5) and E_{cc} =‘equivalent’ secant modulus of elasticity at peak stress (f_{cc}/ε_{cc}).

Eq. 33 relates $\varepsilon_{eff,st}$ to ε_{cc} and indirectly to f_{cc} ; however, it is well-known that the strength and ductility gains are related to the amount of confinement provided to the columns together with the stress value in the confinement reinforcement (Sheikh & Uzumeri, 1980). This is an implicit problem, traditionally solved by assuming that the transverse reinforcement reaches the yield limit at the peak stress (Mander & Priestley, 1988, Nagashima et al., 1992, Li et al., 1994). Conversely, Cusson & Paultre, 1995 introduced an iterative procedure to provide a solution: equilibrium is attained when the effective deformation in confining steel $\varepsilon_{eff,st}$ determined from eq. 36 is consistent with the effective stress $f_{eff,st}$ got from eq. 32.

Finally to complete the proposed stress-strain relationship for confined concrete the ultimate strain is determined through the following expression:

$$\varepsilon_{ccu} = \varepsilon_{cc50} = \varepsilon_{c50} + 0.15(f_1 / f_{co}) \quad f_1 = k_s \rho_{st} f_{y,st} \quad (37)$$

where ε_{cc50} =concrete strain corresponding to 50% of residual strength associated to ultimate strain value for confined concrete; ε_{c50} =concrete strain corresponding to 50% of residual strength associated to ultimate strain for unconfined concrete (suggested value, $\varepsilon_{c50}=0.004$).

In the determination of ε_{cc50} from equation 37 the effective confinement pressure f_1 with steel stress set equal to the yielding value is adopted, being expected that at such large deformations, the transverse rebars should be yielding.

The stress-strain relationship for confined concrete can be completely defined given two points: the confined compressive strength f_{cc} corresponding to a strain ε_{cc} , and the post-peak axial strain ε_{cc50} .

The ascending branch is equal to Mander & Priestley, 1988 formulation (see eq. 27). The descending branch is a modification of the relationship originally proposed by Fafitis & Shah, 1985 to model confined column in compression:

$$f_c = f_{cc} \exp\left[k_1 (\varepsilon_c - \varepsilon_{cc})^{k_2}\right] \quad \varepsilon_c \geq \varepsilon_{cc} \quad (38)$$

$$k_1 = \frac{\ln 0.5}{(\varepsilon_{cc50} - \varepsilon_{cc})} \quad k_2 = 0.58 + 16(f_1 / f_{co})^{1.4} \quad (39)$$

For well-confined concrete, k_1 is large and produces a smooth falling branch, while for light-confined concrete, k_1 is small and produces a steep falling trend. The

coefficient k_2 controls the curvature of the descending branch. For well confined concrete, k_2 is large and produces a convex falling branch, while for light-confined concrete, k_2 is small and produces a concave falling branch.

Setting $k_2 = 1.5$, the proposed model can be used also for the prediction of unconfined concrete behaviour.

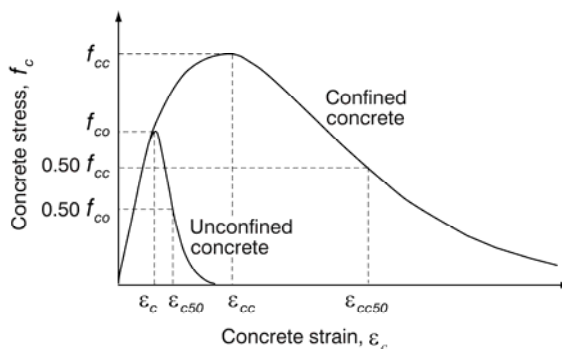


Fig. 156: Adopted stress-strain model for concrete (Cusson & Paultre, 1995)

4.2.4. Razvi model (1999)

Razvi & Saatcioglu, 1999 propose a model for confined NSC and HSC columns using extensive test data provided by own test results (Razvi & Saatcioglu, 1996) as well as by other research studies (Yong et al., 1988, Itakura & Yagenji, 1992, Nagashima et al., 1992, Cusson, 1994), for a total of 266 columns' tests. These included full size specimens characterized by different shapes, sizes, reinforcement configurations, tie yield strength (400 to 1387 MPa) and concrete strengths (30 to 130 MPa). The parameters incorporated in this model are type, volumetric ratio, spacing, yield strength, and arrangement of transverse reinforcement, distribution and amount of longitudinal steel as well as concrete strength and section geometry. Similarly to Cusson & Paultre, 1995, the authors state the problem of evaluating the real degree of confinement of RC section, considering not only geometry an arrangement of stirrups, but also effective stress $f_{eff, st}$, that could be sensible lower than yielding one. The authors conclude that supposing yielding of transverse steel for computing confined concrete strength produces fairly accurate predictions for NSC confined with normal-strength steel (Saatcioglu & Razvi, 1992). On the other hand, lateral confinement pressure required for HSC may be significantly higher than NSC.

Based on regression of available data, the following formulation is proposed for determining the effective stress $f_{eff,st}$ on confining rebars, replacing the iterative procedure proposed by Cusson & Paultre, 1995.

$$f_{eff,st} = E_s \left(0.0025 + 0.04 \sqrt[3]{\frac{k_2 \rho_c}{f_{c,0}}} \right) \leq f_{y,st} \quad k_2 = 0.15 \sqrt{\left(\frac{c_{x,y}}{s} \right) \left(\frac{c_{x,y}}{w_{x,y}} \right)} \leq 1 \quad 40)$$

where c_x, c_y =the dimension of confined core to the centreline of the hoop; w_x, w_y =distances between two longitudinal bars along the two main directions (x, y) in the cross section plane; s =spacing of transverse reinforcing; E_s =steel elastic modulus; $f_{c,0}$ =unconfined concrete strength.

The average confining pressure f_l is computed as reported in equation 32. For rectangular and square columns with different pressure in two orthogonal directions, resulting from different tie arrangements in two directions, a weighted average should be used:

$$f_l = \frac{f_{l,x}' c_x + f_{l,y}' c_y}{c_x + c_y} \quad 41)$$

where c_x, c_y = the dimension of confined core to the centreline of the hoop and $f_{l,x}', f_{l,y}'$ are the confining pressure along the two orthogonal direction of the section.

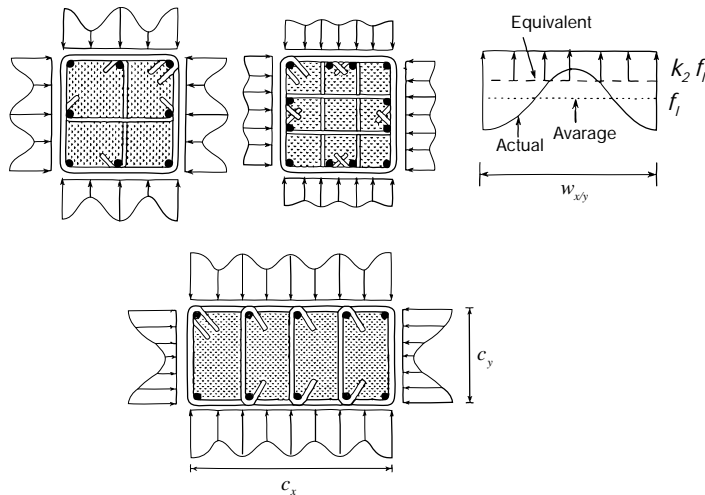


Fig. 157: Lateral confining action (Razvi & Saatcioglu, 1999)

The peak compressive strength is defined as:

$$f_{cc} = f_c + k_1 f_l' \quad k_1 = 6.7 (f_l')^{-0.17} \quad (42)$$

A two part stress-strain model get proposed by the authors in the form of an ascending parabolic branch up to peak and a linear descending branch up to 20% of the peak stress (Fig. 158). For the ascending branch the formulation made by Mander & Priestley, 1988 is adopted (equation 27). The descending branch is the same proposed by Saatcioglu & Razvi, 1992 in their original model developed for NSC. The slope of this segment is defined by the strain corresponding to 85% of the peak stress ϵ_{cc85} , with the role played by concrete and steel strength, introduced through the coefficients k_3 and k_4 , respectively.

$$\epsilon_{cc} = \epsilon_c (1 + 5k_3 K) \quad K = \frac{k_1 f_l'}{f_c} \quad (43)$$

$$\epsilon_{cc85} = 260k_3 \rho_{st} \epsilon_{cc} [1 + 0.5k_2 (k_4 - 1)] + \epsilon_{c85} \quad (44)$$

$$k_3 = \frac{40}{f_c} \leq 1.0 \quad k_4 = \frac{f_{yd}}{500} \leq 1.0 \quad (45)$$

If no available experimental data, an estimation for ϵ_{c85} and ϵ_c is provided by equation 46:

$$\epsilon_c = 0.0028 - 0.008k_3 \quad \epsilon_{c85} = \epsilon_c + 0.0018k_3^2 \quad (46)$$

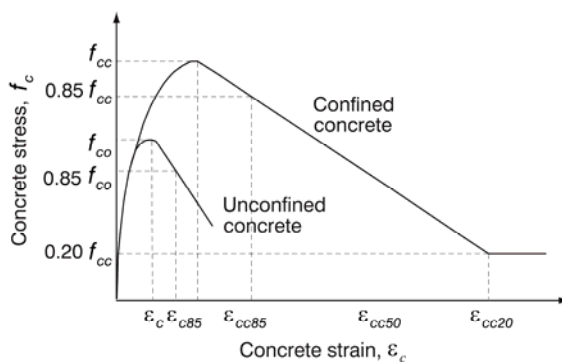


Fig. 158: Adopted stress-strain model from Razvi & Saatcioglu, 1999

4.2.5. Legeron model (2003)

Based on the work made by Cusson & Paultre, 1995, Légeron & Paultre, 2003, define a compressive concrete model suitable for both NSC and HSC. The model is validated on 210 square and circular columns tested under concentric compression. Also 50 square and circular columns under constant axial load and reversed cyclic bending are used to assess of the model effectiveness for seismic-type loading. The authors adopt an expression similar to equation 32 for computing the effective confinement pressure f_l' , with the only different that the average confinement ratio ρ_{st} , is replaced by the confinement ratio considering the total rebar area $A_{st,y}$, parallel to considered bending direction.

$$f_l' = k_s \rho_{st,y} f_{eff,st} \quad \rho_{st,y} = A_{st,y} / (s c_y) \quad (47)$$

The authors propose to adopt the same effective confinement index $I_e' = f_l' / f_{cc}$ as defined in eq. 33 for evaluating both the peak stress and corresponding strain. Based on the work by Cusson & Paultre, 1995, new relations are introduced for f_{cc} and ε_{cc} that cover a broader concrete strength range.

$$f_{cc} = f_c \left[1 + 2.4 (I_e')^{0.7} \right] \quad (48)$$

$$\varepsilon_{cc} = \varepsilon_{c0} \left[1 + 35 (I_e')^{1.2} \right] \quad (49)$$

The iterative procedure for determining the effective confinement index value (Cusson & Paultre, 1995) and in particular the effective lateral pressure f_l' , is replaced by a simplified graphical method. The approach is based on the strain compatibility hypothesis, namely the assumption that the outer concrete is strained to the same level of ties (see equations 48 and 49 together with equations 33 and 36). Assuming $E_{cc} = \alpha f_{cc} / \varepsilon_{cc}$, where $\alpha > 1$, the 'strain compatibility condition' lead to following expression:

$$\frac{\varepsilon_{eff,st}}{\varepsilon_c} = \left[1 + 35 (I_e')^{1.2} \right] \left[\nu_{cc} - \frac{1 - \nu_{cc}}{\alpha} \times \frac{I_e'}{1 + 2.4 (I_e')^{0.7}} \right] \quad (50)$$

where ν_{cc} is the 'equivalent' Poisson coefficient for confined concrete.

Fig. 159 presents experimentally determined $\varepsilon_{eff,st} / \varepsilon_c$ values obtained from 80 columns tested under uniaxial compression (Sheikh & Uzumeri, 1980, Sheikh &

Toklucu, 1993, Mander et al., 1984, Nagashima et al., 1992, Cusson, 1994). Fig. 159 also reports equation 50 for $\nu_{cc} = 0.43$ and $\alpha = 1.1$. Considering the high level of uncertainties in the measurement of strain in ties, the predictions are in good agreement with experimental results. The following simpler formulation which also provide good correlation with the test data is reported by Cusson & Paultre, 1995:

$$\frac{\epsilon_{eff,st}}{\epsilon_c} = 0.25 + 10I_e' \quad \nu_{cc} \geq 0.43 \tag{51}$$

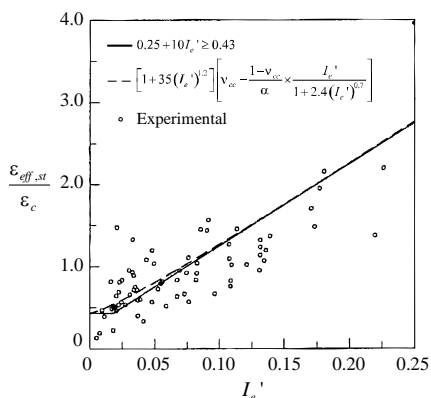


Fig. 159: strain compatibility condition

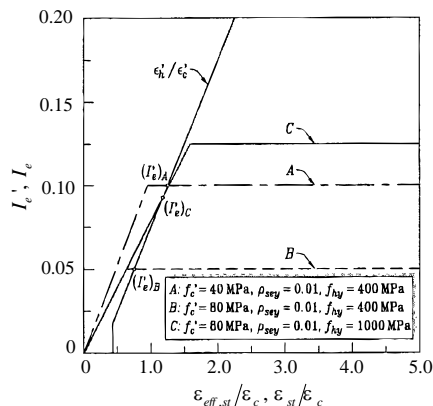


Fig. 160: Graphic determination of $\epsilon_{eff,st}/\epsilon_c$

On the same graphic it is also possible to plot the normalized stress-strain relationship of the confining steel:

$$\bar{\sigma} = I_e = \rho_{st,y} \frac{\sigma_{s,st}}{f_c} \quad \bar{\epsilon} = \frac{\epsilon_{s,st}}{\epsilon_c} \tag{52}$$

This relation is plotted in Fig. 160 for 3 column configurations considering elastic, perfectly plastic steel's relationship. Equation 51 is also plotted. Since both equations 51 and 52 should be satisfied simultaneously, the peak strength of concrete should occur at the intersection point. The iterative procedure mentioned for the Cusson & Paultre, 1995 model, is intended to find this intersection point. The abscissa of this point graphically determined, provides the effective confinement index I_e' .

From this equation, it is evident that the more a column is confined, the more it is able to effectively stress the yield transverse reinforcement to yield limit. This fact confirms that even normal-strength-rebar may not yield if un-sufficient confinement ratio ρ_{st} is provided, as reported by Sheikh & Uzumeri, 1980 and Cusson, 1994.

Finally to define the stress-strain relationship for confined concrete following expression is proposed for evaluate the post-peak strain ε_{cc50} , corresponding to strain at 50% of the maximum stress

$$\varepsilon_{ccu} = \varepsilon_{cc50} = \varepsilon_{e50} [1 + 60I_{e50}] \quad (53)$$

where I_{e50} = effective confinement index at ε_{cc50}

From the experimental evidence, it is demonstrated that even if ties do not reach yield at peak strength, they always yield at ε_{cc50} ; this is mainly due to the large concrete expansion that take place after peak. Hence I_{e50} is computed setting $f_{eff,st} = f_{y,st}$ and then only the force equilibrium is necessary:

$$I_{e50} = \rho_{st,y} \frac{f_{y,st}}{f_c} \quad \rho_{st,y} = k_s \frac{A_{st,y}}{SC_y} \quad (54)$$

Being the strain ε_{cc50} difficult to measure experimentally, it is possible to use $\varepsilon_{cc50}=0.004$ as suggested by Cusson & Paultre, 1995.

The stress strain formulation is equivalent to Cusson & Paultre, 1995 (see Fig. 156) with the ascending and post-peak branch defined by eq. 37 and 38, respectively. Only the formulation of k_2 coefficient in eq. 39 is modified.

$$k_2 = 1 + 25(I_{e50})^2 \quad (55)$$

4.2.6. Cusson model (2008)

Cusson & Paultre, 2008 propose a modification to Légeron & Paultre, 2003 model. A new simple and direct approach is developed to compute the effective ties' stress $f_{eff,st}$, and consequently the effective confinement index I_e' . It is taken as a starting point for the new approach, the estimation of the minimum stress in the confining steel at peak concrete stress, assuming that the concrete column meets the minimum requirements for non-seismic design. In other words, it is assumed initially that the lateral confinement pressure is small ($f_l = 0$). Based on compatibility of strains and equilibrium of forces in the column section, the minimum possible stress in the confining steel is calculated as follows:

$$f_{st,MIN} = \nu_{cc} \varepsilon_{c0} E_s \leq f_{y,st} \quad (56)$$

where ν_{cc} = 'equivalent' Poisson coefficient for confined concrete (assumed 0,4 from experimental tests on HSC columns); ε_{c0} =unconfined concrete strain at peak strength, E_s =steel Young modulus

The minimum effective confinement pressure ($f'_{l,min}$) at concrete peak stress, corresponding to the lateral pressure typically achieved in lightly confined concrete columns, is found as follows

$$f'_{l,MIN} = k_s \rho_{st} f_{st,MIN} \tag{57}$$

Usually this value should not exceed 5 MPa. Based on the regression analysis, the following relationship for $f_{eff,st}$ is proposed:

$$f_{eff,st} = f_{st,MIN} + 0,33E_s \left(\frac{f'_{l,MIN}}{0,85f_{c0}} \right)^{1,7} \leq f_{y,st} \tag{58}$$

For the definition of the stress-strain compressive concrete curve the same model as defined by Légeron & Paultre, 2003 should be used.

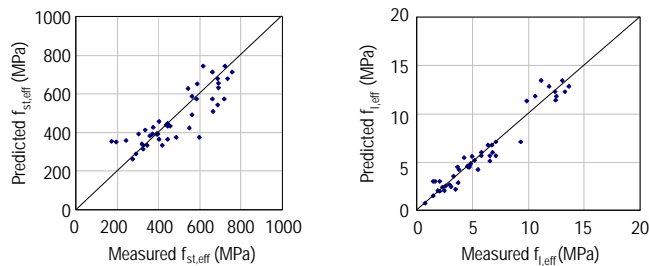


Fig. 161: Predicted vs. experimental lateral reinforcement stress and provided confining pressure (Cusson & Paultre, 2008)

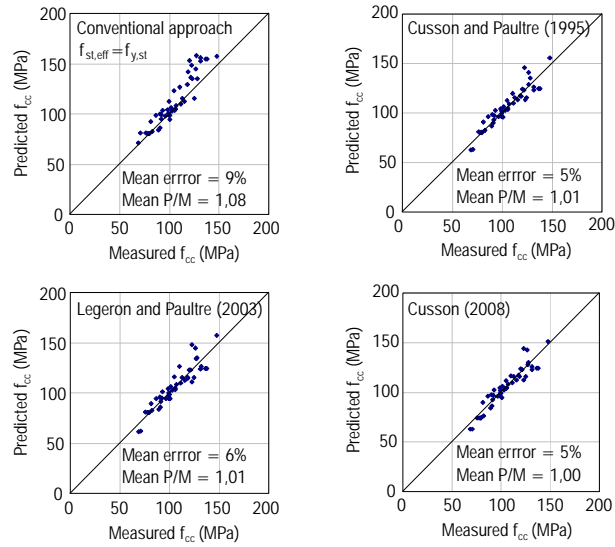


Fig. 162: Predicted vs. experimental concrete peak strength (Cusson & Paultre, 2008)

4.2.7. Cui and Sheikh model (2010)

Differently from the above reported ones, the Cui & Sheikh, 2010 model is based on regression fitting on data provided by compressive test on active confined specimens, using fluid pressure. The model deals with a wide range of strength, ranging between 25 to 110 MPa. Sargin, 1971 non-dimensional mathematical expression is taken as the base form of the stress-strain curve (eq. 59).

$$\frac{f_c}{f_{cc}} = \frac{A(\varepsilon_c / \varepsilon_{cc}) + B(\varepsilon_c / \varepsilon_{cc})^2}{1 + C(\varepsilon_c / \varepsilon_{cc}) + D(\varepsilon_c / \varepsilon_{cc})^2} \quad (59)$$

Following formulations are adopted for prediction about peak stress f_{cc} and corresponding strain ε_{cc} , based on plain concrete input parameters f_{c0} and ε_{c0} .

$$\frac{f_{cc}}{f_{c0}} = \left(1 + 10 \frac{f_l'}{f_{c0}} \right) \quad f_{c0} \leq 60 \text{ MPa} \quad (60)$$

$$\frac{f_{cc}}{f_{c0}} = \left(1 + 10 \frac{f_l'}{f_{c0}} \right) \quad f_{c0} > 60 \text{ MPa}$$

$$\frac{\varepsilon_{cc}}{\varepsilon_{c0}} = 1 + (70 - 13 \ln(f_{c0})) \left(\frac{f_l'}{f_{c0}} \right) \quad (61)$$

Further details about parameters A, B, C, D can be found in literature. To apply this models to predict concrete behaviour on real samples, an additional formulation is required to estimate the equivalent confinement pressure provided by passive confinement in substitution of fluid pressure input parameter. The approach proposed by Cusson & Paultre, 2008 is adopted to this purpose.

4.2.8. Provisions for concrete ductility

Independently from the adopted model and stress-strain relationship, the input parameter ϵ_{cu} , namely the ultimate strain for unconfined concrete play a fundamental key-role in determine the concrete ductility level, both for unconfined and confined conditions. The proposal made by Légeron & Paultre, 2003 and Cusson & Paultre, 1995 to assume a flat value $\epsilon_{cu}=0.004$, independently from considered concrete grade, appears at least approximate from this point of view. Other authors do not provide further details on this topic and reference is thus made to Codes' provisions. In the following table values reported in EN 1992-1-1:1993 (European Committee for Standardization, 1993), EN 1992-1-1:2005 (European Committee for Standardization, 2005a), EN 1998-3:2005 (European Committee for Standardization, 2005d), CEB-FIP Model Code 90 (Internation Federation for Structural Concrete (FIB), 1993), CEB-FIP Model Code 2010 (Internation Federation for Structural Concrete (FIB), 2010) for different concrete classes are compared. For CEB-FIP Model Code 90, the value ϵ_{c50} , corresponding to a 50% drop of residual strength, is assumed as reference ultimate strain.

	C12	C20	C30	C40	C50	C60	C70	C80	C90	C100	C120
EN 1992-1-1:1993	3,6	3,4	3,2	3,0	2,8	-	-	-	-	-	-
MC 90 (1993)	5,0	4,2	3,7	3,3	3,0	2,8	2,6	2,4	-	-	-
EN 1992-1-1:2005	3,5	3,5	3,5	3,5	3,5	3,2	3,0	2,8	2,8	2,8	-
EN 1998-3:2005	4,0	4,0	4,0	4,0	4,0	4,0	4,0	4,0	4,0	4,0	4,0
MC 2010 (2010)	3,5	3,5	3,5	3,5	3,4	3,3	3,2	3,1	3,0	3,0	3,0

Table 11: Ultimate strain for unconfined concrete as provided by different Codes

Looking at values reported in Table 11, there is a general trend in unconfined HSC ductility increase from older to most recent Codes, probably justified considering the improvement of HSC concrete performance attained in the last 20 years, through proper mix-design technologies. Looking at EN 1998-3:2005 (dealing with existing structures' retrofitting) a constant value for all concrete classes is given, equal to

0.004, similarly to proposal made by Légeron & Paultre, 2003. On the contrary, remaining Codes reports a clear dependency between concrete strength and ductility level. In the following reference is made to sufficiently conservative provisions reported by UNI-EN-1992-1-1:2005:

$$\varepsilon_{cu} = 2,8 + 27[(98 - f_{cm})/100]^4 \leq 3,5 \quad f_{cm} = f_{ck} + 8MPa \quad 62)$$

To keep a unitary framework, even the unconfined peak strength is assumed from provisions reported in the same Code:

$$\varepsilon_{c0} = 2,0 + 0,085(f_{ck} - 50)^{0,53} \geq 2\% \quad 63)$$

4.2.9. Provisions for concrete strength

A particular issue to take into consideration for correct concrete modeling, is the effective compression strength, in particular for HSC concrete. A reference formulation to evaluate expected columns' compressive strength under pure axial compression is reported in ACI 318-08 (ACI Committee 318, 2008):

$$P_0 = \alpha f_c (A_g - A_s) + f_y A_s \quad \alpha = 0,85 \quad 64)$$

where P_0 =pure axial load capacity of columns (ACI 318); f_c =concrete compressive strength; f_y =steel yielding stress; A_g =gross cross sectional area; A_s =area of longitudinal steel;

A coefficient $\alpha=0,85$ for all concrete classes is introduced. This coefficient is missing in both current Italian design code and Eurocode. It does not take into consideration possible strength reduction due to 2nd order effect (in NTC 2008 a coefficient 0,8 is introduced for this purpose). Conversely, it accounts for difference between concrete strength provided by cylindrical concrete specimens and the one provided by real scale column samples. In this regard, Sharma et al., 2005 report a ratio 0.88 vs. 1 when comparing concrete strength of plain unreinforced column and the one measured from standard concrete cylinders, thus very close to assumption about α reduction parameter reported in ACI 318-08.

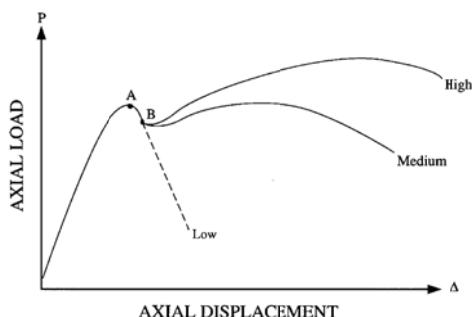


Fig. 163: Schematic behaviour of HSC columns subjected to concentric axial loads, incorporating low, medium, and high amounts of transverse reinforcement

Fig. 163 shows a schematic load-axial deformation response under concentric loads of HSC columns with transverse reinforcement. As concrete strength increases, the ascending portion of the curve approaches a straight line. Point A in Fig. 163 indicates the loading stage at which cover concrete spalls off. Experimental compression tests performed in the past reported how spalling of the cover concrete tends to occur prior to achieving the expected compressive strength of unconfined section (see eq. 64), contrary to the observed behavior of concrete columns made of NSC. The behavior of HSC columns beyond this point depends on the relative areas of the column and the core and on the amount of transverse reinforcement provided. Following spalling of the cover concrete, the load-carrying capacity of columns generally drops to point B. Beyond this point Cusson, 1994 reports that it is possible to increase the maximum axial strength of columns up to 150 percent of that calculated by the ACI 318-08 provisions, and obtain a ductile behavior, by providing sufficient transverse reinforcement.

Different explanations have been proposed to explain observed early spalling of cover concrete in HSC columns. According to Collins et al., 1993, the low permeability of HSC leads to drying shrinkage strain in cover concrete, while the core remains relatively moist. As a result, tensile stresses are developed in the cover concrete. A different explanation is reported by Cusson, 1994. He states that early spalling of concrete cover may also be initiated by the presence of a closely spaced reinforcement cage that separates core and cover concrete, creating planes of weakness. Cusson, 1994 even suggests to disregard completely concrete cover for evaluate HSC column axial strength: comparing experimental values when splitting of cover concrete take place (point A in Fig. 163), with P_0 corresponding to unconfined strength of the total concrete cross section, setting unitary α coefficient, a ratio varying from 0,85 (for $f_c=20$ MPa) to 0,7 (for $f_c=94$ MPa) is reported by Cusson, 1994. Similar trend was noticed by Razvi & Saatcioglu, 1996.

This is aligned with provisions required by Canadian Code for Design of Concrete

Structures (2004), which reports following formulation for coefficient α :

$$\alpha = (0,85 - 0,0015f_c) \geq 0,67 \quad 65)$$

This could suggest that more conservative α coefficient for HSC design should be adopted. It must be underlined that equation 65 refers to combined axial and bending solicitations. Further details on this topic are reported in par. 9.2. When just pure axial loading is considered, also Canadian Code reports a formulations similar to ACI 318 ones (eq. 64). The ratio $P_{\text{exp,MAX}}/P_0$ (P_0 evaluated as in eq.64) reported by Cusson, 1994 ranges between 0,87 and 1,4 (average 0,99), with lower values for higher concrete grades and lower confinement. Conversely experimental tests performed by Sharma et al., 2005, indicate a variability range for P_{exp}/P_0 (eq.64) comprises between 0,93 and 1,07 (average value 1), thus a considerably reduced range if compared with previous experimental tests. This could be a further suggestion about the HSC performances' improvement, especially in term of ductility, attained in the last 20 years (cf. Table 11) through proper mix-design of this material. Hence, it appears reasonable the adoption of coefficient $\alpha=0,85$ for calculating compressive strength of columns, as suggested by ACI 318-08 and also already adopted by Nagashima et al., 1992 (see eq.29) and Cusson & Paultre, 2008 (see eq. 58) in their formulations. When adopting EN 1992-1-1:2005 for design, the quantitative effect played by α reduction coefficient might be substituted by the long term effect coefficient.

4.2.10. Models' validation

To asses the capability of above reported concrete models to reproduce real response of confined columns under axial loading, a comparative study is performed, making reference to 4 compressive tests provided by Sharma et al., 2005, relative to RC columns with different concrete grade and lateral steel arrangement (Table 12). The experimental force vs. displacement curves are filtered in order to remove cover concrete contribute and get the equivalent stress vs. strain relationship for confined concrete. The filtering procedure adopted by Sharma et al., 2005 is the same originally defined by Sheikh & Uzumeri, 1980. For all considered models, the same input parameters for unconfined concrete are adopted. In particular a constant reduction factor $\alpha=0,85$ for the concrete strength is assumed, as discussed in chapter 4.2.9. Despite deformation at peak strength ε_{c0} for unconfined concrete is provided by experimental tests, equivalent values

reported by EN 1992-1-1:2005 (cf. eq.62) are considered for comparative study. Nevertheless, a good agreement is recognizable between experimental and Code's values. Similarly, the ϵ_{cu} values, corresponding to ultimate strain for plain concrete, are taken from provisions in EN 1992-1-1:2005 (cf. eq. 63)

sample	f_c (MPa)	f_y (MPa)	ϵ_{c0} exp (%)	ϵ_{c0} EC2 (%)	ϵ_{cu} EC2 (%)	s (mm)	d_b (mm)	layout
SA	62.20	412	2,37	2,6	3,0	50	8	
SC	61.85	520	2,37	2,6	3,0	50	8	
SD	63.35	412	2,37	2,6	3,0	50	8	
SH	81.80	520	2,60	2,8	2,8	50	8	

Table 12: Reference column tested by Sharma et al., 2005

For each column sample, following output parameters from analytical models are compared with experimental data:

- Lateral pressure
- Maximum strength (f_{cc})
- Ultimate strain (assumed corresponding to ϵ_{cc50})
- Enveloped area by the stress-strain curve (dissipated energy)

For ultimate strain's analytical values comparison also formulation proposed by Panagiotakos & Fardis, 2001 (see eq. 26) is considered.

- Test SA

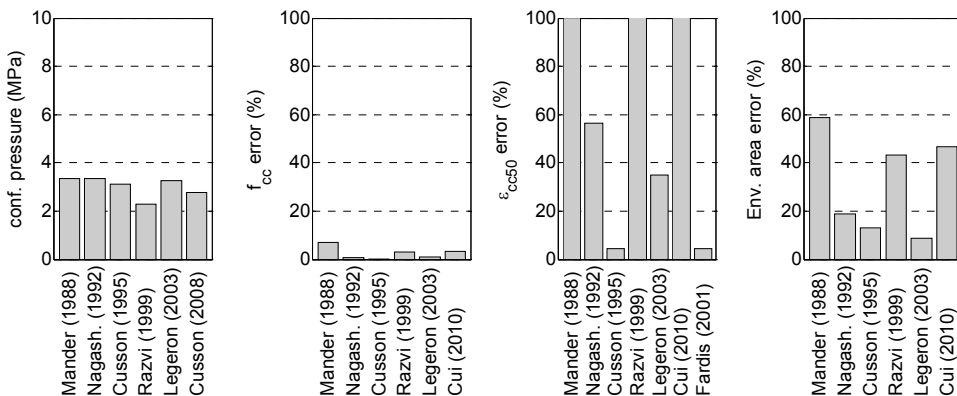


Fig. 164: Confined concrete output parameters comparison for column sample SA

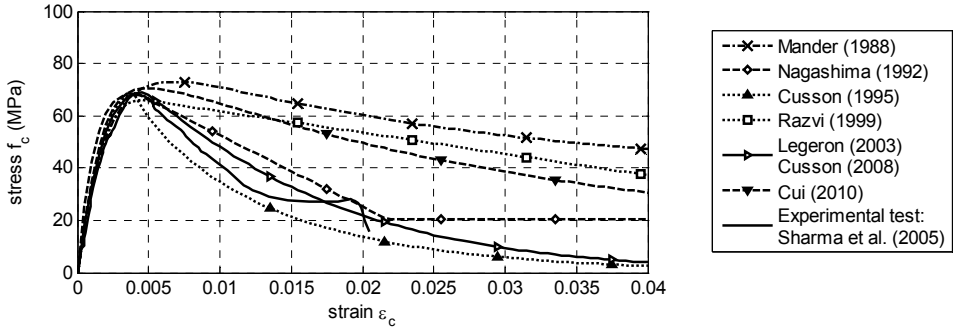


Fig. 165: Confined concrete models comparison for column sample SA

- Test SC

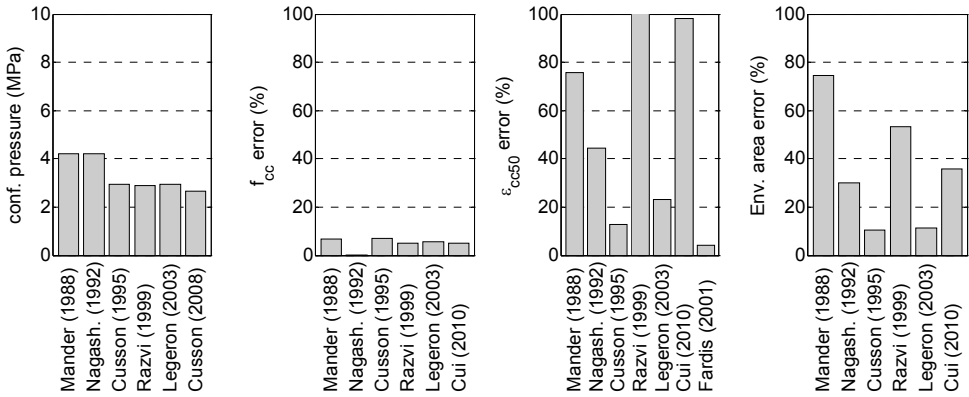


Fig. 166: Confined concrete output parameters comparison for column sample SC

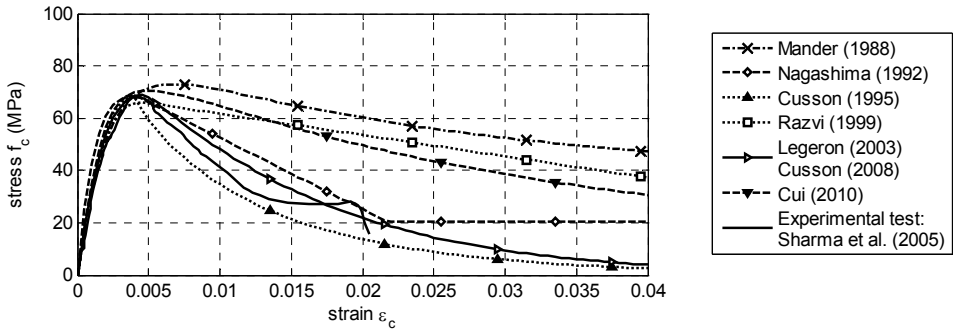


Fig. 167: Confined concrete models comparison for column sample SC

- Test SD

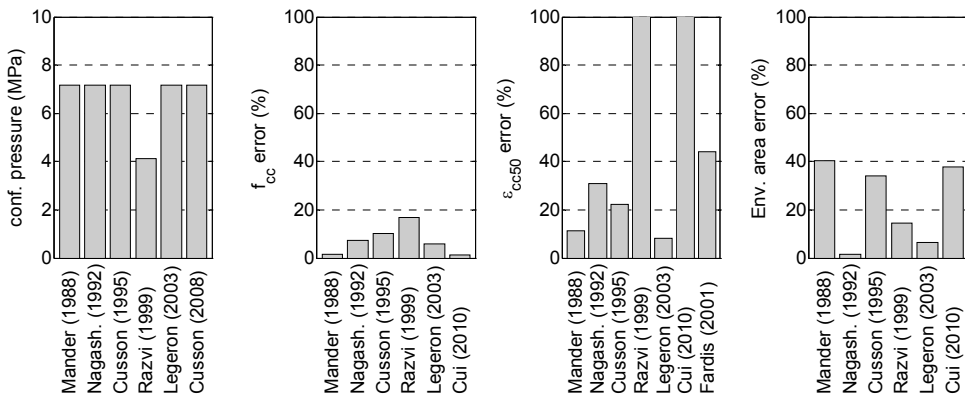


Fig. 168: Confined concrete output parameters comparison for column sample SD

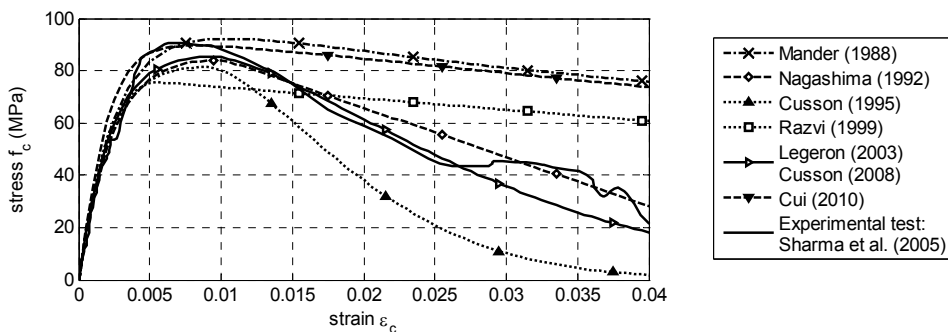


Fig. 169: Confined concrete models comparison for column sample SD

• Test SH

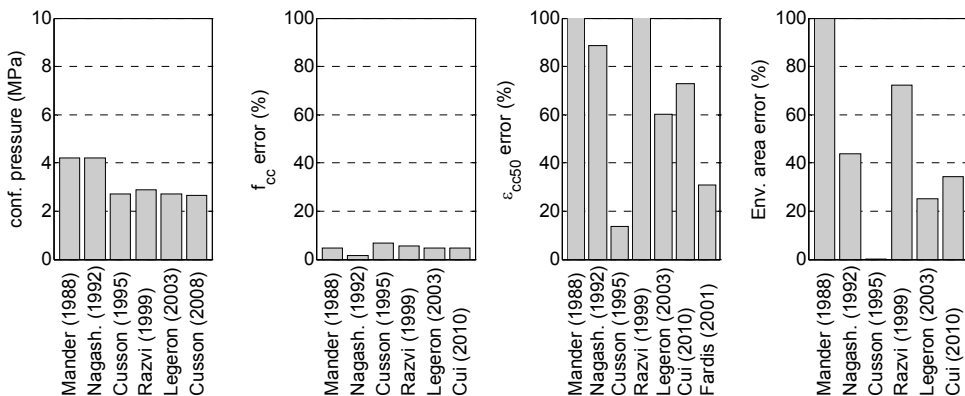


Fig. 170: Confined concrete output parameters comparison for column sample SH

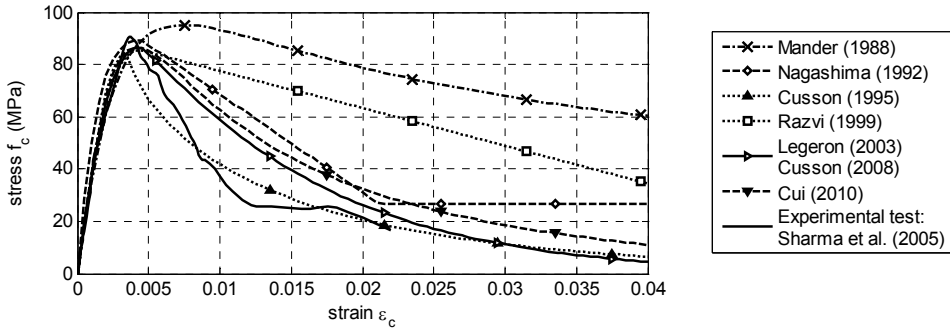


Fig. 171: Confined concrete models comparison for column sample SC

Lateral confinement is the first considered aspect to evaluate analytical models' sensitivity on input parameters. Considered approaches lead to rather different estimations for this value, depending from their capability to deal with real stress level on lateral reinforcement, that might be sensibly lower than yielding one. Adopting the yielding hypothesis generally provides an overestimation of confining pressure, in particular with HSC samples (Sheikh & Uzumeri, 1980), as in the considered cases. This justify lower confinement level estimated by Cusson & Paultre, 1995, Razvi & Saatcioglu, 1999, Légeron & Paultre, 2003, Cusson & Paultre, 2008 formulations. Generally the values they provide are rather uniform, with exception of Razvi & Saatcioglu, 1999 model applied to sample SD, which seems excessively conservative. Nevertheless, all considered formulations furnish an excellent estimation for the confined concrete strength f_{cc} , with errors always below 20%. Best prediction comes from Cui & Sheikh, 2010 (less than 1% error) and Nagashima et al., 1992 and Légeron & Paultre, 2003 (less than 5% error). Considerably much more scatter and rough estimations are related to the ultimate strains, which account for the shape of the softening branch in the stress-strain curves and thus for the ductility level of the response, clearly the most sensitive aspect to be captured by an analytical model. Worst estimations are generally provided by Mander & Priestley, 1988, Razvi & Saatcioglu, 1999 and Cui & Sheikh, 2010 models, that predict a much more ductile response as compared to experimental evidences. For the Mander & Priestley, 1988 model this appears reasonable, considering it is developed for NSC ($f_c < 50\text{MPa}$) applications and thus tends to overestimate ductility for higher concrete classes. Formulation for ultimate strain proposed by Panagiotakos & Fardis, 2001 seems to provide a better estimation for ultimate strain and should be adopted together with Mander & Priestley, 1988 model when dealing with HSC. Satisfactory results are provided by Cui & Sheikh, 2010 only within the limits of sample SH, the one with the highest concrete grade. Similar deductions follow the analysis of the amount of dissipated

energy, another parameter related to the shape of the stress-strain relationship, analogously to the ultimate strain value. Looking at considered parameters, the Nagashima et al., 1992, Cusson & Paultre, 1995 and the Légeron & Paultre, 2003 (considering modifications proposed by Cusson & Paultre, 2008) models estimate the actual experimental curves more closely as compared to the other models employed in the study. Among them, the Légeron & Paultre, 2003 model provides the best analytical response. This evidence is supported by objective comparison and even confirmed by naked-eyes comparison between analytical and experimental responses.

Beyond this result, it is surprising how the nearly 20 year old Nagashima et al., 1992 model is able to provide a good simulation, despite limited number of available data used to fit the model and despite the rough hypothesis about lateral ties yielding, independently from sample's geometry and materials. In this regard, in a recent investigation performed by Husem & Pul, 2007 comparing several analytical model for HSC against their own experimental tests, the Nagashima et al., 1992 resulted the most proper. It is pointed out that Cusson & Paultre, 1995 and Légeron & Paultre, 2003 models were not considered for that survey.

In the following analyses in next chapters, the Légeron & Paultre, 2003 model is adopted as reference to estimate non-linear concrete behaviour in compression. It is adopted for both NS and HS concrete grades. When not available by experimental testing, input data for unconfined plain concrete as assumed as reported by UNI-EN-1993-1-1 (cf. eq. 62 and 63). Furthermore a reduction coefficient $\alpha=0.85$ should always be accounted for unconfined concrete peak strength .

4.3. Numerical implementation of concrete models

4.3.1. *Tensile behaviour*

The two basic ideas of non-linear fracture mechanics are that some tensile stress can continue to be transferred after micro-cracking has started, and that this tensile stress depends on the crack opening, which is a displacement, rather than on the strain (as it does in the elastic region, see Fig. 172). The area under the tensile stress versus crack opening curve equals an energy which is denoted as fracture energy, G_f . This is assumed to be a material parameter.

In numerical FE approach, an effective method to model the crack opening inside a continuum is the smeared crack approach. Differently from discrete cracking, consisting in explicit crack modelling through model re-meshing, smeared approach consists basically in modification of constitutive material parameter inside single elements (in particular elastic modulus is drastically reduced). This means that the deformation of one crack is smeared out over a characteristic length.

To make the numerical simulation independent from currently adopted mesh size in term of total dissipated energy during damaging process (mesh dependency issue), the tensile stresses versus strain used should be a direct function of the of the element mesh size.

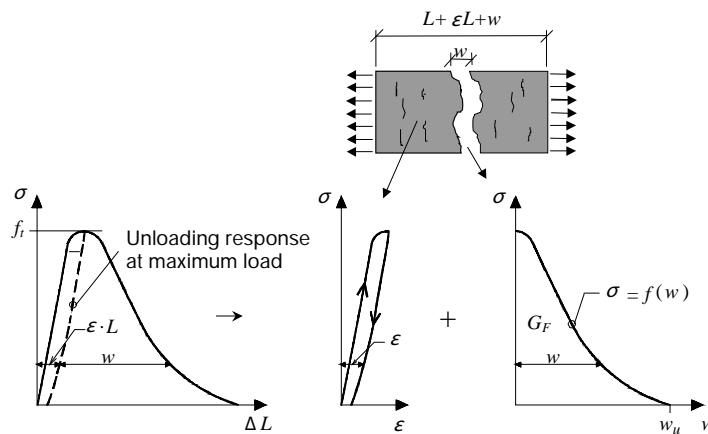


Fig. 172: Crack opening mechanism (Lundgren, 1999)

From equation 66 and 67 it results straightforward the switching from tensile stress vs. crack opening ($\sigma(w)$) to tensile stress vs. crack deformation ($\sigma(\varepsilon)$) by supposing that stress field could be assumed as constant over the single element length (l_{EF}). In this way the fracture energy G_f , is transformed into a fracture energy density g_f , direct function of current mesh size. Identification of correct characteristic element length is not always a trivial task, in particular when the dimensions of the elements are not the same in all directions. If the crack pattern is known before the analysis is carried out, the most accurate assumption would be to use the size of the element perpendicular to the crack plane. If, however, the crack pattern is not known in advance (Fig. 173 a), or when cracks appear in more than one direction in an element (Fig. 173 b,c), a mean value is usually preferred. This means that the ductility of the concrete (dissipated energy) is overestimated in one direction (the length of the elements), and underestimated in the other direction (the width of the elements). The easiest and simplest solution to this problem is of course to use meshes in which the elements have about the same size in all directions. As an

alternative, when this is not possible, the best value for average mesh size should be identified by the designer.

$$G_f = \int_0^{w_c} \sigma(w) dw \quad \rightarrow \quad G_f = \int_0^{\varepsilon_c} \sigma(\varepsilon) \cdot l_{EF} d\varepsilon \quad 66)$$

$$g_{fEF} = \frac{G_f}{l_{EF}} = \int_0^{\varepsilon_c} \sigma(\varepsilon) d\varepsilon \quad 67)$$

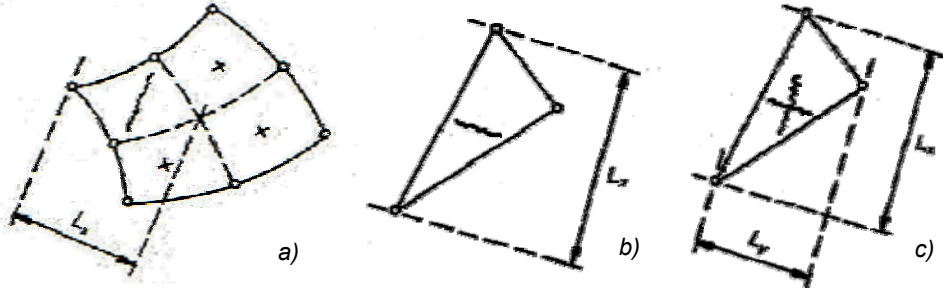


Fig. 173: Characteristic element length during fracture damaging process

In current work, to model concrete in tension, a non linear decreasing branch is assumed to for traction vs. strain relationship, based on models proposed by Hordijk et al., 1986 (see eq. 68 and Fig. 174). By integration of the enveloped area, the ultimate strain is defined as reported in equation 69. It result a direct function of the required fracture energy density. To estimate the fracture energy, which is a required input parameter, the formulation reported in CEB-FIB Model Code 2010 (Internation Federation for Structural Concrete (FIB), 2010) is adopted (eq. 70).

$$\frac{\sigma(\varepsilon)}{f_t} = \begin{cases} \left(1 + \left(c_1 \cdot \frac{\varepsilon}{\varepsilon_u} \right)^3 \right) \exp\left(-c_2 \frac{\varepsilon}{\varepsilon_u} \right) - \frac{\varepsilon}{\varepsilon_u} (1 + c_1^3) \exp(-c_2) & 0 \leq \varepsilon < \varepsilon_u \\ 0 & \varepsilon \geq \varepsilon_u \end{cases} \quad 68)$$

where $c_1=3$; $c_2=6,93$

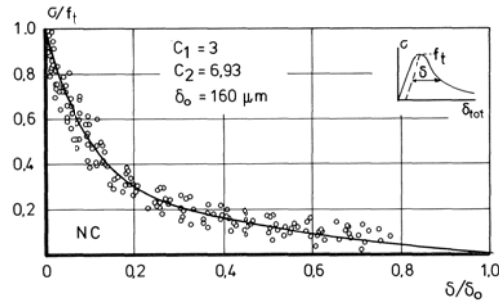


Fig. 174: Experimental vs. analytical formulation for concrete in traction (Hordijk et al., 1986)

$$\varepsilon_u = 5,136 \frac{G_f}{l_c^{(e)} \cdot f_t} = 5,136 \frac{g_f}{f_t} \quad 69)$$

$$G_f = 73(f_{cm})^{0,18} \quad 70)$$

4.3.2. Compressive behaviour

Since cracks are easy to spot, localisation of the deformations in a tensile failure of concrete is not difficult to understand. However, there is also localisation of the deformations in a crush failure. Experimental tests show that the compression softening behaviour is related to the boundary conditions and the size of the specimens (Model Code 90, Lundgren, 1999). These effects are likely partly due to localisation of the crushing deformations (Fig. 175b). Markeset, 1993 has presented a model where a damaged zone, L^d was defined. When strain gradients were present, they were assumed to depend on the depth of the damaged zone. Reinforcement probably affects the length of the damaged zone also. This model can serve as a tool for analyses of beams and columns with uniaxial compression. However, there is at present no convenient way to take the effect of localisation into account in a generalised material model suited for FE analysis, especially not for a general case with triaxial stress states. One problem is that the number of elements in which the compressive region will localise is not known when the analysis is started. In tension, it seems reasonable to assume that a crack will localise in one single element; an assumption that is not so obvious for compression. In the presented analyses, simple stress versus strain relations for the compressive behaviour are used without taking into account the size of the elements.

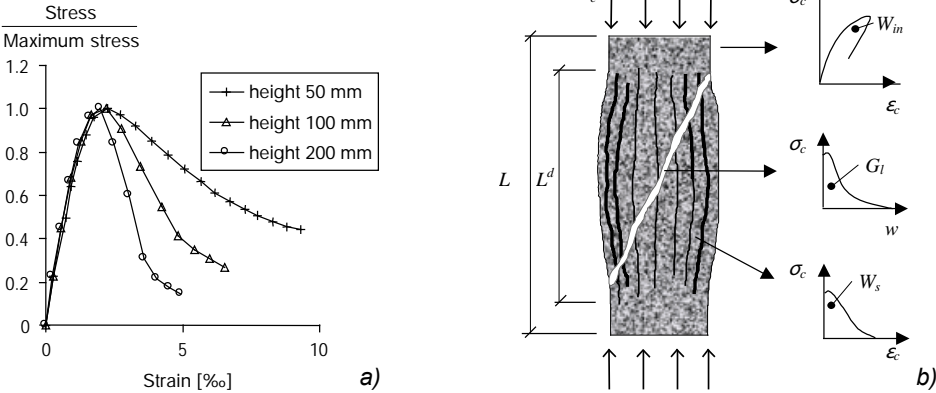


Fig. 175: a) Compression tests on plain concrete specimens with different length; b) compression model from Markeset, 1993

5. LATTICE GIRDERS' PARAMETRIC OPTIMIZATION

5.1. Introduction

Referring to investigated precast joint prototype, lattice girders are adopted to restore beams' continuity and to provide force transfer capability across the core joint. An alternative solution could be the positioning of additional straight rebars, analogously to a cast-in-place joint.

Such an approach, for example, is adopted for precast systems developed by Park & Bull, 1986 consisting in threaded rebars settled inside U-shell beams and furtherly updated and tested by Lee et al., 2004 and Park et al., 2008, Lignola et al., 2010. Despite limited differences, all tests showed good load-carrying capacity and deformation capacity, which are comparable to those of conventional monolithic RC joint. Contrariwise, both the energy dissipation capacity and stiffness of the specimens are significantly less than those of the cast-in-place specimen due to slippage of rebars occurred at the beam-column connection, as suggested by severely pinched hysteresis curves. Beam-to-column joint performances under monotonic and cyclic loading with beam continuity provided by threaded rebars has been investigated by Amato et al., 2010. Also in this case rebars' slippage, in particular under negative bending moment, is identified to be the main cause for severe pinching of hysteresis loop independently from adopted detailing, even after limited imposed top drift. This is probably related to the problem of jointing different monolithic precast elements, namely column and beam members, and force them to behave analogously to a cast-in-place joint. To provide full interaction among these components a stiffer and stronger connection should be provided. This justify the adoption of lattice girders made by plain rebars in place of longitudinal threaded reinforcement. Illustrative experimental tests are those performed by Scotta & Tesser, 2011 on beam to column joint under cyclic loading (chapter 1.6.5). In spite of encouraging results, limited attention has been focussed at present on lattice girder geometry, simply adopting standard products provided by precasters. This is

still an open issue, since force transfer among lattice and concrete relies on web truss capability to bear against concrete, but no design provisions are available with reference to lattice's geometry, minimum rebars' diameter or overlapping length. This is even more relevant considering that at present adopting lattice girders to provide beam continuity is becoming commonplace for real case applications.



Fig. 176: Real cases example of lattice girders applications

Reference could be made to experimental pull-out tests aiming to investigate longitudinal shear transfer mechanisms of web trusses in CSTC beam, whose role is compared to that of classical shear studs in a composite members. Different failure modes have been identified but the interaction phenomena between truss and concrete appear still not fully comprehended and analytical formulations provide rather rough prediction of experimental evidence (Colajanni et al., 2011). Furthermore this kind of tests appear not suitable to describe the role played by lattice girder, since shear transfer mechanism on beams and force transfer mechanism on lattice girder crossing the core-joint are rather different. This latter deal with axial forces induced by bending solicitations' decomposition, normally considerable higher than shear forces and acting over a limited length, corresponding to the overlapping one (Fig. 177). To deepen this topic some numerical pull-out tests are presented in this chapter, conceptually analogous to classical experimental pull-out tests commonly adopted to study bond phenomena of rebars (Eligehausen et al., 1983, Pochanart & Harmon, 1989; Mazzarolo et al., 2012). Lattice girder get solid modelled as embedded inside a concrete block; an axial pull-out force is subsequently applied on lattice ends, while the reaction force is exerted on the concrete block. Numerical model is build in Ansys V.11.0 (ANSYS Inc., 2007) to take advantage of the possibility offered by this tool to define the model through scripting. This allows for a parametric investigation about lattice

girder behaviour as a function of its geometry. Longitudinal bars' diameter, web trusses' diameters and lattice length (v-spans' number) are assumed as parametric quantities. On the basis of numerical results, the force transfer mechanisms provided by lattice girder are investigated and the minimum geometrical requirements to guarantee sufficient stiffness and strength to this component are identified. Finally to check about adequateness of these provisions, the bending strength of lattice-concrete composite section is evaluated and compared with expected values coming from RC beam formulations, assuming perfect interaction hypothesis between rebar and concrete and plain sections hypothesis.

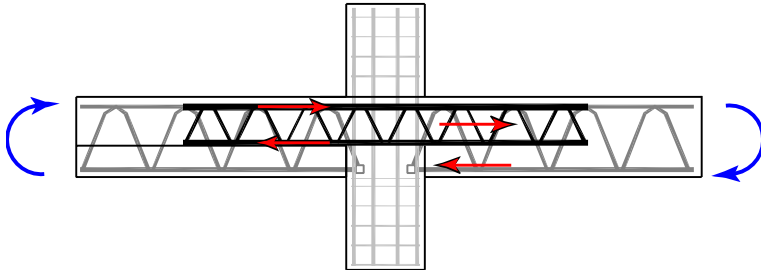


Fig. 177: Bending-moment-induced axial forces acting on lateral truss girders

5.2. Numerical parametric pull-out tests

Numerical model consists in a lattice girder completely embedded inside a concrete block, 200 millimetres depth and 800 millimetres height, assuring this way a large enough frontal surface, acting as fixed restraint during tests. Length of the block is variable and depends from lattice's v-spans number. To increase computational efficiency just half sample is modelled, accounting for its symmetry with reference to longitudinal-vertical median plane and introducing equivalent boundary conditions (fixed Z translations in the symmetry plane) to restore the full model condition (Fig. 180). The model is built in Ansys V.11.0 (ANSYS Inc., 2007), through scripting using the native APDL (Ansys Parametric Design Language) which allows for a parametric definition of the model.

The whole sample is solid modelled with 8-nodes SOLID65 hexahedral elements for concrete (average mesh size 40 mm) and 8-nodes SOLID45 hexahedral elements for lattice components (average mesh size 15 mm). This latter is reproduced in detail, even introducing 30 mm straight segments among inclined trusses to account for bent bar's geometry. To make possible the adoption of mapped quadrangular mesh for the whole model, a square section is adopted for trusses.

Two different models' family are considered with longitudinal bars' diameter (edge) d_1 equal to 20 and 30 millimetres, respectively. To capture the role played by web truss, a parametric analysis is conducted, varying web truss diameter d_2 between 10 to 30 millimetre (by increment of 5 millimetres), with upper limit given by longitudinal rebar cross size. For each web and longitudinal rebars' diameter combination, 5 models are built, with v-spans number varying between 1 and 5. This brings to a total of 15 and 25 models considered respectively for 20 (Table 13) and 30 (Table 14) millimetres longitudinal rebars' diameter. Between lattice girder and surrounding concrete a surface contact get modeled to account for mutual interaction (relative sliding, bearing and loss of contact), implementing a Mohr-Coulomb constitutive model with friction coefficient $\mu=0.4$ and null cohesion. For concrete a uniaxial stress-strain relationship in compression is implemented, accounting for a limited confinement condition. This choice allows to consider behaviour of the lattice girder in tension under negative bending moment, when cracking of surrounding concrete limits drastically the confining action. A fictitious confining pressure equal to 0.2 MPa is considered. A concrete class C25/30 is considered. Shear retention factor β for non-linear concrete modelling is assumed 0.8 and 0.2 for un-cracked and cracked section respectively. Being available in Ansys just a brittle model for concrete in tension, fracture energy G_f is not required as input parameter. Other mechanical parameters for concrete and steel modelling are reported in Table 15. An increasing monotonic imposed displacement is applied at one end of longitudinal rebars. Reaction force acts against restrained frontal concrete surface. The maximum expected reaction force corresponds to rebar failure. Best performance corresponds to model that allows to attain the maximum strength, limiting damaging of surrounding concrete, together with minimum amount of required steel.

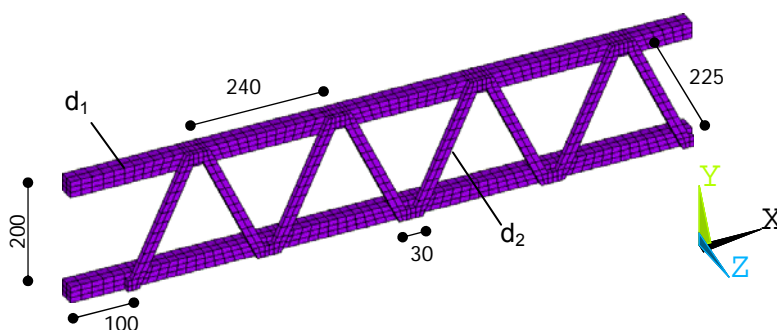


Fig. 178: Lateral truss girder model

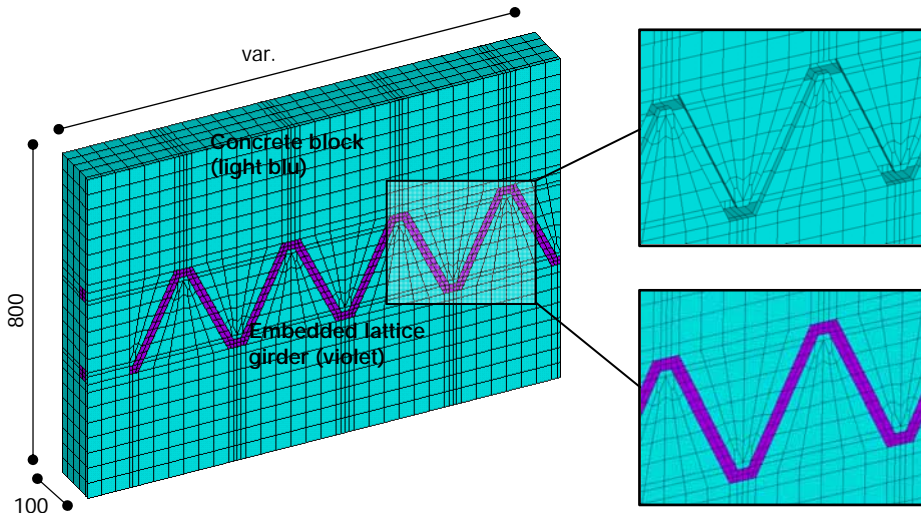


Fig. 179: lateral truss model

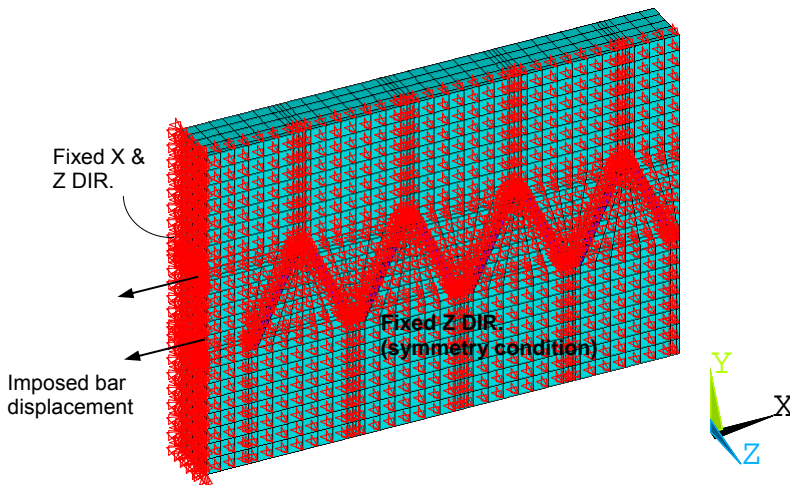


Fig. 180: boundary condition applied to the pull-out F.E. model

Model no	d ₁	d ₂	v-span no
1	20	10	1
2	20	10	2
3	20	10	3
4	20	10	4
5	20	10	5
6	20	15	1
7	20	15	2
8	20	15	3
9	20	15	4
10	20	15	5

Model no	d ₁	d ₂	v-span no
11	20	20	1
12	20	20	2
13	20	20	3
14	20	20	4
15	20	20	5

Table 13: Parametric pull-out test models with ϕ 20 (d₁) longitudinal rebars

Model no	d ₁	d ₂	v-span no
1	30	10	1
2	30	10	2
3	30	10	3
4	30	10	4
5	30	10	5
6	30	15	1
7	30	15	2
8	30	15	3
9	30	15	4
10	30	15	5

Model no	d ₁	d ₂	v-span no
11	30	20	1
12	30	20	2
13	30	20	3
14	30	20	4
15	30	20	5
16	30	25	1
17	30	25	2
18	30	25	3
19	30	25	4
20	30	25	5

Model no	d ₁	d ₂	v-span no
21	30	30	1
22	30	30	2
23	30	30	3
24	30	30	4
25	30	30	5

Table 14: Parametric pull-out test models with ϕ 30 (d₁) longitudinal rebars

Concrete				Steel rebars				
f _c (MPa)	f _t (MPa)	E (MPa)	G _f (N/mm)	f _y (MPa)	E (MPa)	E _{pl} (MPa)	ε _y (%)	ε _u (%)
30	2.9	30590	NaN	450	2e6	1400	0.2	7.5

Table 15: Mechanical parameter for material model definition

Fig. 181 and Fig. 182 report the computed pull-out reaction force vs. lattice girder slippage curves, from models with longitudinal rebar diameter (d₁) equal respectively to 20 and 30 millimeters. It should be noted that in the latter case analysis was forced to larger imposed displacement. This is due to the switching of

iterative numerical procedure from implicit to explicit scheme. It means that when convergence is not achieved anymore, tolerance on residual force is disregarded, and time increment reduced drastically to 1/1000 of total.

As expected, not all the models attain the maximum strength corresponding to yielding of longitudinal rebars.

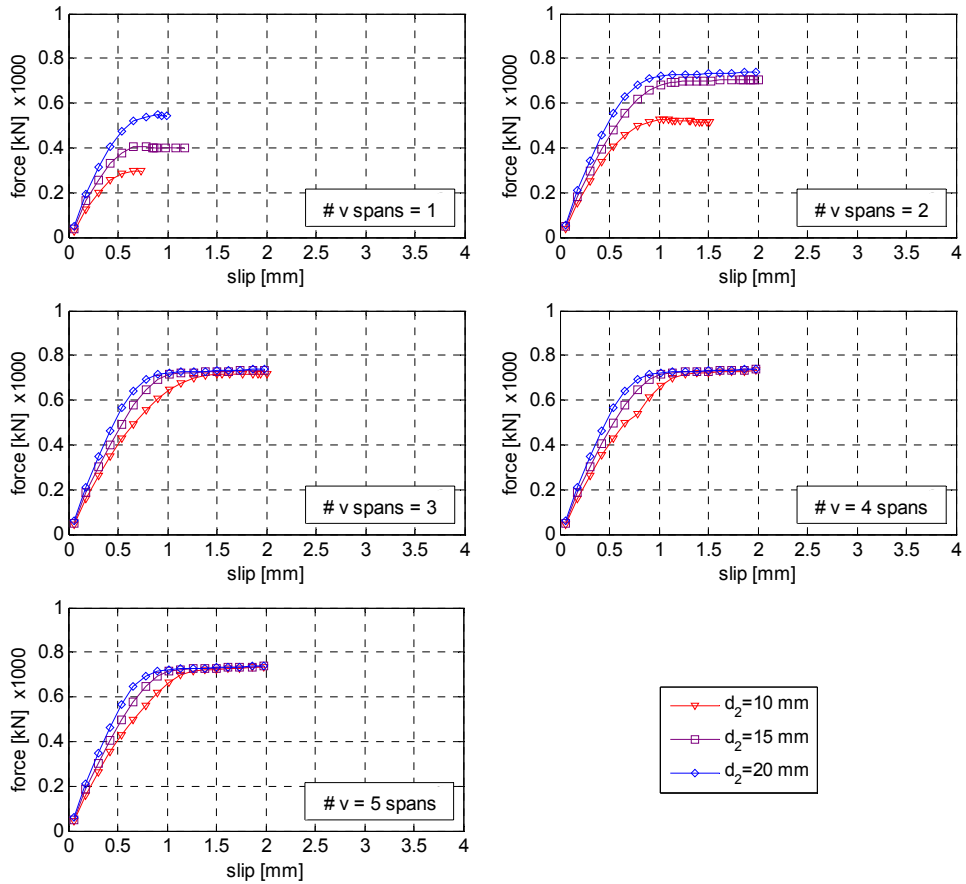


Fig. 181: Pull-out force vs. rebar slip.; $\phi 20$ (d_1) longitudinal rebars

Analysis and development of an innovative prefabricated beam-to-column joint

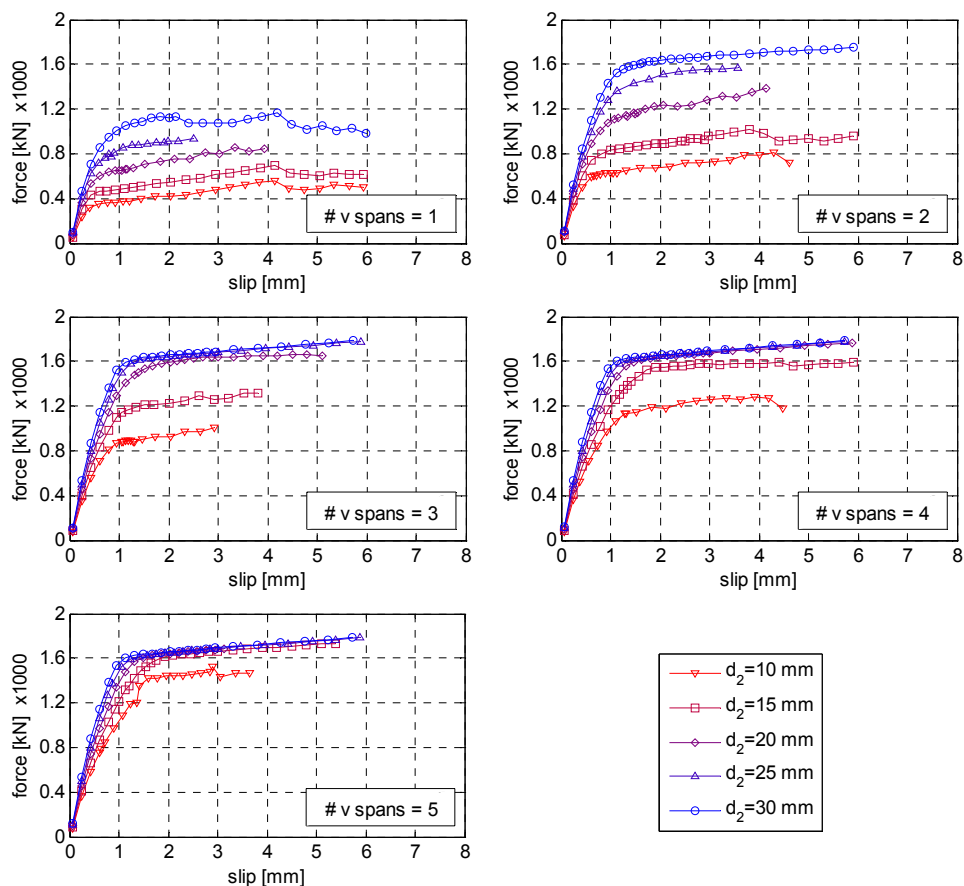


Fig. 182: Pull-out force vs. rebar slip.; $\phi 30$ (d_1) longitudinal rebars

To highlight effect played by lattice geometry, results 'contours relative to $d_1=30$ mm and $d_2=10,20,30$ mm are reported respectively for a v-span number equal to 2 and 4. From Fig. 183 to Fig. 185 is reported the stress intensity factor on concrete at the end of test, that means when achieving numerical converge is not possible anymore. From Fig. 186 to Fig. 188 are plotted the corresponding Von Mises stresses on steel truss. Web truss diameter plays two main effect. First of all, the larger it is, higher concrete area is involved in bearing load. This means lower compression stresses and higher strength capacity. Secondary higher diameter corresponds to higher stiffness and higher strength of web truss, allowing thus a better stress redistribution among v-spans along lattice girder.

Looking at Fig. 186a, being rebar diameter not sufficient, plastic hinges take place on web trusses, approximately 50 mm far from truss node. As soon as web rebar is bent and yielded, global slip of lattice increases, due to progressive crushing of surrounding concrete (Fig. 183a). A longer girder allows to support higher pull-out

force, despite still plastic hinging on web rebars occurs, due to insufficient web-truss strength (Fig. 183b and Fig. 186b). It is interesting to note as similar web-rebar's plastic hinging phenomena is observed also in some experimental pull-out tests performed by Aiello et al. (2009) (see Fig. 190). A possible analytical explanation for this behaviour is provided by analytical model for inclined truss in CSTC beam proposed by Colajanni et al., 2011. Maximum bending moment take place at both side of inclined truss, at a certain distance from truss ends (see Fig. 191). When it exceeds maximum strength, a plastic hinge take place.

This can be considered as a validation of goodness of proposed numeric model, able to capture this aspect when not enough strength is provided to web-trusses.

When lattice girder is long enough, increasing of web-truss diameter allows to get a more favorable force distribution along the whole lattice's length (Fig. 184b) with limited concrete damaging (Fig. 185b). Slip is mainly due to yielding of longitudinal bar stubs, where displacement gets applied, while the remaining lattice's portion remain elastic (Fig. 187b, Fig. 188b). For the model with v-span number equal to 4 and web-trus diameter equal to longitudinal rebar one, nearly no damage is observed inside concrete block (Fig. 185b) and initial stiffness in the force vs. slip curve correspond to longitudinal bars' elastic stiffness. Conversely if an insufficient number of v-span is provided, maximum strength increase together with web diameter, but consistent damaging of surrounding concrete cannot be avoided.

Such a behaviour is confirmed by Fig. 189, where normalized force distribution at failure along upper longitudinal rebars is plotted against monitored position. In case just 2 v-spans are modeled, higher amount of force is supported by the second span, being the first one surrounded by severely crushed concrete. This effect is much higher as lower web diameters are considered. Web diameter affects deeply also force distribution along specimen in case of 4 v-spans lattice models. Higher web-truss diameters are associated to an exponential decreasing of force along truss. It means that bearing action of frontal inclined web truss against concrete is strong enough to guarantee force transfer from concrete to longitudinal rebar. As rebar decrease, exponential trend tend to become linear, corresponding to uniform force transfer distribution along the whole lattice. In case of insufficient strength ($d_2=10$; $d_2=15$), progressive concrete crushing and web rebar yielding in the front of specimen, force the farthest web inclined truss to bear higher amount of load.

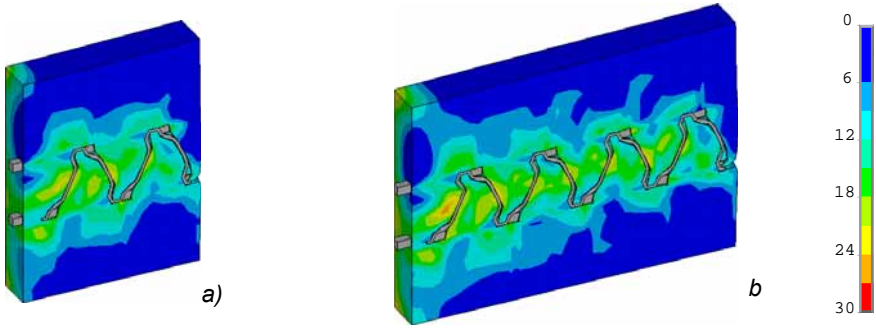


Fig. 183: Stress intensity on concrete (MPa); $d_1=\phi 30$ $d_2=\phi 10$

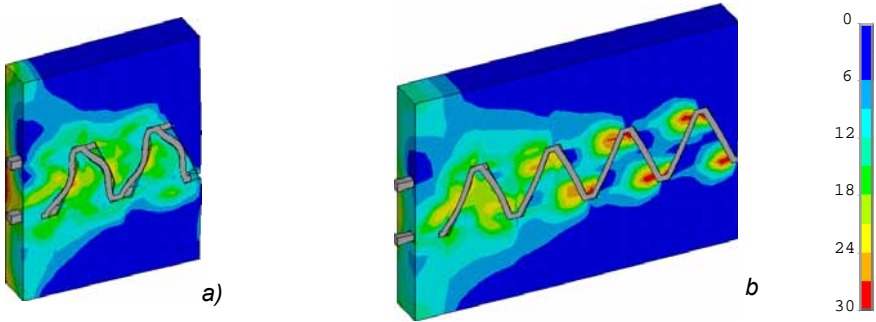


Fig. 184: Stress intensity on concrete (MPa); $d_1=\phi 30$ $d_2=\phi 20$

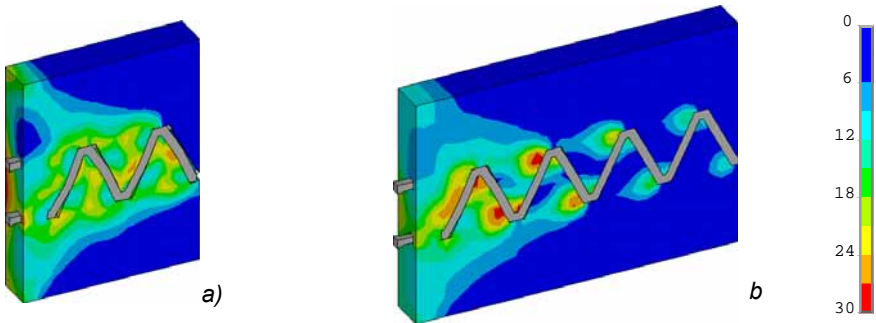


Fig. 185: Stress intensity on concrete (MPa); $d_1=\phi 30$ $d_2=\phi 30$

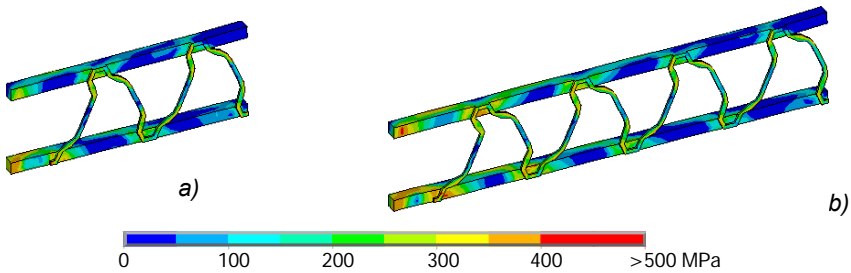


Fig. 186: Von Mises stresses on lattice; $d_1=\phi 30$ $d_2=\phi 10$

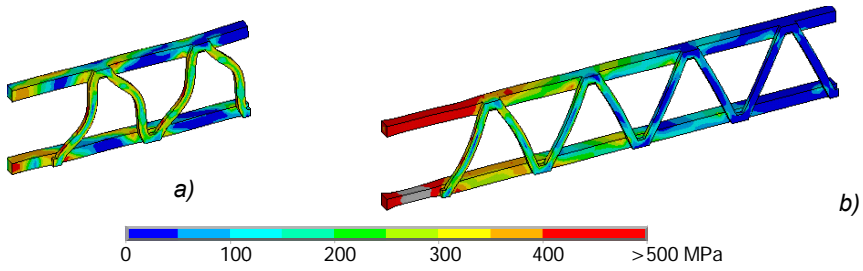


Fig. 187: Von Mises stresses on lattice; $d_1=\phi 30$ $d_2=\phi 20$

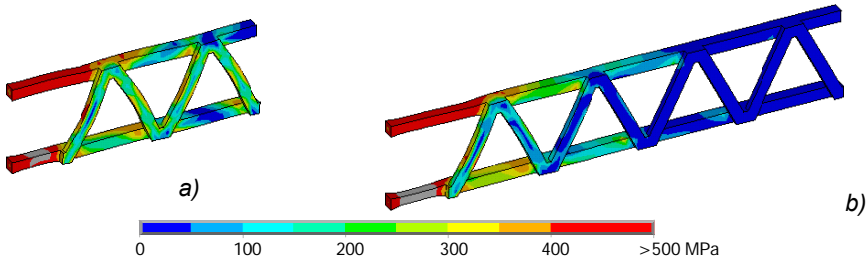


Fig. 188: Von Mises stresses on lattice; $d_1=\phi 30$ $d_2=\phi 30$

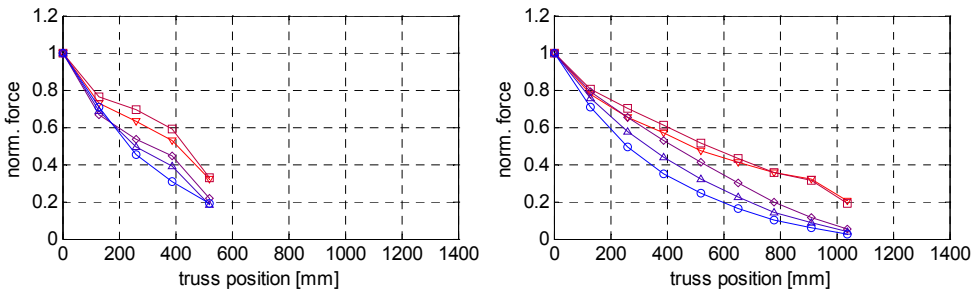


Fig. 189: Normalized force distribution along truss; $v\text{-spans} = 2$ (left) and $v\text{-spans}=4$ (right)



Fig. 190: Particular pull-out failure; experimental tests by Aiello et al., 2009

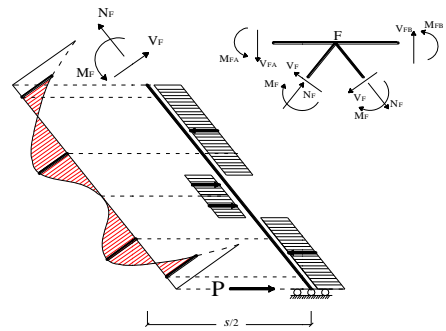


Fig. 191: Analytical model for web truss (Colajanni et al., 2011)

To better sensitize pull-out numerical results a tridimensional representation is proposed, where lattice girder's geometry (web truss diameter and number of v-spans) is plotted against maximum strength. Fig. 192 and Fig. 193 correspond to numerical simulations adopting longitudinal rebar diameter (d_1) equal to 20 and 30 mm, respectively.

Yield limit is reached when enough strength is provided. Giving analytical interpretation of numerical results is not trivial, being these influenced by non-linear behaviour of both concrete and steel. Also experimental results to confirm numerical evidences should be provided. However some general rules could be derived. To guarantee the full longitudinal rebars' plasticization following geometric limitations should be guaranteed:

$$\begin{aligned}
 & d_2 / d_1 \geq 0.7 \\
 & \# \text{ v-span} \geq 4
 \end{aligned}
 \tag{71}$$

where d_2 =incline truss diameter; d_1 =longitudinal rebar diameter

Specimens with these limitations attained the maximum strength during numerical pull-out tests, without web rebars' yielding, both considering $\phi 20$ and $\phi 30$ longitudinal rebars.

Further aspect to consider is the possibility of lateral truss girder to transfer the maximum axial load level under oligocyclic fatigue loading (seismic input). To fulfill this requirement lateral truss layout should be chosen among specimens that evidenced limited concrete damaging under monotonic loading.

Limitations in equation 71 allow to consider this aspect by dismissing lattices' layouts with limited web diameter (see Fig. 183b) or limited number of v-span (see Fig. 185a), even though maximum strength is guaranteed.

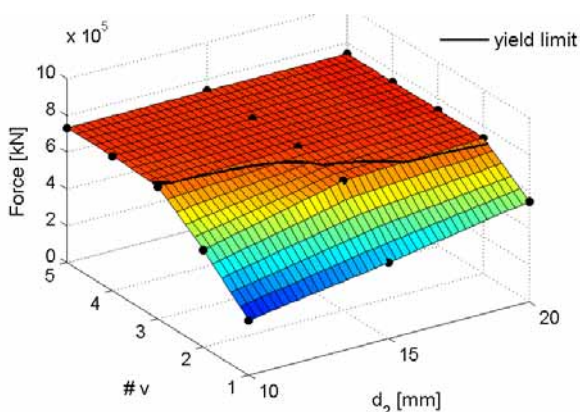


Fig. 192: Pull-out strength domain vs. truss layout; FE models with $\phi 20$ longitudinal bar

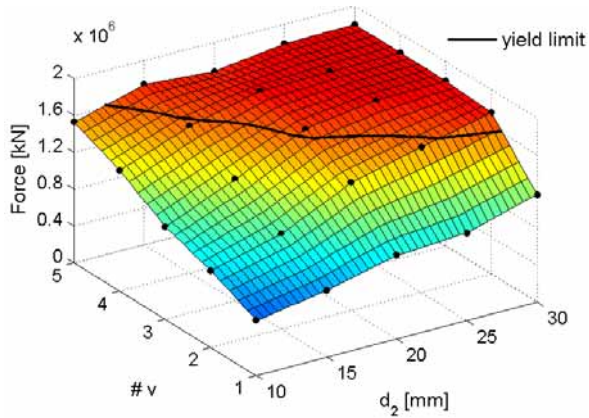


Fig. 193: Pull-out strength domain vs. truss layout; FE models with $\phi 30$ longitudinal bar

5.3. Bending strength

To check adequacy of proposed geometry limitations for lattice girder (see eq.71), performances of a cantilever beam subjected to positive and negative bending are investigated. The FE model is analogous to those adopted for pull-out tests, with the main differences that the truss is shifted 50 mm far from the upper edge of the beam and an elastic 100 mm transition zone is defined in the front of cantilever to redistribute stresses to the whole beam's section. The global geometry of the defined cantilever reproduce the final configuration of lateral truss girder, when mounted in the investigated precast joint. 6 v-spans are modeled to make the slenderness of the beam large enough to avoid shear failure phenomena and highlight bending performance. Two different concrete properties are considered. In the lower part, corresponding approximatively to the concrete precast base in CSTC beam, a certain confinement effect is considered, accounting for $\phi 8$ stirrups with 60 mm interaxis (about 1 MPa equivalent confining pressure). In the upper part a less ductile stress-strain curve is assigned to considered for limited Poisson in the tensile zone. A fictitious confining pressure of 0.2 MPa is here supposed. This configuration is particularly suited to evaluate to cantilever performance under negative bending. Conversely, when subject to positive bending, confinement action for concrete in the upper beam side could be underestimated. However high reinforcement ratio given by lattice girder balance this effect and good ductility to the system is the same provided.

Longitudinal rebar diameter and web rebar are taken respectively equal to 20 and 15 mm, thus fulfilling requirement reported in equation 71.

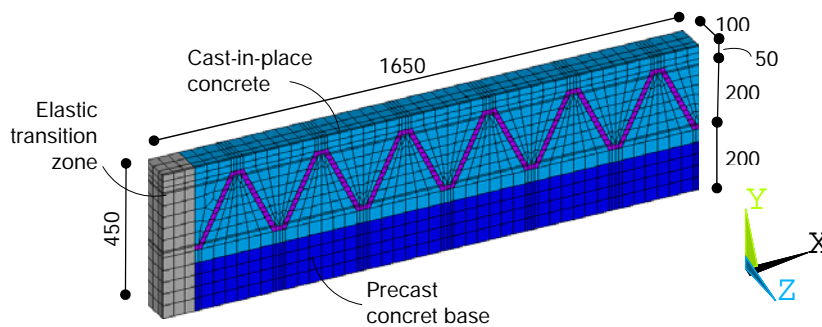


Fig. 194: Cantilever FE model for lattice-concrete composite beam

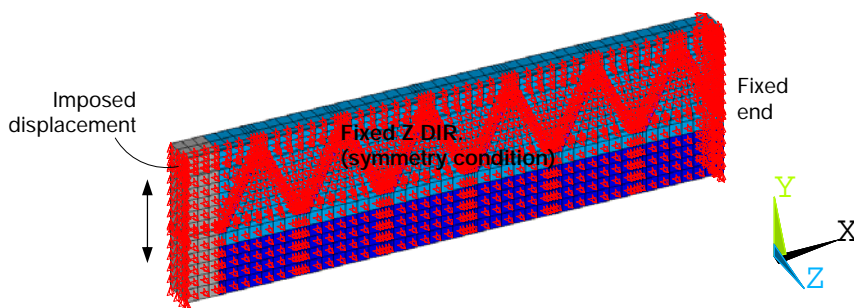
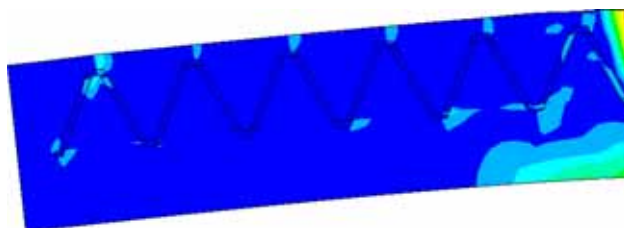


Fig. 195: Boundary conditions applied to lattice-concrete composite beam

From Fig. 196 to Fig. 199 the numerical response under monotonic negative bending is presented. The plastic hinge is located near the fixed end, with a main crack at the end of the beam (Fig. 196) and a lattice's yielding penetration of approximately 500 mm (nearly 2 v-spans). The shear force transfer take place though a truss and tie mechanism among the lattice girder and surrounding concrete. In Fig. 197 and Fig. 198, respectively compressed concrete struts and tension inclined ties are recognizable. Moment vs. displacement curve evidences global high ductility of the cantilever. The numerical yielding moment agrees satisfactory with the value computed adopting simplified rigid-plastic theory (see eq. 72 and 73).



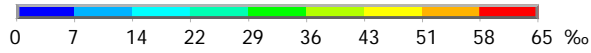


Fig. 196: Cantilever lattice-concrete beam subject to hogging bending: strain intensity

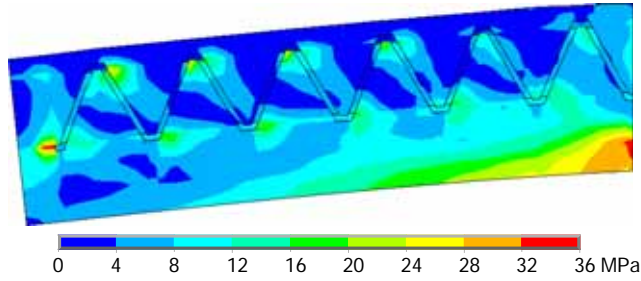


Fig. 197: Cantilever lattice-concrete beam subject to hogging bending: concrete stress intensity

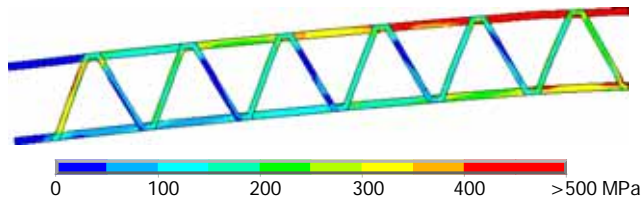


Fig. 198: Cantilever lattice-concrete beam subject to hogging bending: Von Mises stress on lattice

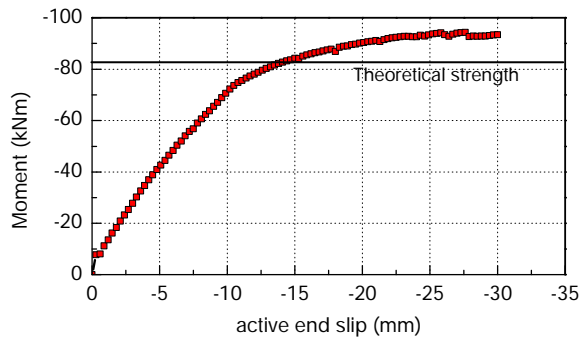


Fig. 199: Hogging moment vs. displacement

$$\begin{aligned}
 x &= f_{yk} \cdot \left(\sum_{i=1}^n A_s^i \right) / (0.85 \cdot f_{cd} \cdot b) \\
 &= 450 \cdot (20 \cdot 20 \cdot 2) / (0.85 \cdot 30 \cdot 100) \\
 &= 141 \text{ mm}
 \end{aligned}$$

72)

$$\begin{aligned}
 M_{pl,Rd} &= \sum_{i=1}^n f_{yk} \cdot A_s^i \cdot (d^i - x / 2) \\
 &= 450 \cdot 20 \cdot 20 \cdot (400 + 200 - 141 / 2 - 141 / 2) \\
 &= 82.6 \text{ kNm}
 \end{aligned}
 \tag{73}$$

Similar results are obtained from positive bending moment tests (Fig. 200 to Fig. 203). Due to missing reinforcement in the lower side of cantilever a main crack spread from to bottom up to the lower longitudinal rebars, in correspondence of the fixed end. The effect is to reduce the effective beam depth. Also in this case compression strut and tension tie mechanism develop between concrete (Fig. 201) and lattice girder (Fig. 202). Plastic hinge penetration is lower compared to negative bending simulation (about 250 mm). Nevertheless global ductility of the specimen is analogous to previous case. Theoretical bending moment evaluated with analytical simplified rigid-plastic theory, agree well with numerical evidences (see eq. 74 and 75).

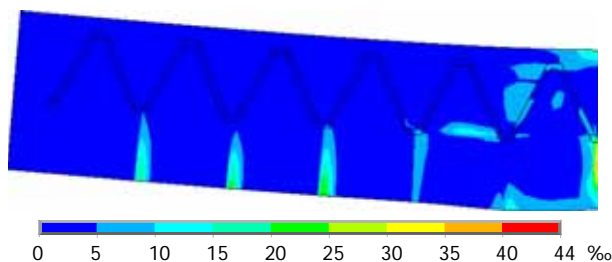


Fig. 200: Cantilever lattice-concrete beam subject to sagging bending: strain intensity

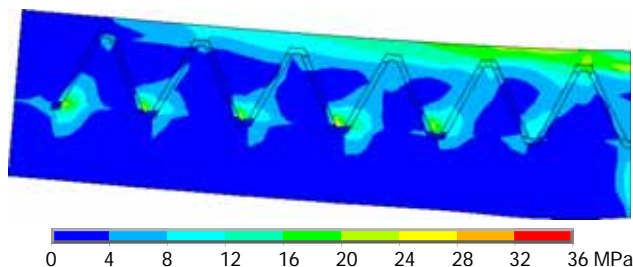


Fig. 201: Cantilever lattice-concrete beam subject to sagging bending: concrete stress intensity

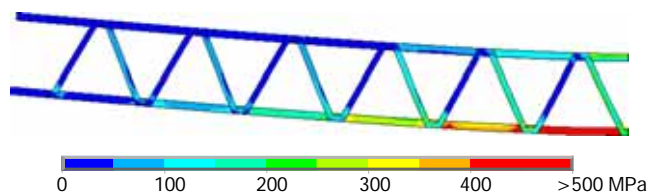


Fig. 202: Cantilever lattice-concrete beam subject to sagging bending: Von Mises stress on lattice

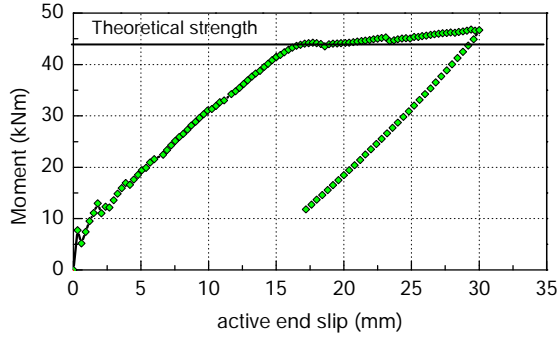


Fig. 203: Sagging moment vs. displacement

$$x = f_{yk} \cdot (A_s - A'_s) / (0.85 \cdot f_{cd} \cdot b) \quad 74)$$

$$= 0$$

$$M_{pl,Rd} = \sum_{i=1}^n f_{yk} \cdot A_s^i \cdot (d^i - x / 2) \quad 75)$$

$$= 450 \cdot 20 \cdot 20 \cdot 250$$

$$= 44.9 \text{ kNm}$$

5.4. Conclusion

In this chapter attention is stressed on structural performances of lateral truss girders. Their main function in the presented precast joint is that of provide beam's continuity through the joint. Experimental tests available from literature evidence better performances of joint with lattice girders than those with classical threaded bar, both in term of strength and stiffness. Still some concern is about the real force transfer capability of such elements. Numerical pull-out tests suggest that minimum requirements on the geometry of the truss should be provided to guarantee that a full interaction with surrounding concrete is possible.

Being adopted plain rebars, longitudinal bars yielding is possible only when inclined truss is stiff enough and a sufficient number of v-spans are provided. In this case

the dowel action of inclined truss bearing against concrete is effective in guaranteeing force transfer between lattice and concrete

From this point of view the adopted pull-out test set-up appears to be more effective than experimental pull-out tests available from literature, since condition of the truss under axial force provided by bending moment decomposition, is better represented.

Finally a bending test on a cantilever lattice-concrete composite beam considering a lattice with adequate geometry, confirmed full interaction between reinforcement and concrete.

To verify numerical performances of the cantilever under positive and negative bending, analytical yielding moment is evaluated for both cases adopting simplified rigid beam theory, as prescribed by Codes for composite sections. Good agreement between analytical and numerical result is obtained, validating this way adopted analytical procedure, based on perfect adherence hypothesis, despite plain rebars are adopted.

6. COMPOSITE-COLUMN'S FE MODEL CALIBRATION

6.1. Introduction

The possibility to fit experimental results via numerical simulation is of great interest since it allows to get reference FE models, suitable for wider study of proposed technology, in substitution of experimental real scale testing.

Experimental survey over static performance of composite-column reported in chapter 3.3 is adopted to this purpose, since the column's geometry is rather simple and collected data provide a comprehensive picture about samples' response during testing. Numerical analyses are conducted using Abaqus V.6.10 FE software (Simulia, 2010). Compared with others, this tool offers the advantage of a straightforward modeling of complex tridimensional RC samples, a wide library of materials' constitutive law (also for concrete) and an improved solution-convergence capability during iterative process.

The capability of numerical model to reproduce experimental evidences is evaluated in terms of global quantities, such as applied global reaction force vs. displacement, and in terms of local quantities, in particular strain data. This procedure allows for a thorough validation of implemented numerical models, both in the matter of geometrical modeling and in the matter of implemented constitutive model, in particular the concrete one (see par. 4.3).

6.2. FE model

The numerical model consists of a full tridimensional representation of composite-column geometry. The 8-nodes hexahedral solid element (C3D8R) is adopted for the whole model, with exception of spiral stirrups inside column, modeled by linear truss elements (B31). Regular mesh is assured by mapped meshing subroutine.

Average mesh size for concrete is 40 mm. Circumference of longitudinal column reinforcement is split 8 times, to reproduce accurately circular section geometry. Steel-joint is meshed with a finer mesh with average edge size approximately 20 mm. Vertical steel plate are split 4 times in the thickness direction, to capture more accurately second order effects.

The concrete cast to fill the core-joint is not modeled, owing to impossibility to simulated sudden concrete splitting failure through adopted concrete plasticity model. At top and bottom of composite-column model, two stiff planes are modeled adopting quadrilateral elements (R3D4). Such planes are introduced to impose boundary conditions on the model more efficiently. The stiffness of the planes allows to better re-distributed stresses over the whole column section and avoids local stress concentration. This way, numerical stability during Newton-Raphson iterative process is considerably improved. All translational degrees of freedom (DOF) are restrained at bottom plane level. Imposed force is applied at a specific reference point located in the mass center of upper rigid plane. A monotonic increasing axial load is applied. Six different models are defined, as many as tested samples (see Table 5). The so defined models consist of 27578 node, 19456 solid, 192 planar and 432 linear elements, for a total of 20080 finite elements. Adopted material properties are reported in Table 3 and Table 4.

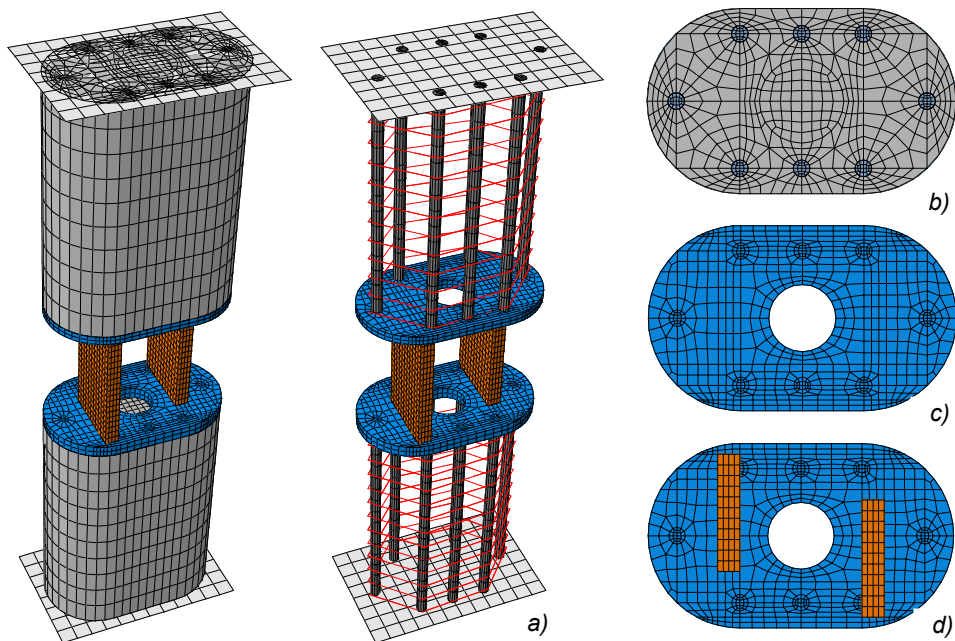
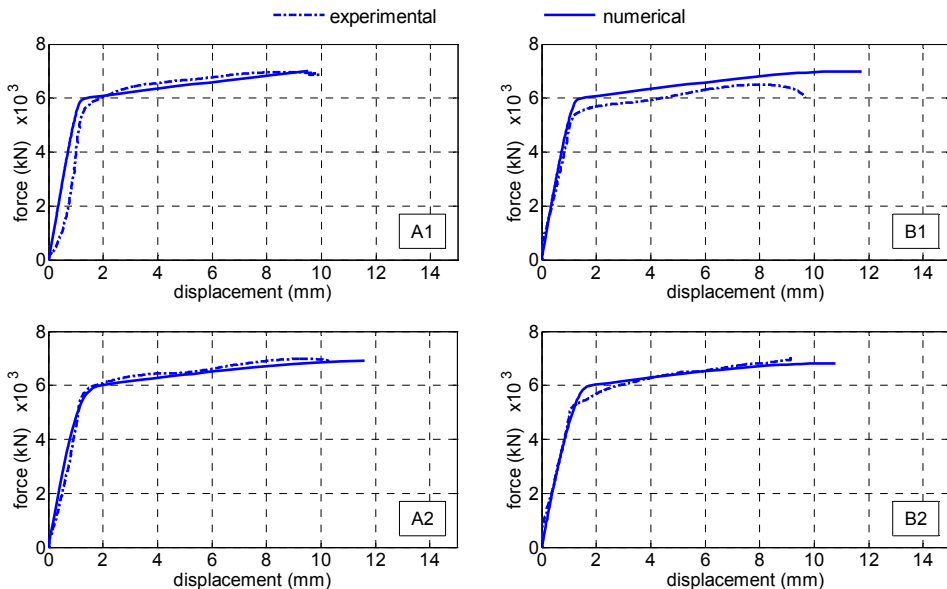


Fig. 204: a) Composite column FE model; b) HSC column mesh; c) horizontal steel plate mesh; d) steel-core-joint mesh

6.3. Experimental vs. numerical response

The first aspect to take into consideration, when checking capability of a FE model to reproduce an experimental response, is to look at global quantities, which summarize the structural behaviour of tested samples. The total applied force vs. axial deformation of steel-core-joint is particularly suited for this purpose (Fig. 205). To provide an objective evaluation to matching level between experimental and numerical response, 4 quantities are considered: displacement and force at yielding (Table 16), ultimate displacement and force at failure (Table 17). The highest average percentage difference is relative to yielding displacement (+9,5%). The lowest corresponds to estimation of ultimate force (+0,06%). Beyond excellent correspondence between experimental and numerical trend suggested by these values, attention should be stressed at amplified (by 5 times) deformed shape of numerical sample at failure (Fig. 206). With only exception for model A1, all the remaining clearly evidence a failure condition associated to vertical steel plates buckling, analogously to experimental response (see Fig. 113). This confirms the robustness of the adopted numerical approach, able to account properly for second order effect.

In Fig. 206 the compression damage map for all samples is also reported. Concrete columns attained limited damage levels, corresponding to experimental evidence, that column performed elastically till the end of testing.



Analysis and development of an innovative prefabricated beam-to-column joint

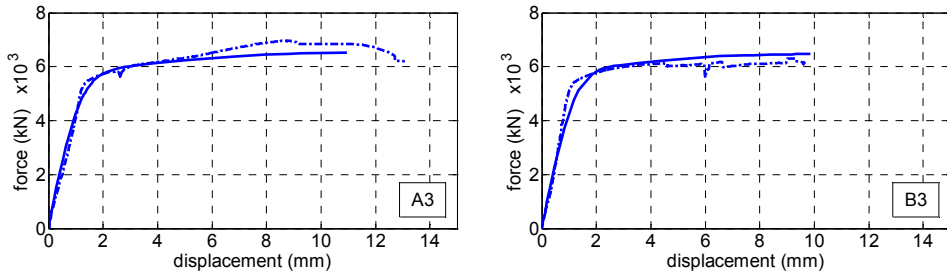


Fig. 205: Experimental vs. numerical results; force-displacement relationship

Sample	F_{y_exp} (kN)	F_{y_FE} (kN)	diff. %	U_{Fy_exp} (mm)	U_{Fy_FE} (mm)	diff. %
A1	5930	5880	-0.85	1.77	1.17	-33.90
A2	5933	5907	-0.44	1.55	1.63	+5.16
A3	5579	5736	+2.81	1.61	1.99	+23.60
B1	5424	5880	+8.4	1.28	1.24	-3.13
B2	5294	5880	+11.06	1.25	1.55	+24.00
B3	5557	5821	+4.75	1.41	1.99	+41.13
average	5620	5850	+4.29	1.48	1.59	+9.48

Table 16: Force and displacement at yielding: numerical and experimental values

Sample	F_{u_exp} (kN)	F_{u_FE} (kN)	diff. %	U_{Fu_exp} (mm)	U_{Fu_FE} (mm)	diff. %
A1	6960	7000	+0.57	1.77	9.53	-4.32
A2	6986	6906	-1.15	1.55	11.60	+13.06
A3	6954	6508	-6.41	1.61	10.94	-16.36
B1	6496	6994	+7.67	1.28	11.75	+21.51
B2	7004	6814	-2.71	1.25	10.76	+17.47
B3	6312	6461	+2.36	1.41	9.85	+1.97
average	6785	6780	+0.06	1.48	9.53	+5.55

Table 17: Force and displacement at failure: numerical and experimental values

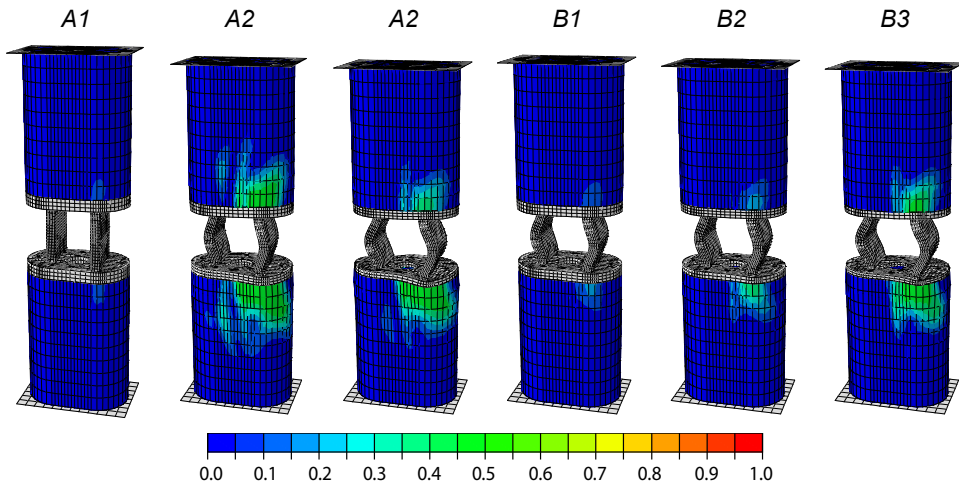


Fig. 206: Compression damage map from different FE models at failure

To check more in detail numerical model reliability to provide an accurate simulation of experimental tests, also strain data recorded during testing are compared with corresponding numerical values.

In the case of concrete this is not a straightforward operation, since concrete modeling suffers of mesh dependency issue, both in tension and in compression (see par. 4.3). Looking at Fig. 208 and Fig. 209, respectively vertical and transversal strains relative to upper HSC column are compared. The good matching in trends suggests that adopted concrete modeling approach is sophisticated enough, to capture not only global, but even local quantities.

Furthermore, FE solution allows to clarify specific experimental evidences, as the non-uniform axial strains distribution on HSC column face. In chapter 3.3.4 it get supposed it is a consequence of asymmetrical vertical plate layout in the core-joint. A column section taken in the model 100 mm far from the flanged connection (Fig. 211a), allows to directly appreciate this effect: compressive stress are considerably higher in correspondence of vertical plate due to high axial stiffness these provide at column base. This disturbing effect tend to vanish rapidly as farer column section are considered (Fig. 211b).

Analysis and development of an innovative prefabricated beam-to-column joint

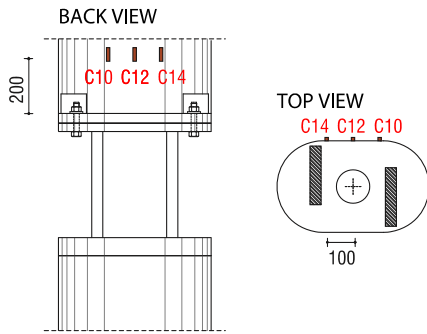


Fig. 207: Concrete strain-gauge location: sensor C10 C12 C14

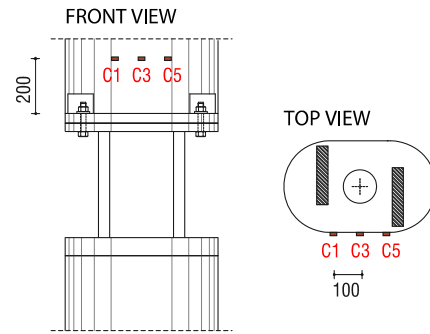


Fig. 208: Concrete strain-gauge location: sensor C1 C3 C5

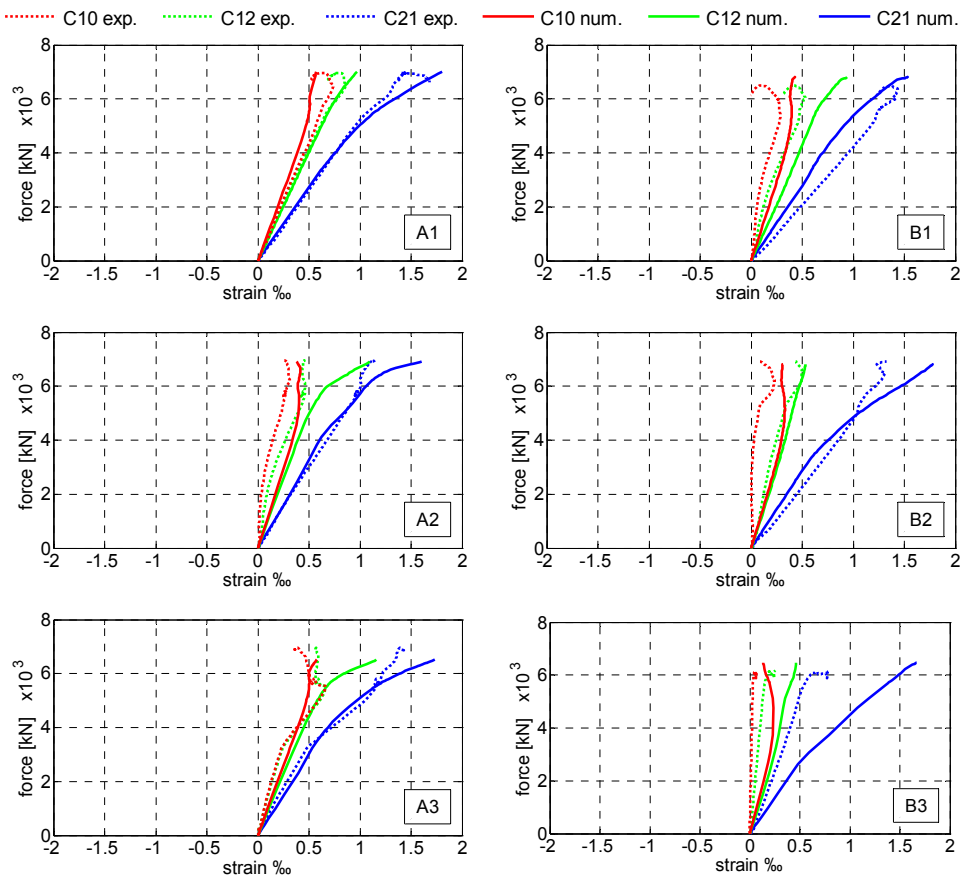


Fig. 209: Experimental vs. numerical static results; vertical strain from sensors C10 C12 C14

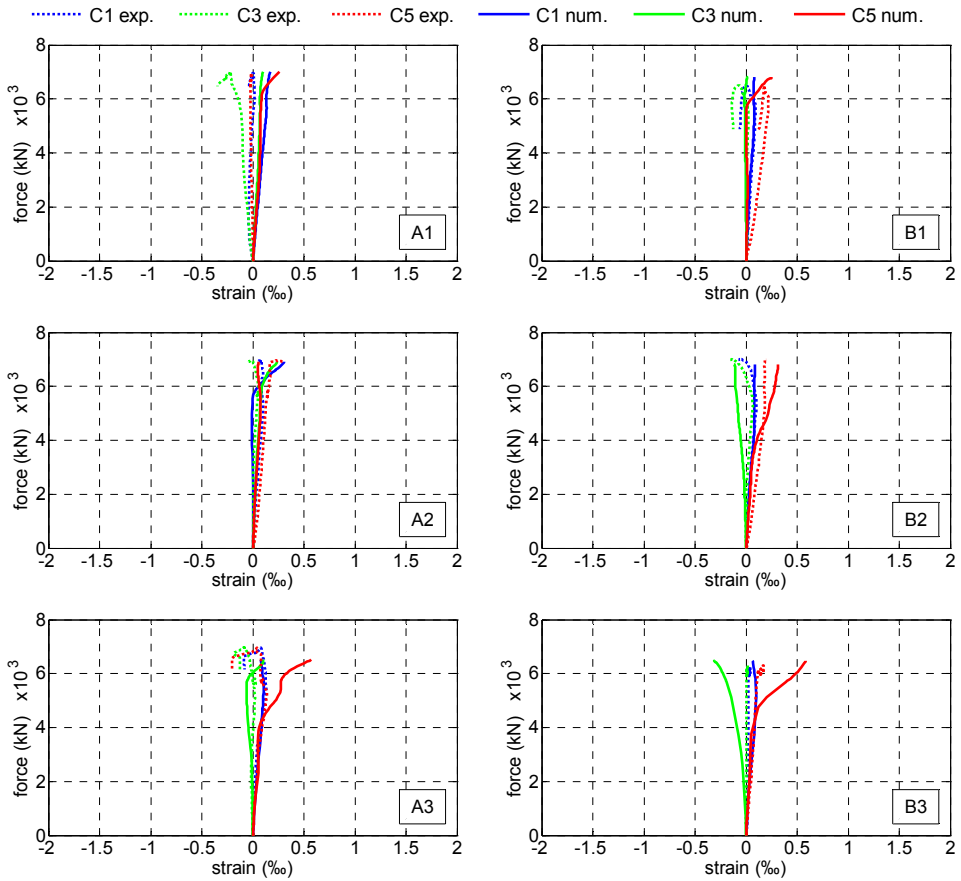


Fig. 210: Exp. vs. numerical static results; horizontal strain from sensors C1 C3 C5

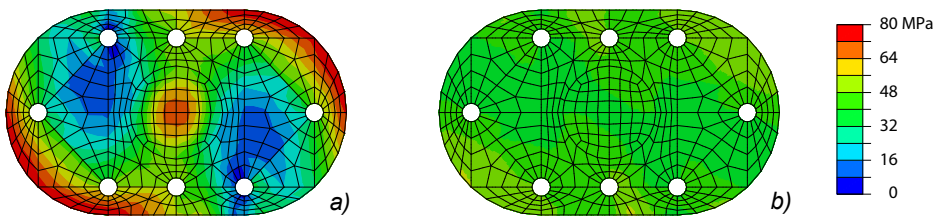


Fig. 211: Upper column axial stress σ_{zz} ; a) 100 mm far from flanged connection; b) 500 mm from flanged connection

Satisfactory numerical response is further confirmed by comparison of in-plane strains on the lowest steel flange belonging to steel-core-joint. From Fig. 214 it can be noticed that deformation level agrees reasonably well between numerical and experimental solutions, even if some sensors appeared to suffers some damaging during data acquisition, probably due to concrete splitting out. Fig. 215 shows as vertical steel plates promotes bending effects on the lower horizontal flange This

explain why strain levels in the X-direction results higher in samples with lower horizontal flange thicknesses. Strains in the Y-direction result sensibly lower and opposite in sign, mainly due to Poisson effect.

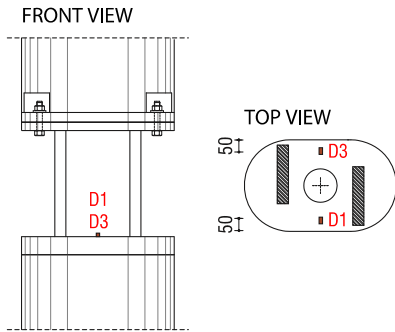


Fig. 212: Concrete strain-gauge location: sensor C24 C32

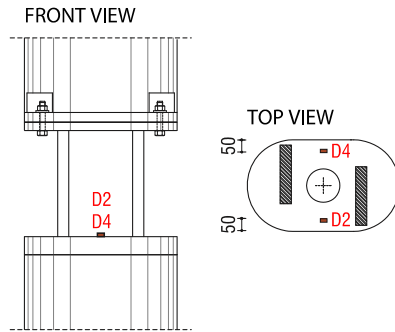
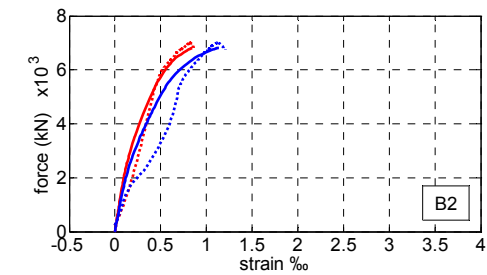
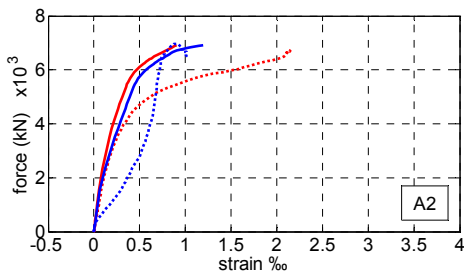
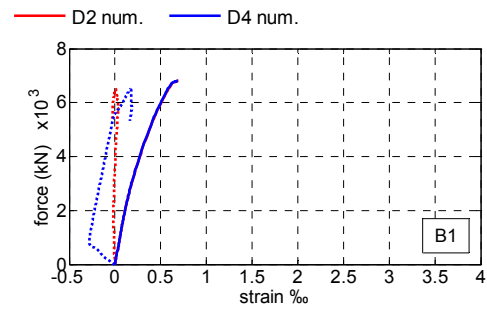
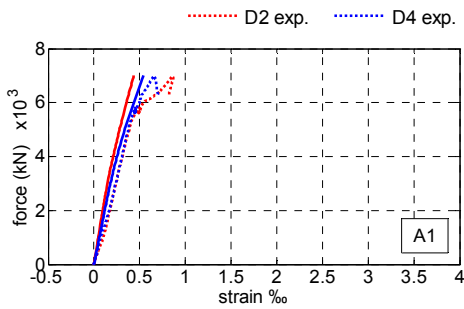


Fig. 213: Concrete strain-gauge location: sensor C24 C32



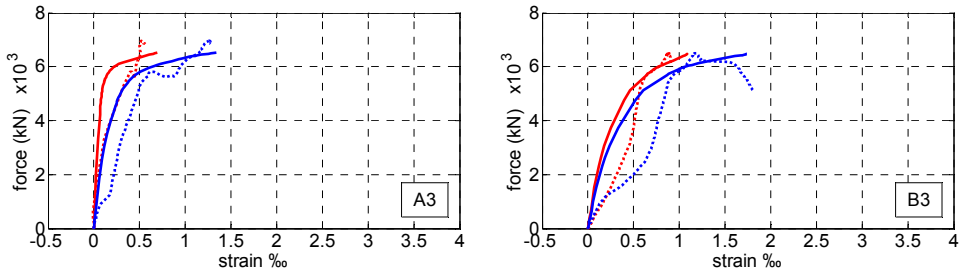


Fig. 214: Experimental vs. numerical static results; strain from gauges D1, D3

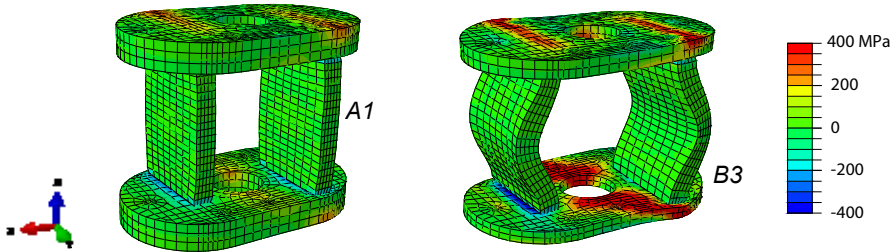
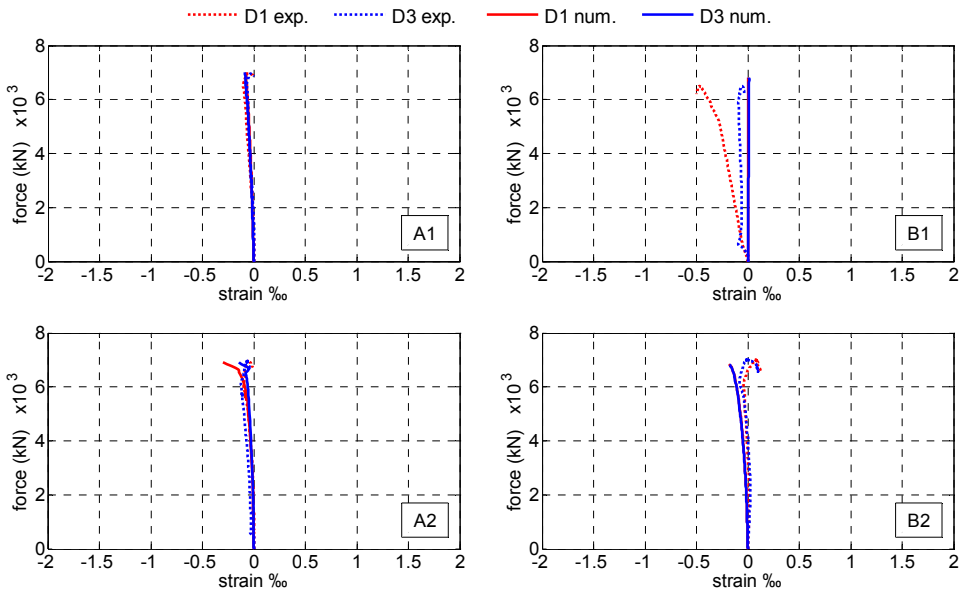


Fig. 215: Stress σ_x ; samples A1 and B3



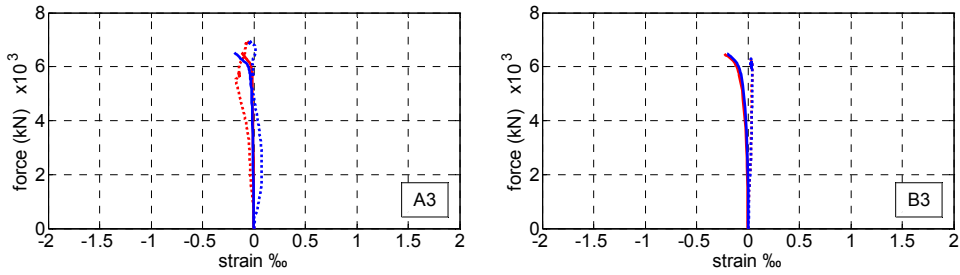


Fig. 216: Experimental vs. numerical static results; strain from gauges D2, D4

Last but not least, even strains data collected by gauges stuck on vertical steel plates are compared with numerical records. As stated in chapter 3.3.6, higher vertical strains than recorded were expected from experimental tests. A part from sample A3, even numerical solutions retrieve strains sensibly higher than experimental ones.

For sample A1, the absence of buckling phenomena during numerical simulation lead to a uniform distribution of strain Fig. 219 (left) and stress levels Fig. 220 (left) on the vertical steel plate. Strain level attains 2.5% (eq. 76) and corresponds to the analytical value expected when buckling is disregarded.

$$\epsilon_{\max,A1} = u_{F_u,A1} / h_{\text{joint}} = 9.53 / 380 = 0.025 \quad (76)$$

For all remaining samples, being horizontal steel plate less stiff than A1, buckling of vertical steel plate is well captured by numerical simulation. As shown in Fig. 219 (left) and Fig. 220 (left) both stresses and strains are no longer uniformly distributed along vertical plates. On the outer faces strain level tends to be lower than the inner face. This cause the vertical strain to be lower for those samples with less stiff horizontal plates, as buckling effect is encouraged. This partially justify the experimental evidence of strains level lower than expected, even if what stated in chapter 3.3.6 remain still valid: both concrete splitting out and vertical plate buckling contributed surely to sensor damaging. The proof in this sense may be identified in experimental sample A3. In this case a unique sensor worked continuously until a strain level slightly higher than 10% was attained, comparable to the value provided by numerical simulation. This suggests that even remaining models provide a realistic estimation of real deformation experienced by steel plate during testing.

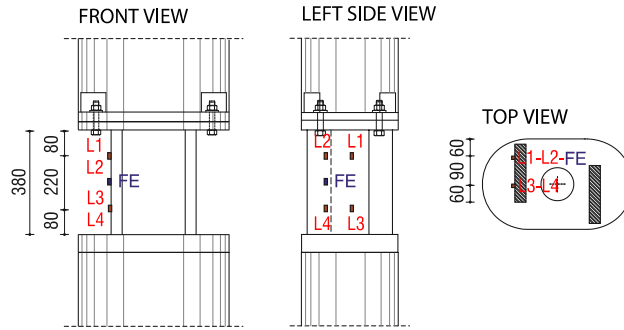


Fig. 217: Vertical steel plate strain-gauge location: sensor L1 L2 L3 L4

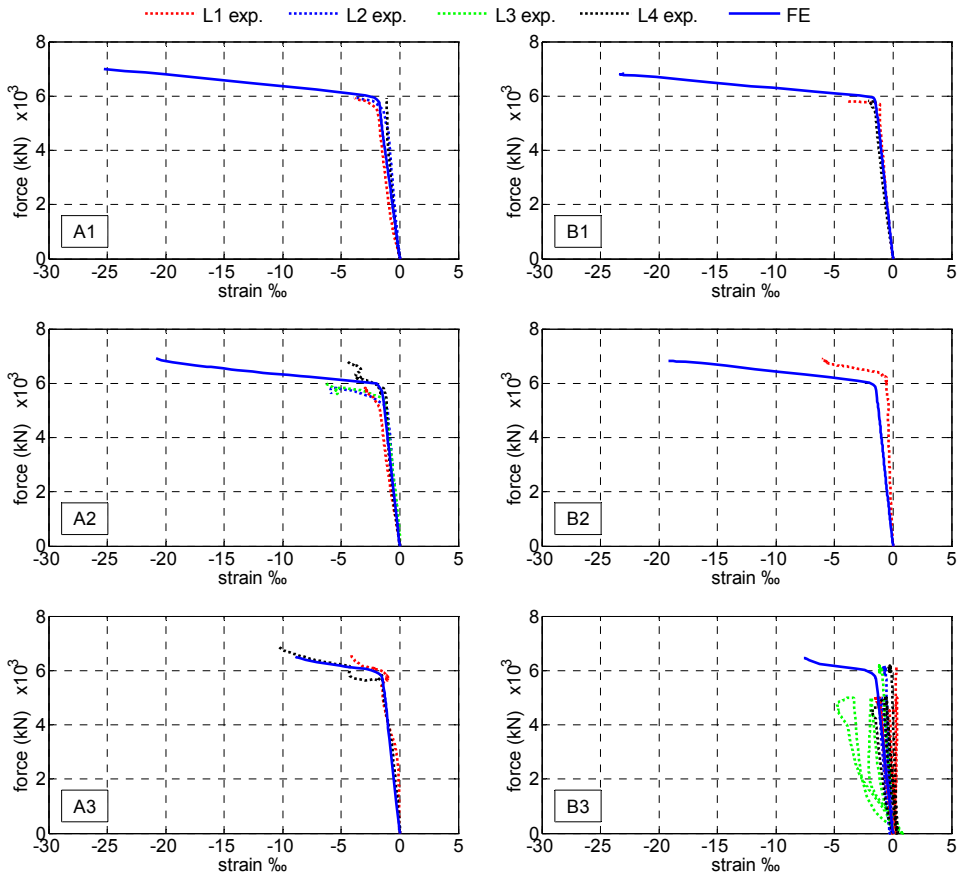


Fig. 218: Exp. vs. numerical static results; strain from sensors on bottom horizontal steel plate L1 L3

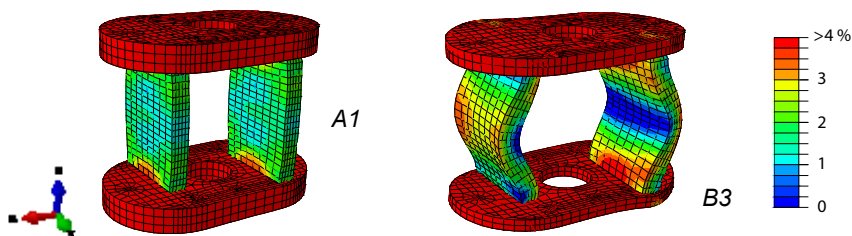


Fig. 219: Strain ε_{zz} ; samples A1 and B3

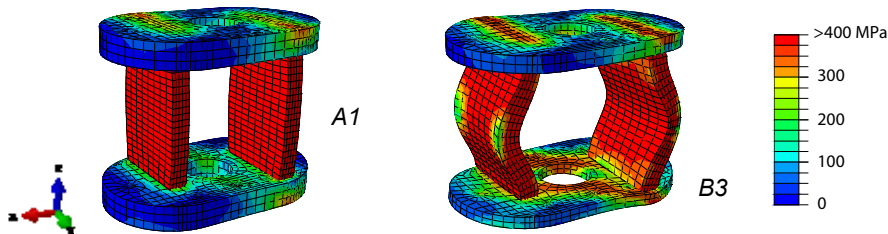


Fig. 220: Von Mises Stress; samples A1 and B3

6.4. Conclusions

With the aim of providing a mathematical model as a reference for all subsequent analysis presented in the following chapters, static lab tests are simulated via numerical model. The adoption of an effective and flexible FE tool, namely Abaqus V.6.10 (Simulia, 2010), allows for a detailed modeling of the geometry of the samples, implementing non-linear constitutive material laws defined in previous chapters.

Global and local quantities provided by experimental campaign are compared to those retrieved by FE models. Global quantities expressed in terms of force vs. displacement relationships show a satisfactory agreement. Realistic simulation of second order effects relative to buckling phenomena of vertical steel plates, is a further proof about the robustness of the adopted numerical approach.

Also local quantities show a rather good correspondence, in particular the one referring to local concrete strains, despite the mesh dependency issue related to numerical modeling of concrete material. This represents an additional validation of constitutive model for concrete defined in chapter 4, and confirms FE software ability to deal with highly non-linear problems.

7. OPTIMIZATION OF COMPOSITE-COLUMNS

7.1. Introduction

This chapter focuses on the estimation of the composite-column's strength domain and on the optimization of the layout of column to core-joint coupling system. The first aspect aims to take major confidence with expected structural performance in term of pure axial loading and combined axial-bending solicitations. The latter has economic implications. Analyses are performed using Abaqus V.6.10 (Simulia, 2010). Numerical models and constitutive laws validated against experimental static tests (cf. ch.6), are taken as a reference to develop the new models presented in this chapter.

In chapter 3.3 it is stated as during static experimental testing, core-concrete was subjected to splitting failure, when approaching an axial load level almost equal to 5000 kN, due to absence of lateral confinement. In real-case applications such a failure is prevented by confining action provided by flooring system. In addition, specific reinforcement cages might be adopted, especially for exterior joint. In this chapter it is assumed that adequate confinement is provided to core-joint, in order to investigate maximum performances available from composite-column system.

Firstly, the reference resistance domain of HSC column and composite core-joint taken as separate are defined. Several analyses are performed imposing increasing rotation at the top of the FE model (corresponding to a concentrate bending action) at different axial load levels, to get the complete M-N strength domain.

Secondly, the above explained approach is adopted to investigate structural performances of composite-column, the latter given by assembling HSC column and composite-core-joint together. Both single flange welded connections and bolted connections are considered. Aiming to identify the optimum layout column-to-column coupling system, a parametric analysis is conducted, varying the thicknesses of flanges. Optimum solution is identified as the one able to provide an adequate stiffness and strength to the composite-column, with the minimum amount

of required steel, to make the proposed precast system still more competitive from the manufacturing costs point of view.

7.2. HSC column numerical analyses

HSC column FE model is derived from reference models adopted for static experimental test simulation (see par. 6.2). The model represents a HSC column stub, 0.79 meter long (Fig. 221a). Longitudinal rebars (in blue in Fig. 221b) and concrete are explicitly solid modeled through hexahedral elements (C3D8R), while confining spiral stirrups (in red in Fig. 221b) are modeled with embedded linear truss elements (B31). Perfect bond between concrete and reinforcement is supposed.

At top and bottom of the model, two rigid planes are meshed with quadrilateral elements (R3D4). These allow to redistribute boundary conditions over the whole column section, avoiding stress concentration at column's ends.

The so defined model consists of 10375 nodes, 7440 solid, 192 planar and 216 linear elements, for a total of 7848 finite elements.

The base is assumed as fixed, while two load steps are considered at top column's end. During the first step, an axial force is applied. Several numerical simulations are performed with axial load level ranging between 0 to N_{MAX} , by step 2000kN. The second step consists on an imposed increasing rotation. Being this step displacement-controlled, softening branch of the global structural response can be monitored. N_{MAX} is evaluated by increasing axial force level until convergence is not attained anymore. This procedure allows to get an accurate estimation of M-N (bending moment vs. axial force) strength domain for HSC column (Fig. 223). Such a domain results fundamental for all subsequent numerical analyses, since it represents the reference limit strength-domain for the composite-column assembly. Fig. 222 shows the numerical response in terms of M- χ (reaction moment vs. curvature) curves at different axial load levels. Considering that model section property is constant, curvature can be estimated simply dividing the imposed rotation value by the samples' height.

$$\chi = \varphi/h \tag{77}$$

where φ =top rotation; h =model's height

Finally, in Fig. 224 the section bending stiffness is plotted as a function of axial load level. Stiffness is evaluated as the secant slope at 75% of maximum strength (M_{MAX}) in the $M-\chi$ diagrams (eq. 78), as suggested by Legeron & Paultre, 2000:

$$EJ_{COL} = 0,75M_{MAX} / \chi_{COL}^{75} \quad (78)$$

where χ^{75} =curvature at 75% M_{MAX}

It should be noticed as estimated maximum axial strength capacity for HSC column is about 15000kN, more than double of the maximum axial force level attained during experimental testing.

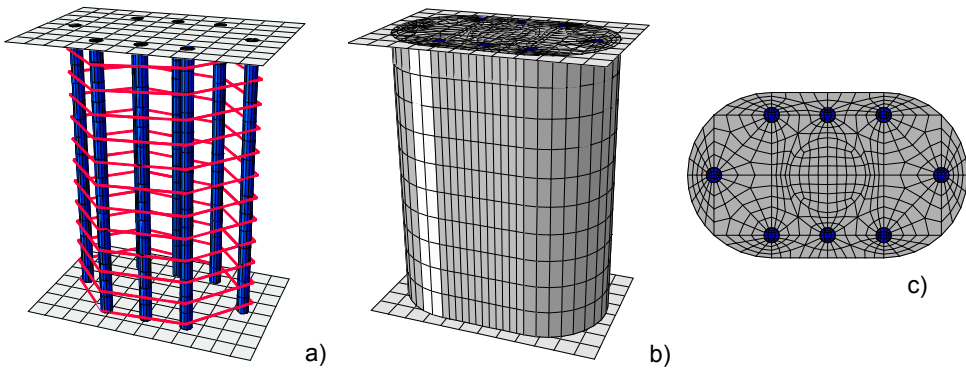


Fig. 221: Column FE model; a) full model; b) embedded reinforcement; c) mesh section

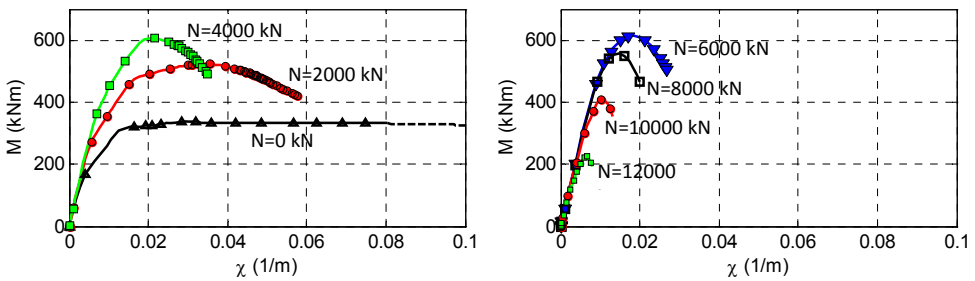


Fig. 222: Moment vs. curvature; F.E. solution from different model and axial load conditions

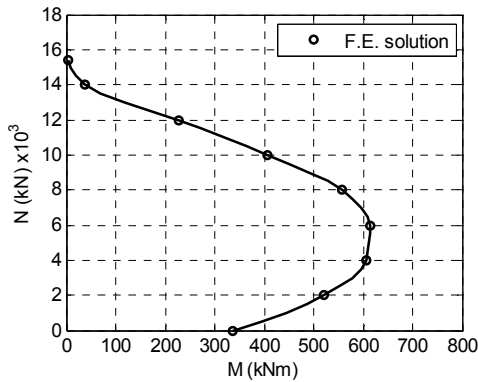


Fig. 223: M-N strength domain for HSC column: FE solution

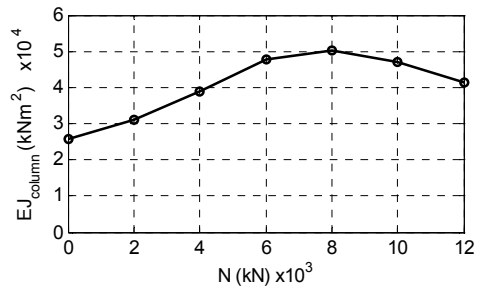


Fig. 224: HSC column stiffness versus axial force: FE solution

7.3. Core-joint numerical analyses

Similarly to HSC column, also the core-joint is modeled separately to get its response in term of strength and stiffness, as a function of acting axial load level.

The FE model is reported in Fig. 225. It consists in two vertical steel plates made in structural steel S355, with section dimensions 210 by 40 mm, embedded in normal strength concrete (C25/30). Both, concrete and vertical plates are modeled through hexahedral elements (C3D8R), with a contact region on the sheared surfaces, to account for interaction phenomena. A classic Mohr-Coulomb constitutive law is adopted for this purpose setting a friction coefficient $\mu=0.4$. Two rigid planes, meshed with quadrilateral elements (R3D4) are introduced to limit stress concentration at both model's ends, where boundaries conditions similar to those adopted for HSC column get applied. The model consists of 10375 nodes and 4168 solid and 192 planar elements, for a total of 4360 finite elements.

Experimental static testing evidenced that, due to absence of passive confinement, concrete core tends to a premature splitting failure, in particular for heavier axial loading conditions. Other confinement contributes should than be considered in order to exploit maximum core-joint strength. For inner joints, such a condition is provided by flooring systems and lateral beams. For external joints specific reinforcement details should be applied to provide required confinement level (cf. ch.12.8). In the following analyses, the core-joint strength domain is computed with reference to interior joints, where adequate confinement is surely provided by flooring system. A conservative estimation for this contribute is provided by

equation 79, based on a formulation developed by Cusson & Paultre, 2008 to account for passive light confinement condition (eq.56):

$$\sigma_{conf} = \nu_c \varepsilon_{c,0} E_c = 0,2 \cdot 0,002 \cdot 32200 / 2 = 6,4 MPa \quad 79)$$

where σ_{conf} =confining pressure; ν_c =Poisson's coefficient evaluated in the elastic range (=0.2); E_c '=equivalent' secant modulus of elasticity at peak stress (f_c/ε_c), assumed as half of reference elastic modulus E_0 .

The estimated value is rounded down to 5 MPa, to take into account the approximation of proposed formulation. Such a pressure is applied on the outer joint surface, during the first load step, while applying axial loading.

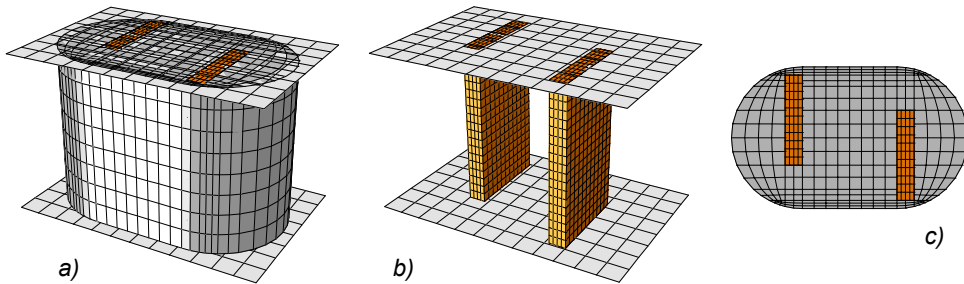


Fig. 225: Core-joint FE model; a) full model; b) embedded steel plates; c) section mesh

The $M-\chi$ curves retrieved by numerical model are plotted in Fig. 226 together with the reference ones, provided by numerical model of bare HSC column.

Also in this case the curvature estimation is based on the assumption of constant section property and thus it is taken as the imposed rotation value divided by the samples' height (eq. 77). Strength domain results wider than HSC column reference one (Fig. 227), suggesting that core-joint should not be considered as a weak component of the precast assembly, at least when proper confinement is assured. Core-joint behaviour is also considerably more ductile compared to HSC column, in particular for axial load levels higher than 6000 kN, mainly thank to larger amount of steel (provided by vertical steel plates) and to NS in place of HS concrete. Section stiffness is estimated through equation 80, adopting the same procedure as for HSC column:

$$EJ_{JNT} = 0.75M_{MAX} / \chi_{JNT}^{75} \quad 80)$$

where χ^{75} =curvature at 75% M_{MAX}

Core-joint's stiffness results higher than HSC column's one for axial load levels lower than 4000kN (Fig. 229). As a result, for higher axial loading, core-joint deformability should be explicitly considered when evaluating composite-column equivalent stiffness.

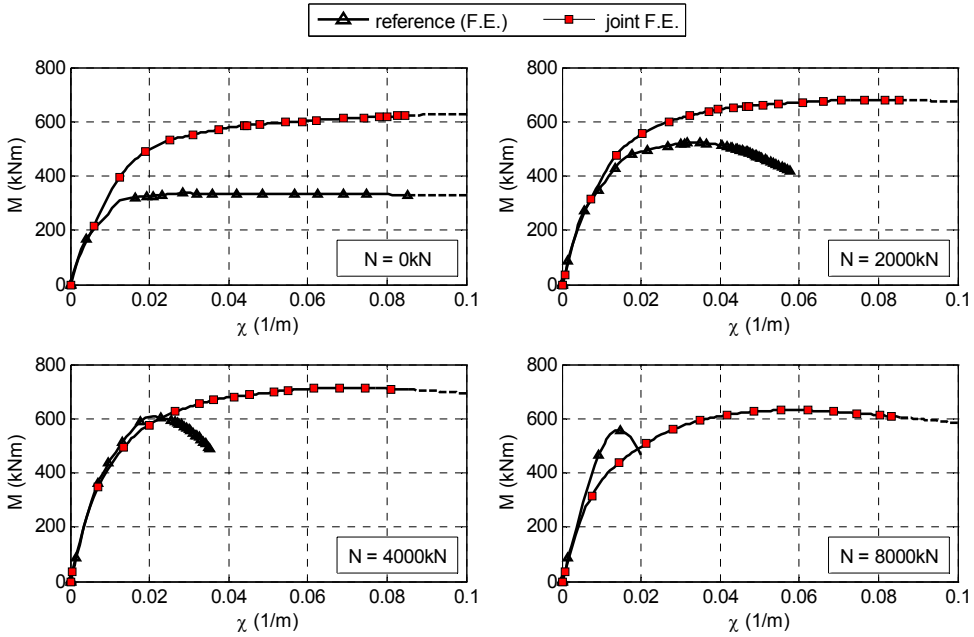


Fig. 226: Moment vs. curvature; F.E. solution from different model and axial load conditions

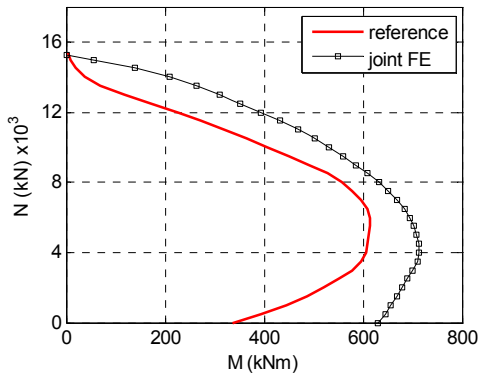


Fig. 227: M-N domain; reference domain vs. domain

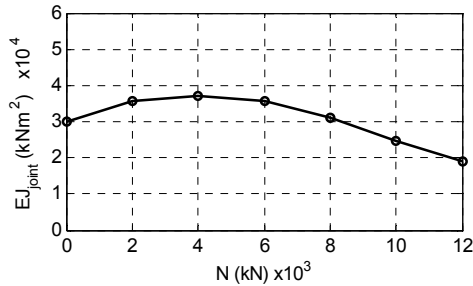


Fig. 228: Core-joint stiffness vs. axial load

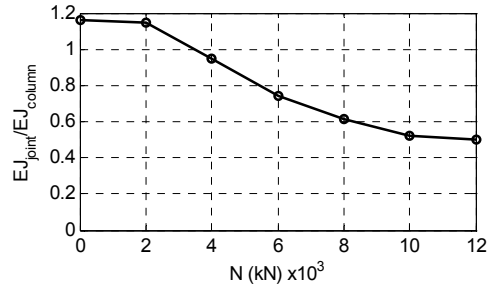


Fig. 229: Core-joint vs. HSC column vs. axial load stiffness ratio

7.4. Column-joint connected with welded flanges

Previous analyses define the strength domain for column and core-joint modeled as separate. In this chapter, a FE model is considered, with the HSC column and the composite-core-joint connected together by an horizontal steel flange. Such a model represents the lower part of the proposed composite-column layout, with the lower column connected to the upper “windowed” steel-joint. The model consists of 16580 nodes, 11758 solid, 192 planar and 216 linear elements, for a total of 12176 finite elements. Reference should be made to chapters 7.2 and 7.3 to get more details about modeling techniques for HSC column and core-joint, respectively.

These analyses aim to investigate the connection’s strength mechanism and to identify the optimum steel-flange layout, through a parametric study, varying flange’s thickness from 20 to 60 mm with steps of 10 mm, for a total of 5 different models.

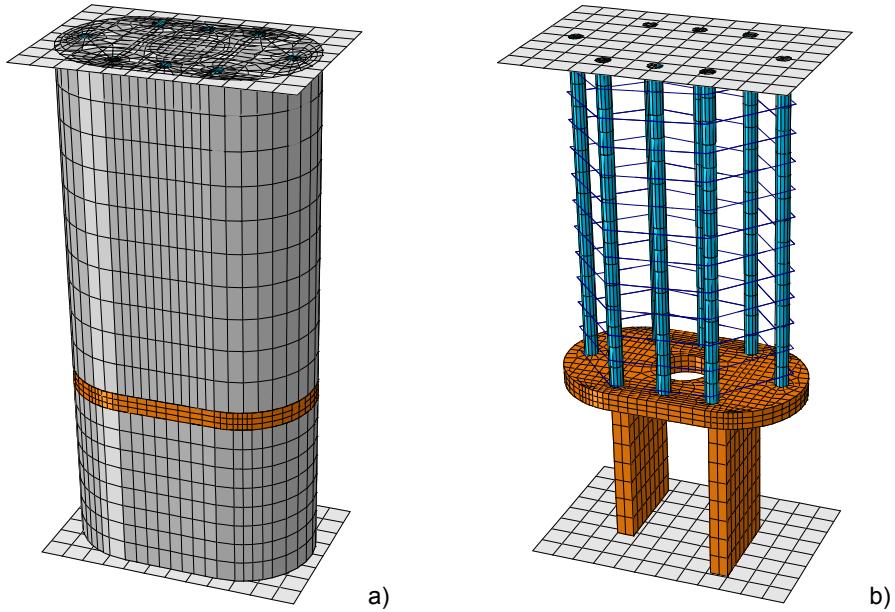


Fig. 230: Single-flange composite-column FE model; a) full model; b) inside steel plates and rebars view

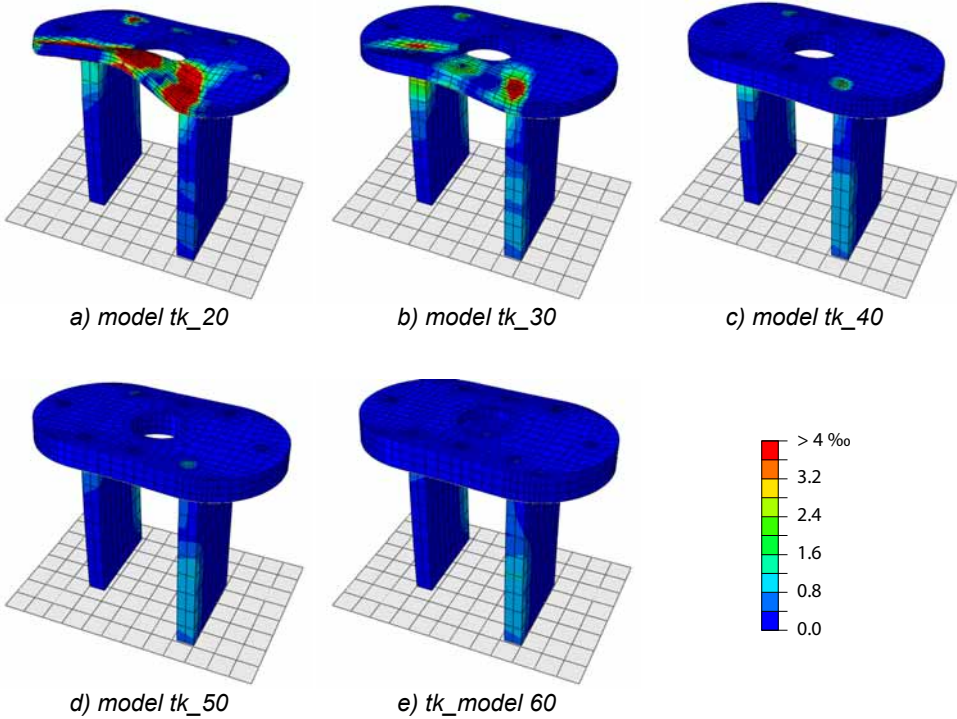


Fig. 231: Plastic strain at column-to-joint interface: single flange welded connection; deformation scale factor 10x

In Fig. 231 the plastic deformations of steel-core-joint are plotted for each considered model. Upper column's rebars in tension provide transversal bending on the horizontal steel flange and induced stresses can increase until yield limit is exceeded. The lower is the flange thickness, the wider is the portion of yielded material, in particular in the zone where horizontal flange is constrained by lower vertical plates welded on it. Steel-joint evidences a global elastic behaviour for flange's thicknesses higher than 40mm. In Fig. 232 the reaction moment vs. curvature is plotted for several models and axial load levels and it is compared with reference curves (provided by HSC column). The section curvature χ is computed from rotation data, through equation 77. In this case, it should be better talking about equivalent curvature χ_{eq} , being section property not constant along the composite-column. Looking at the strength domain plotted in Fig. 233, Increasing flange's thickness lead to a better fitting of reference strength domain provided by HSC column. A clearer global representation of composite-column strength capacity compared to HSC column is better reported in Fig. 234a. For axial load levels lower than 4000kN, all samples are able to withstand more than 95% of the reference bending strength. In the range between 4000 and 10000kN, only model with flange thickness bigger than 40 mm can withstand more than 90% of the reference strength. Increasing flange's thickness from 40 to 60 mm leads to a limited performance improvement. For axial load levels bigger than 10000kN, models with thickness equal to 20, 30 and 40 mm drop down to less than 60% of the reference strength, while the remaining reach satisfactory strength level. In Fig. 234 a similar analysis is reported, comparing stiffness of the composite-column and HSC column. Stiffness get evaluated as the secant stiffness when 75% of maximum strength is attained in the loading branch of the M- χ curves. Worst performances characterize samples with flange thickness lower than 40 mm, when axial load level is lower than 2000kN. For all the remaining samples, bending stiffness is comparable with reference one provided by HSC column (more than 90% of the reference value), with exception for axial load levels bigger than 10000kN. Increasing flange thickness from 40 to 60 mm leads to a limited performance improvement. In the light of these observation, it can be stated that numerical sample with flange thickness equal to 40 mm is the best compromise between performance and required amount of steel. Potentially, there are two main reasons for that. On the one hand, limited performance in terms of strength is evidenced only for axial loads bigger than 10000kN, which is however a value never attained considering design solicitations (cf. ch.9.4 and eq. 64). On the other hand, limited performance improvement is obtained increasing flange thickness more than 40 mm.



Analysis and development of an innovative prefabricated beam-to-column joint

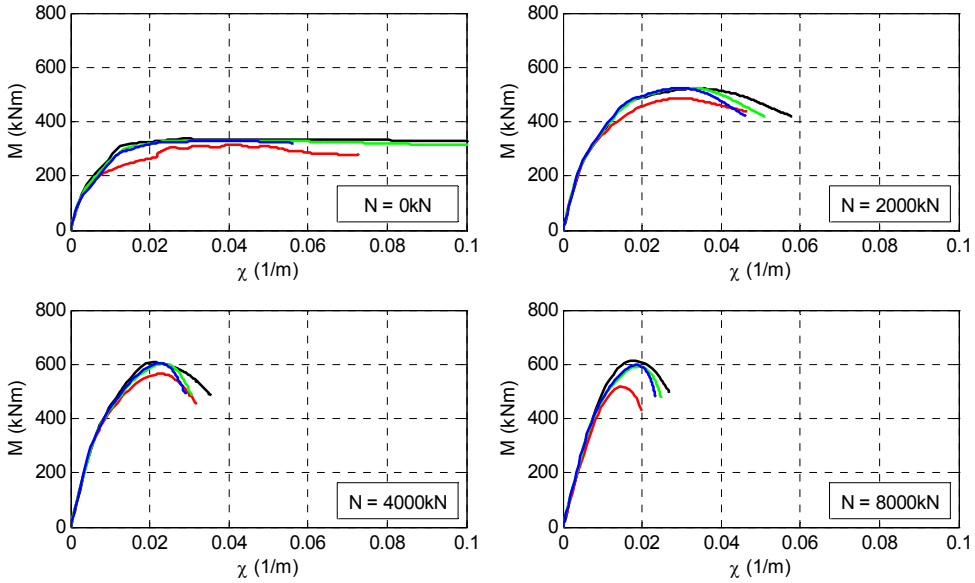


Fig. 232: Mom. vs. curvature (FE solution); composite-column with single flange welded connection

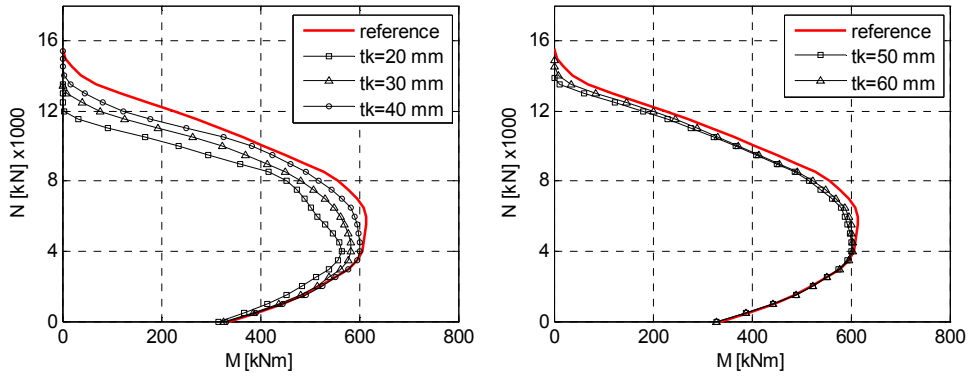


Fig. 233: M-N domain (FE solution); composite-column with single flange welded connection

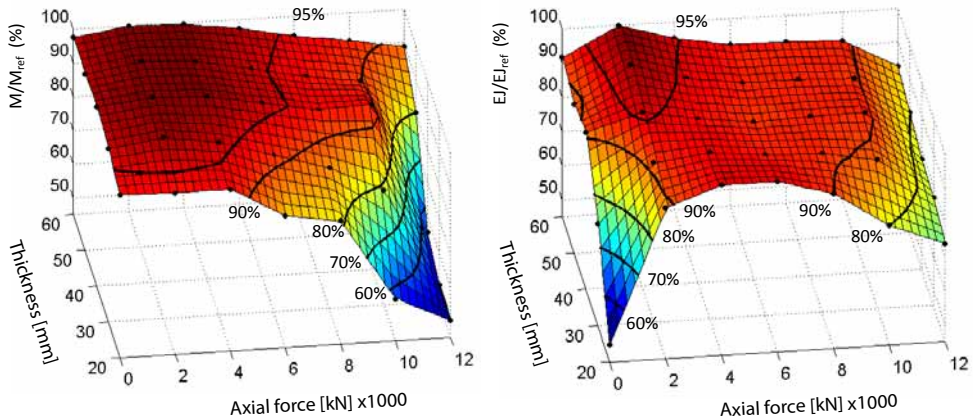


Fig. 234: Composite-column with single flange welded connection; global performances in term of strength ratio (left) and stiffness ratio (right)

7.5. Column plus bolt-connection (4 bolts)

In this chapter, the structural performances of a composite-column considering a bolted joint-to-column connection are investigated. The bolted coupling system is accurately reproduced by solid modeling of bolts and nuts (Fig. 235). Between horizontal steel-flanges and outer bolts' surface, a contact surface is introduced, to account for sliding, gap-openings and over-closures. A Mohr-Coulomb constitutive model is adopted for this purpose, setting the coefficient $\mu=0.4$ and null cohesion. The whole models get meshed by hexahedral solid elements (C3D8R), with the only exception of spiral stirrups in the column, truss modelled with R3D4 elements. To get more details, about modeling and material property adopted for HSC column and composite-core-joint, reference should be made to chapter 7.2 and 7.3. Boundary conditions correspond to those applied for previous analyses. The so defined models consist of 27791 nodes, 19414 solid, 192 planar and 216 linear elements, for a total of 19822 finite elements. Also in this case, main objectives of the analyses is clarify the connection strength-mechanisms and mechanics, as well as identify the most favourable layout in term of both performance and needed steel metal. Towards this aim a parametric study is conducted varying horizontal flanges' thicknesses. To reduce the number of possible combinations, 6 have been chosen on the basis of engineering judgement, namely 20/20, 20/30, 20/40, 30/30, 30/40, 40/40, where the first and the second number is the thickness for respectively, lower and upper flange.

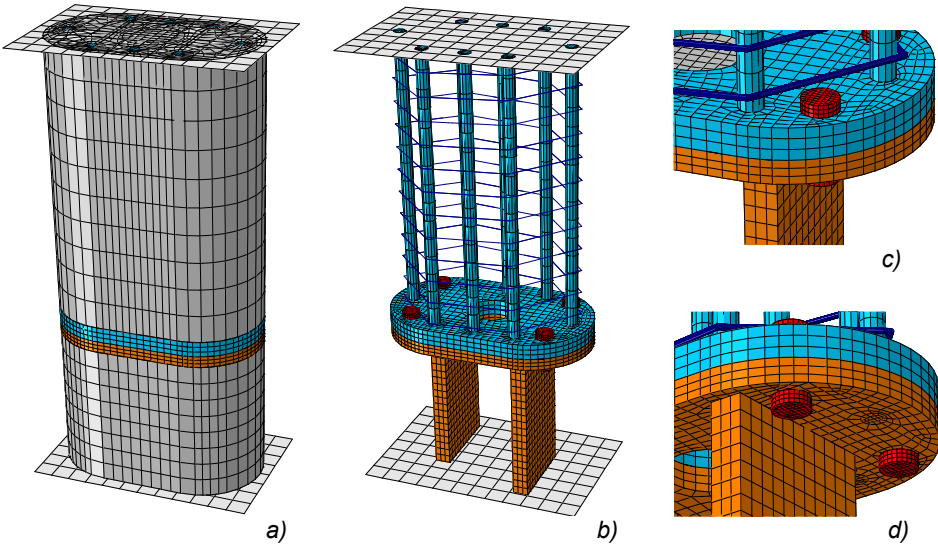


Fig. 235: Double flange-composite-column FE model: 4 bolts layout ; a) full model; b) inside steel plates and rebars; c) d) detailed view of bolts modeling

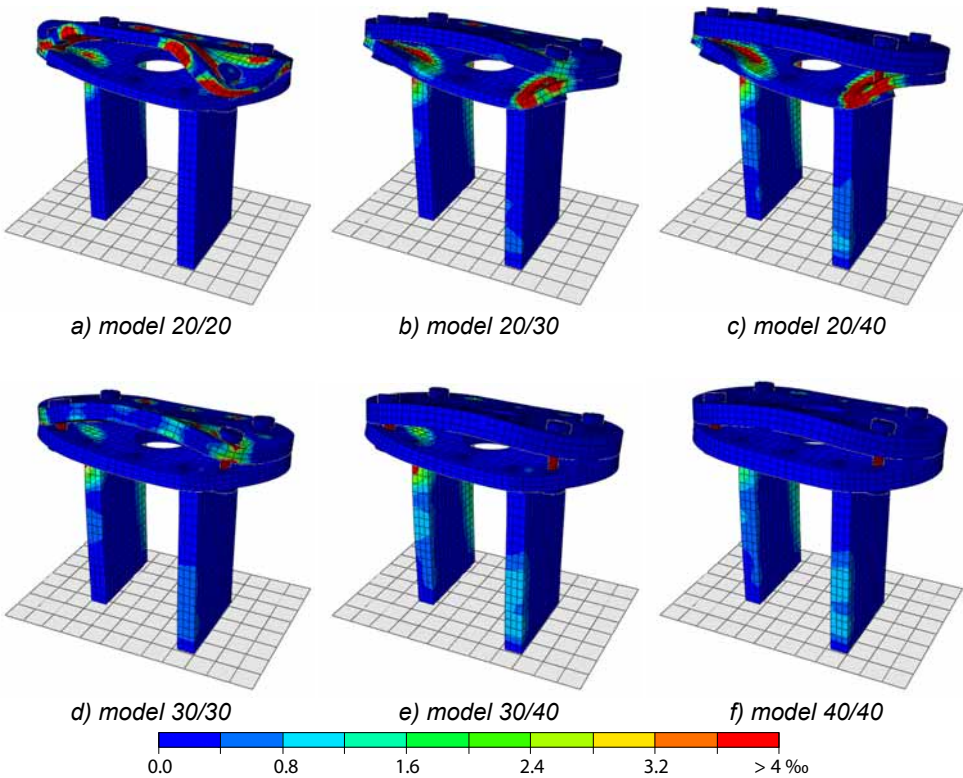


Fig. 236: Plastic strain at column-to-joint interface: 4 bolts flanged-connection; deformation scale factor 10x

Looking at equivalent plastic strains plotted in Fig. 236, several failures' type are recognizable depending of flanges' thicknesses. In model 20/20 the upper flange results excessively slender to withstand bending moment introduced by column's rebars in tension and therefore, several plastic hinges develop till to form a kinematic mechanism. Trend behaviour in model 30/30 is similar, although stiffer plates allow to limit the plastic strains spreading and the plastic mechanism does not fully develop. In models 20/30 and 20/40 as well, the weak element becomes the lower flange. Plastic hinges on this element develop in proximity of vertical steel plate as a result of excessive bending provided by bolts in tension, while upper flange perform still elastically. For all these models, behaviour of connection could be associated to "Mode 2" failure described in EN 1993-1-8:2005, characterized by both flanges and bolts yielding. In remaining models, flanges are stiff and strength enough to provide elastic performance until failure. Such a behaviour recalls the rigid mechanism ("Mode 3" failure) reported in EN 1993-1-8:2005, characterized by bolts yielding.

In Fig. 237 the reaction moment M vs. curvature χ is plotted for different models and axial load levels and compared with reference curves (provided by HSC column). From the strength point of view, increasing flange thicknesses leads to an general improvement of composite-column performances. Models "30/30", "30/40" and "40/40" fit reasonably well reference domain, with the exception of very low axial load levels (≈ 0 kN). This implies that bolted connection could represent a weak component of the assembly when limited axial loading is provided. Also composite-columns' equivalent stiffness results sensibly affected by low axial load levels, independently from connection layout (Fig. 238b). According to these observations, it is possible to identify model "30-30" as the optimum sample among the considered ones, since further increasing flange thickness does not provide any appreciable performance improvement neither in term of strength nor in term of stiffness. An alternative bolts' layout is presented in the next chapter, to improve connection performances when limited axial loading might be provided, as in the case of low storey frames or upper storeys in high-rise structures.

Analysis and development of an innovative prefabricated beam-to-column joint

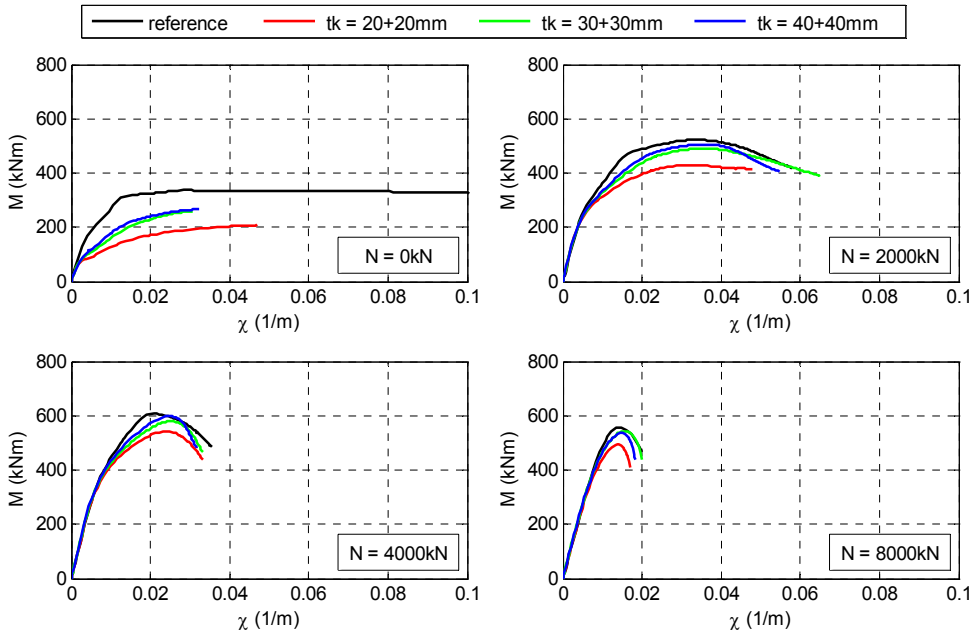


Fig. 237: Mom. vs. curvature (FE solution); composite-column with double flange bolted connection (4 bolts)

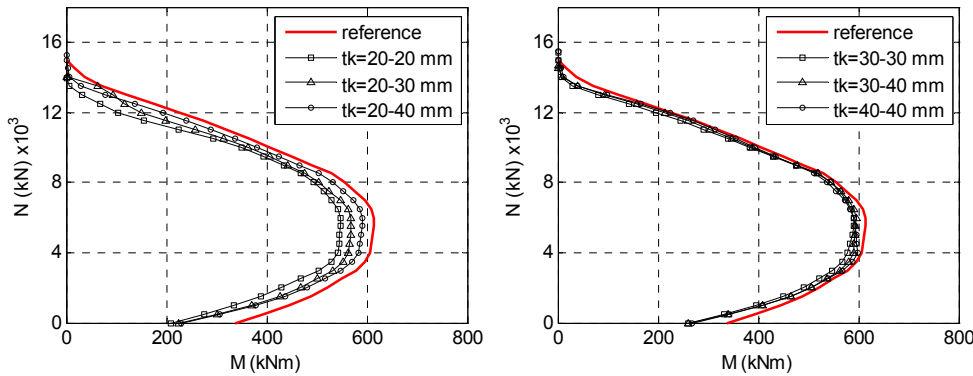


Fig. 238: M-N domain (FE solution); composite-column with double flange 4 bolts connection

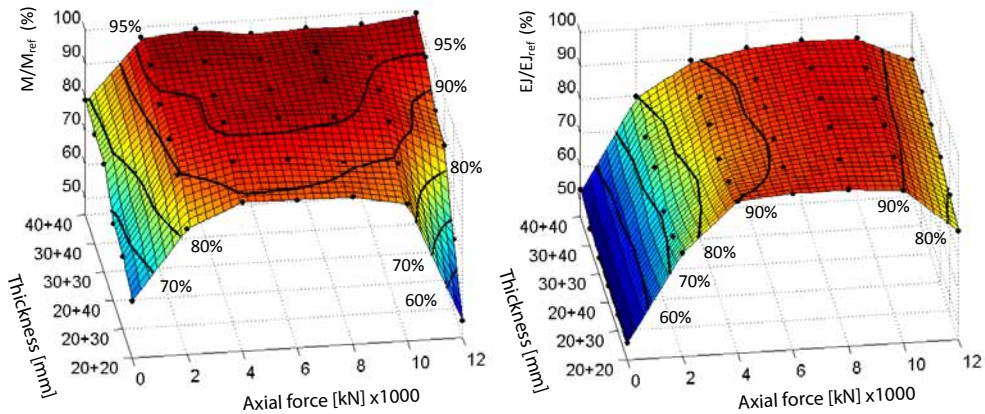


Fig. 239: Composite-column with double flange bolted connection (4 bolts); global performances in term of strength ratio (left) and stiffness ratio (right)

7.6. Column plus bolts-connection (6 bolts)

Analyses in paragraph 7.5 evidence how bolted flange connection considering four M24 10.9 bolts are satisfactory, both in term of strength and stiffness, assuming that enough axial load level is acting on the column (>2000kN).

To remove this limitation a bolted connection layout with two additional bolts is presented and investigated

Supplementary bolts get axially aligned with respect to a couple of column's longitudinal rebars, due to space restrictions. As a consequence bolts should be pre-welded on the upper steel flange directly on factory, before welding of longitudinal reinforcement.

The implemented numerical models consist of 26819 nodes, 18593 solid, 192 planar and 216 linear elements, for a total of 19001 finite elements.

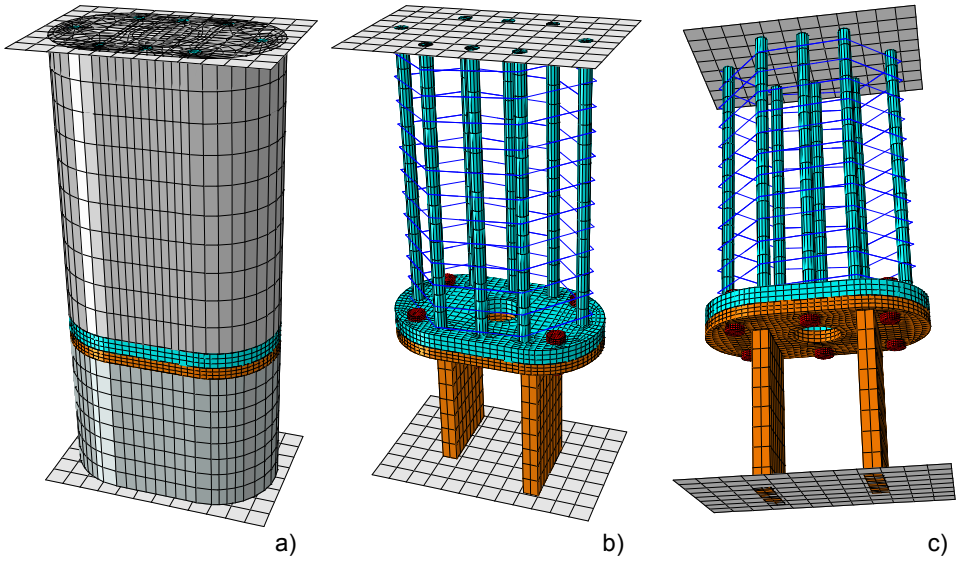


Fig. 240: Double flange-composite-column FE model: 6 bolts layout ; a) full model; b) inside steel plates and rebars view; c) bottom view

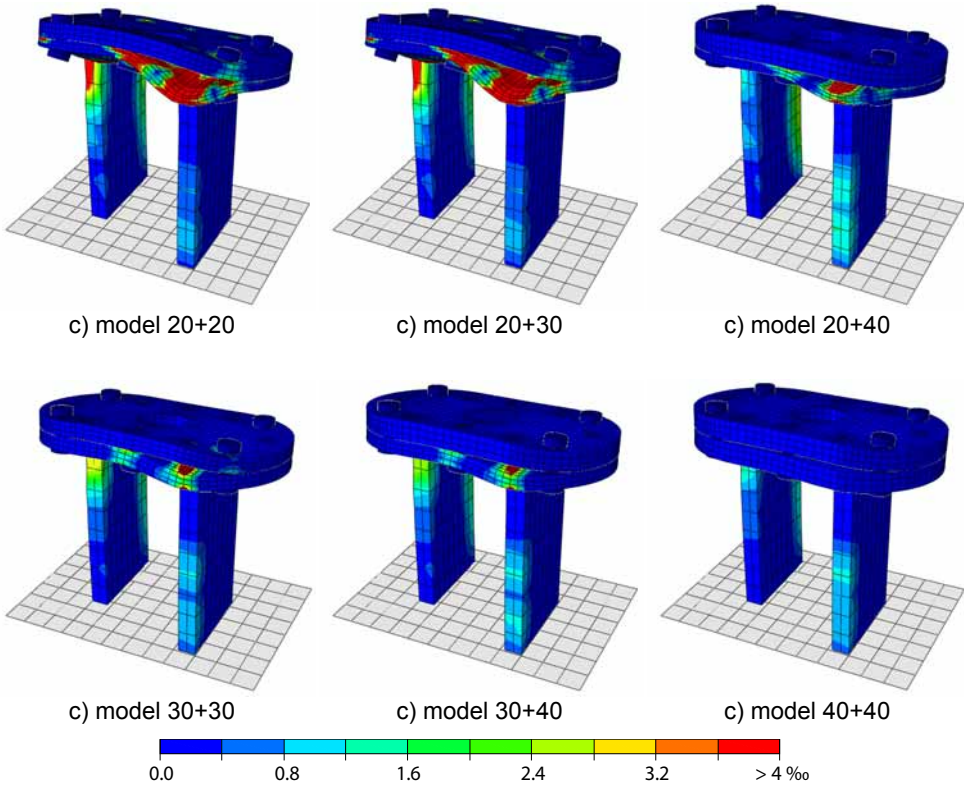


Fig. 241: Plastic strain at column-to-joint interface: 6 bolts flanged-connection; deformation scale factor 10x

The proposed bolts configuration affects sensibly stresses' distribution on horizontal flange compared to previous solution, as suggested by equivalent plastic strain contour reported in Fig. 241. The lower flange is the most stressed, independently from adopted flange thicknesses, due to bending solicitations induced by central bolt in tension acting on the whole span between vertical steel plates. Looking at Fig. 242 and Fig. 243, it appears evident as the strength gap between computed and reference domain at lower axial load level, get completely recovered. This is even more evident comparing tridimensional strength domain reported in Fig. 244a with the one in Fig. 239a. Less appreciable is the global stiffness improvement provided by supplementary bolts in connection. Better performances are attained for models "30/30", "30/40" and "40/40", with a stiffness gain of about 20% and 10% for load levels ranging between 0-2000 and 2000-4000kN, respectively (Fig. 244b). It can be concluded that, increasing the number of bolts in the connection is an effective way to attain adequate strength level in particular when limited axial loading is provided. Nevertheless, flanged connection still represents a structural discontinuity in the composite-column assembly. Connection stiffness should be explicitly considered for frame seismic design, to account for additional frame's deformability under lateral load and for a more realistic solicitations' distribution among members (cf. ch.8).

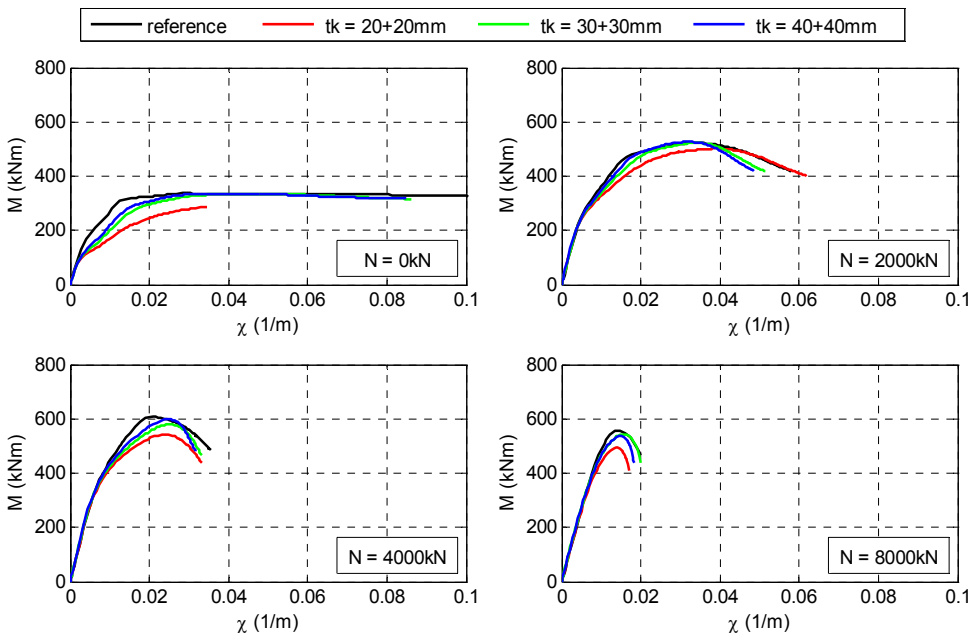


Fig. 242: Moment vs. curvature (FE solution); composite-column with double flange bolted connection (6 bolts)

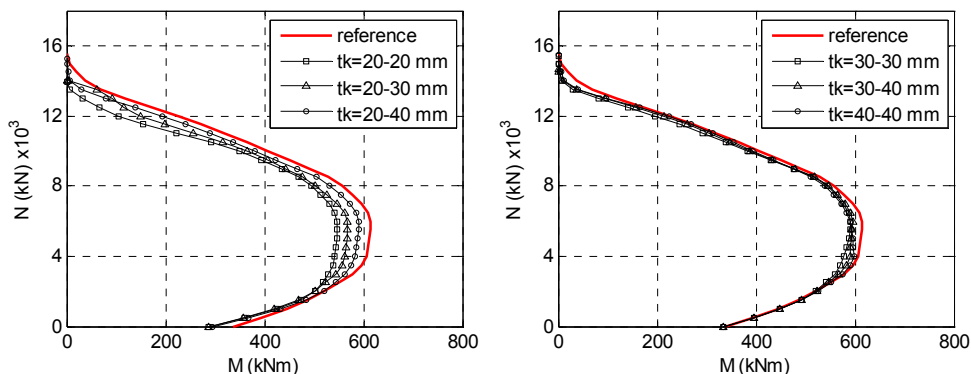


Fig. 243: M-N domain (FE solution); composite-column with double flange 6 bolts connection

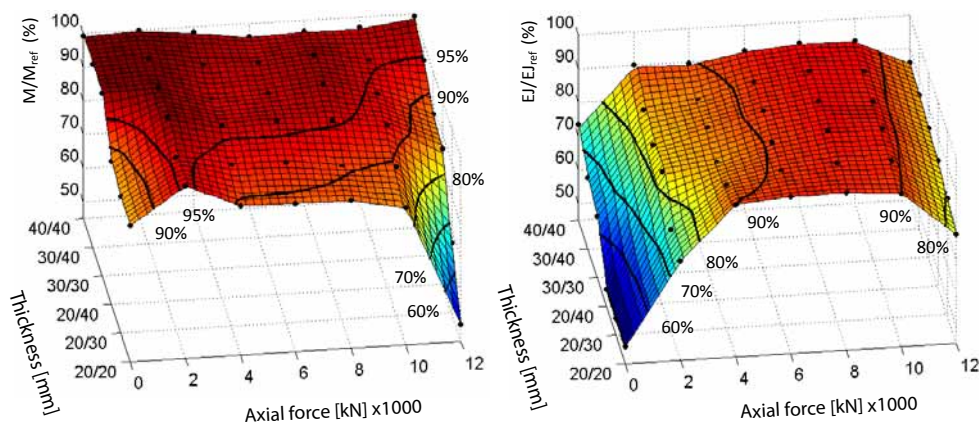


Fig. 244: Composite-column with double flange bolted connection (6 bolts); global performances in term of strength ratio (left) and stiffness ratio (right)

7.7. Conclusion

This chapter deals with the numerical investigation of structural performance of composite-column and composite-column's base components. Firstly the HSC column and composite-core-joint are numerically studied as separate, enabling the evaluation of corresponding strength domains. This comparison allows to classify core-joint as a strong component of the assembly, able to withstand higher axial-bending solicitations before failure, as long as adequate confinement to concrete core-joint is provided. This information results particularly important for seismic design consideration, since it allows to exclude the development of undesired

bending failure mechanism at joint level. Referring to static performance, maximum pure axial bearing capacity of the column attains almost 15000 kN, more than double the maximum force level attained during experimental testing, corresponding to bearing capacity available in the temporary phase (almost 6000kN cf. ch.3.3).

Secondly the connection interface between column and composite-joint is studied with the aim to identify resistant mechanisms and optimum flanges thicknesses' distribution corresponding to the best compromise between material saving and performance, both in term of stiffness and strength.

In the case of single flange welded connection, the best solution corresponds to a flange thickness equal to 40 mm. In bolted connection with 4 bolts, the best solution is identified in 30 mm thick flanges. Analyses allowed to identify a possible weak mechanism, corresponding to this type of connection in conjunction with low axial load levels. To remove this limitation, in particular for column's design of low storey frames or upper storeys in high-rise structures, a slightly modified layout is considered, introducing two more bolts. This improvement allows to gain the strength gap compared to reference HSC column strength domain, but not the stiffness gap. This suggests that bolted connection represents a structural discontinuity of the column-assembly and confirms the importance of explicitly considering its deformation contribute, especially during design of frame systems subject to lateral or earthquake loading (cf. ch.11.4).

8. ROTATIONAL STIFFNESS OF COLUMNS' COUPLING SYSTEMS

8.1. Introduction

In the current practice of analysis and design of steel, concrete or composite frame structures, the actual behavior of member to member coupling is simplified to the two idealized extremes of either fully-rigid behavior or ideally-pinned behavior. Although the adoption of such an idealized connection behavior greatly simplifies the analysis and design process, the predicted response of the idealized structure may be quite unrealistic compared to the response for the actual structure, in particular when dealing with non linear analyses (Elliott et al., 2004, Sassone & Bigaran, 2007, Pique & Burgos, 2008). From the practical point of view then, connection between members should nearly always be considered as semi-rigid (Ferreira et al., 2011). This is still more relevant when dealing with a precast structures, made by monolithic element assembled together with different jointing system. For the proposed precast system, particular care should be spent on the column-to-column connection system, since analyses reported in chapter 7 clearly evidence as it affects sensibly the global stiffness of the composite-column. This chapter deals with the explicit estimation for this deformation contributes, expressed in term of rotational stiffness, adopting as input data, those provided by numerical analysis in chapter 7. A particularly suited method to investigate this aspect is the so-called “components approach”, based on the assumption that global performance of a structural assembly may be described as the sum of the contributes provided by its base components. Such an approach is usually adopted in steel structures design, specifically to evaluate structural performances of flanged/bolted connections. Some applications are also reported in literature, to describe the behaviour of composite steel-concrete joints (Zordan, 2004, Briseghella, 2005). In the following, two formulations are proposed. The first one could be considered as a “reverse-component-approach” and is based on $M-\varphi$ (Moment vs. rotation) curves obtained by numerical analysis. The second formulation is an analytical component method approach based on elasticity theory.

Rotational stiffness estimations provided from both approaches are compared together, to check on consistency of proposed formulations.

8.2. Reverse component approach

The first method could be considered as a reverse application of the so-called “components approach”, since starting from the global response of the composite-column, expressed in term of M-φ (Moment vs. rotation) curves, the responses estimated for HSC column and core-joint are removed to filter out the contribute provided by mere interface connection. With reference to equation 81, the (absolute) top rotation of composite column could be defined as the integral of each section’s curvature over the whole model. The same integral could be expressed by summing up different rotation’s contributes, namely the core-joint, the interface and the HSC column ones. For the first and the latter contributes, integration become trivial, being curvature constant. Rearranging equation 81, the interface contribute can be highlighted. Such expression states that interface-connection M-φ curves could be obtained by subtracting from the composite-column’s M-φ curves, those relative to column and composite-core-joint as schematised in Fig. 245.

$$\varphi_{TOT}(M) = \int_0^{\ell} \chi(x) dx = \int_0^{h_{JNT}} \chi_{JNT}(M) dx + \varphi_{INT}(M) + \int_0^{h_{COL}} \chi_{COL}(M) dx \quad 81$$

$$\varphi_{INT}(M) = \varphi_{TOT}(M) - \varphi_{JNT}(M) - \varphi_{COL}(M) \quad 82$$

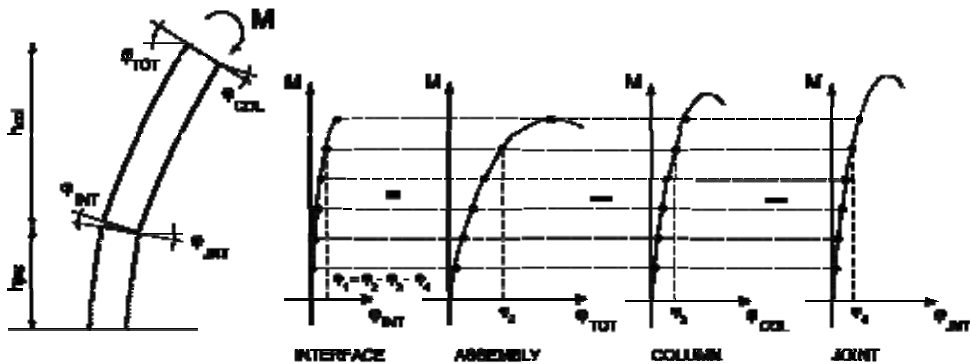


Fig. 245: Calculation of interface connection stiffness: “reverse components method”

Once the M - φ relationships for the interface are available, stiffness is assumed as the secant slope of the curve at 75% of maximum bending moment (Legeron & Paultre, 2000):

$$K_{INT} = \frac{0.75M_{MAX}}{\varphi_{INT(0.75M_{MAX})}} \quad 83)$$

8.3. Analytical component approach

The analytical component approach is based on an analytical formulation derived from elasticity beam theory, aiming to a simplified expression to calculate interface-connection stiffness. Given a composite-column, top deflection due to concentrate bending acting at column's end can be expressed as the summation of deflection contribute due to column (Δx_{COL}), composite core-joint (Δx_{JNT}) and interface connection (Δx_{INT}) (see eq. 84 to 86 and Fig. 246).

The top chord rotation (not to be mistaken with the absolute or total rotation) of the assembly can be expressed as in equation 87.

$$\Delta x_{COL}(M) = \frac{M \cdot h_{COL}^2}{EJ_{COL}} \quad 84)$$

$$\Delta x_{JNT}(M) = \frac{M \cdot h_{JNT}^2}{2S_{JNT}} + \frac{M \cdot h_{JNT} \cdot h_{COL}}{S_{JNT}} \quad 85)$$

$$\Delta x_{INT}(M) = K_{INT} \cdot h_{COL} \quad 86)$$

$$\varphi_{CHORD}^{ASS} = (\Delta x_{COL} + \Delta x_{JNT} + \Delta x_{INT}) / (h_{JNT} + h_{COL}) \quad 87)$$

The equivalent composite-column chord stiffness at a certain bending moment level, can be expressed as:

$$K_{CHORD}(M) = M / \varphi_{CHORD}(M) \quad 88)$$

Actually, the chord stiffness is an unknown quantity, since the rotation quantity recorded from numerical model is the total (or absolute) top rotation and not the chord rotation.

However, it is still possible to assume that the ratio α between the chord stiffness of mere HSC column and composite-column is equal to the ratio between their absolute stiffness.

$$\alpha = \frac{K_{CHORD}^{ASS}}{K_{COL}^{COL}} = \frac{K_{TOT}^{ASS}}{K_{TOT}^{COL}} \tag{89}$$

where ASS=assembly; COL=HSC column; CHORD=cord rotation; TOT=total or absolute top rotation.

At this point the parameter α is a known quantity. Rearranging equation 89 leads to the following expression:

$$K_{CHORD}^{ASS} = \alpha \cdot K_{CHORD}^{COL} = \alpha \cdot 2EJ_{COL} / h_{COL} \tag{90}$$

Finally, rearranging expressions 87, 88 and 90, following analytical formulation can be defined to express secant stiffness of connection system between HSC column and composite-core-joint. All quantities are known. In particular EJ_{COL} and EJ_{JNT} are defined in chapters 7.2 and 7.3.

$$K_{INT} = h_{COL} \cdot \left[\frac{h_{COL} + h_{JNT}}{2\alpha \cdot EJ_{COL} / h_{COL}} - \frac{h_{COL}^2}{2EJ_{COL}} - \frac{h_{JNT}^2}{2EJ_{JNT}} - \frac{h_{JNT} \cdot h_{COL}}{2EJ_{JNT}} \right]^{-1} \tag{91}$$

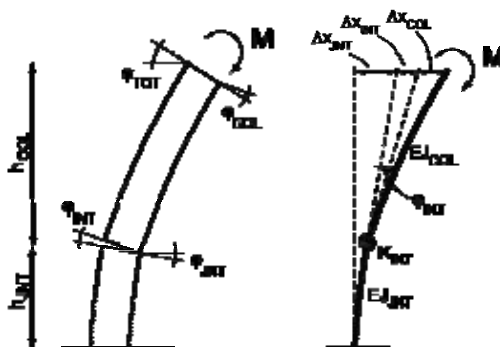


Fig. 246: Calculation of interface connection stiffness: analytical approach

8.4. Rotational stiffness of column-to-joint interface

To evaluate consistency of both presented formulations, estimated interface rotational stiffness values are directly compared ones against the others. Three different comparison are reported relative to single flange welded connection (Fig. 247) and double flange connection with 4 (Fig. 248) and 6 bolts (Fig. 249). Values above 10^6 kNm/rad, are limited in order to highlight behaviour at low axial load level. Looking at results, it can be seen as there is a good agreement between complementary formulations, and this could be considered as a sort of validation about goodness of their theoretical background. In general, for all kind of connections, there is a clear relationship between axial loading and stiffness values. Less influence is provided by flange thicknesses. Among all layouts, higher stiffness values are provided by single-flange solutions for all axial load levels. Related to double-flange bolted connection, it appears that improvement in terms of stiffness due to additional bolts is limited. Base on these results, the strength and deformation contributes provided by column to column coupling systems can be explicitly accounted, in particular for modeling of frame structures adopting proposed precast solution. In the following reference is made to “reverse components approach”, which provide more uniform results without local jumps or discontinuities in plotted tridimensional response surfaces.

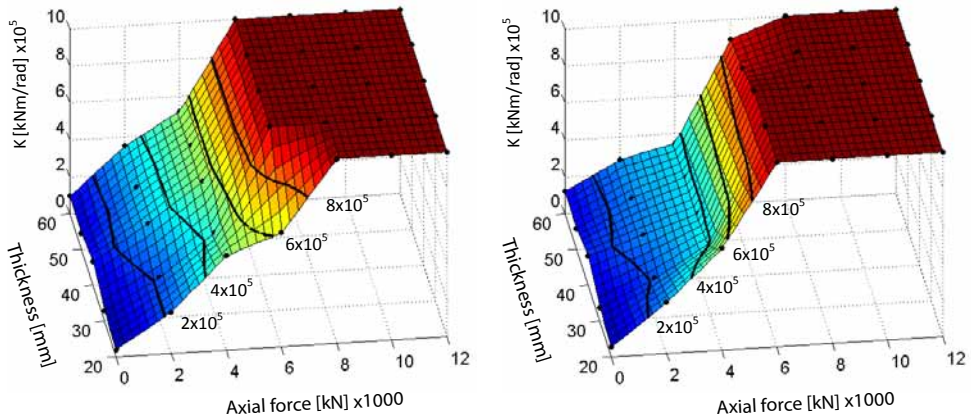


Fig. 247: Stiffness estimation for single flange welded connection: “reverse components method” (left) and analytical approach (right)

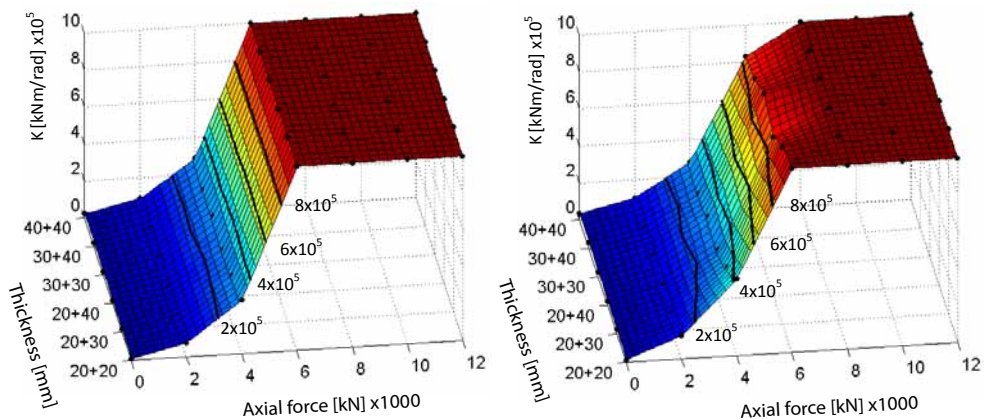


Fig. 248: Stiffness estimation for double flange bolted connection (4 bolts): “reverse components method” (left) and analytical approach (right)

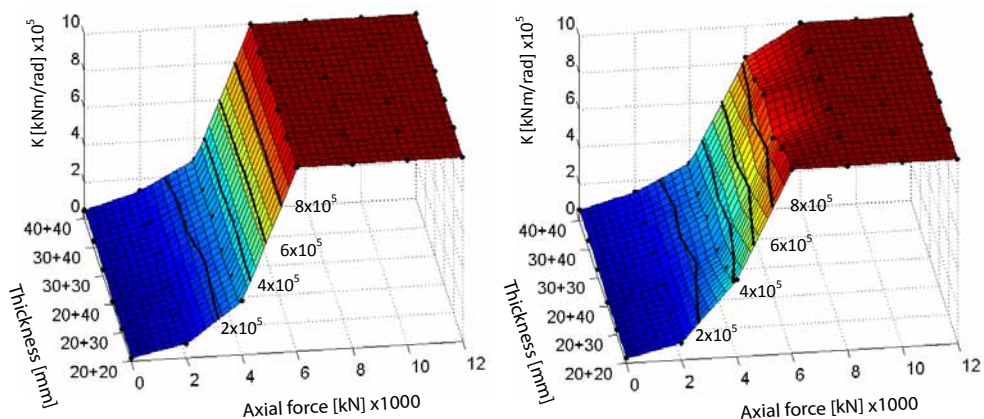


Fig. 249: Stiffness estimation for double flange bolted connection (6 bolts): “reverse components method” (left) and analytical approach (right)

8.5. Column-to-joint interface classification

In the chapter 8.4 the rotational stiffness of different column-to-joint interfaces considered in this study, is explicitly estimated. Nothing is still said about their classification. All structural connections are comprised between two limit categories, namely pinned and fully-rigid.

To reflect the relative stiffness between the rotational stiffness of each end connection and the attached member, the following “end-fixity factor” r is adopted (Monforton & Wu, 1963, cf. Fig. 237). It could be interpreted as the ratio of the

rotation α of the end of the member to the combined total rotation ϕ of the member and the connection due to a unitary end-moment.

$$r = \frac{\alpha}{\phi} = \left(1 + \frac{3EJ}{KL}\right)^{-1} \tag{92}$$

where K is the end-connection spring stiffness and EJL is the flexural stiffness of the attached member.

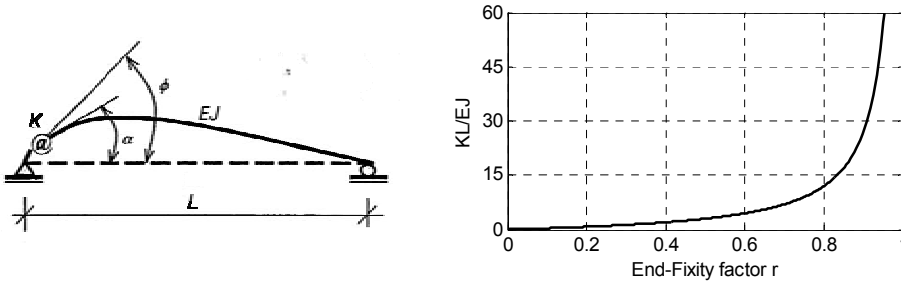


Fig. 250: End fixity factor "r"

For flexible or so-called pinned connections, the rotational stiffness of the connection is idealized as zero; thus the value of the end-fixity factor is zero ($r = 0$). For fully restrained or so-called rigid connections, the factor is unity ($r = 1$), since the connection rotational stiffness is infinite. A semi-rigid connection has an end-fixity factor between zero and unity.

By definition, for a connection to be rigid it requires infinite stiffness. Therefore, theoretically speaking, no connection should be considered as rigid

The concept of the end-fixity factor is very important for structure design, since it provides a physical sense of the extent of rigidity available in a certain connection.

It is evident from Fig. 254 that, the relationship between connection stiffness and end-fixity factor is almost linear when the connection is relatively flexible with a value of the end-fixity factor between 0.0 and 0.5. As the end-fixity factor approaches unity, the required increase of connection stiffness is more than proportional. As a consequence, for a specific increase in the end-fixity factor, the corresponding increment in connection stiffness might be quite different depending on whether the connection is considered to be flexible or rigid. There is then more advantage to characterize semi-rigid behaviour using the end-fixity factor rather than connection stiffness.

Elliott et al., 2004 have reported a classification for connection, based on end-fixity factor, that can help to identify the connection category. The connection flexural stiffness below $0.5EJ/L$ (zone 1) and above $25EJ/L$ (zone V) have been associated

to ideally-pinned and fully-rigid performance. These limits are assumed as suggested in Eurocode.

Among these values a connection should be considered as semi-rigid. Three sub-classes are identified depending on actual rotational stiffness values. Flexural stiffness limit $2EJ/L$ identify limited strength connections. Between 2 and $6EJ/L$ are identified semi-rigid connection with moderate strength. Finally, between 6 and $25EJ/L$ are identified semi-rigid connection with high strength (Table 18)

Connection flexural stiffness		0.5 EJ/L	2 EJ/L	6 EJ/L	25 EJ/L						
Fixity factor	0.0	0.1	0.2	0.3	0.4	0.5	0.6	0.7	0.8	0.9	1.0
Zone classification	I		II		III		IV		V		

Table 18: End-fixity-factor classification (Elliott et al., 2004)

The end-fixity factor above mentioned, is used to provide a classification to column-to-joint interface connection presented in this study.

The stiffness EJ of the column is above reported in Fig. 224. The connection stiffness K is taken from Fig. 234, Fig. 239 and Fig. 244 for single flange connection, double flanged connection with four bolts and double flanged connection with 6 bolts, respectively. Finally, the length of the member is assumed as 3 meters. Results are reported in Fig. 251 and Fig. 252.

In general, all connections' classifications range from moderate to high strength semi-rigid for lower axial load levels. When load level increases, connections become fully rigid.

Single-flange welded connection confirms the stiff performance already evidenced in previous analysis. Specifically, considering 40 mm flange thickness (identified as the optimum layout in chapter 7.4), end-fixity factor is always bigger than 0.8 and exceed 0.9 as axial load levels attains 2000kN. This confirms as in most cases deformability contribution provided by this connection could be disregarded.

Double flange connections appear less stiff.

For the four bolts layout, connection is classified as semi-rigid with moderate strength (zone III in Fig. 252) when axial loading is lower than 2000kN. Between 2000kN and 5000kN, it behaves like a semi-rigid high strength connection. For higher axial load levels, it becomes fully rigid. A slight performance improvement is given by adding the couple of bolts, especially for the lower axial load levels.

This means that in most of cases connection deformability should be considered, especially during modeling of frame system for non-linear analysis.

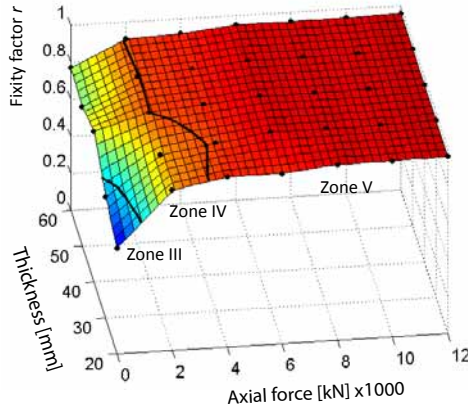


Fig. 251: End fixity factor for single flange welded connections

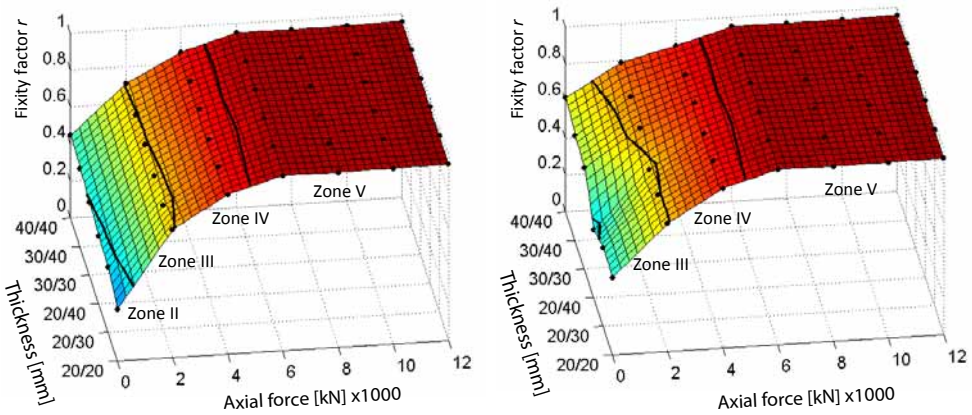


Fig. 252: End fixity factor for double flange bolted connections: 4 bolts (left) and 6 bolts (right) layout

8.6. Conclusions

This chapter deals with the issue of estimating the equivalent spring stiffness, provided by column to core-joint and column to column interface connection. Two formulations are presented based on components approach. Both of them provide similar results and this is taken as a proof of their validity. To provide a classification about rotational stiffness value of connection, the end-fixity factor is introduced. This parameter confirms as single flange welded connection should be considered as fully rigid, even when limited axial loading is provided. Conversely, bolted

connections result less stiff compared to adjoining members and get classified as semi-rigid. For this reason their deformation contributes should be always considered when modeling frame systems adopting proposed composite-column layout for vertical members.

9. ANALYTICAL STUDY OF COMPOSITE-COLUMNS

9.1. Introduction

Besides numerical modeling, an important aspect is the identification of simplified analytical approaches to model composite-columns behaviour, in particular for the design phase. A first issue to consider is the possibility to get the strength domain of composite-column's components taken as separate: HSC column, composite-core-joint and bolted connection. Related to this aspect is the correct accounting for concrete strength, in particular when dealing with HS concrete. In chapter 4.2.9 considerations are reported with reference to pure axial loading conditions, taken by literature and Codes. In this chapter considerations are extended to combined axial and bending conditions. To validate simplified analytical approach for design, numerical analyses results are taken as a reference.

Secondly, the analytical fitting of numerical $M-\varphi$ curves is investigated. This validation is fundamental to assess the possibility of adopting analytical approach for computation of end-members' plastic hinges' non-linear relationships.

Finally developed analytical approach is adopted to estimate the reference design strength domain for considered composite-columns, accounting for partial safety factor imposed by Codes and allowing to estimate the limit number of storeys for frames adopting proposed precast technology.

9.2. Provisions for HSC column bending strength

As stated in chapter 4.2.9, a correction coefficient for concrete strength $\alpha=0.85$ should be adopted for design independently from concrete grade. It accounts for difference between concrete strength provided by cylindrical concrete specimens and the one provided by real scale column samples.

The correct design of HS reinforced concrete sections under combined axial and bending solicitations need for some additional considerations, in particular to account for the different behaviour of HSC compared to NSC samples.

In ACI 318-08 (ACI Committee 318, 2008), the reduction factor α used for compressed members is substituted by the equivalent rectangular stress-block correction factor $\eta=0.85$. For the depth of the rectangular compression block λ (cf. Fig. 253) following equation is assumed:

$$\lambda = 0,85 - 0,05 \cdot (f_c - 40) / 6,9 \leq 0,85 \tag{93}$$

This formulation is analogous to that in ACI 318-89 and NZS 3101:2006 (New Zealand Standard, 2006).

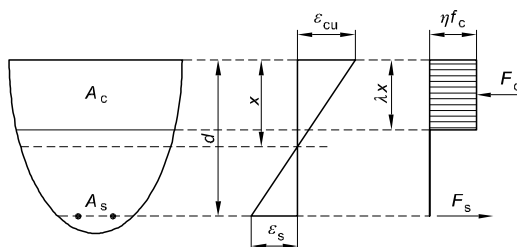


Fig. 253: Stress-block approach as reported in ACI 318-08

Several studies (Li et al., 1991) indicate that ratios of the experimental flexural strength to that calculated according ACI formulations are less than 1, when considering HSC columns subjected to high axial load levels. Conversely, ACI provisions provide from 10% to 25% less flexural strength when dealing with NSC columns. Based on these evidences, an equivalent rectangular compressive stress block is suggested (Li et al., 1991):

$$\begin{aligned} \eta &= 0,85 & f_c &\leq 55 \\ \eta &= 0,85 - 0,004(f_c - 55) \geq 0,75 & f_c &\geq 55 \end{aligned} \tag{94}$$

To explain different bending behaviors between NSC and HSC columns, Azizinamini et al., 1994 assume that typical stress-strain curves in compression for HSC are characterized by an ascending portion that is primarily linear, with maximum strength achieved at an axial strain between approximately 0.0024 and 0.003. Therefore, it might be more appropriate to use a triangular compression stress block (Fig. 237) for calculating the flexural strength when f_c exceeds approximately 70 MPa, with the maximum compressive stress limited to $0.85 f_c$. Considering the equilibrium of horizontal forces and moments, the equivalent

rectangular compression block shown in Fig. 254 has the following properties: intensity of compression stress equals $0.63 f_c$ (analogous to Li et al., 1991) rather than $0.85 f_c$ (the value currently specified in ACI 318-08), and the depth of the rectangular compression block λ equals 0.6 times the depth of the neutral axis, corresponding approximately to current ACI requirements.

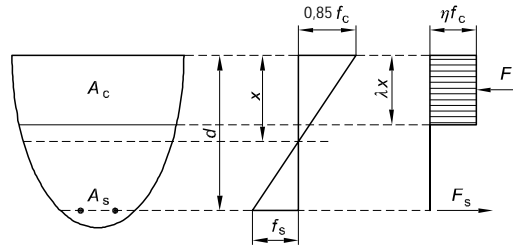


Fig. 254: Stress-block modified approach for HSC sections (Li et al., 1991)

EN 1992-1-1:2005 accounts for these experimental evidences with specific formulations for concrete strength respectively lower or higher than 50MPa:

$$\begin{aligned} \eta &= 1 & f_{ck} &\leq 50 \text{ MPa} \\ \eta &= 1 - (f_{ck} - 50) / 200 & f_{ck} &\geq 50 \text{ MPa} \end{aligned} \quad 95)$$

$$\begin{aligned} \lambda &= 0,8 & f_{ck} &\leq 50 \text{ MPa} \\ \lambda &= 0,8 - (f_{ck} - 50) / 400 & f_{ck} &\geq 50 \text{ MPa} \end{aligned} \quad 96)$$

In equations 95 the strength reduction coefficient $\alpha=0.85$ is missing, but the long term actions coefficient might be adopted for this purpose.

An alternative formulation is reported by the CSA A23.3-04 (CSA Standard, 2010):

$$\eta = 0,85 - 0,0015 f_c \geq 0,67 \quad 97)$$

$$\lambda = 0,97 - 0,0025 f_c \geq 0,67 \quad 98)$$

The Canadian Code also allows to adopt concrete non-linear stress-strain curves with peak stresses no greater than $0.9 f_c$, to accounts for differences between the in-place strength and the strength of standard cylinders.

From analysis of provisions suggested by Code and literature, it appears clear that influence of concrete grade should be explicitly considered to evaluate appropriate concrete strength for design. In particular a first coefficient α should be used to account differences between the in-place strength and the strength of standard

cylinders, similarly to what stated in 4.2.9 when pure axial condition is considered. In addition, a further coefficient η should be considered for design of HSC concrete members subjected to axial-bending solicitations. In the following an estimation for η coefficient is proposed, based on numerical results provided by chapter 7 and compared to above reported formulations.

9.3. Analytical modeling of composite-column

9.3.1. *MATLAB subroutine*

In order to define through analytical approach, the strength domain of general layout RC sections, a specific computer program is developed in MATLAB (MathWorks Inc., 2011). Implemented subroutine uses a layered representation of the section, each layer being separated into a confined core layer and an unconfined cover layer with the corresponding material properties and characterized by a specific average dimensions $b(y)$ and distance y from the neutral axis (Fig. 234). The confined concrete material properties account for the effectiveness of the confinement reinforcement and the yield strength of the transverse steel reinforcement (Legeron concrete model, cf. ch.4.2.5). The longitudinal reinforcement is also represented by layers, with the appropriate material properties. The program calculates the moment-curvature response by an incremental iterative procedure based on the plane section hypothesis and on fulfilling of axial and bending solicitations equilibrium conditions:

$$N = \int_0^x \sigma_c(y) \cdot b(y) \cdot dy + \sum_{i=1}^N \sigma_{s,i} \cdot A_{s,i} \quad 99)$$

$$M = -\int_0^x \sigma_c(y) \cdot b(y) \cdot y \cdot dy - \sum_{i=1}^N Z_i \cdot y_i \quad 100)$$

Firstly, a certain axial load level N is fixed. Secondly, the ε_c value is assumed at top edge of concrete section. As first tentative, neutral axis is located at middle height. The neutral axis is then moved iteratively upwards and downwards through a bisection method, until axial load equilibrium is achieved (eq. 99). The resulting bending moment is then calculated (eq. 100). Afterwards, a new increased value for ε_c is assumed and the iterative process starts again. In this way, the complete $M-\chi$

curve is analytically defined for a certain axial load level. Failure corresponds to the attainment of either ultimate confined concrete strain ϵ_{ccu} , ultimate steel strain ϵ_{su} or 80% of residual bending strength (Cusson & Paultre, 2008). Critical points such as yielding of longitudinal reinforcement, onset of cover spalling, and ultimate curvature are also stored. Repeating the process for different axial load levels, the complete M-N strength domain is defined.

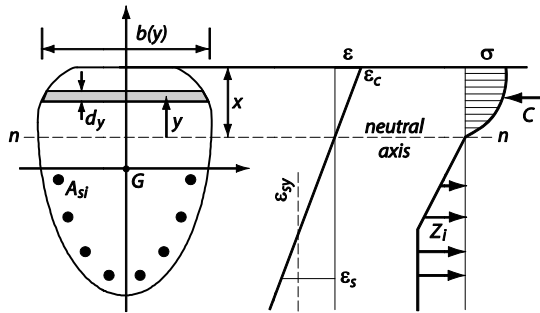


Fig. 255: RC section discretization for MATLAB subroutine

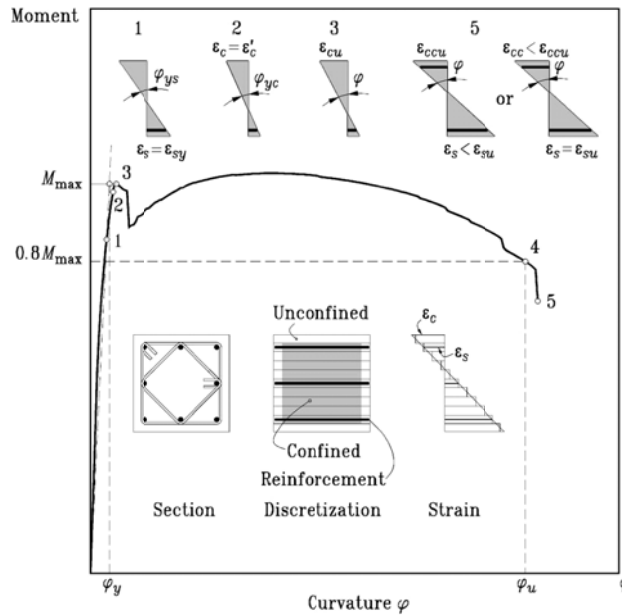


Fig. 256: MATLAB subroutine: example of $M-\chi$ response (Cusson & Paultre, 2008)

9.3.2. HSC column

In Fig. 257 the HSC column strength domains, obtained from numerical (see Fig. 223) and analytical approaches, are plotted together and compared.

Coefficient α is assumed unitary, being this reduction factor disregarded during numerical analyses. To reproduce the strength domain when both axial and bending conditions are considered, two values for η are defined: 0.85 and 0.95.

Analytical formulation with $\eta=0,95$ better agrees with numerical results for axial loading lower than 8000kN. $\eta=0,85$ leads to a better fitting of resistance domain for higher axial load levels. For axial loading lower than 4000kN, strength domain is well captured by both coefficients, being the role played by concrete secondary.

Analytical results confirm the importance of introducing a strength reduction for HSC. The fact that numerical simulation captures similar evidence those of experimental test reported from literature, concerning to lower performance of HSC columns compared to NSC ones, is an additional confirmation of goodness of the adopted numerical approach. For a safe analytical estimation of HSC column strength domain, $\eta=0,85$ should be assumed. This agrees with equation 95, taken from EN 1992-1-1:2005. In proximity of pure axial loading condition, numerical strength domain is characterized by an apparent axial strength increase. This phenomena is correctly simulated assuming $\eta=1$. Such a factor is also suggested by experimental evidences.

In Fig. 258, the $M-\chi$ curves obtained from numerical and analytical approaches are compared. It is clear as analytical solution is able to capture accurately the numerical trend. It should be taken as a verification about the possibility to adopt such an approach to generalize HSC column results when different rebars layout and diameter are adopted, than those adopted for numerical investigations.

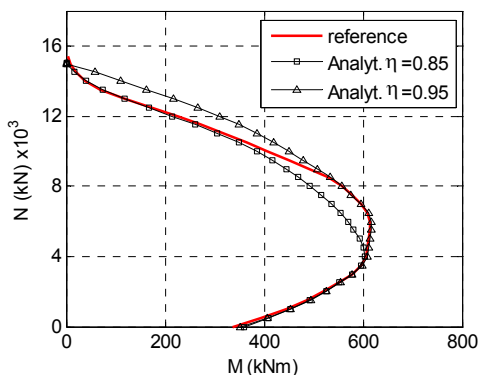


Fig. 257: Numerical vs. analytical estimation of strength domain for HSC column

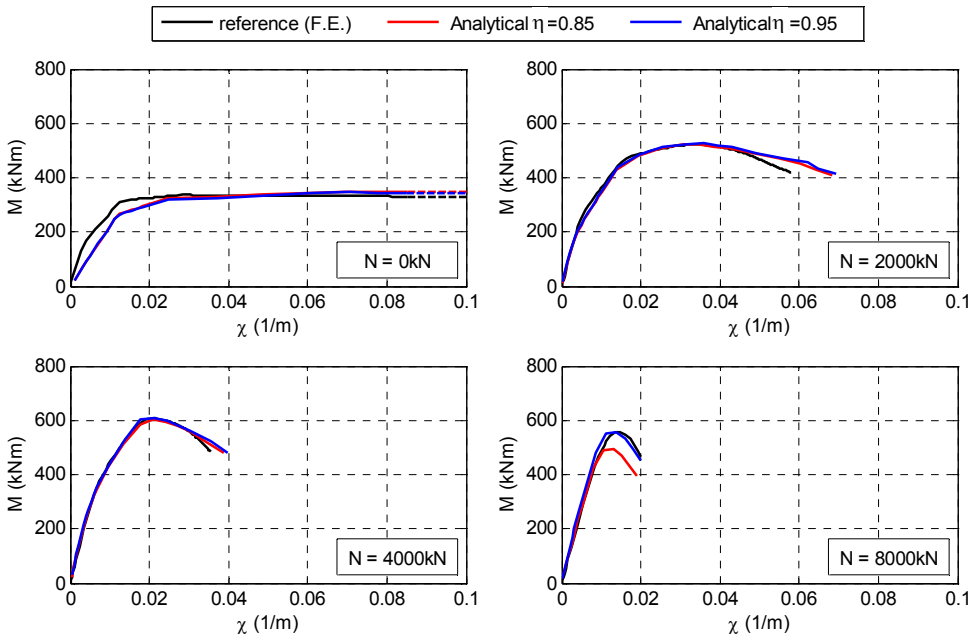


Fig. 258: Numerical vs. analytical estimation of M - χ curves for HSC column

9.3.3. Composite-core-joint

To reproduce the bending response of composite core-joint adopting analytical approach, vertical steel plates are splitted into 7 parts. This means that the 210 by 40 mm vertical plate section is represented by 7 rebars with dimension 30 by 40 mm, arranged to reproduce the plate section geometry.

For concrete a confinement pressure equal to 5 MPa is considered (cf. ch.7.3). Coefficient α is taken as unitary as for numerical analysis. Coefficient η is also taken as unitary as stated by equation 95 (NSC is here considered). As it can be seen in Fig. 259, there is a good agreement between numerical and analytical studies. This confirms the possibility to adopt simplified analytical approach to design the composite-core-joint.

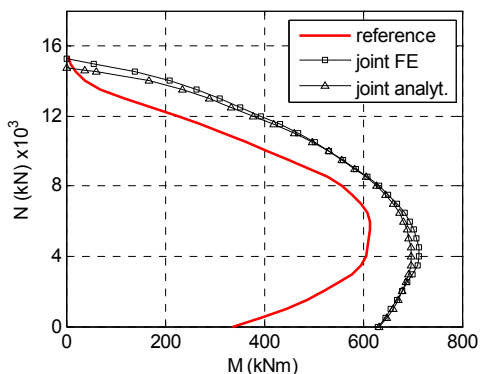


Fig. 259: Numerical vs. analytical estimation of strength domain for composite-core-joint

9.3.4. Bolted connection

To complete the analytical study of composite-column, performances of bolted connections are evaluated. The same MATLAB subroutine can be used, simply substituting the σ - ε relationship for concrete, with an equivalent material corresponding to S355 steel (the same of horizontal steel flanges). Due to the fact that subroutine recognizes S355 steel still as concrete, no resistance contribute is provided in tension. In this way opening and bearing between the two bolted flanges can be simulated. The hypothesis is introduced about deformed plain sections, rather realistic considering flanges' deformed layout when adequate thickness is provided (cf. ch.7.4 to 7.6). In Fig. 260 the analytical strength domain is compared with the reference one relative to HSC column. Results are consistent with numerical evidences reported in chapters 7.5 and 7.6, characterized by a reduced bending strength for axial loads lower than 2000kN when considering a 4 bolts connection. On the contrary, 6 bolts provide adequate strength to gain this resistance gap. When pure bending condition is considered, connection strength provided by four bolts is around 280kNm, similarly to what found from composite-column numerical results (Fig. 238b). For higher axial load levels, strength provided by bolted connection is much higher than reference domain, thus representing a strong component of the assembly.

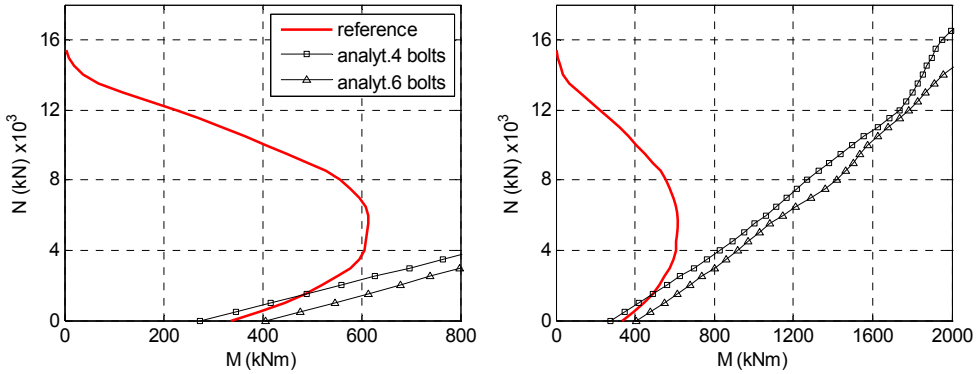


Fig. 260: Analytical estimation of strength domain for bolted connection

9.4. Design domain for composite-column

In chapter 9.3 the simplified analytical approach is demonstrated to be an effective tool to reproduce the numerical results. In this chapter the same approach is applied to get strength domain for design of composite-column, adopting base material's safety factor's required by Codes.

The concrete strength reduction coefficient α and η are also considered (cf. ch.9.2). The first one accounts for differences between cylindrical concrete strength and real size specimens strength and is assumed equal to 0.85. This coefficient is missing in current Italian Code NTC 2008, but could be quantitatively substituted by the long-term actions coefficient. The latter accounts for concrete grade influence in determining maximum members' bending strength, in particular when dealing with HSC. The formulation reported in equation 95, taken from EN 1992-1-1:2005 provide the best agreement with numerical results reported in chapter 9.3.2.

HSC base materials' properties and corresponding partial safety factors are reported in Table 15, taking as reference provisions reported in UNI-EN-1992-1-1:2005 and Italian Code NTC2008. Parabolic-rectangular and elastic-perfectly plastic stress-strain relationships are assumed respectively for concrete and steel.

Concrete			Steel rebars		
Grade	f_{ck} (MPa)	γ_c	Grade	f_{yk} (MPa)	γ_s
C75/90	75	1,5	B450C	450	1,15

Table 19: HSC base materials' properties and partial safety factors

HSC column strength design domain is plotted in Fig. 261 together with reference numerical strength domain.

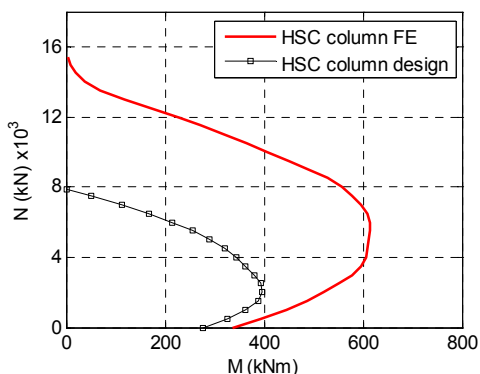


Fig. 261: Design strength domain for HSC column

Maximum axial bearing capacity of HSC column is computed from equation 101, assuming η coefficient lower than unity, despite experimental tests suggest that this coefficient affects only bending performance of members.

$$\begin{aligned}
 P_{MAX} &= \alpha \eta \frac{f_{ck}}{\gamma_c} (A_c - A_s) + \frac{f_{yk}}{\gamma_s} A_s \\
 &= 0,85 \cdot 0,875 \cdot \frac{75}{1,5} \left(158000 - 8 \frac{30^2 \pi}{4} \right) + 8 \frac{450}{1,15} \frac{30^2 \pi}{4} \\
 &= 7878 kN
 \end{aligned}
 \tag{101}$$

In a similar way reference strength domain for composite core-joint get estimated. Material properties and corresponding safety coefficients are reported in Table 20.

Concrete			Steel rebars		
Grade	f_{ck} (MPa)	γ_c	Grade	f_{yk} (MPa)	γ_s
C25/30	25	1,5	S355	345	1,05

Table 20: Composite-core-joint base materials' properties and partial safety factors

Confining pressure acting on core-joint is assumed equal to 2,5MPa (half of the value applied for numerical simulations, cf. ch.7.3). According to UNI-EN-1992-1-1:2005, confined concrete strength is equal to:

$$f_{ck} = f_{ck} (1,125 + 2,5 \cdot 2,5 / f_{ck}) = 34MPa \quad 102)$$

Maximum axial bearing capacity of composite core-joint is computed from equation 103. Based on equation 95 for considered concrete grade (C25/30), η coefficient is taken as unitary.

$$\begin{aligned} P_{MAX} &= \alpha \eta \frac{f_{ck}}{\gamma_c} (A_c - A_s) + \frac{f_y}{\gamma_s} A_s \\ &= 0,85 \cdot 1 \cdot \frac{34}{1,5} \cdot (158000 - 210 \cdot 40 \cdot 2) + \frac{345}{1,05} \cdot 210 \cdot 40 \cdot 2 \\ &= 8240kN \end{aligned} \quad 103)$$

Complete strength design domain is plotted in Fig. 262 together with reference strength domain provided by numerical core-joint solution. The HSC column domain is completely enveloped by core-joint domain, confirming the possibility to classify it as a strong component of the assembly.

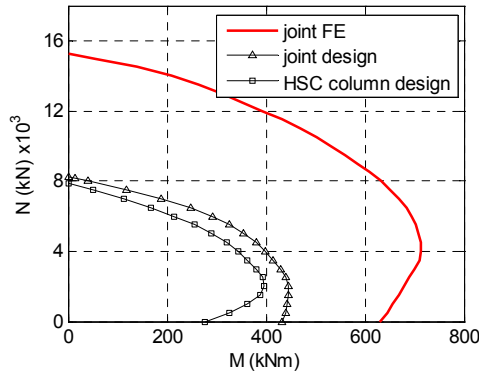


Fig. 262: Design strength domain for composite-core-joint

The analytical composite-column's design strength domain get adopted as a reference point to provide an estimation of the maximum number of storeys for frames adopting proposed precast system. Loads considered for this analysis are reported in Table 24. Wind effects are also considered to account for additional bending moment acting on base column at ground level. A reference wind speed equal to 27 m/s is assumed (an average value over the Italian Territory). The equivalent wind load is estimated in 0.5 kN/m^2 , increased by a specific wind profile factor $c_e(z)$ as specified by NTC 2008 prescriptions. Verification process make reference to Ultimate Limit State (ULS) conditions (eq. 104). Load's amplification factors γ suggested by NTC 2008 are reported in Table 21.

$$L = \gamma_{G_1} G_1 + \gamma_{G_2} G_2 + \gamma_{Q_1} Q_1 + \sum_{j>1} \psi_{0,j} Q_j \tag{104}$$

	Comb. Factor ψ_0	Ampl. factor γ
Structural dead load (G_1)	-	1.3
Non-structural dead load (G_2)	-	1.5
Live load (crowd) (Q_1)	-	1.5
Wind load (Q_2)	0.6	1.5

Table 21: Static load amplification factor

Reference is made EN 1992-1-1:2005 provisions (eq. 105) to estimate single columns' eccentricity to account for second order effects due to possible frame's elevation irregularities:

$$\begin{aligned} \theta_i &= \theta_0 \cdot \alpha_h \cdot \alpha_m \\ \alpha_h &= 2 / \sqrt{\ell}; \quad \frac{2}{3} \leq \alpha_h \leq 1 \\ \alpha_m &= \sqrt{0.5(1 + 1/m)} \end{aligned} \tag{105}$$

where θ_0 =reference base eccentricity, to be taken equal to 1/200; α_h =reduction factor to account buildings height; α_m =reduction factor to account for number of vertical element; ℓ =total frame's height; m =number of vertical elements considered

Considering a interstorey span equal to 3.2 meters, the reference eccentricity is estimated as 7.5 mm, rounded up to 10mm. Regular plain frame numerical model are built in SAP2000 V.11.0 (Computer and Structures, 2010). Reference should be done to chapter 11.5.1 for further details. Each storey in the model is horizontally shifted with respect to the lower one to provide elevation irregularities and a non-linear geometry analysis is performed to account for second order effects. Maximum allowable number of storeys result equal to 10 and 8 for frames with bays span 6 and 8-meters-long, respectively.

The force distribution in term of axial forces and bending moments computed for these frames are reported in Fig. 263 and Fig. 264. The worst solicitations' combinations for the two frame typology are plotted together with the reference strength domain in Fig. 265. It should be noticed as strength domain limit is nearly attained. Identified maximum number of storeys should be considered as a conservative lower limit, since taller frame are feasible considering lower live loads the those assumed for current analyses.

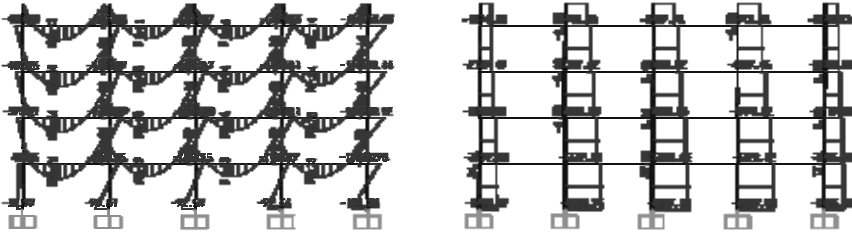


Fig. 263: Lower storeys solicitations for frame with 6-meters-long bays span

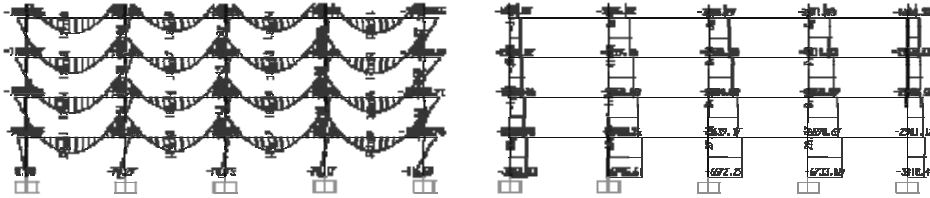


Fig. 264: Lower storeys solicitations for frame with 8-meters-long bays span

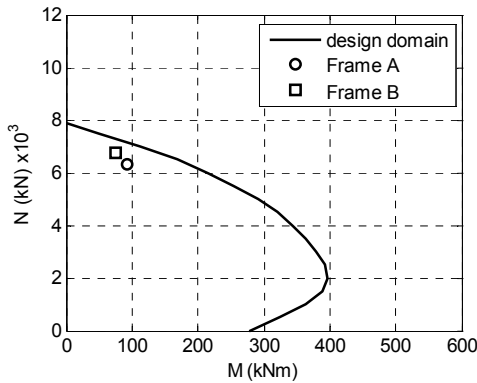


Fig. 265: Worst solicitations' combination for base columns and reference strength domain

9.5. Conclusions

The objective of this chapter is the definition of analytical tools, to study the behaviour of base components of composite-column, namely HSC column, composite-core-joint and bolted connection. Furthermore, the role played by concrete strength reduction factor is investigated, making reference to experimental evidences available from literature, Code Regulations and numerical results provided by composite-column analyses.

Analytical approach evidence a satisfactory agreement with results provided by numerical analysis: strength domains is accurately reproduced as well as $M-\phi$ curves got by numerical analysis of HSC column. This validate the possibility to adopt the analytical approach as a viable alternative to time-costing numerical analyses.

Besides, analytical approach allows to define reference strength domain to be adopted for every-day design, considering material properties and safety factor coefficients required by Codes. It allows to get an estimation about maximum number of storeys allowable by proposed precast technology. On the basis of numerical models build in SAP2000 V.11.0 (Computer and Structures, 2010) this limit is estimated equal to 10 and 8 for frames with bays span 6 and 8-meters-long, respectively. Identified maximum number of storeys should be considered as a conservative lower limit, since taller frame are feasible considering lower live loads than those assumed for current analyses.

10. NUMERICAL JOINT CYCLIC PERFORMANCE

10.1. Introduction

Energy dissipation capability affects sensibly the seismic performance of a beam-to-column joint. When an emulative approach is adopted, as for the proposed precast system, it is expected that non-linear behaviour remains concentrated at beams' end, while the column performs elastically as required by a beam sidesway mechanism.

In experimental cyclic testing, a combined bending-shear crisis of lower column led to a premature test abruption, although column overdesign should have prevented such a possibility. Reasons for this behaviour are identified in unforeseen boundary conditions imposed by test equipment, different from those supposed during preliminary test planning. The challenge for the purposely implemented joint's numerical model is to reproduce experimental test, despite the encountered unusual boundary conditions. Such model is an upgraded development of the reference composite-column FE model for static lab tests' simulations.

In partial substitution of the experimental phase, the same joint's numerical model is adopted in order to estimate the cyclic performance of the precast system, assuming boundary conditions analogous to those typically experienced by a joint on a framed structure subjected to lateral loading.

Numerical results allow to get an estimation about energy dissipation capability and equivalent damping factor, which are relevant to characterize the non-linear performance of the proposed precast system.

10.2. Numerical model

The numerical model consists of a full tridimensional representation of precast joint geometry as reported in Fig. 122. Most components of the model are meshed with 8-nodes hexahedral solid element (C3D8R), namely HSC column and corresponding longitudinal rebars, core joint and lateral beam. Average mesh size for concrete elements is almost 40 mm. Circumference of longitudinal column reinforcement is split 8 times, to reproduce accurately circular section geometry. Steel-joint is meshed with a finer mesh with average edge size approximately 20 mm. Vertical steel plate are split 4 times in the thickness direction, to capture more accurately second order effects. Stirrups, both from the column and beam side, truss girders and beam's trusses are modeled with linear truss elements (B31) supposing full interaction with surrounding concrete. This enable to keep mesh of the model rather regular despite, complicate reinforcement arrangement, in particular in the beam-to-joint interface. To improve numerical simulation, bolted connection is explicitly solid modeled. Contact surfaces are introduced to accounts for flange-to-flange and bolts-to flange-interaction, based on Mohr-Coulomb constitutive model with friction coefficient $\mu=0.4$ and null cohesion. At members' ends a rigid plane is modeled adopting quadrilateral elements (R3D4) to redistribute boundary condition aver the whole members' section. The models consist of 41757 nodes, 28288 solid, 452 planar and 1528 linear elements, for a total count of 30268 finite elements. Adopted material properties are reported in Table 3 and Table 4: C75/90 concrete grade for HSC column, C30/37 concrete grade for precast beams' base, C25/30 concrete for in-place casting, B450C steel for column reinforcement and beam's stirrups and structural steel S355J for remaining components, namely steel-core-joint and horizontal flanges, lattice girders restoring beam continuity and beams' trusses. Adopted material's constitute laws are reported in chapter 3.2.

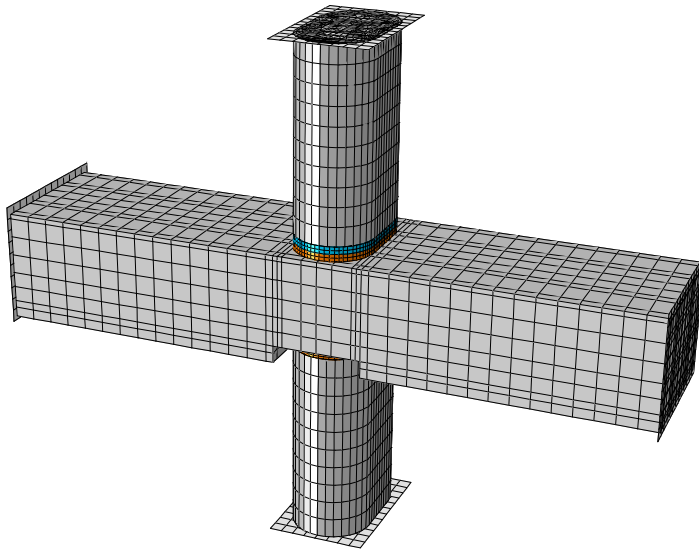


Fig. 266: Joint FE model; full view

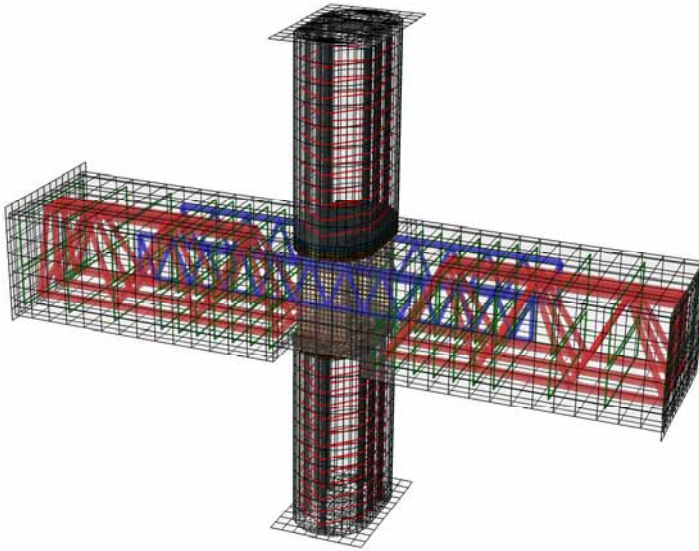


Fig. 267: Joint FE model; full view plus reinforcement

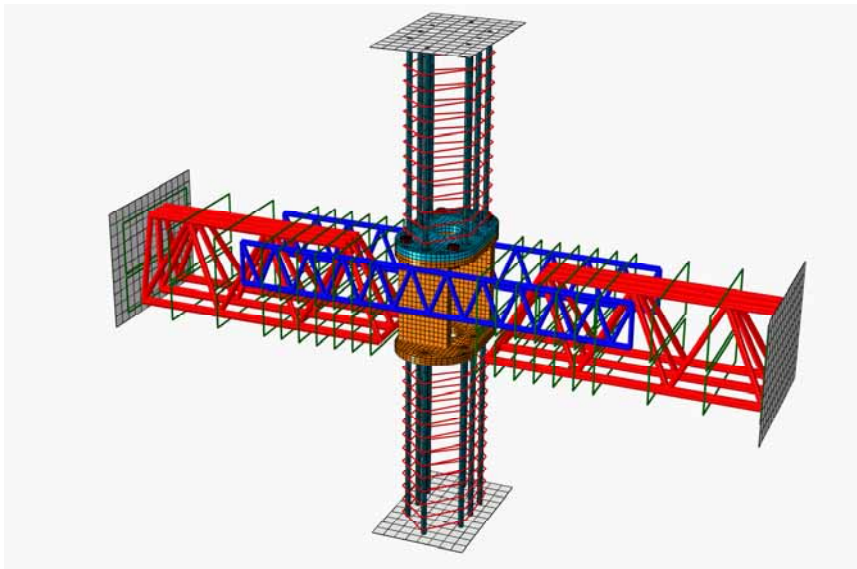


Fig. 268: Joint FE model; naked reinforcement view

10.3. Implementation of experimental static test

For the numerical implementation of experimental cyclic tests, reference is made to sample D2, the only one not strengthened with FRP fabric and thus more straightforward to be modelled.

The difficulty of identifying applied boundary conditions, given the machinery adopted for cyclic testing (Fig. 124), lies in the appraisal of real supports' fixity degree provided by test machinery at member's ends.

Concerning lower column's base, where input-displacements get applied, end-member's rotation was prevented during D2 testing. This is consistent with the S-shaped deformed layout for base column at the end of testing (Fig. 269), typical of beams fixed at both ends, subjected to relative vertical movement of end-supports.

Other supports are assumed as hinged and fixed for top column-end and beams-end, respectively, despite rotational and translational springs would be probably more representative of real boundary conditions, at the expense of introducing calibration issue for the stiffness values. The limit case of either perfect hinged or fixed restrain is just an ideal approximation, assumed on the basis of engineering judgement. Numerical analyses are displacement-controlled and adopt the same displacement history of experimental testing, reported in Fig. 125. Before cyclic

loading an axial force equal to 2000kN get applied at the upper column's end, to account for axial loading condition on the sample.

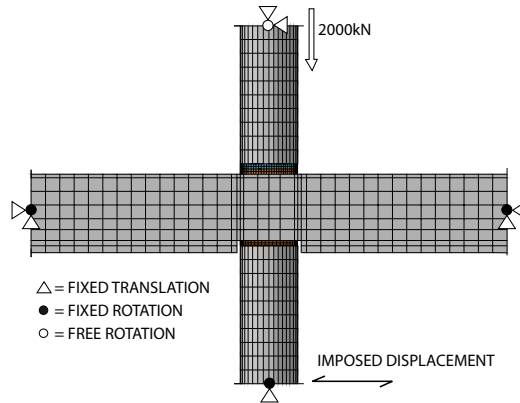


Fig. 269: Boundary conditions for FE simulation of experimental cyclic testing

Numerical simulation of sample D2 provides excellent response concerning the failure mode, analogous to that experienced during lab testing, with lower column's strength decreasing rapidly due to progressive concrete crushing, while the remaining parts of the model are still elastic. Also attained lateral force level is consistent with the one got from lab test (728 kN, Fig. 270a). Main difference among numerical and experimental behavior deals with global stiffness of the sample during loading process, resulting experimental response 4 time less stiff than numerical one.

This behaviour is not ascribable either to materials' properties or numerical approach, whose reliability is verified by tests reported in chapter 6. Discrepancy between numerical and experimental trends probably deals with boundary conditions and might be partially explained considering that adopted end-members' supports, either pinned or fixed, are just an approximation of real fixity-degree. Besides a sort of fictitious stiffness might have been introduced in the experimental sample's response, due to improper restraining of the whole testing machinery, causing a sort of free body movement (cf. ch.3.4). This is still an open issue that would require further laboratory testing to be checked. In Fig. 270b comparison between numerical and experimental response is done referring to filtered experimental data reported in Fig. 140. In this case a rather good agreement between numerical and lab responses is evident, also in term of global sample's stiffness.

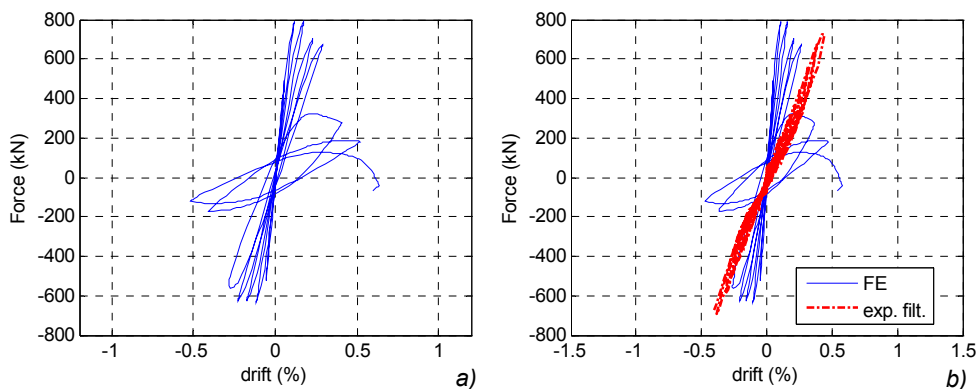


Fig. 270: Hysteretic response from FE simulation of cyclic lab tests

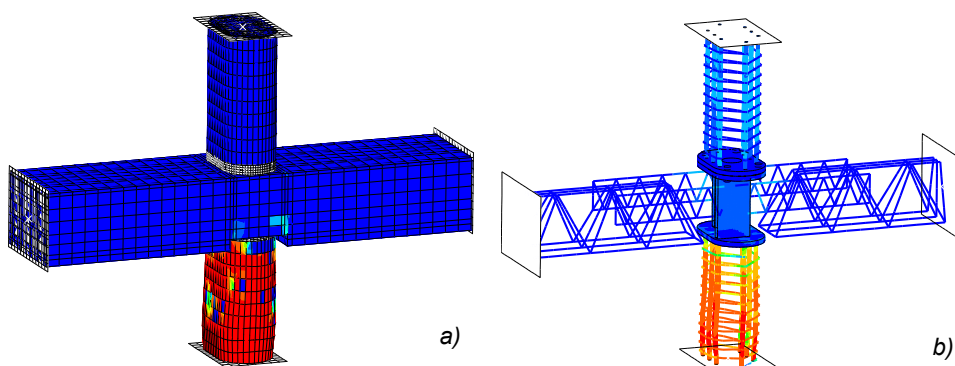


Fig. 271: FE simulation of cyclic lab tests; a) compression damage on concrete; b) Von Mises stresses on reinforcement

10.4. Expected cyclic behaviour for precast joint

For the simulation of real cyclic performance of the proposed precast joint different boundary conditions are considered, compared to the ones adopted for experimental testing. To reproduce a realistic solicitations' distribution among the joint's members, similar to that experienced by the same joint on a framed structure subjected to a seismic input, fixed supports are removed and beam's ends are provided with a roller support (Fig. 272). This allows the members' ends in the joint sample to become contra-flexural point for the bending moments' diagram.

The numerical response retrieves high ductility response, with broad hysteretic cycles and failure attained due to bar's fracture at inter-storey drift slightly exceeding 3%, thus considerably higher than the reference limit for design, usually

ranging from 1 to 2% (Fig. 273a). Equivalent viscous damping, calculated in accordance with the equation: $\xi_{eq} = E_d / (4\pi \cdot E_{el})$, where E_d is the hysteretic damping and E_{el} is the elastic energy of each cycle, ranges between 20% to 40% for inter-storey drift levels comprises between 0.5% to 3%, similarly to a classic RC joint's performance (Fig. 273b).

Energy dissipation capability is given by plastic hinging on beams' end, mainly thank to high straining capacity of longitudinal bars belonging to lattice girders (Fig. 274). Conversely CSTC beam's truss performs elastically for most part of test, resulting ineffective in providing strength contribute in the plastic hinge region (Fig. 275).

To better present the role played by lattice girder, four points belonging to this component's longitudinal bars, get monitored (Fig. 276). These show similar responses, characterized by considerable straining in tension until fracture strain (22%) is attained in one bars, identifying the failure condition of the test (Fig. 277). Unloading compressive strains are limited during initial load cycles and increase progressively with concrete damaging to restore equilibrium condition on the beam section. Larger plastic deformations are experienced by upper reinforcement during last cycles, due to the limited beam's depth under positive bending, this latter caused by missing continuity reinforcement on the lower side of the beam. Due to structural discontinuity between precast concrete base and adjoining cast core-joint a wide opening tend to spread from the lower beam side, located at beam-to-joint interface, causing the aforementioned beam's depth reduction. To estimate the dimension of this opening, total deformation of plastic hinge's are plotted as a function of the lateral force level. Two different values are reported, referring to the upper and lower beam side respectively. On both side a smeared cracking take place, that may be approximatively assumed as equal. Removing this contribute from the lower deformation's records, the discrete opening is estimate to be almost 6 millimetres just before failure (Fig. 278).

Analysis and development of an innovative prefabricated beam-to-column joint

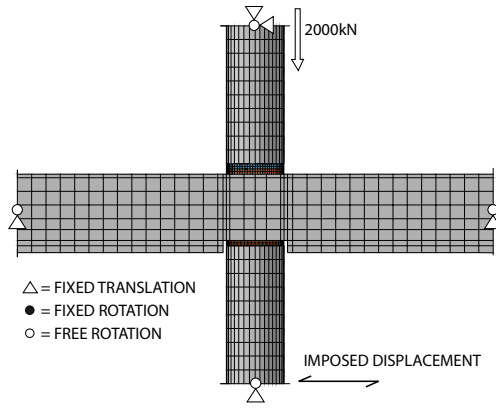


Fig. 272: Boundary condition for FE simulation of cyclic testing

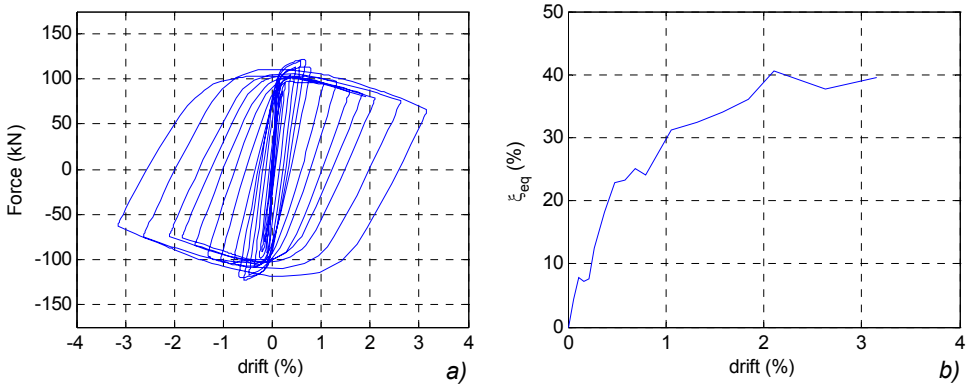
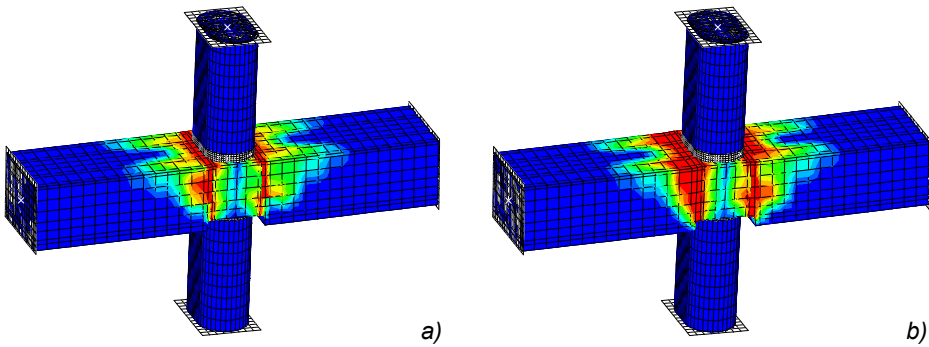


Fig. 273: a) hysteretic numerical response; b) equivalent damping



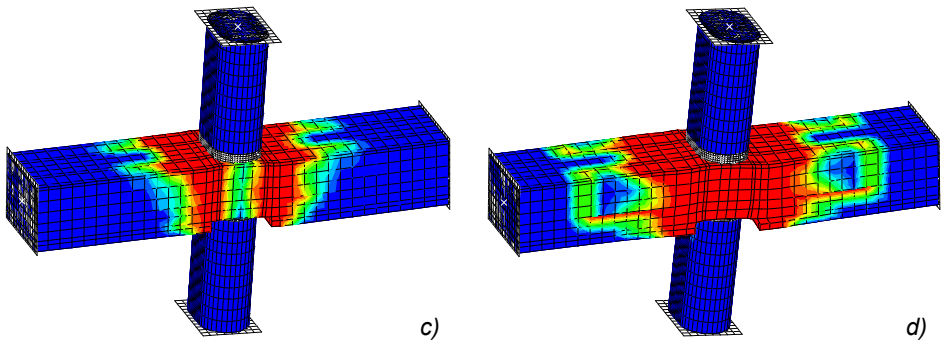


Fig. 274: Tension damage evolution at different drift levels: a) 0.5%; b) 1%; c) 2%; d) 3%

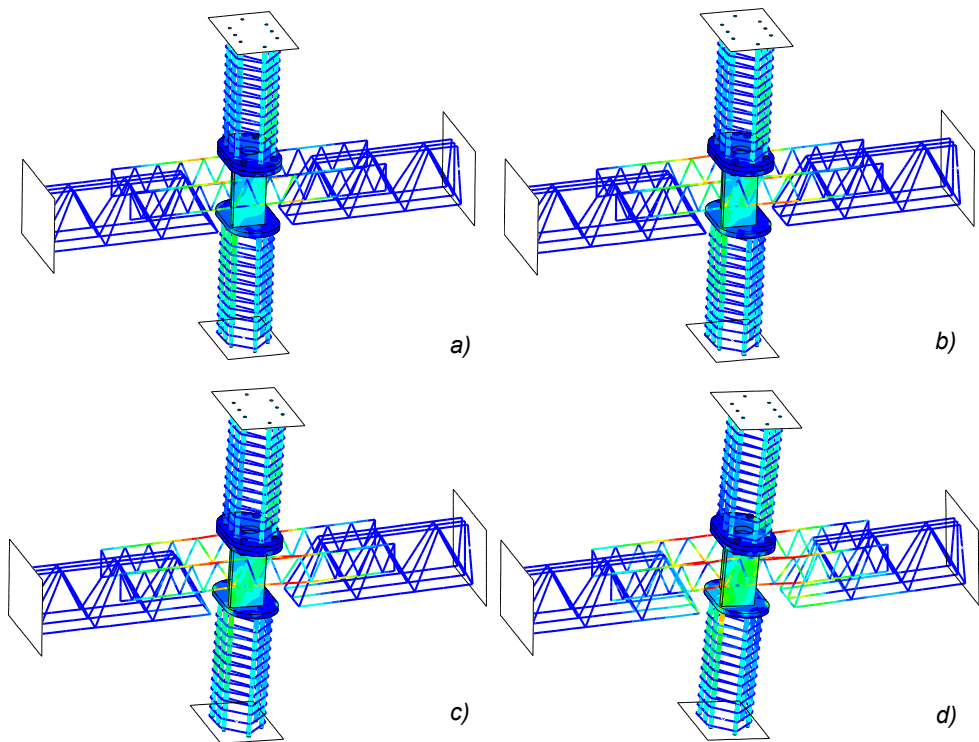


Fig. 275: Von Mises stresses at different drift levels: a) 0.5%; b) 1%; c) 2%; d) 3%

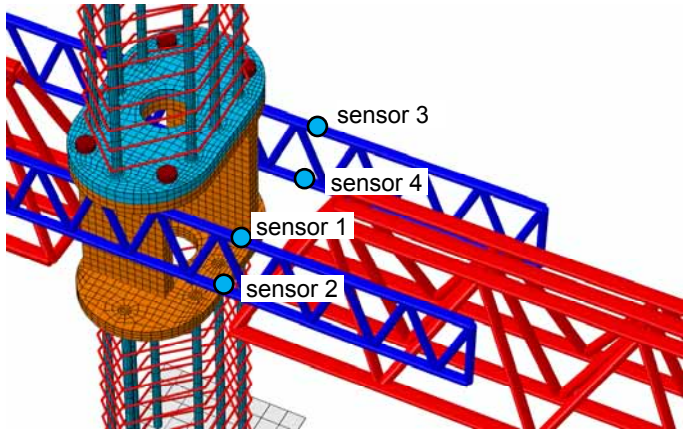


Fig. 276: Monitored numerical point on lattice girder

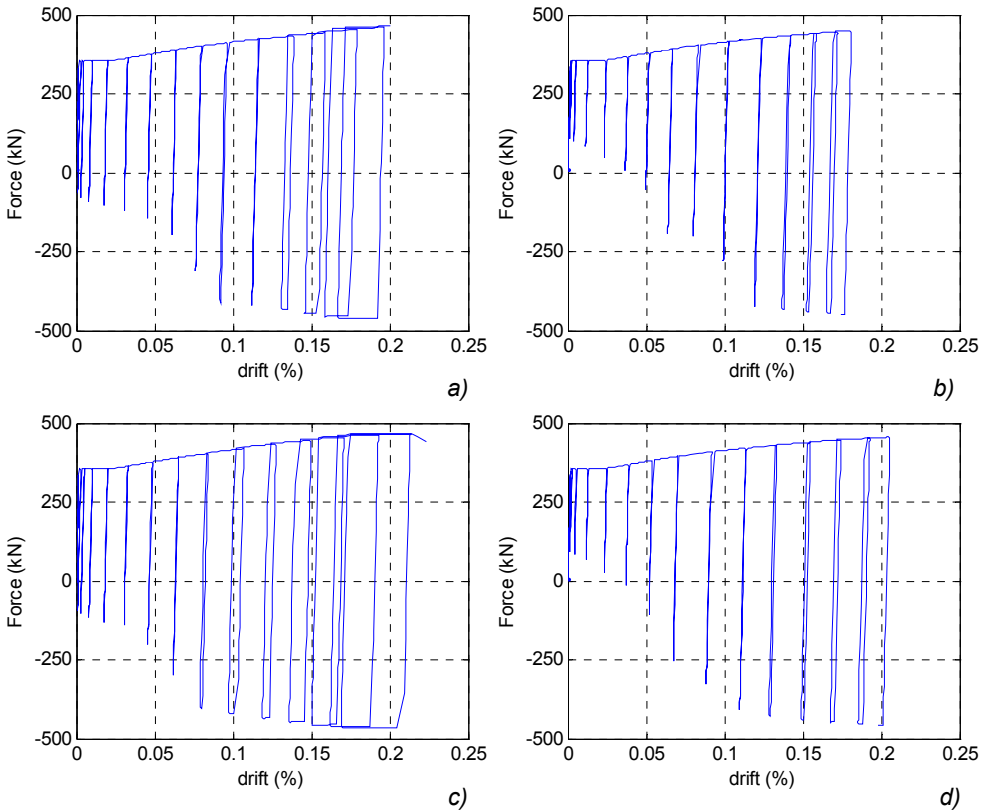


Fig. 277: Stress vs. strain relationship on truss girder: a) sensor 1; b) sensor 2; c) sensor 3; d) sensor 4

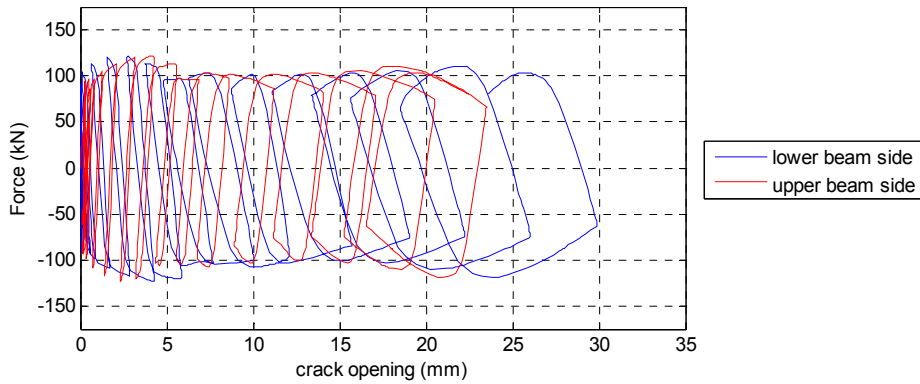


Fig. 278: Crack opening at plastic hinge

10.5. Conclusion

Numerical analyses reported in this chapter provides important contributes on the study of the performance of the proposed precast joint under cyclic loading.

The numerical model implemented for this purpose is an accurate representation of joint geometry. It allows to capture main evidences provided by experimental cyclic testing, like the brittle failure mode of lower column, despite adopted boundary conditions are rather unusual for cyclic testing of beam-to-column joint samples. Based on the same model a further numerical simulation is conducted, imposing boundary conditions representative of the joint behaviour inside a framed structure subjected to lateral loading, this latter characterized by contraflexure point of the bending diagram located at members mid-span, corresponding to members' end in the numerical samples. Numerical response is encouraging and suggest high dissipation and deformation capability of the joint, comparable to the one of an equivalent RC cast-in-place joint. The credit for this performance is mainly related to lattice girders, able to restore beam through joint continuity and high deformation capability in the plastic hinge zone, when properly designed.

11. ESTIMATION OF SEISMIC VULNERABILITY

11.1. Introduction

Moment seismic resisting frames present undoubted benefits compared to alternative structural solutions, which requires for additional seismic resistant elements such as bracing systems, dissipative devices or shear walls, to withstand the earthquake action. As an example, the possibility to create wide opening without interferences, sensibly improving the architectural freedom about final building layout and living space's arrangement. Moreover, a consistent economical saving, being the same skeleton structure able to withstand both gravity and dynamic solicitations.

A fundamental issue for completing the study concerning the performance of the new proposed precast joint, is the assay of the possibility to adopt this technology for moment resisting frames in seismic areas. This aspect increases in relevance if the modularity of precast members, columns in particular, is considered. In fact, this implies fixity of member's section dimensions, independently from frame's layout, thus causing an upper limit on the maximum available strength. The limitation imposed by this characteristic needs to be investigated. Current survey is mainly oriented to National territory, being the Italian market the expected main reference for the proposed solution.

To this purpose, an innovative approach is adopted. The evaluation of the seismic performance is based on maximum allowable ground accelerations, introducing a seismic vulnerability parameter expressed as a direct function of Italian territory percentage, where the proposed precast technology can be used depending on real seismic action and ground category.

In fact, it is ineffective at present, considering a reference value for ground acceleration as for past seismic code OPCM 3431, which subdivided the whole National territory into four main seismic regions. On the contrary, proposed vulnerability-based approach complies with the actual design code NTC2008, which refers to a grid of 10751 points, each of them characterized by specific input

seismic action expressed in terms of both, ground acceleration and shape acceleration spectra.

Different frames' layout are taken into account, varying beams' span, reinforcement arrangement and total storey number. Towards this aim, an iterative fully automated verification algorithm is implemented in MATLAB (MathWorks Inc., 2011), based on results provided by non linear pushover analyses, these latter conducted on regular plain frames FE models built in SAP2000 V.11.0 (Computer and Structures, 2010). In order to favor a more realistic non-linear structural response, great effort is spent on accurate modeling of members' property, namely equivalent cracked members' stiffness and non-linear moment vs. rotation relationships for members' ends. Specific formulations are defined to account for the different behaviour of the proposed precast framing system compared to an equivalent RC frame cast-in-place. In particular, the interaction between precast elements and connections' deformability (cf.ch.8) are explicitly considered, treasuring evidences collected in previous chapters through experimental and numerical studies to check on mechanics and resisting mechanisms of proposed precast joint system.

11.2. Plastic hinges' reference theory

In considered pushover analyses, frames' non-linear behaviour is concentrated in rigid-plastic hinges at members' ends, while remaining portions perform elastically. A realistic estimation of the non-linear Moment vs. Rotation ($M-\varphi$) curves as well as a proper value for the effective elastic stiffness of cracked RC members, are then fundamental input values for the calculation of seismic force and deformation demands on considered frames. A tentative estimation for such input data could be provided by FEMA 356 (Federal Emergency Management Agency (FEMA), 2000), even if Panagiotakos & Fardis, 2001 report as those provisions, retrieve generally conservative values that lead to underestimating real section ductility.

A better estimation for input data is provided by the moment vs. curvature curves computed for each frame's member, thus accounting for specific geometry and reinforcement, using the implemented MATLAB subroutine defined in chapter 9.3.1. The first step consists in transforming these curves into a bi-linear piecewise equivalent representation, with a certain elastic and post-yielding stiffness. As suggested by Legeron & Paultre, 2000 a reasonable estimation for the elastic section stiffness EJ is provided by the secant slope at 75% of M_{MAX} . The elastic

branch is then supposed to be straight until M_{MAX} (corresponding to M_y) is reached. The ultimate curvature χ_u is associated to one of the following events:

- Concrete attains (corresponding to a drop of 50% of peak compressive strength)
- Reinforcement fractures;
- The global residual strength drops down to 80% M_{MAX} .

The ultimate moment M_u is finally calculated assuming that the global area A_d subtended to the $M-\chi$ curve remain unvaried, to assure equivalence of dissipated energy:

$$M_u = \frac{2A_d - M_y \chi_y}{\chi_u - \chi_y} - M_y \quad (106)$$

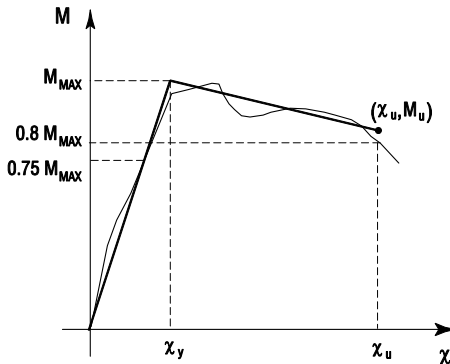


Fig. 279: Bilinear $M-\chi$ representation

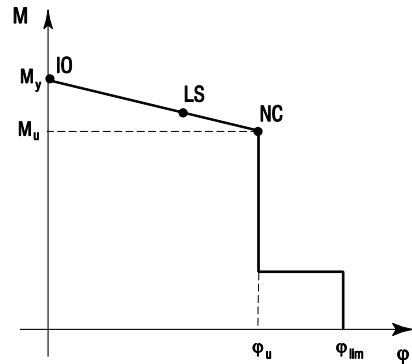


Fig. 280: Plastic hinge's $M-\phi$ relationship

The ratio M_y/χ_y is assumed as the effective flexural rigidity EJ of the cracked section. This value, however, still does not reflect many important effects, such as those of inclined cracking and shear deformations along the member, as well as any fixed-end rotation due to bar pullout from the anchorage zone.

Based on fitting over 963 experimental tests, following expression is proposed by Panagiotakos & Fardis, 2001 to estimate the member's chord rotation at yielding:

$$\phi_y = \frac{\chi_y L_v}{3} + 0.0025 + a_{sl} \frac{0.25 \varepsilon_y d_b f_y}{d - d' \sqrt{f_c}} \quad (107)$$

where χ_y =yielding curvature; L_v =shear span; a_{sl} =end-slip correction coefficient (0÷1); ε_y =yielding strain, d_b =rebars' diameter, $d-d'$ =lever arm between tension and compression rebars

The first term on the right side of equation 69 represents the drift or chord rotation at yield θ_y that is due to flexural deformations. The shear span L_V correspond to the Moment vs. Shear ratio at members' ends. Estimating this quantity for all members could be quite frustrating, but Mpampatsikos et al., 2008 suggest to replace it by $L/2$, where L is the member total length.

The second term on the right side of equation 69 refers to shear distortion. Finally, the third term accounts for the fixed-end rotation owing to slipping. Coefficient a_{sl} equals 1 if slippage of longitudinal steel from its anchorage zone beyond the end section is possible, or 0 if it is not.

Based on above formulation, EN 1998-3:2005 reports a similar expression for the estimation of yielding rotation of RC members

$$\varphi_y = \chi_y \frac{L_V + a_v z}{3} + 0.00135 \left(1 + 1.5 \frac{h}{L_V} \right) + \frac{0.13 \varepsilon_y d_b f_y}{d - d' \sqrt{f_c}} \quad (108)$$

where χ_y =yielding curvature; L_V =shear span; $a_v z$ =is the tension shift of the bending moment diagram; ε_y =yielding strain, d_b =rebars' diameter, $d-d'$ =lever arm between tension and compression rebars

Expression 107 is substantially equivalent to 108, with the main differences that the tension shift of the bending moment is considered for the flexural deformation contributes, the shear deformation is made explicitly dependant from the shear span and the rebar debonding contribute is half considered, but the a_{sl} coefficient is missing.

Get the equivalent flexural rigidity EJ of cracked members is now trivial, considering that the elastic deformation contribute is spread on the whole column or beam element:

$$EJ_{EQ} = \frac{M_y L_V^3}{3\varphi_y} \quad (109)$$

Once the equivalent elastic stiffness for frames' members is computed, being inertia modulus J a geometric input of the numerical model, the equivalent elastic modulus can be computed (E_{EQ}) and expressed as ratio of the initial elastic modulus E_0 .

Let's focus now on the issue relative to calculation of complete Moment vs. Rotation curve, to be implemented in members' end region for the pushover analyses.

A quantity to determine is the plastic hinge length L_{pl} , that is the portion of beam or column where non-linearities concentrate, namely the members' portion where rebar's yielding is expected. Panagiotakos & Fardis, 2001 suggest that L_{pl} should be

a function of two main variables, namely the shear span L_s and the product $d_b f_y$. If L_{pl} is taken as a linear function of these two variables, the following expressions provide the best fit to the 875 tests for which values of φ_u were available, both for cyclic and monotonic loading:

$$L_{pl,cyc} = 0.12L_v + 0.014\alpha_{sl}d_b f_y \quad (110)$$

$$L_{pl,mon} = 0.18L_v + 0.021\alpha_{sl}d_b f_y \quad (111)$$

where L_v =shear span; α_{sl} =end-slip correction coefficient (0÷1); d_b =rebars' diameter

EN 1998-3:2005 reports a more conservative expression:

$$L_{pl} = \frac{L_v}{30} + 0.2h + 0.11 \frac{d_b f_y}{\sqrt{f_c}} \quad (112)$$

where L_v =shear span; h =section height; d_b =rebars' diameter

Once the L_{pl} quantity is known, the ultimate chord rotation Near Collapse (NC) for the considered member can be calculated as reported in equation 113 (EN 1998-3:2005, Panagiotakos & Fardis, 2001). The NC condition is equivalent to the CP (Collapse Prevention) condition reported in FEMA 356.

$$\varphi_{u,NC} = \frac{1}{\gamma_{el}} \left(\theta_y + (\chi_u - \chi_y) L_v \left(\frac{1 - 0.5L_{pl}}{L_v} \right) \right) \quad (113)$$

where γ_{el} =safety coefficient for primary members (1.5) χ_y =yielding curvature; χ_u =ultimate curvature; L_v =shear span; L_{pl} =plastic length

To get a rigid plastic Moment vs. Rotation relationship, just the plastic contribute should be considered from 113:

$$\varphi_{pl,NC} = \frac{1}{\gamma_{el}} \left((\chi_u - \chi_y) L_v \left(\frac{1 - 0.5L_{pl}}{L_v} \right) \right) \quad (114)$$

The LS (Life Safety) plastic rotation limit is then obtained as (see par. A.3.2.3 in EN 1998-3:2005):

$$\varphi_{pl,LS} = 3/4 \varphi_{pl,NC} \quad (115)$$

Finally the residual strength to define the failure branch in M-φ relationship is taken as 20% of the maximum value, as suggest in FEMA 356.

11.3. Beams' plastic hinges

11.3.1. Adopted formulations

Expressions reported in chapter 11.2 can be used to estimate beam's input data for pushover analysis, even if some modifications should be accounted, to consider the specific beams' layout in proposed solution.

In particular the horizontal frame members are constituted by CSTC beam, whose structural continuity is provided by specific lattice girder passing through the core-joint. It would be wrong to consider the whole beam section as uniform.

To calculate the yielding rotation (i.e. the equivalent stiffness) equation 108 is used, but considering two different flexural contribute: the one provided by CSTC beam and the one provided by lattice girder-concrete composite section.

Some hypotheses need to be introduced. It is supposed that the influence of the lattice girder should be accounted for a length equal to that required by CSTC rebars to become effective in bearing bending moment. This length is assumed to be equal to half the plastic hinge length as defined in equation 112.

$$\varphi_{y,gir} = \chi_{y,gir} \frac{L_{pl} / 2}{3} \quad (116)$$

The rotation contribute provided by CSTC beam is assumed as:

$$L_{V,red} = L_V - L_{pl} / 2 \quad (117)$$

$$\varphi_{y,CB} = \frac{M_y L_{V,red} / L_V}{EJ_{CB}} \frac{L_{V,red}}{3} \quad (118)$$

where $\varphi_{y,CB}$ =rotation at yielding for the CSCT beam; $L_{V,red}$ =reduced shear length; EJ_{CB} =section stiffness of CSCT beam (estimated as $6.1 \times 10^{13} \text{ Nmm}^2$).

The rotation contributes defined in equations 116 and 118 can be applied into equation 108, leading to the following expression:

$$\varphi_y = \chi_{y,gir} \frac{L_{pl}}{6} + \frac{M_y L_{v,red} / L_v}{EJ_{CB}} \frac{L_{v,red}}{3} + 0.00135 \left(1 + 1.5 \frac{h}{L_v} \right) + 0.25 \frac{0.13 \varepsilon_y d_b f_y}{d - d' \sqrt{f_c}} \quad (119)$$

where χ_y =yielding curvature; L_v =shear span; a_{vz} =is the tension shift of the bending moment diagram; ε_y =yielding strain, d_b =rebars' diameter, $d-d'$ =lever arm between tension and compression rebars

Compared with eq. 108, the tension shift has been disregarded and a reduction coefficient for the debonding contribute is assumed ($a_{sl}=0.25$). This is due to the fact that lattice girder's debonding is limited, when properly designed (cf. ch.5.2 and eq. 71)The equivalent section stiffness EJ can then be calculated adopting equation 109. Finally, concerning the complete rigid-plastic $M-\varphi$ relationship issue, under the hypothesis that CSCT beam's truss does not provide any significant contribute, the mere truss girder reinforcement should be considered. Numerical analyses about cyclic performance of the precast joint reported in chapter 10, supports this hypothesis, showing as the plastic hinge length L_{pl} is not long enough to guarantee a full interaction of the confinement provided by CSTC beam, that remains thus elastic during the whole test (cf. Fig. 275). Equations 114 and 115 should then be adopted.

11.3.2. Computed plastic hinges

In Fig. 281 and Fig. 282 are reported detailed beam's section dimensions and effective reinforcement to be adopted for plastic hinge calculation under negative and positive bending respctively. In the first case (Fig. 281 Fig. 282) longitudinal reinforcement provided by lattice girders is fully considered. Experimental tests reported by Scotta & Tesser, 2011 and numerical evidences (cf. ch.5) have evidenced as inclined trusses belonging to these components can provide enough bearing action against concrete to restore the perfect bond conditions between plain-bar and concrete. Among the lower longitudinal reinforcement provided by truss inside CSCT beam, just two of them are considered effective in providing some resistance contribute to the compressed beam portion, taking suggestion from experimental results provided by Badalamenti et al., 2008.

Under positive bending, just lattice girders are considered as effective, while reinforcement provided by CSCT beam is totally disregarded. Due to missing reinforcement in the lower side of cantilever a main crack spread from to bottom up

to the lower longitudinal rebars, in correspondence of the fixed end (Fig. 200). To account for this effect a reduced effective beam depth is considered.

In Fig. 283 and Fig. 284 are reported the analytical $M-\chi$ curves for positive and negative bending respectively. For all cases failure is reached by exceeding of maximum steel strains. In Fig. 285 and Fig. 286 are reported the equivalent $M-\phi$ curves, for $\phi 16$ and $\phi 28$ longitudinal lattices' bars, respectively. To perform this transformation, equations 109, 114, 115 and 119 are adopted. It should be noticed as the equivalent stieffness E_{fess} is sensibly reduced compared to the uncracked section stieffness E_0 and in some case is also sensibly lower than 30%, suggested by ACI 318-08 as a reference value. Similar evidences have been also reported by Panagiotakos & Fardis, 2001. Main input parameters to define plastic hinges for Pushover analyses are reported in Table 22.

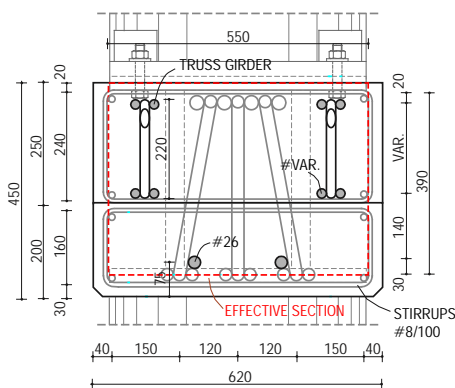


Fig. 281: beam section dimensions under negative bending

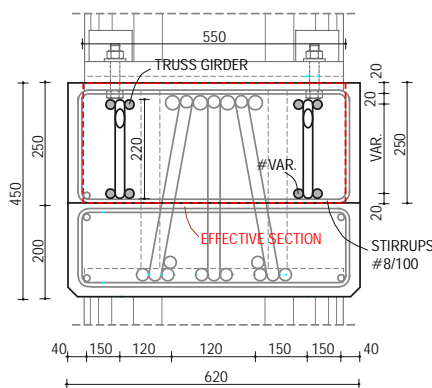
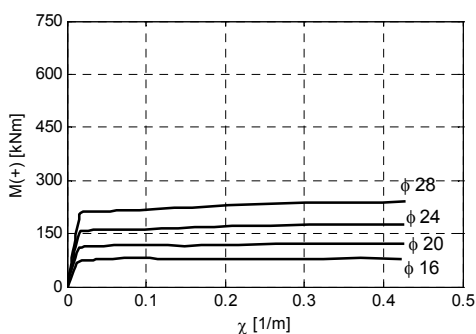
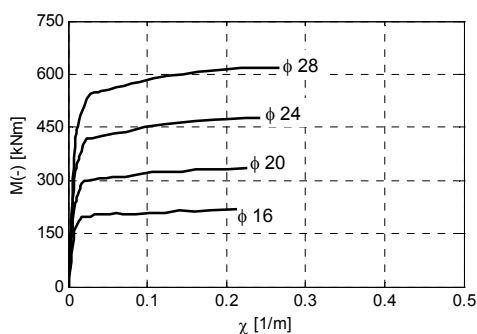


Fig. 282: beam section dimensions under positive bending



max.steel strain failure for all sections

Fig. 283: $M-\chi$ curves for beams under positive bending



max.steel strain failure for all sections

Fig. 284: $M-\chi$ curves for beams under negative bending

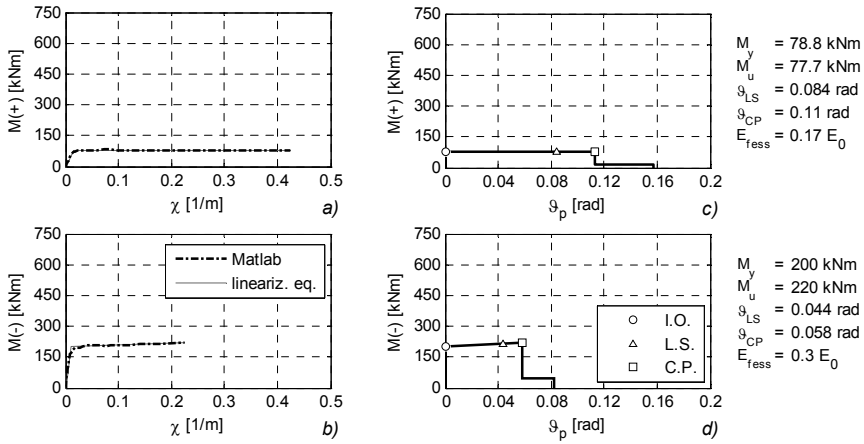


Fig. 285: M - χ vs. M - ϕ transformation for $\phi 16$ beam's reinforcement

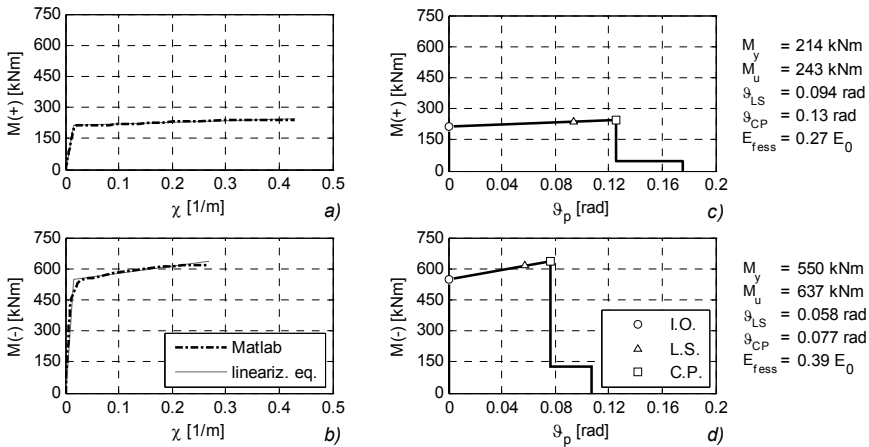


Fig. 286: M - χ vs. M - ϕ transformation for $\phi 28$ beam's reinforcement

φ _b (mm)	Positive bending					Negative bending				
	M _y (kNm)	M _u (kNm)	φ _{LS} (rad)	φ _{CP} (rad)	$\frac{E_{fess}}{E_0}$	M _y (kNm)	M _u (kNm)	φ _{LS} (rad)	φ _{CP} (rad)	$\frac{E_{fess}}{E_0}$
16	79	78	84	112	0.16	200	220	43.8	58	0.29
18	97	98	86	115	0.18	251	274	44.7	60	0.32
20	117	121	88	117	0.20	304	339	45.7	61	0.34
22	139	147	89	119	0.22	360	416	47.3	63	0.35
24	162	176	91	121	0.23	420	491	50.3	67	0.36
26	187	209	93	123	0.25	482	566	53.9	72	0.37
28	214	243	94	125	0.26	550	637	57.6	77	0.38

Table 22: Plastic hinges' properties

11.4. Columns' plastic hinges

11.4.1. Adopted formulations

Similarly to beams, also for columns the procedure reported in chapter 11.2 is adopted to estimate input data for Pushover analyses, although some modifications should be introduced to the original plastic-hinge formulations, to consider in particular the deformation contributes provided by column-to-column connection system (cf. ch.8) and the core-joint, as well (cf. ch.7.3). These affect in particular the hinges' yielding rotation that means the equivalent stiffness columns' E_{fess} . The connections' contribute should be computed as:

$$\varphi_{INT} = M_y / K_{INT} \quad 120)$$

where φ_{INT} =rotation contribute ; M_y =yielding moment; K_{INT} =stiffness of bolted or welded connection

The core-joint contribute is assumed as:

$$\varphi_{JNT} = \frac{M_y}{EJ_{JOINT}} \left[\left(\frac{h_{JOINT}}{2} \right) + \frac{1}{2} \left(\frac{h_{JOINT}}{2} \right)^2 \right] \cdot L_V \quad 121)$$

where φ_{JNT} =core-joint rotation contribute ; M_y =yielding moment; h_{JOINT} =height of core-joint; L_V =shear span

The total column's chord rotation when yielding is reached is then computed putting these contributes together into equation 108 and the following expression is then provided:

$$\varphi_y = \chi_y \frac{L_V}{3} + 0.00135 \left(1 + 1.5 \frac{h}{L_V} \right) + 0.25 \frac{0.13 \varepsilon_y d_b f_y}{d - d' \sqrt{f_c}} + \varphi_{INT} + \varphi_{JNT} \quad 122)$$

Compared with 108, the tension shift has been disregarded and a reduction coefficient for the debonding contribute is assumed ($a_{sl}=0.25$). This is due to the fact that column's reinforcement is welded at ends against horizontal steel flanges, thus reducing sensibly debonding phenomena.

11.4.2. Lateral confining steel

The considered HSC columns are characterized by a highly automated precast assembling process. In particular a specific machinery is able to coil-up the $\phi 6$ spiral stirrups around the longitudinal rebars. Adopting such a reinforcement diameters is allowed by the Italian Regulation Code NTC2008, also when dealing with seismic design. However strict reinforcement geometry limitations are required. These could represent a limiting aspect for the proposed precast columns if high-ductility seismic design is chosen (Class Ductility “A” design), since they should be satisfied along the whole columns’ length. Conversely when a low ductility design is chosen (Class Ductility “B” design), such restrictions should be considered only in the dissipation zones (i.e. plastic hinges). In a typical frame structure, a beam sidesway mechanism is usually adopted for seismic design: plastic hinges take place at beams’ ends, while column remain elastic, to avoid soft-storey failures. Just columns’ base at ground level could be subjected to plasticization, without reducing global structure stability and safety. More accurate confinement detailing should then be adopted just for a limited columns’ portion, without affecting sensibly the final costs of the proposed solution. The idea is that of hand-placing higher diameter stirrups during the precast process, once longitudinal rebars have been welded on lower horizontal flange (Fig. 287a and b). Stirrups could be inserted from the top and made slide down till the required position. A limited welding is required to fix them in the right position. Such an operation is required just for the column at base floor, for a stub length approximatively equal to 500mm, as the expected plastic hinge length. In the remaining column portion non-seismic detailing for lateral reinforcement can be adopted (i.e. the coiled $\phi 6$ stirrups, see Fig. 287c). For the remaining columns at superior storeys, coiled stirrups can be adopted for the length (Fig. 287d and Fig. 288)

With reference to required lateral reinforcement in columns’ plastic regions, reference should be made to Paultre & Légeron, 2008.

They developed new equations for the determination of confinement reinforcement for rectangular and circular concrete columns applicable to concrete strength up to 120 MPa and confinement steel strength up to 1,400 MPa. These equations were developed from a comprehensive study considering experimental results given by 93 square and circular columns’ test. Such research provided the basis for the new confinement requirements of the new Canadian Standard Association (CSA) (document CSA A23.3-04 “Design of concrete structures”).

First of all, minimum amount of transverse reinforcement is determined by prescriptions usually adopted in codes for non-seismic reasons to avoid buckling failure:

$$\frac{A_{sh,MIN}}{s} = 0.09 \frac{f_{cd}}{f_{ywd}} b_c \quad (123)$$

where b_c =cross-sectional dimension of column core measured center-to-center of outer legs of the transverse reinforcement comprising area A_{sh} ($\approx 490\text{mm}$); s =stirrups' spacing; f_{ywd} =transverse reinforcement yield design strength (390MPa); f_{cd} =concrete design strength (38MPa)

A similar expression is adopted also by NTC 2008 to design column dissipative regions in “CD B” seismic design.

In above expressions, however, no reference is still made to axial load level, nor to confined sections geometry, which affects sensibly experimental results. A second expression is then provided by Paultre & Légeron, 2008 for moderately ductile frames:

$$\frac{A_{sh,MIN}}{s} = 0.15 k_n k_p \frac{A_g}{A_{ch}} \frac{f_{cd}}{f_{ywd}} h_c \quad (124)$$

Where $k_n = n/(n-2)$; n =longitudinal rebars' number ($n=8$); k_p =ratio of applied vs. pure axial load column capacity; h_c =height of confined core section ($\approx 270\text{mm}$); A_g =gross area-section ($\approx 1580\text{cm}^2$); A_{ch} =confined core area ($\approx 1021\text{cm}^2$); f_{ywd} =transverse reinforcement yield design strength (390MPa); f_{cd} =concrete design strength (38MPa)

Expression 123 provide a required stirrups amount equal to $4295 \text{ mm}^2/\text{m}$. Making reference to 124 and considering an axial load level equal to 4000kN ($k_p \approx 0.5$), required stirrups amount is equal to $3870 \text{ mm}^2/\text{m}$.

A conservative solution could be the adoption of stirrups $\phi 12$, spaced 50 mm , corresponding to $4520 \text{ mm}^2/\text{m}$ (Fig. 289).

The over-reinforced columns at ground level is in the following indicated as “base column”. The others are indicated as “upper columns”.

To guarantee accurate frame models implement for Pushover analyses, both plastic hinges for base columns and the upper columns have been calculated.

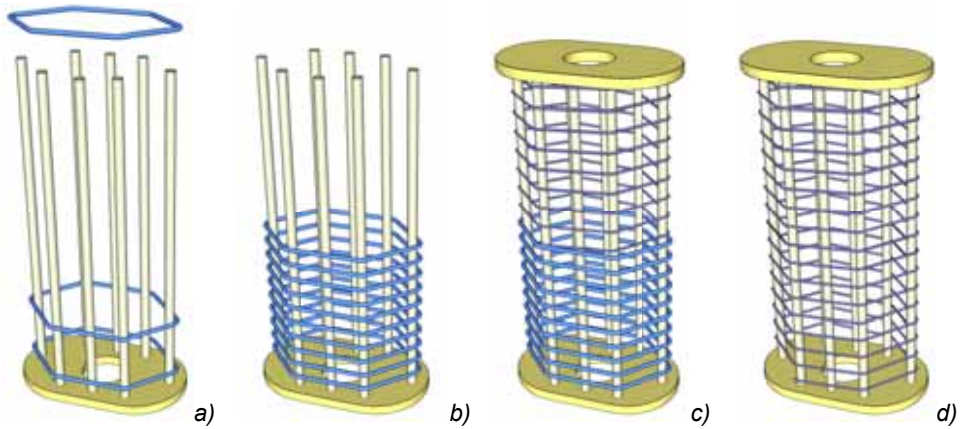


Fig. 287: a) b) precast assembling process for base columns; c) base column layout; d) standard column layout

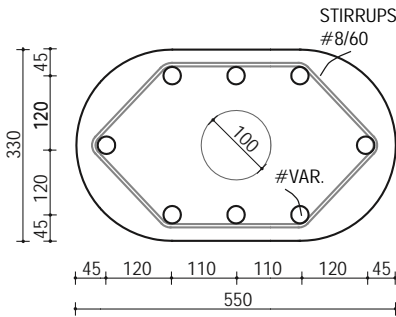


Fig. 288: Column section dimensions

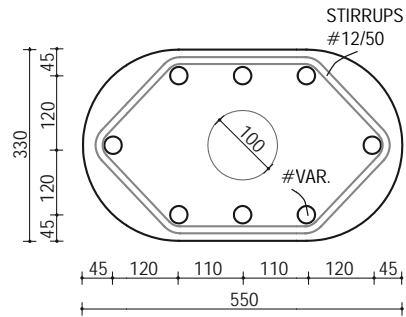


Fig. 289: Base column section dimension

11.4.3. Column plastic hinge

In Fig. 290 and Fig. 291 are reported the M-c curves computed for upper and base columns, respectively. In the latter case it can be seen as the over-reinforcement provided by higher diameter stirrups cause a considerable increase in section ductility. In general lower longitudinal rebars' diameter allow to get higher ductility level at lower axial load levels. As applied axial force exceed 2000kN, this trend is less evident. Failure is never attained for exceeding of maximum steel strain. At lower axial loads failure is due to concrete crushing, while for higher loads failure is attained for excessive reduction of section residual strength.

In Fig. 292 is reported an example of the transformation of such curves into M- ϕ ones. To perform this operation equations 109, 112, 114, 115 and 122 are adopted. It should be noticed as the equivalent stieffness E_{fess} is sensibly reduced compared to the uncracked section stieffness E_0 and always lower than 70%, suggested by

ACI 318:1995 as a reference value. Similar evidences have been also reported by Panagiotakos & Fardis, 2001, even if in this case such results could be partially justified also by introduction of connection deformability.

Finally main input parameter to define plastic hinges for Pushover analyses are reported in Table 23.

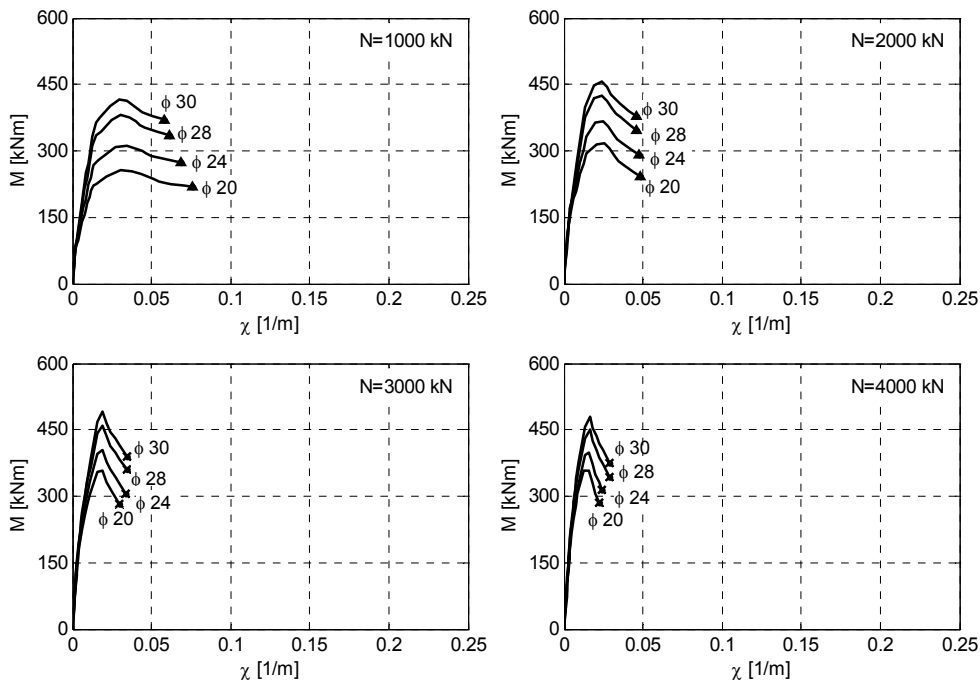
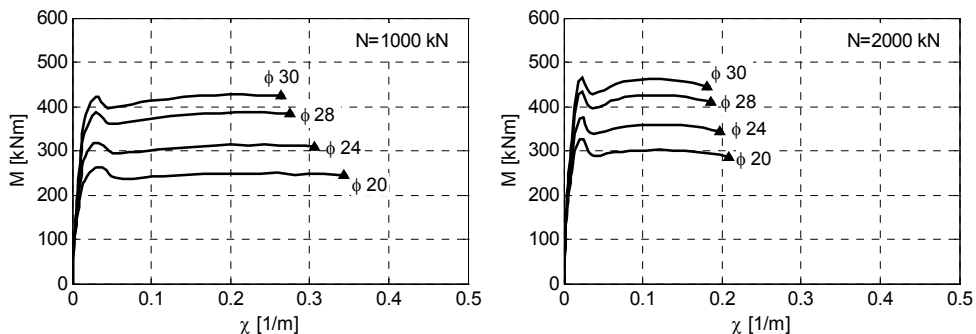


Fig. 290: $M-\chi$ curves for column with standard reinforcement



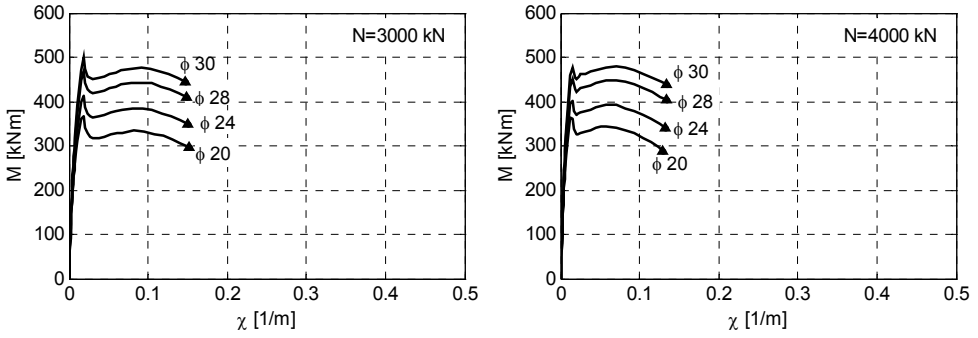


Fig. 291: $M-\chi$ curves for base column

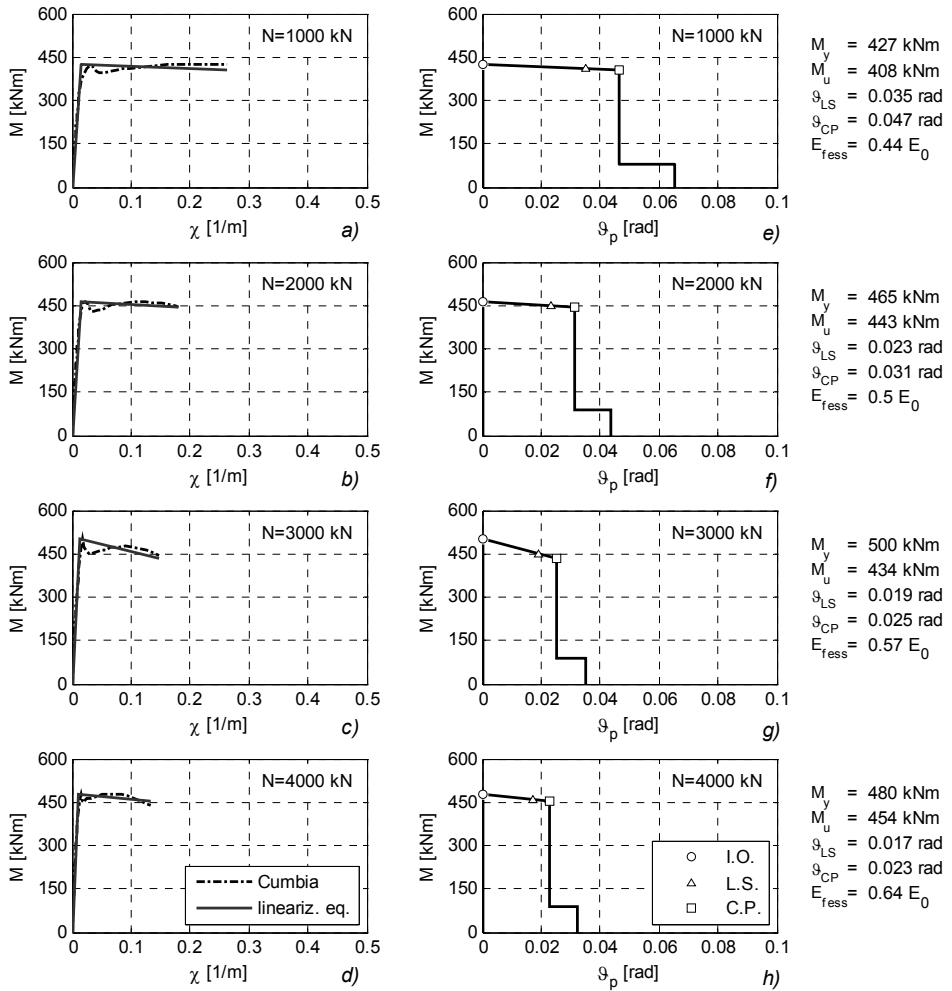


Fig. 292: $M-\chi$ vs. $M-\phi$ transformation for $\phi 30$ base column

Analysis and development of an innovative prefabricated beam-to-column joint

ϕ_b (mm)	N (kN)	Standard columns					Base columns				
		M_y (kNm)	M_u (kNm)	ϕ_{LS} (rad)	ϕ_{CP} (rad)	$\frac{E_{fess}}{E_0}$	M_y (kNm)	M_u (kNm)	ϕ_{LS} (rad)	ϕ_{CP} (rad)	$\frac{E_{fess}}{E_0}$
20	0	168	156	25.7	34.3	0.19	172	160	50.2	66.9	0.18
22	0	197	186	22.0	29.3	0.22	206	191	49.5	66.0	0.22
24	0	230	219	19.0	25.4	0.25	243	225	48.1	64.1	0.25
26	0	265	252	17.1	22.8	0.29	282	262	53.8	71.8	0.29
28	0	301	289	15.1	20.1	0.32	327	301	56.3	75.1	0.32
30	0	341	327	13.7	18.2	0.36	372	343	56.5	75.3	0.35
20	1000	255	226	8.0	10.6	0.29	264	230	42.2	56.3	0.30
22	1000	283	253	7.5	10.1	0.31	291	262	40.9	54.6	0.32
24	1000	311	283	7.2	9.6	0.34	318	299	38.9	51.9	0.35
26	1000	346	311	6.8	9.0	0.36	354	331	37.8	50.4	0.37
28	1000	381	342	6.4	8.5	0.39	388	370	36.0	48.1	0.40
30	1000	415	378	6.0	8.0	0.42	427	408	35.0	46.6	0.43
20	2000	316	270	4.5	6.0	0.39	326	273	25.0	33.4	0.41
22	2000	340	294	4.5	6.0	0.40	351	303	24.6	32.8	0.42
24	2000	366	318	4.4	5.9	0.42	376	334	24.5	32.7	0.43
26	2000	394	345	4.4	5.9	0.44	404	369	24.2	32.3	0.45
28	2000	424	373	4.4	5.9	0.46	434	405	23.7	31.6	0.47
30	2000	456	404	4.4	5.8	0.49	465	443	23.4	31.2	0.50
20	3000	357	319	2.3	3.0	0.48	368	284	17.9	23.9	0.50
22	3000	381	344	2.2	3.0	0.48	390	311	18.1	24.1	0.51
24	3000	404	339	2.8	3.8	0.49	414	338	18.3	24.5	0.52
26	3000	431	366	2.8	3.8	0.51	441	368	18.5	24.6	0.53
28	3000	459	395	2.8	3.8	0.52	469	401	18.7	24.9	0.54
30	3000	491	425	2.9	3.8	0.54	500	434	18.9	25.2	0.56
20	4000	359	318	1.6	2.2	0.56	364	296	15.4	20.6	0.59
22	4000	378	322	1.9	2.5	0.57	381	325	15.9	21.1	0.59
24	4000	400	346	1.9	2.5	0.58	402	354	16.2	21.7	0.61
26	4000	425	342	2.4	3.2	0.59	425	387	16.6	22.1	0.61
28	4000	451	372	2.4	3.2	0.60	449	421	17.0	22.7	0.63
30	4000	479	406	2.4	3.2	0.61	480	454	17.3	23.1	0.64

Table 23: Column plastic hinge properties

11.5. Vulnerability-based approach

11.5.1. Frame models

The verification of seismic performances of current precast technology is conducted on regular plain moment-resisting multi-storey frames, with 5 bays and interaxis equal to 6 meters, the latter imposed by structural limit of the adopted flooring technology (200 mm thick hollow core slabs) Two layout are considered with bays span equal to 6 (Fig. 293) and 8 meters (Fig. 294), respectively.

The number of storeys get progressively increased from 3 to 10 and 8 for frames with respectively 6 and 8-meters-long bays span. The upper number of storeys limit is defined on the basis of static strength considerations (cf. ch.9.4). Aiming to identify the most proper reinforcement arrangement and corresponding ductility factor R (eq. 137, 138), for each frame, two different lattices' bar diameters are considered. The first determined from static design of hogging moments acting at beams' ends in Ultimate Limit State condition. The second determined by a bending strength overdesign of almost 100kNm. It should be recalled as lattice girders' reinforcement is the only one able to restore beam continuity across the core joint (Fig. 281 and Fig. 282). A total of four different frame's layouts are thus considered:

- frame type A: 6 meters bays; $\phi 18$ lattice bar diameter;
- frame type B: 6 meters bays; $\phi 22$ lattice bar diameter;
- frame type C: 8 meters bays; $\phi 24$ lattice bar diameter;
- frame type D: 8 meters bays; $\phi 28$ lattice bar diameter.

To simplify frames' numerical modeling the same reinforcement amount is assigned to all beams at different storey level. For base columns, $\phi 30$ longitudinal rebars are supposed for all the considered frames. Columns' reinforcement diameter get progressively reduced for upper storeys, paying attention that enough strength is provided, in order to avoid column sidesway mechanisms. Static loads acting on frames are reported in Table 24. Considered live load is usually associated to very busy living spaces, like markets and malls for example. Considering less strict load conditions, even higher storey number could be attained for the considered precast system. Non linear analyses are conducted adopting SAP2000 V.11.0 (Computer and Structures, 2010). Frames are modeled through simple 2 nodes beam elements. To get a realistic non-linear numerical response, particular care is spent to account for the different behaviour of the proposed precast framing system compared to an equivalent RC cast-in-place structure. In particular, the interaction between precast elements and coupling connections' deformability (cf. ch.8) are explicitly considered through the modification of the elastic modulus for cracked

Analysis and development of an innovative prefabricated beam-to-column joint

members' section and through the definition of specific formulations for plastic hinges at members' ends as well (cf. ch.11.3.1 and 11.4.1).

	LOAD TYPE	Coeff. Ψ_{2j}	Load (Kg/m ²)
	STRUCTURAL DEAD LOAD		
	Hollow core section flooring system 20+5	-	450
G ₁	TOT. STRUCTURAL DEAD LOAD	-	450
	NON-STRUCTURAL DEAD LOAD		
	Finishing screed tk. 10 cm (1500kg/m ³ by 0,1m)	-	150
	Paving	-	50
	Ceilings	-	50
G ₂	TOT. NON-STRUCTURAL DEAD LOAD	-	250
G ₁ + G ₂	DEAD LOAD	-	650
	LIVE LOAD		
	Crowd	0.6	400
Q	TOT. LIVE LOAD		400
G ₁ + G ₂ + Q	TOT. LOAD (non seismic condition)		1050
G ₁ + G ₂ + Ψ_2Q	TOT. LOAD (seismic condition)		890

Table 24: Applied load on frames

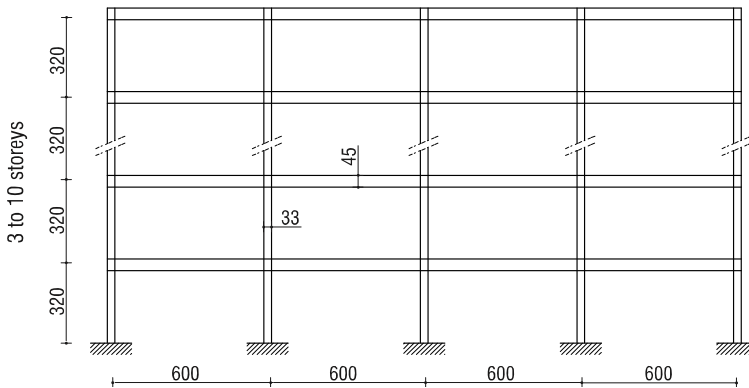


Fig. 293: Typical frame layout with 6 meters beams' span

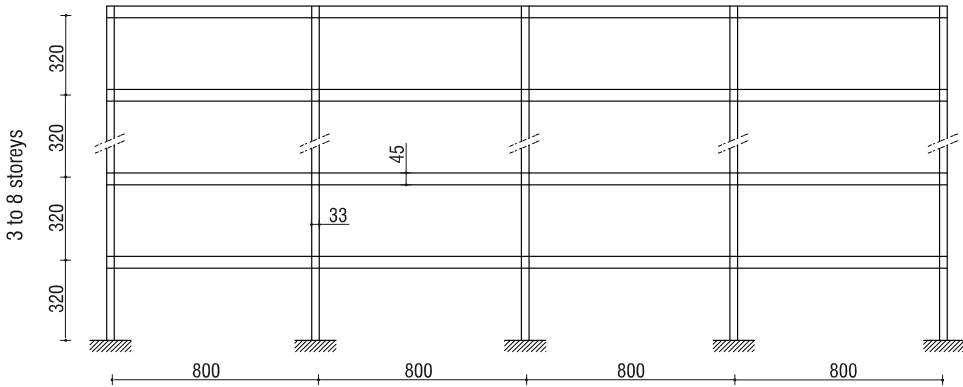


Fig. 294: Typical frame layout with 8 meters beams' span

11.5.2. Reference seismic action

The investigation about seismic performance of proposed precast system needs for a reference seismic action to be defined. Current survey is mainly oriented to National territory, being the Italian market the expected main reference for the proposed solution. The current Italian Code for seismic design (NTC2008), differently from overseas Codes, refers the input seismic action to a grid with span 10 by 10 km, that covers the whole Italian territory, identifying 10751 points, each characterized by a specific value for Peak Ground Acceleration (PGA) a_g and a specific shape for the reference elastic Acceleration Spectra $S_a(T)$ (Fig. 296). This latter get completely defined by the definition of two parameters: F_0 and T_C^* . The first one provides the peak pseudo-acceleration of the equivalent Single Degree of Freedom (SDOF) system (between natural periods T_B and T_C in Fig. 296). The latter is directly related to T_C as a function depending from site classes (ground categories). As it can be seen from Fig. 297 to Fig. 299, there is a wide variability for seismic parameters over the Italian territory that make impossible identifying a reference seismic action as for past seismic code OPCM 3431, which referred to four main seismic regions. To comply with current Italian seismic Code a vulnerability-based approach is adopted, that allows to express the performance of the proposed precast technology not in term of allowable ground acceleration, but as percentage of the territory where considered framed structures are able to withstand the earthquake event. This approach requires a recursive extension of the verification procedure to the whole Italian Territory, namely to 10751 seismic points. This operation is made possible through a user defined MATLAB subroutine, adopting as input data pushover curves coming from non-linear static analyses on

regular plain frames (cf. ch.11.5.1) and seismic parameter provided by Code, the latter referred to seismic events with an exceeding probability of 10% during 50 years, thus assuming a return period equal to 475 years (Fig. 295). Further details about adopted procedure are reported in chapter 11.5.3.

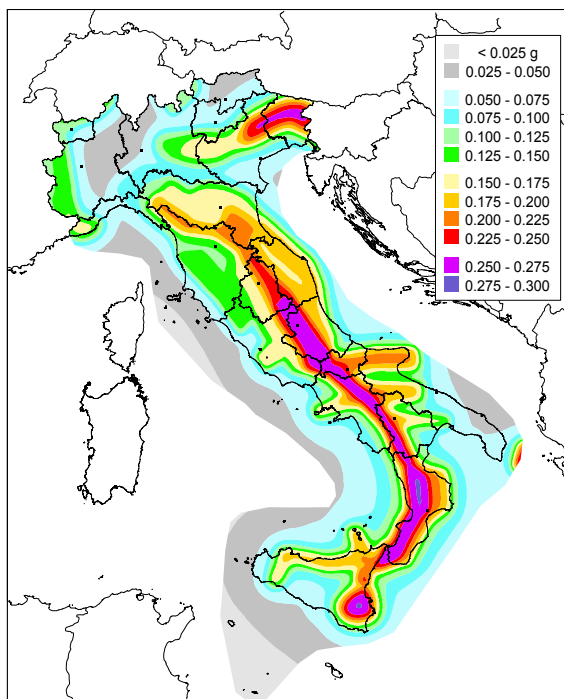


Fig. 295: Reference ground acceleration for the Italian Territory with reference to return period equal to 475 years and Ground Category A, as reported in OPCM 28 April 2006 n.3519, All.1b

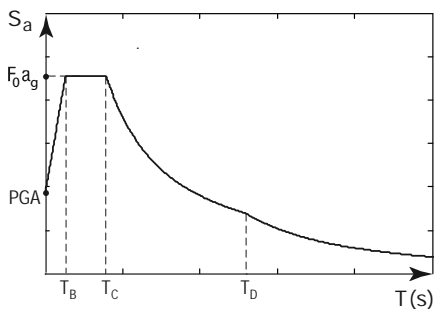


Fig. 296: Acceleration design spectra

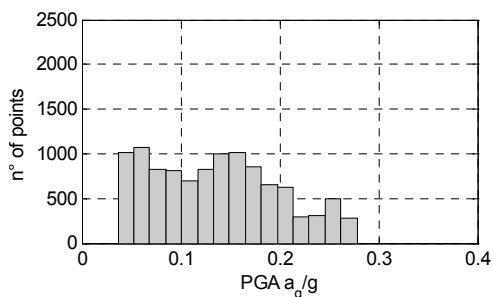


Fig. 297: Reference PGA; return period 475

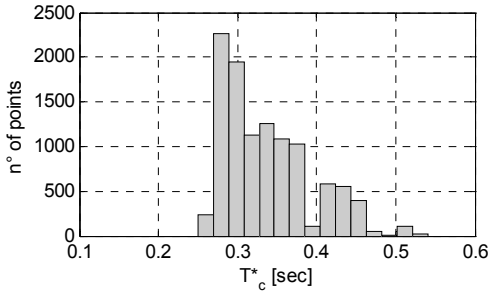


Fig. 298: T_c^* ; return period 475

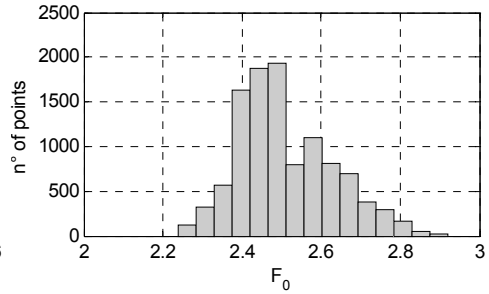


Fig. 299: F_0 ; return period 475

11.5.3. Verification procedure

To shed light on seismic performance of proposed precast technology, the first verification step consists in the determination of the non-linear response of considered frames under earthquake loading. Pushover analyses are adopted for this purpose in order to get the frames' response expressed in term of *capacity curve*, namely base-shear force versus top displacement relationship obtained by monotonically increasing lateral load applied on the structure. The distribution of the horizontal forces F_i is obtained by multiplying the floor masses m_i by a specific displacement profile $\Phi(z)$.

$$F_i = m_i \phi(z)_i \quad (125)$$

Every reasonable profile $\Phi(z)$ could be used, but often the contributions of the higher modes of vibration of the structure are negligible and the displacement shape of the first mode of vibration can be used to define vector Φ . However, it is recommended that the analysis is repeated by two displacement profiles that bound the actual seismic response of the structure. As suggested by NTC 2008 a linear triangular and constant displacement profile are adopted:

$$\phi(z)_i^{LIN} = 1 / h_{tot} \cdot h_{i-th} \quad (126)$$

where h_{tot} =frame total height; h_{i-th} =considered storey height

$$\phi(z)_i^{COS} = 1 \quad (127)$$

For each computed capacity curves, an ultimate top displacement is defined, depending on which of the following event take place before (Fig. 300):

- Plastic rotation of at least one single plastic hinge exceeds the Life Safety (LS) limit.
- Residual strength attains 85% of the peak strength V_{MAX} (as suggested by NTC 2008).

The first of these two events define the so called Performance Point (PP) of the structure, corresponding to the maximum allowable top displacement before failure take place.

To perform seismic design of building, the N2 method proposed by Fajfar & Gašperšič, 1996 is used. Such an approach need the capacity curve to be linearized into equivalent elasto-plastic curves (Fig. 300). The basic idea is to leave unchanged the area A enveloped by original capacity curve until PP (i.e. global energy remains unchanged). For current analyses, the initial elastic stieffness K is evaluated as the secant slope crossing 75% V_{MAX} . The yielding displacement d_y is then estimated as:

$$d_y = 0.5 \left[2d_u - (4d_u^2 - 8A / K)^{0.5} \right] \tag{128}$$

where A =enveloped area; K =elastic stieffness; d_u =ultimate displacemnt (PP)

Getting the yieldign shear force V_y is trivial:

$$V_y = d_y K \tag{129}$$

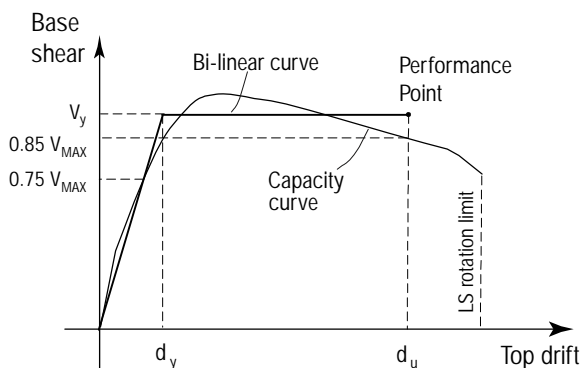


Fig. 300: Capacity curve bi-linearization

Next step is the trasformation of the linearized MDOF (Multi Degrees of Freedom) capacity curve into the equivalent SDOF (Single DOF) curve, related to a single pendulum equivalent to the whole frame structure.

The perform this operation the quantities m^* (equivalent SDOF mass) and Γ (modal mass participation factor) need be defined:

$$m^* = \sum m_i \phi_i \quad 130)$$

$$\Gamma = \frac{\sum m_i \phi_i}{\sum m_i \phi_i^2} \quad 131)$$

The equivalent SDOF system has a mass equal to m^* and its response parameters (force V^* and displacement D^*) may be obtained from the corresponding parameters of the MDOF system (base shear V and top displacement D) by means of the following equations:

$$V^* = V / \Gamma \quad 132)$$

$$D^* = D / \Gamma \quad 133)$$

The force V^* could be better expressed in adimensional form:

$$v^* = V^* / m^* \quad 134)$$

The equivalent fundamental period of the SDOF system is defined as:

$$T^* = 2\pi \sqrt{\frac{m^*}{d_y^*} F_y^*} \quad 135)$$

In order to judge the inelastic response of the structure under examination, it is necessary at this point to relate the capacity curve to a specific PGA value. The elastic acceleration spectra $S_{a,el}(T)$ has been already defined in Fig. 296 and is recalled in Fig. 301. This spectra can be transformed into the equivalent elastic displacement spectra $S_{d,el}(T)$ (Fig. 302) though the expression:

$$S_{D,el}(T) = \frac{T^2}{4\pi} S_{A,el} \quad 136)$$

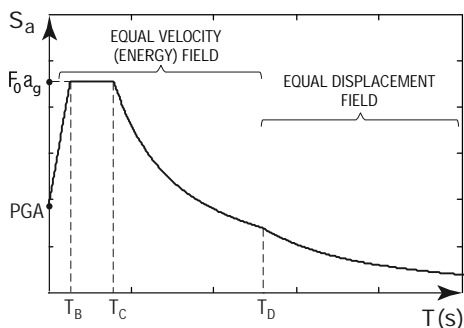


Fig. 301: Elastic pseudo-acceleration design spectra $S_{a,el}(T)$

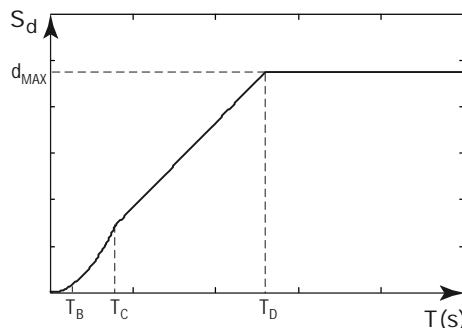


Fig. 302: Elastic displacement design spectra $S_{d,el}(T)$

Adopting $S_{d,el}$ and $S_{a,el}$ as abscissa and ordinate respectively, a specific spectra is defined, named $S_A S_D$ (elastic acceleration-displacement) spectra.

In the N2 method proposed by Fajfar & Gašperšič, 1996, the expected target displacement (TD) $S_{d,pl}(T^*)$ demand of the inelastic SDOF system, is related to the displacement of the corresponding elastic structure, and may be defined as a function the spectral value $S_{d,el}(T^*)$, being T^* the fundamental period of the SDOF system.

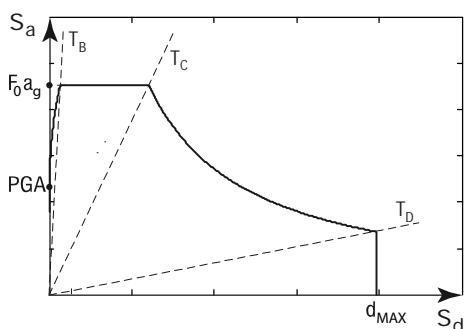


Fig. 303: S_a - S_d spectra

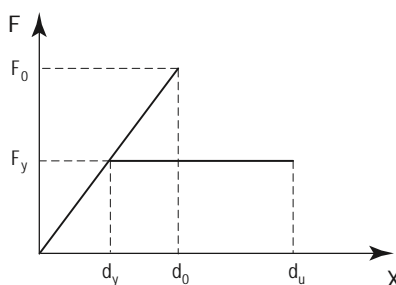


Fig. 304: Linear vs. non linear response

A fundamental parameter to introduce is the *reduction factor R*. It accounts for the reduction of the input elastic force, when inelastic structural responses are considered. Looking at Fig. 304 it could be defined as:

$$R_\mu = \frac{S_{A,el}(T^*)}{S_{A,pl}(T^*)} = \frac{F_0}{F_y} = \frac{\delta_0}{\delta_y} \tag{137}$$

Vidic et al., 1994 define such a parameter as:

$$\begin{aligned}
 R_\mu &= \mu && \text{when } T^* \geq T_C \\
 R_\mu &= (\mu - 1) \frac{T^*}{T_C} + 1 && \text{when } T^* < T_C
 \end{aligned} \tag{138}$$

For natural period $T^* \geq T_C$, equation 138 is derived by equivalence displacement between elastic and inelastic system (Fig. 305a). For natural period $T^* < T_C$, assumption is done about energy equivalence of the elastic and inelastic system (Fig. 305b)

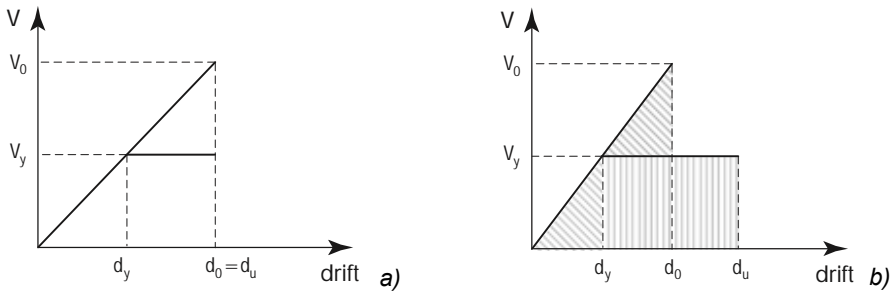


Fig. 305: a) displacement and b) energy equivalence principle

A further parameter directly related to system inelastic response is the *displacements ductility ratio* μ , usually expressed as:

$$\mu = d_u / d_y \tag{139}$$

Then:

$$d_u = \mu d_y = \mu \frac{\delta_0}{R_\mu} \tag{140}$$

In term of spectral displacement, equation 140 can be formulated as:

$$S_{D,pl}(T^*) = TD = \frac{\mu}{R_\mu} S_{D,el}(T^*) \tag{141}$$

Then:

$$\begin{aligned}
 S_{D,pl}(T^*) &= S_{D,el}(T^*) && \text{when } T^* \geq T_C \\
 S_{D,pl}(T^*) &= \frac{\mu}{(\mu - 1) \cdot T^*/T_C + 1} S_{D,el}(T^*) = && \text{when } T^* < T_C
 \end{aligned} \tag{142}$$

The N2 method consists basically in a graphical approach, with the SASD spectra and v^* -D* curve plotted together (Fig. 306 and Fig. 307).

The target displacement is defined as the point in the bilinear Pushover curve that respect equations 142. Contemporarily an inelastic SASD spectra could be defined adopting both equations 138 and 141. It can be seen as the previously defined Target Displacement (TD) point is crossed by the new defined inelastic spectra (blue line in Fig. 306 and Fig. 307).

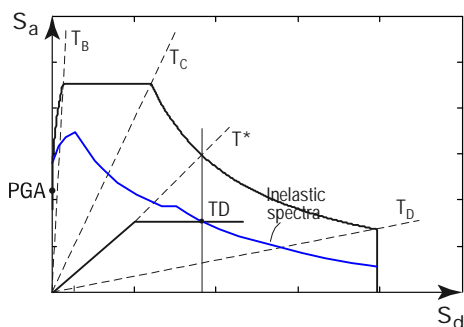


Fig. 306: N2 method; $T^* \geq T_C$

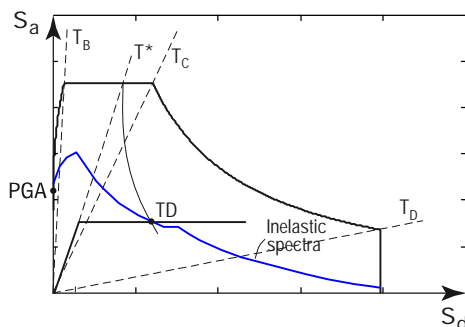


Fig. 307: N2 method; $T^* < T_C$

At this point is possible to compare TD and PP. In N2 design procedure if $PP > TD$, structure should be considered safe with respect to reference seismic input and verification process is considered positive (Bosco et al. (2009)).

Conversely, for the considered analyses a further step is required. Aim of such analysis is found out the maximum allowable PGA acceleration (A_g) to be compared with the reference PGA (a_g).

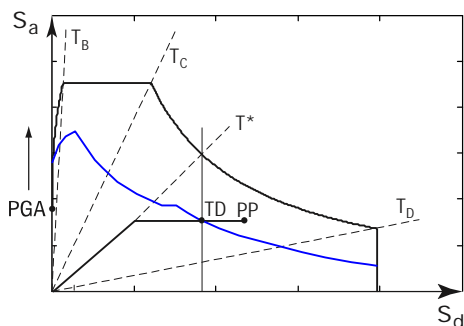


Fig. 308: Iterative procedure ($PP > TD$)

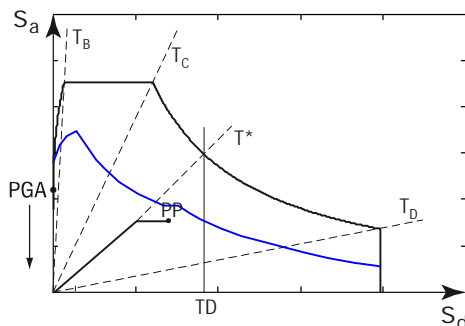


Fig. 309: Iterative procedure ($PP < TD$)

A specific iterative procedure is adopted varying A_g once fixed reference F_0 and T_C^* values, until $PP = TD$ (with an imposed tolerance of 1 ‰). A specific MATLAB subroutine is implemented to perform this task. Some examples of the adopted

iterative procedure are reported in Fig. 310. The goodness of adopted approach is conformed by the plotting of the inelastic spectra, which cross exactly the PP in all considered cases. At this point A_g and reference a_g values can be compared. If $a_g > A_g$ the verification process results positive. Such a procedure is extended to the whole Italian Territory defined by 10751 regularly spaced points. The percentage of positive verification (P_{POS}) compared to the whole points' number is assumed as an estimation about percentage of the Italian Territory (P_{POS}), where such a precast system could be adopted. Seismic vulnerability SV get expressed as the complementary to 100 of this percentage:

$$SV(\%) = 100 - P_{pos}(\%) \tag{143}$$

0 means a fully applicable system; 100 is related to totally unsatisfactory performance. Through a fully automated user defined algorithm implemented in MATLAB, this scoring approach is extended to the all frames' layout introduced in chapter 11.5.1 and to ground categories reported in NTC 2008, namely A to E, in order to get a

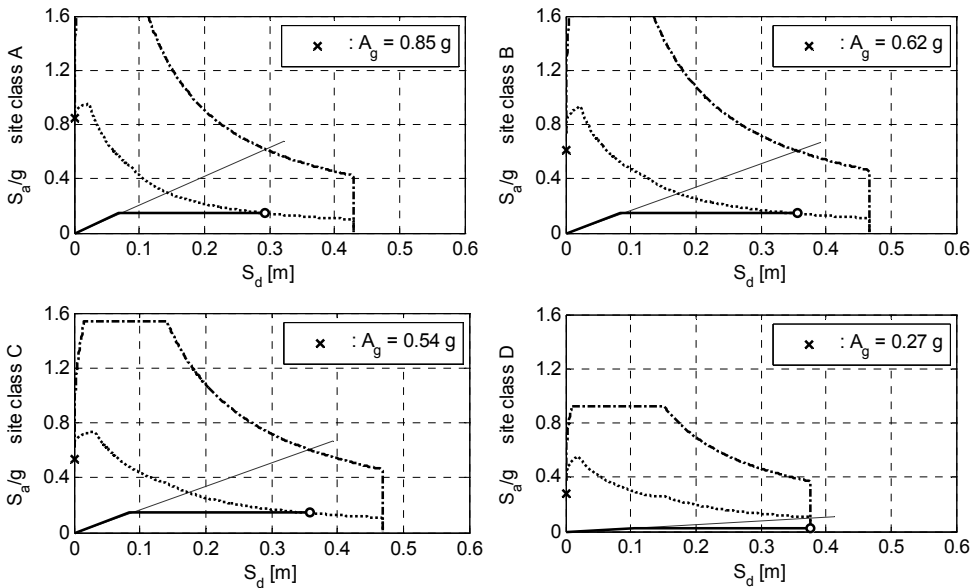


Fig. 310: Some examples of adopted iterative verification procedure

11.6. Seismic analyses results

11.6.1. Layout A frames

In Fig. 311 are reported pushover curves for layout A frames, characterized by 6 meter long bays span and $\phi 18$ lattice girders' longitudinal bars. Number of storeys ranges from 3 to 10 and both triangular and uniform lateral load distributions are considered. Looking at Fig. 314 and Fig. 315 referring respectively to 3 and 10 storey frames, a mixed sidesway plastic hinging mechanism develops before failure, consistent with the one suggested by Code, requiring for columns in the elastic range, with only exception of ground floor column's base. Maximum experienced base shear diminishes as the number of storeys increases, due to increasing bending solicitations. For lower frames, failure is attained due to exceeding of maximum allowable plastic hinge rotation. Whereas, when the number of storeys is greater than 6, failure is due to a rapid degradation of residual strength, as a consequence of bending moments introduced into ground columns by second order effects (Fig. 311). The natural period ranges from 1.5 to 4.5 for the shortest and tallest buildings, respectively (Fig. 312). On the other hand, the ductility factor R (eq. 138) is characterized by an inverse trend: rather high values ($R > 4.5$) are associated with structures lower than 7 storeys, with progressively lower R values for taller buildings, finally reaching $R=2.5$ for a 10 storey structure.

This is related to a less effective plastic hinges' distribution in taller frames, which involves just beams at lower storeys, while the remainder perform elastically (Fig. 315). In Fig. 316 and Fig. 317 the verification process over the whole Italian territory is reported. The grey points represent the maximum allowable seismic input A_g computed for each of 10751 seismic points defined by Code, while the black line reports to the corresponding reference acceleration values a_g (sorted in ascending). Looking at seismic vulnerability parameters plotted in Fig. 318, it appears clear as frames' performance is highly affected by considered storey number and site classes as well. In particular taller frames suffer more than lower ones the seismic input and performance are rather unsatisfactory when site classes D (stiff soil) and E (soft clay soil) are considered.

Analysis and development of an innovative prefabricated beam-to-column joint

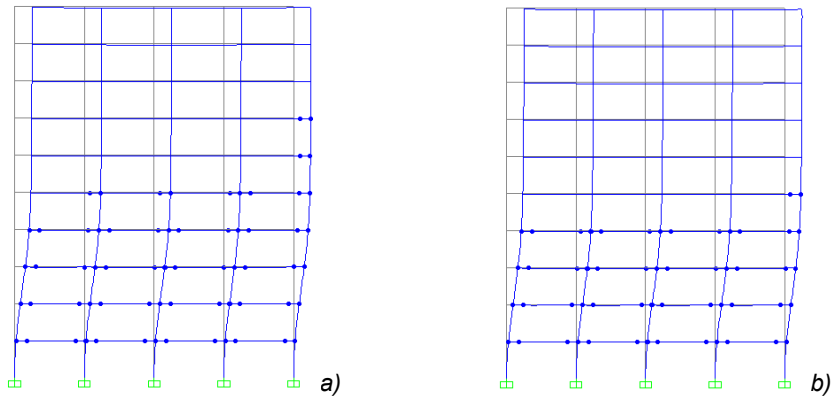


Fig. 315: Plastic hinges on 10-storey type A frame; a) triang. and b) unif. load distribution

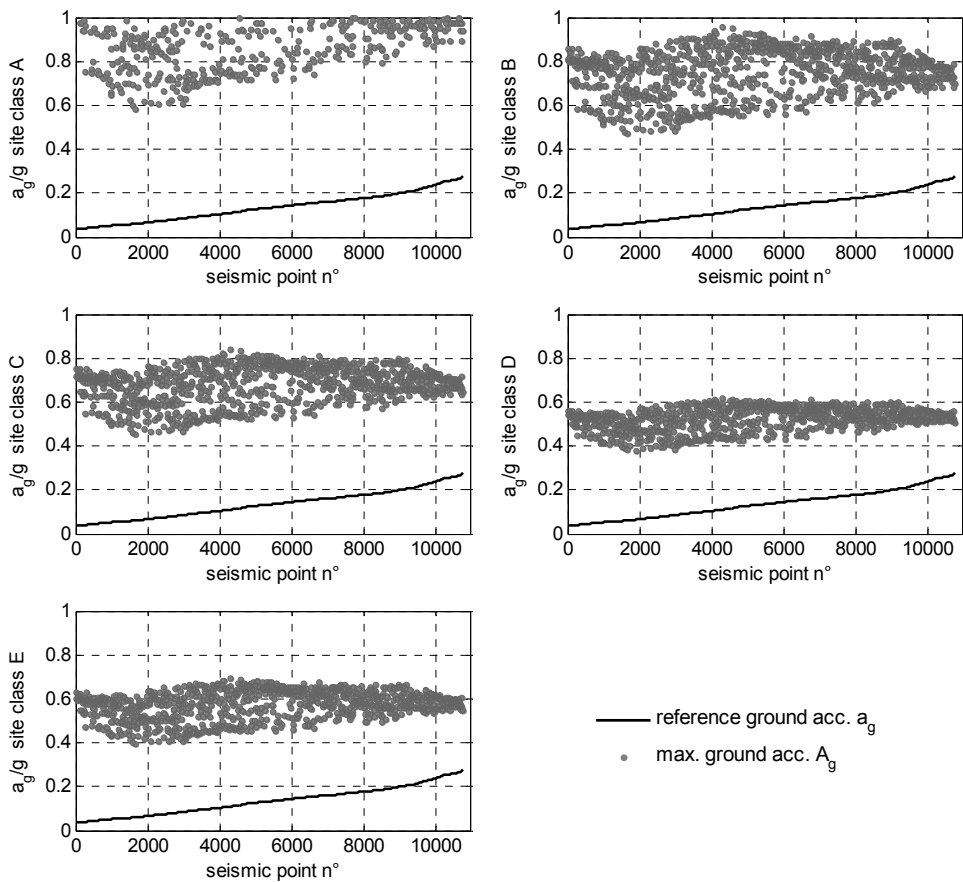


Fig. 316: Seismic verification procedure; 3-storey layout A frame

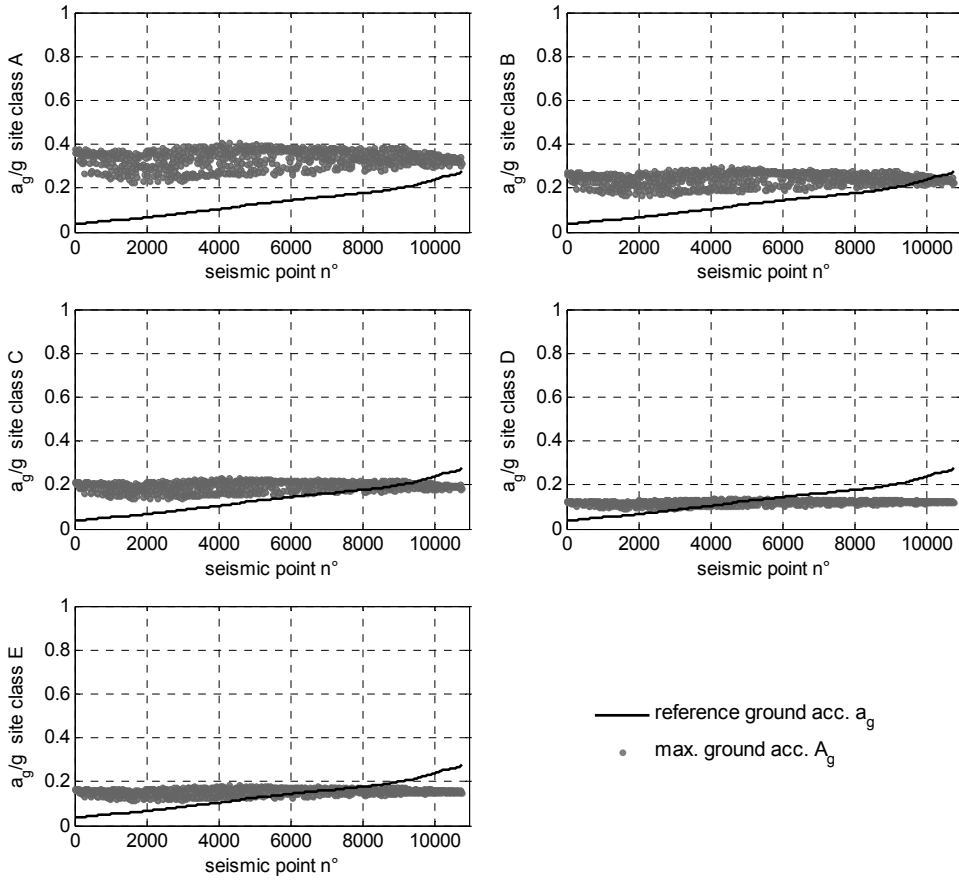


Fig. 317: Seismic verification procedure; 10-storey layout A frame

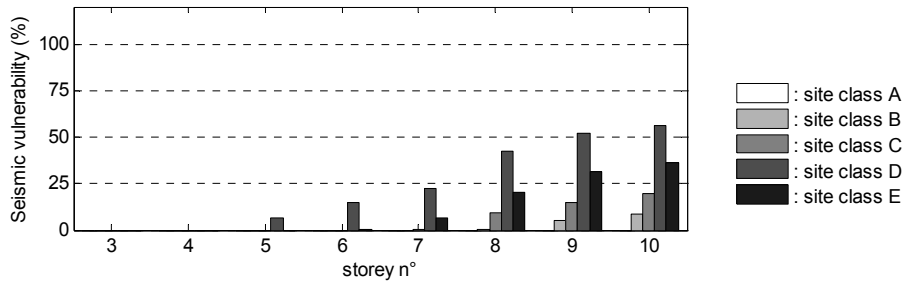


Fig. 318: Seismic vulnerability parameter; layout A frames

11.6.2. Layout B frames

Layout B consists in 3 to 10-storeys frames with 6 meter bays and $\phi 22$ lattice girders' longitudinal bars. Corresponding pushover curves are plotted in Fig. 319. Similarly to analyses for frame layout A, failure is attained due to exceeding of maximum allowable plastic hinge rotation for lower frames. Whereas, when the number of storeys is greater than 6, failure is due to a rapid degradation of global residual strength, mainly due to bending moments introduced into ground columns by second order effects induced by high drift levels. Also frames' natural period remains substantially the same as for frames type A, thank to nearly unchanged vertical members' stieffness (Fig. 322). On the contrary considerably higher base shear is attained due to beams' overstrength provided by higher longitudinal bars diameter. Ductility factor R remains substantially constant, namely $R=3.5$, while the number of storeys ranges between 3 to 8 and it decrease to $R=2.5$ for taller frames (Fig. 323). Generally lower value for ductility factor compared to those relative to frame type A are a consequence of a less effective plastic hinges' distribution, which involves just beams at lower storeys, while the remainder perform elastically (Fig. 321), even when the 3-storey frame is considered (Fig. 320). Nevertheless global seismic performace of frame layout B are sensibly higher, as confirmed by vulnerability parameter (Fig. 318 and Fig. 324). If site classes A/B (rock), C (very dense soil and soft rock) and E (soft clay soil) are considered, the investigated moment resisting precast frames are proper for use on almost 100% of National Territory. Not even a class D site (compact clay) is considered to be a limiting factor with respect to the feasibility of the proposed system, since specific earthquake-resistant components (shear walls, dampers, etc) are necessary in less than 10% and 30% of the Nation's territory, respectively, when considering structures of less than or greater than 9 floors. This indicate how important is the proper choice of ductility factor and corresponding reinforcement arrangement to maximize performance of the considered structures.

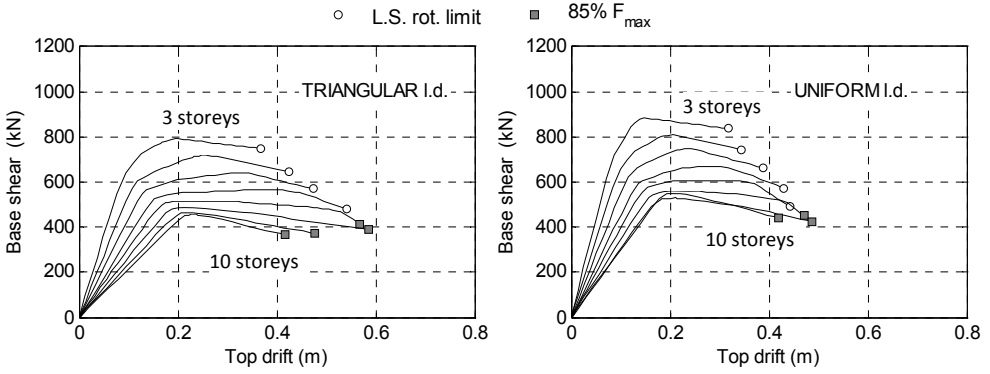


Fig. 319: Pushover curves; layout B frames

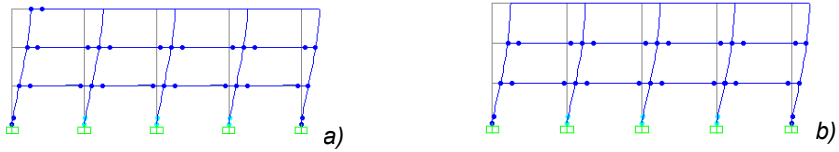


Fig. 320: Plastic hinges on 3-storey type B frame; a) triang. and b) unif. load distribution

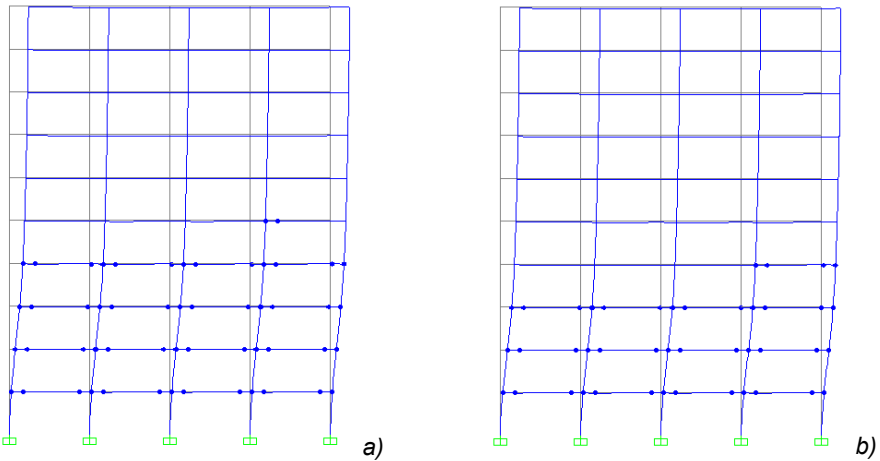


Fig. 321: Plastic hinges on 10-storey type B frame; a) triang. and b) unif. load distribution

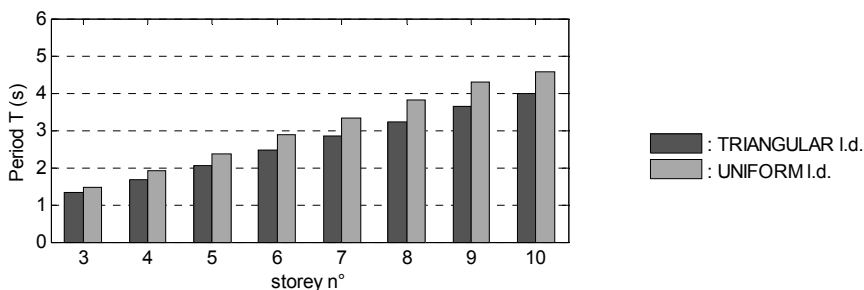


Fig. 322: Natural period; layout B frames

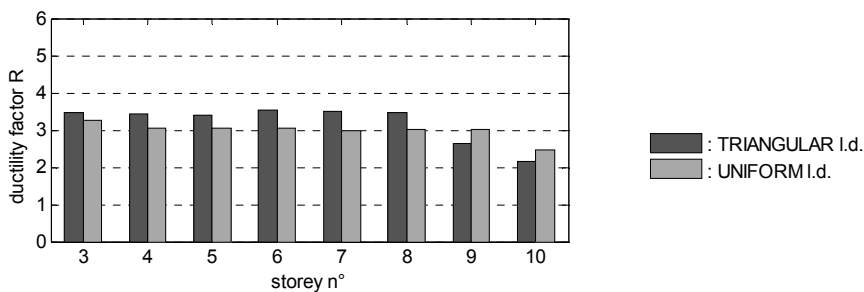


Fig. 323: Ductility factor; layout B frames

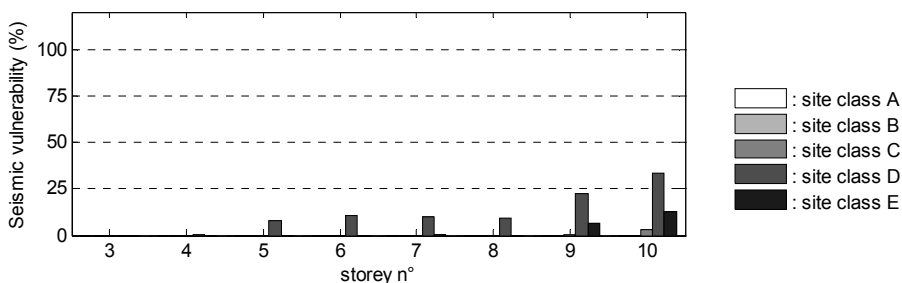


Fig. 324: Seismic vulnerability parameter; layout B frames

11.6.3. Layout C frames

Layout C frames consists in 3 to 8-storeys, bays span 8 meters long and $\phi 24$ lattice girders' bars. Corresponding pushover curves are plotted in Fig. 325.

The wider bays span compared to type A and B frames cause a higher axial load acting on ground columns considering the same number of storeys, thus favouring a less ductile response of those columns and consequently of the whole structure, testified by a ductility factor around 2 independtly from number of storeys (Fig. 329).

Base shear attains levels comparable to those of layout B frames although the equivalent SDOF base shear is sensibly lower due to the larger amount of seismic participating mass. This latter contributes to a 0.5-1 second upward shifting of natural periods (Fig. 328) compared to those of layout B frames, despite higher axial loads and consequently higher stiffness on columns. Performance of layout C frames are resumed in Fig. 330 through the corresponding vulnerability parameter expressed as a function of number of storeys and site classes. If class A/B (rock), C (very dense soil and soft rock) and E (soft clay soil) sites are considered, the investigated earthquake resisting precast frames are proper for use over almost 100% of Italian territory. They are feasible also on more than 90% and 75% of the territory when, respectively, class sites E (soft soil) and D are considered, with exception of slightly worst performance for frames with a number of storeys equal to 4 and 5. In this case lower frames tend to perform slightly worst than taller ones as a consequence of their higher stiffness.

Overall satisfactory performance of layout C frame, comparable to those of layout B frame, are a proof of the fact that limited ductility factor's values do not entail limited feasibility of proposed precast technology.

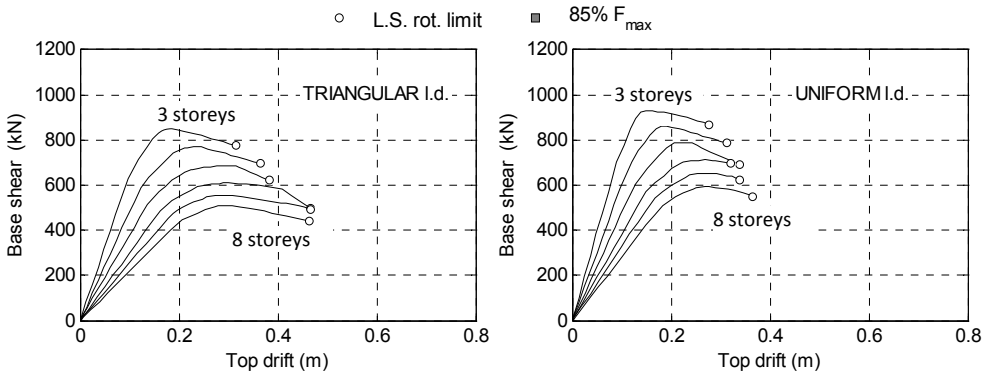


Fig. 325: Pushover curves; layout C frames

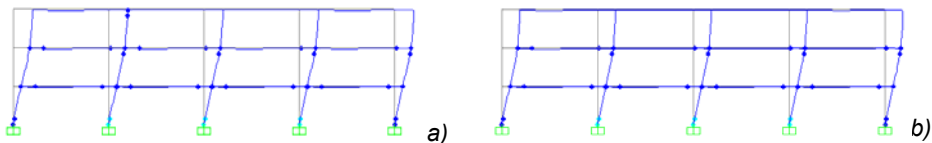


Fig. 326: Plastic hinges on 3-storey type C frame; a) triang. and b) unif. load distribution

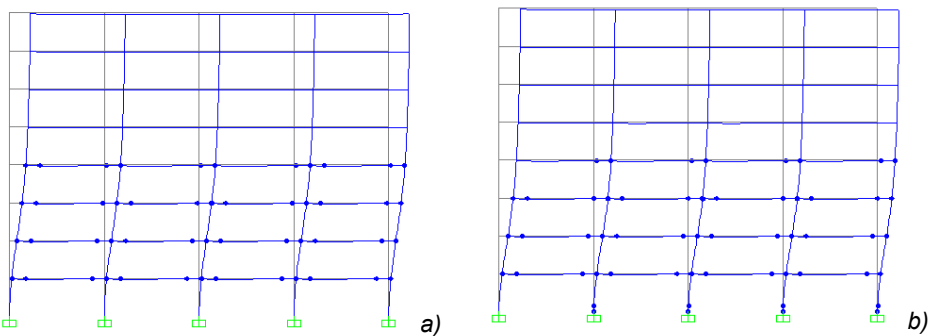


Fig. 327: Plastic hinges on 8-storey type C frame; a) triang. and b) unif. load distribution

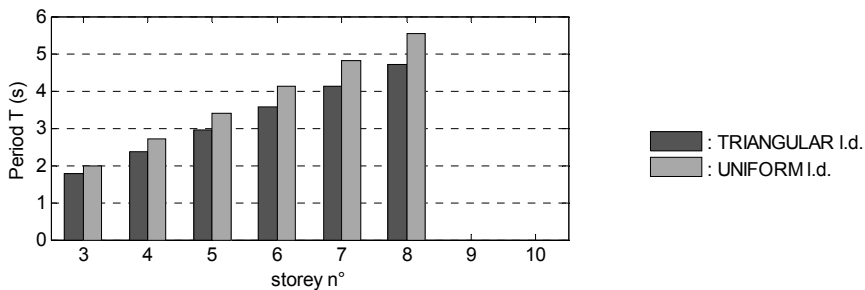


Fig. 328: Natural period; layout C frames

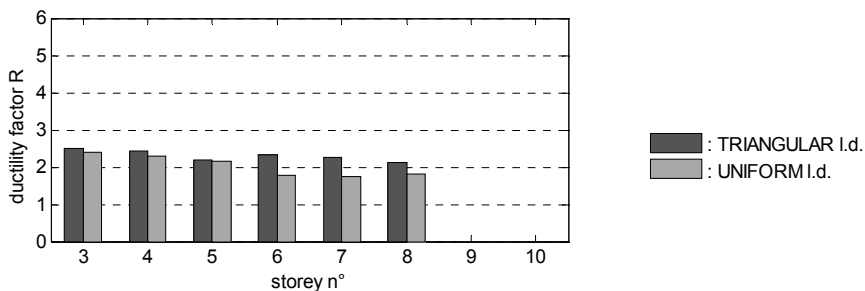


Fig. 329: Ductility factor; layout C frames

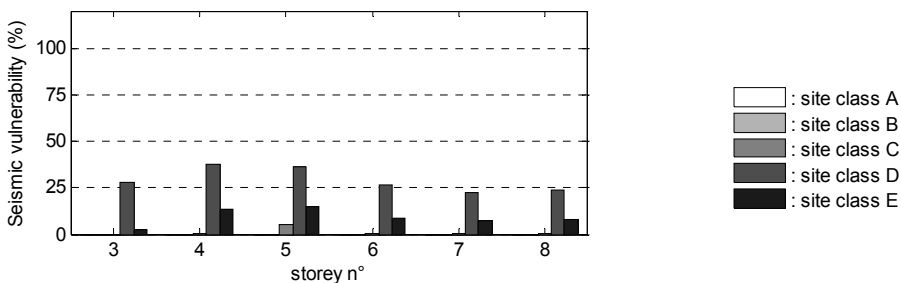


Fig. 330: Seismic vulnerability parameter; layout C frames

11.6.4. Layout D frames

Layout D consists of 3 to 8- storey frames, characterized by 8-meters-long bays span and $\phi 28$ lattice girders' longitudinal rebars, these latter corresponding to an overdesign of almost 100kNm compared to layout C frames (cf.ch.11.5.1)

Observing push-over curves plotted in Fig. 331, the response is nearly elastic with a limited plastic branch for all considered frames, mainly due to two complementary reasons. Firstly, the higher axial loads acting on ground columns of frames with 8-meters-long bays span compared to those with 6-meters-long bays span, favouring a less ductile response of those columns. Secondly, the beams' overstrength, that limits consistly the plastic hinging development, confinign it on lower storeys beams. As a consequence attained base shear is even higher than those retrieved from layout C frames and a premature base columns' failure take place at limited top drift levels, affecting sensibly the ductility factor R , the latter decreasing progressively from 2 to 1.5 from the 3 to the 8-storey frame (Fig. 335), the lowest values among different frames' layout. This has an unfavourable impact on global seismic performance of layout D frames, in particular with reference to class D (stiff soil) sites, unfeasible over 30% to nearly 50% of National territory, depending on considered number of storeys. This suggests as a certain minimum ductility level should always be guarantee to exploit maximum performances of considered frames.

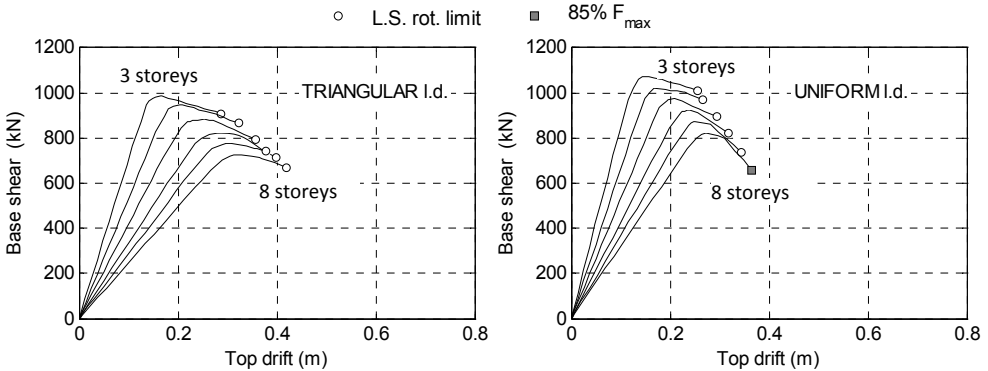


Fig. 331: Pushover curves; layout D frames

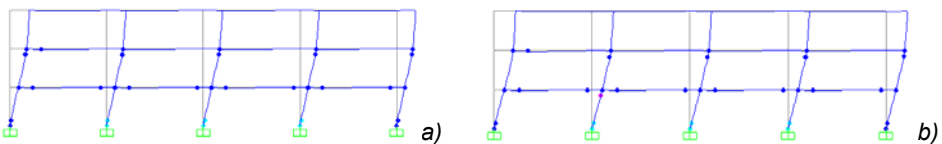


Fig. 332: Plastic hinges on 3-storey type D frame; a) triang. and b) unif. load distribution

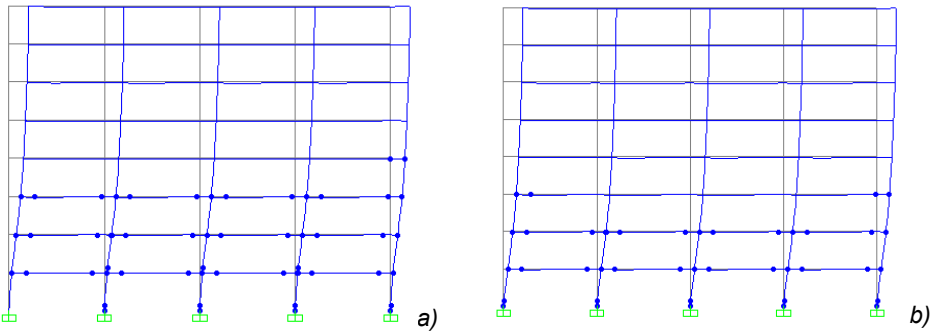


Fig. 333: Plastic hinges on 8-storey type D frame; a) triang. and b) unif. load distribution

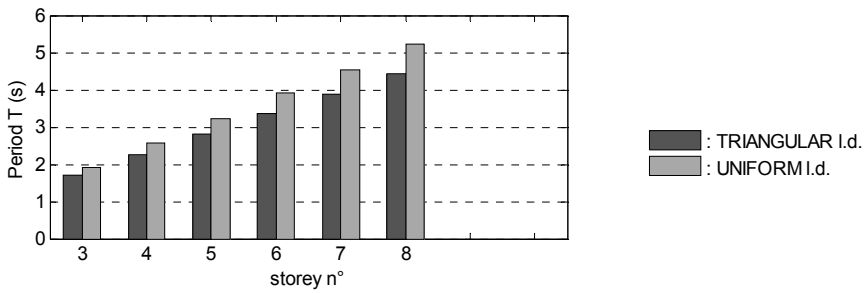


Fig. 334: Fundamental period; layout D frames

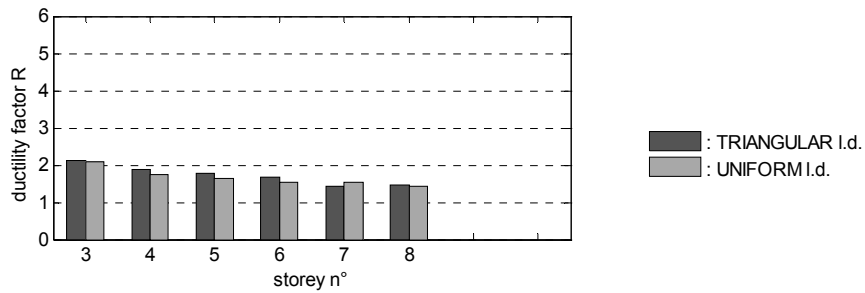


Fig. 335: Ductility factor; layout D frames

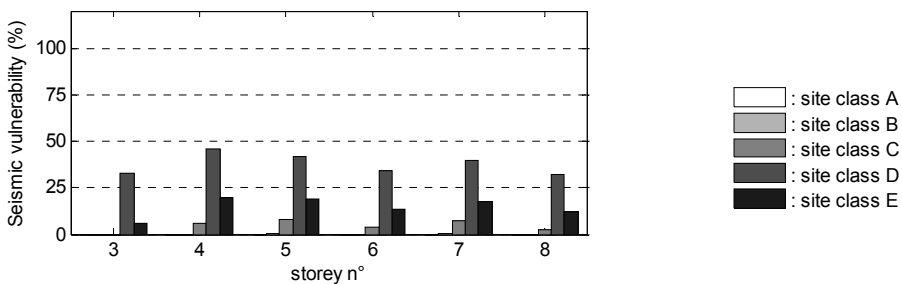


Fig. 336: Seismic vulnerability parameter; layout C frames

11.7. Reduction factor identification

The reduction factor R is the parameter adopted for a force-based seismic design method to define the member's solicitations as a fraction of the one computed by linear elastic analyses.

$$R = R_{\mu} R_s \quad (144)$$

R_{μ} is the *ductility dependent reduction factor*, or simply *ductility factor*, defined as the ratio of elastic strength demand to inelastic strength demand F_y , adopting equation 138.

R_s is the *overstrength factor*, defined as the ratio of the actual strength (inelastic strength demand) to design strength (Fajfar, 1996). R_s could be reasonably assumed as 1.2.

In equation 145 is reported the reduction factor formulation adopted by EN 1998-1:2005 and NTC 2008 for RC equivalent monolithic precast frames considering low ductility design. It is recalled that high ductility design is not fulfilled by presented precast technology, due to columns' lateral reinforcement limitations (cf. ch.12.4.2).

$$R = 3\alpha_1 / \alpha_u \quad (145)$$

where α_1/α_u overstrength factor between first plastic hinge opening and attainment of a sufficient plastic hinge number to get global structural instability

α_1/α_u is taken equal to 1.3 for multi-column multi-spans frames, leading to a ductility factor $R=4$. Looking at analyses commented in chapter 11.6, best seismic performance expressed in term of vulnerability parameter correspond to layout B and C frames, when considering respectively 6 and 8-meters-long bays span. Corresponding R_{μ} factors are listed below:

- $R_{\mu}=3.0$ 6-meters-long bays span, 3 to 7-storey frame;
- $R_{\mu}=2.5$ 6-meters-long bays span, 8 to 10-storey frame;
- $R_{\mu}=2.0$ 8-meters-long bays span, 3 to 8-storey frame.

Considering an overstrength factor $R_s=1.2$ following reduction factors should be adopted (cf. eq.144):

- $R_{\mu}=3.5$ 6-meters-long bays span, 3 to 7-storey frame;
- $R_{\mu}=3.0$ 6-meters-long bays span, 8 to 10-storey frame;
- $R_{\mu}=2.5$ 8-meters-long bays span, 3 to 8-storey frame.

Such values are lower than those reported by Codes for equivalent monolithic precast frames, but should be taken as a safe reference on the basis of conducted non-linear analyses.

11.8. Conclusions

This chapter reports an essay about the possibility to adopt proposed precast technology for moment resisting frames in seismic areas. A specific vulnerability parameter is introduced, which allows to express the performance of structure, not in terms of maximum allowable ground acceleration, but like percentage of the National territory where those frames are able to withstand Code-reference seismic events, with a return period equal to 475 years, considering different ground categories, ranging from A (rock) to E (soft clay). Non linear response of precast structure is expressed in term of pushover curves got from numerical models of regular plain frames implemented in SAP2000, with different number of storeys, beams' reinforcement arrangement and bays span, the latter 6 and 8-meters long, for a total of four frames' layout, identified as A, B, C, D. Analyses allowed to identify the proper ductility factor and corresponding reinforcement arrangement, able to exploit maximum seismic performance of considered structures. In particular to favor a high-ductility response (cf. layout A) or conversely to favor a nearly linear response through beams' overdesign (cf. layout D), leads to a rather unsatisfactory response, in particular when site classes D and E and taller frames are considered. Proper ductility factors R_{μ} are identified with reference to frame-layouts B and C. Corresponding reduction factors R should be taken as 3 to 3.5 and 2.5 when dealing with frame with bays span respectively 6 and 8-meters-long. It should be noticed as these factors are lower than those suggested by Code, mainly owing to adoption of HSC for column, subjected to a less ductile response than ordinary NSC columns.

Best performance are retrieved with reference to frame-layout B. If site classes A/B (rock), C (very dense soil and soft rock) and E (soft clay soil) are considered, the investigated moment resisting precast frames are proper for use on almost 100% of National Territory. Not even a class D site (compact clay) is considered to be a limiting soil category with respect to the feasibility of the proposed system, since specific earthquake-resistant components (shear walls, dampers, etc) are necessary in less than 10% and 30% of the Nation's territory, respectively, when considering structures of less than or greater than 9 floors.

Referring to frame-layout C, if class A/B (rock), C (very dense soil and soft rock) and E (soft clay soil) sites are considered, the investigated earthquake resisting precast frames are proper for use over almost 100% of Italian territory. They are feasible also on more than 90% and 75% of the territory when, respectively, class E (soft soil) and D sites are considered. Overall satisfactory performance of layout C frame, comparable to those of layout B frame, are a proof of the fact that limited ductility factor's values do not entail limited feasibility of proposed precast technology.

12. PRACTICAL DESIGN PROVISIONS

12.1. Introduction

In this chapter are reported some practical design formulations for the proposed precast solution, based on results obtained from previous analyses and referring to Codes' provisions reported by ACI 318-08 (ACI Committee 318, 2008), Eurocodes (European Committee for Standardization, 2005a) and Italian NTC 2008 (Ministero delle Infrastrutture, 2008).

Bending and brittle shear failure mechanisms are considered, both for static and seismic design conditions. Furthermore attention is paid on reinforcement detailing to provide adequate confinement to concrete sections.

Design formulations for the following joint's components are considered:

- Continuity lattice girder
- CSCT beam
- HSC column
- Bolted connection
- Core joint

At the end of this chapter a new joint layout is proposed, which is an update of the previous one. It keep advantages of the original solution (Mazzarolo et al., 2010, cf. ch.2), with specific reinforcement detailing to enhance core-joint confinement, especially for exterior joints, where action provided by floor slabs is limited.

With these improvements the proposed joint comply with considered Codes' provisions, thus removing any limitation for use also in high-seismicity regions.

12.2. Continuity lattice girder design

12.2.1. Design for bending

Lattice girder represents a fundamental component of the proposed composite joint, since it restores beams' continuity through the core-joint, after the in-site concrete casting. In this phase the resisting mechanisms should be associated to those of an equivalent CSTC beam. In 2009 the Italian Superior Council of Public Works released specific provisions to settle the issue about CSTC beam design and stated that reference should be done to steel-concrete composite beam design provisions (Consiglio Superiore dei Lavori Pubblici, 2009). According to EN 1994-1-1:2005 and NTC 2008, it is possible to compute the design bending strength of a composite beam by rigid-plastic theory only if the composite cross-section is in Class 1 or in Class 2. Such an approach can be adopted for CSTC beam since the compressed steel section belongs to Class 1. Still according to EN 1994-1-1:2005 the tensile strength of concrete shall be neglected. The plastic bending strength of the composite cross-section can be computed assuming the following hypotheses: full interaction between steel truss and concrete; the steel truss chord area is stressed to its design yield strength in tension or in compression; the effective area of concrete in compression resists a stress of 85% of its design cylinder strength f_{cd} , constant over the whole depth between the neutral axis and the most compressed fibre of concrete. It may be assumed that there is full interaction between truss and concrete and the composite cross-section remains plane if the shear connection is designed in accordance to the same Eurocode's provisions (cf. ch.12.2.3).

The ultimate limit state is defined in terms of maximum and minimum strains, i.e. it is equal to -3.5‰ for the compressive concrete and to +10‰ for the tensile steel, even if higher limit could be assumed, being a structural steel S355 adopted for lattice components.

Following formulations for computing plastic resistance moment for CSTC beams are derived from equivalent stress-block approach for RC sections:

$$\xi = f_{yd} \cdot \left(\sum_{i=1}^n A_s^i \right) / (0.85 \cdot f_{cd} \cdot b) \quad 146)$$

where ξ =neutral axis depth

$$M_{pl,Rd} = \sum_{i=1}^n f_{yd} \cdot A_s^i \cdot (d^i - \xi / 2) \approx \sum_{i=1}^n f_{yd} \cdot A_s^i \cdot 0.9 \cdot d^i \quad 147)$$

Considering $\phi 28$ longitudinal rebars, following reference hogging and sagging bending strength can be estimated as:

$$M_{Rd}^{(-)} = \frac{28^2 \pi}{4} \cdot 4 \cdot \frac{355}{1.05} \cdot 0.9 \cdot (360 + 170) \approx 400 \text{ kNm} \quad 148)$$

$$M_{Rd}^{(+)} = \frac{28^2 \pi}{4} \cdot 4 \cdot \frac{355}{1.05} \cdot 0.9 \cdot (200) \approx 150 \text{ kNm} \quad 149)$$

Alternatively to the above reported approach, also elastic analysis and non-linear theory may be adopted. In the latter case suitable non-linear materials' relationships should be considered (cf. ch.4) together with a proper iterative subroutine to get the full response of section (cf. ch.9.3.1)

12.2.2. Design for shear

The determination of the shear resistance provided by lattice-concrete composite beam has to take account of many structural differences compared with a classical composite steel and concrete section. EN 1994-1:2005 reports that the plastic shear resistance of a composite-beam should be taken equal to that provided by bare web steel section unless the value for the contribution from the reinforced concrete part of the beam has been established. In the case of the lattice-concrete composite beam some preliminary considerations can be drawn. The first important aspect is that, being the structural steel part a truss without solid web, its shear stiffness is lower than a typical composite beam's one. In addition, the shear stiffness of a solid web concrete section of the same depth is higher before the cracking occurs. Therefore it can be expected that the first shear resistant mechanism of the beam deals mainly with the concrete section. Reference should be done to equation 164.

After the tensile concrete strength is reached the steel lattice can provide resistance for the tensile stresses. The fact that the truss diagonal bars are not homogeneously distributed, but rather disposed with a certain step, suggests that a Ritter-Mörsch shear mechanism can be established after the concrete cracking. Referring to this static scheme a new composite truss can be considered in which: the truss bottom chord can maintain its role, the top chord is composed by the concrete section and the steel top bars, the diagonal members are alternated in tension and in compression and are respectively constituted by only steel bars or by composite steel bars and concrete. Hence it's important to notice that the diagonal

bars that can absorb the tensile stresses are only those orthogonal to the cracks and not both of the truss diagonal bars. To estimate shear strength both contributes should be estimated, namely the one provided by concrete struts (eq. 150) and steel ties (eq. 151). Both formulations are taken from EN 1992-1-1:2005. Being the two strength contributes acting in series, the global shear strength is ruled by the lowest one (eq. 152).

$$V_{Rsd} = 0.9 \cdot d \cdot \frac{A_{sw}}{s} \cdot f_{yd} \cdot (\text{ctg} \alpha + \text{ctg} \theta) \cdot \sin \alpha \quad 150)$$

$$V_{Rcd} = 0.9 \cdot d \cdot b_w \cdot f_{cd} \cdot (\text{ctg} \alpha + \text{ctg} \theta) / (1 + \text{ctg}^2 \theta) \quad 151)$$

$$V_{Rd} = \min(V_{Rcd}, V_{Rsd}) \quad 152)$$

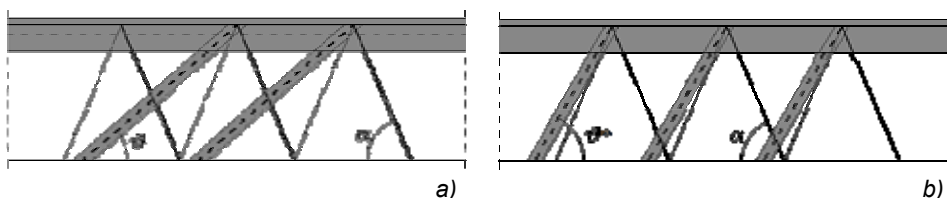


Fig. 337: Alternative Ritter-Mörsch shear resistant mechanism proposed by Colajanni et al., 2011: a) "Model 1" mechanism; b) "Model 2" mechanism

Different angles for inclined struts may be assumed. EN 1992-1-1:2005 provides the following limitation:

$$1 \leq \text{cotg} \theta \leq 2.5 \quad 153)$$

Colajanni et al., 2011 introduce a further limitation for the steel ties inclination:

$$\text{cotg} \alpha \leq \text{cotg} \theta \quad 154)$$

Depending on the value assumed for the angle θ , different Mörsch-Ritter mechanism may be assumed (Fig. 337), corresponding to different shear strength. To get an estimation about this angle, reference should be done to numerical analyses reported in chapter 5. Looking in particular on contours plotted in Fig. 197 and Fig. 201, shear strength mechanism identified as "model 2" (Fig. 337b) by Colajanni et al., 2011, appears to be the closest to numerical evidences. Based on these evidences, values of 45° and 60° , respectively for α and θ are assumed.

Assuming a $\phi 20$ web truss diameter, the shear strength provided by lattice girders is equal to:

$$V_{Rsd} = 0.9 \cdot 200 \cdot \frac{2 \cdot 20^2 \cdot \pi / 4}{180} \cdot \frac{355}{1.05} \cdot (\text{ctg}60 + \text{ctg}45) \cdot \sin 60 = 200kN \quad 155)$$

$$V_{Rcd} = 0.9 \cdot 200 \cdot 500 \cdot \frac{0.85 \cdot 30}{1.5} \cdot (\text{ctg}60 + \text{ctg}45) / (1 + \text{ctg}^2 45) = 1200kN \quad 156)$$

$$V_{Rd} = \min(V_{Rcd}, V_{Rsd}) = 200kN \quad 157)$$

The reference shear seismic overdemand solicitation should be computed with reference to bending strength in equations 148 and 149, adopting formulation in EN 1998-1:2005 to avoid brittle beam failure due to shear (eq. 158). Reference is made to a 6-meters-long bays span.

$$V_{Sd} = \gamma_{Rd} (M_{Rd}^{(+)} + M_{Rd}^{(-)}) / \ell = 1.2 \cdot (400 + 150) / 6 = 130kN \quad 158)$$

Comparing equations 157 and 158 it can be stated that adequate shear strength is provided adopting a $\phi 20$ web truss diameter.

12.2.3. Shear-connection design

Being the through-joint continuity beam compared to an equivalent composite beam section, according to the EN 1004-1:2005 adequate stiffness and strength should be provided by shear-connector to restore full-interaction between concrete and steel, ignoring the effect of natural bond-slip between the two (plain rebars are adopted). In other words shear connectors shall be capable of preventing separation of the concrete element from the steel element, assuring this way the validity of plane-section hypothesis. In the case of the CSTC beams the diagonal trusses are the connectors between the longitudinal rebars and the concrete web. The number of inclined web trusses should be at least equal to the total design shear force for the ultimate limit state (eq. 158), divided by the design resistance of a single connector. Several experimental tests investigated this aspect (Puhali & Smotlack, 1980; Tullini et al., 2006; Aiello, 2008; Badalamenti et al., 2008; Aiello et al., 2009). Colajanni et al., 2011 also suggest specific analytical formulations to be

adopted for design, even if scatter of results compared with experimental ones appears still appreciable.

In chapter 5 a conservative approach is adopted to resolve this issue. It is assumed that adequate interaction between steel and concrete is assured if during lattice's pull-out tests, the yielding limit get at least attained. Based on numerical results, provisions reported in equation 71 are proposed to define the shape of the lattice girder geometry. Such an approach could be considered for future updating of the code provisions.

Base on proposed formulations, 4 triangular meshes should be at least adopted at each joint side, together with $\phi 20$ inclined truss diameter, even considering $\phi 28$ longitudinal rebars.

Looking at these limitations, problems arise with reference to outer joints, for whom core-joint depth is not long enough to contain a sufficient number of triangular meshes. In this case it is suggested that a specific plate be welded at the end of the longitudinal rebars (Fig. 341) to increase interaction between truss and concrete, through bearing action of the steel plate embedded in concrete. Such a solution take inspiration from DDB technology developed by Englekirk, 2002 (cf. ch.1.5.3).

12.3. CSTC beam design

The CSTC beam has to possess adequate performances before and after the hardening of the in place concrete cast. This moment distinguishes two phases (or stages) in the life of the beam that are characterized by distinct resistant sections and different mechanics. During the first phase the beam behaves as a prefabricated steel truss that works in a simple supported static scheme. The loads are usually its own weight, the weight of the slab and the weight of the concrete cast. Concrete contribute should be disregarded in tension and so the mere steel truss result effective in bearing load. The limiting factor in this phase is related to possible buckling of the compressed steel reinforcement in the middle beam span. This is also influenced by the possibility to develop hinging at truss node, due to eccentricities related to bending of the inclined truss (Tesser, 2009).

During the second phase the previous truss collaborates with the hardened concrete, defining the classical CSCT beam section layout. Formulations reported in chapter 12.2 fro lattice-concrete composite section, may be used for design of such component.

12.4. HSC column axial and bending strength

12.4.1. Flexural strength for seismic design

The Codes recommend expressions to preclude formation of plastic hinges in columns. Such expressions aim essentially at providing oversized columns with flexural strength more than the one provided beams, obtained considering over-strength factors. In this way the beam's sidesway mechanism for beams is guaranteed and the column's sidesway one is prevented, together with the possibility of weak storey failure type.

ACI 318-08 recommends that the sum of the nominal flexural strengths of the column sections above and below the joint should not be less than 1.2 times the nominal flexural strength of the beam sections at the joint faces.

$$\sum M_C^{Rd} \geq 1.2 \sum M_B^{Rd} \quad 159)$$

where M_C^{Rd} = nominal flexural strength of column; M_B^{Rd} = nominal flexural strength of beam

EN1998-1:2005 suggests the following condition to be satisfied at all joints:

$$\sum M_C^{Rd} \geq 1.3 \sum M_B^{Rd} \quad 160)$$

NTC 2008 allows to consider a less conservative over-strength for low ductility class building:

$$\sum M_C^{Rd} \geq 1.1 \sum M_B^{Rd} \quad 161)$$

Reference beams' strength is provided by equations 148 and 149, which account for $\phi 28$ longitudinal rebars. The amplified nominal flexural strength provided by beams (right side into equation 160) is equal to 585 kNm.

The maximum columns' flexural strength is derived by strength domain in Fig. 261 amplified by two, to account for upper and lower column (assuming the same $\phi 30$ longitudinal reinforcement). The maximum axial load experimented by frames under seismic analyses never exceed 4000kN. In Fig. 338a, the so defined flexural strength provided by beams and columns convergent to the same node are plotted together. It should be noticed as equation 160 is always fulfilled, with exception of axial loads lower than 500kN. It means that for upper storeys, lower diameter for

longitudinal rebars should be adopted. Just considering $\phi 26$ rebars' diameter equation 160 is respected over the whole reference axial load range (Fig. 338b).

These results are consistent with pushover analyses in chapter 11, characterized by a beam sideway mechanism for all the considered frames (see Fig. 314, Fig. 315, Fig. 320, Fig. 321, Fig. 326, Fig. 327, Fig. 332 and Fig. 333).

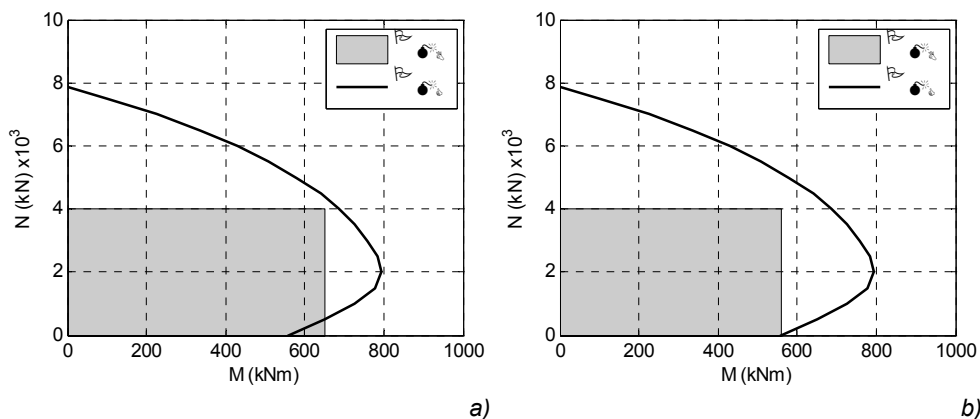


Fig. 338: Comparison between flexural strength provided by beam and column convergent at the same node; a) $\phi 28$ lattice; b) $\phi 26$ lattice

12.4.2. Shear strength design and minimum confinement

To assure a global ductile behaviour under seismic action to frame structures, the codes recommend expressions to preclude brittle shear failure in columns

Shear forces to be considered for design are derived by column's equilibrium conditions, considering nominal flexural strength provided by column, amplified by an overstrength factor

$$V_{Sd} = \gamma_{Rd} \cdot \frac{M_{Rd}^L + M_{Rd}^U}{l_c} \tag{162}$$

where γ_{Rd} =over-strength factor (=1.1); M_{Rd}^L =nominal flexural strength of lower column's end; M_{Rd}^U =nominal flexural strength of upper column's end; l_c =column length.

The nominal flexural strength is a function of the considered axial load level. Under the hypothesis that the same reinforcement is adopted at both column's ends, equation 162 may be written as:

$$V_{Sd}(N) = 1.1 \cdot 2M_{Rd}(N) / l_c \tag{163}$$

Estimated value for V_{Sd} at axial load levels ranging between 0 to 6000kN are reported in Table 26.

To estimate the column shear strength V_{Rd1} , reference is made to formulation reported in NTC2008 and analogous one in EN 1992-1-1:2005.

First of all, the shear strength V_{Rd1} for members without lateral reinforcement is considered.

$$\begin{aligned} V_{Rd1} &= (0.18 \cdot k \cdot (100 \cdot \rho_l \cdot f_{ck})^{1/3} / \gamma_c + 0.15 \sigma_{cp}) b_w d \\ k &= 1 + (200 / d)^{1/2} \leq 2 \\ \rho_l &= A_{sl} / (b_w \cdot d) \leq 0.02 \\ \sigma_{cp} &= N_{Ed} / A_c \end{aligned} \quad 164)$$

where d =column section height from rebar to compressed edge (280 mm); b_w =minimum section width (220 mm, see Fig. 288); ρ_l =longitudinal reinforcement ratio; σ_{cp} =average compression stress; N_{Ed} =considered axial load; A_c = section area (158000mm²); f_{ck} =concrete characteristic strength (should be further multiplied by $\alpha=0.85$ and $\eta=0.875$)

Secondly is reported the expression for calculating the shear strength V_{Rd2} of laterally reinforced members:

$$V_{Rd2} = 0.9 \cdot d \cdot A_{sw} / s \cdot f_{yd} \cdot (\text{ctg} \alpha + \text{ctg} \theta) \cdot \sin \alpha \quad 165)$$

where d =column section height from rebar to compressed edge (280 mm); A_{sw} =lateral reinforcement area; s =stirrups span; θ =shear crack inclination (assumed as 30°); α =lateral reinforcement inclination ($\approx 90^\circ$)

Finally a further expression is reported in EN 1998-3:2005, with reference to seismic shear strength V_{Rd3} under cyclic loading:

$$V_{Rd,3} = \frac{1}{\gamma_{el}} \left[\frac{h-x}{2L_v} \min(N; 0.55 A_c f_{cd}) + (1 - 0.05 \min(5; \mu^{pl})) \cdot \left[0.16 \max(0.5; 100 \rho_{tot}) \left(1 - 0.16 \min\left(5; \frac{L_v}{h}\right) \right) \sqrt{f_{cd}} A_c + V_{wd} \right] \right] \quad 166)$$

where γ_{el} =global safety factor (1.15); h = is the depth of cross-section (330 mm); x = is the compression zone depth (see Table 25); N =compressive axial force; A_c = $b_w d$ (220 by 280 mm); L_v =shear length, assumed half column length (1600mm); ρ_{tot} = is the total longitudinal reinforcement ratio; μ_{pl} = ductility factor of the transverse deflection of the shear span or of the chord rotation at member end: $\mu_{pl} = \mu - 1 = 3$ (cf. Fig. 292); f_{cd} =concrete design strength (37MPa); V_{wd} = shear strength provided by lateral reinforcement (corresponding to V_{Rd2})

N(kN)	x/h
0	1/4
2000	1/2
4000	3/4
6000	1

Table 25: Approximated compression zone depth

In the following table, results of such calculations are reported for different lateral reinforcement arrangement: $\phi 6/60$, $\phi 6/40$, $\phi 8/60$

Values in kN		$\phi 6/60$		$\phi 6/40$		$\phi 8/60$		
N	V_{Sd}	V_{Rd1}	V_{Rd2}	V_{Rd3}	V_{Rd2}	V_{Rd3}	V_{Rd2}	V_{Rd3}
0	192	65	156	163	240	236	285	275
2000	275	181	156	325	240	366	285	435
4000	240	298	156	342	240	415	285	454
6000	138	416	156	521	240	594	285	633

Table 26: Calculated column shear with different formulations and reinforcement layout (grey cells means not adequate strength)

Looking at results reported in Table 26, two main evidences appear clear. Firstly when sufficient axial load is provided, no lateral reinforcement appears necessary. Secondly, formulation reported in EN 1992-1-1:2005 and NTC 2008 result more strict than the one reported in EN 1998-3:2005. This could be justified looking at the fact that this latter is addressed to verification of existing buildings.

To attain adequate shear strength at different axial load levels, higher amount of lateral reinforcement should be considered, than the one provided by original solution consisting in $\phi 6/60$ stirrups. Among the two investigated alternatives, namely $\phi 6/40$ and $\phi 8/60$, the latter one appear to be the most favorable choice.

12.4.3. Lateral reinforcement to provide confinement

Beside adequate lateral reinforcement to withstand shear forces, codes requires strict reinforcement's geometrical limitations to provide adequate concrete confinement. Making reference to NTC2008 such restrictions should be considered only in the dissipation zones (i.e. plastic hinges) when a low ductility design is chosen (Class Ductility "B" design). In a typical frame structure, a beam sidesway mechanism is usually adopted for seismic design: plastic hinges take place at

beams' ends, while columns remain elastic, to avoid soft-storey failures. Just columns' base at ground level may be subjected to plasticization, without reducing global structure stability and safety.

Higher amount of lateral steel should then be provided just for base column. This issue is investigated in chapter 11.4.2. It results that lateral reinforcement constituted by $\phi 12/40$ stirrups should be adopted in the columns' plastic hinge region.

12.5. Bolted connection

12.5.1. Bending strength

Differently from a classic RC frame structure, beside HSC column also bolted connection able to provide vertical structural continuity to frame should be considered and subjected to the same design provision adopted for columns. The flexural strength domain defined for columns should then be taken as a reference. This issue is investigated in chapter 9.3.4. It results that four bolts M24 10.9, are able to assure adequate strength, with exception of axial load level acting on the column lower than 1000kN. An alternative solution consisting in six bolt M24 is able to provide adequate strength even when limited axial load is provided. Reference should be done to chapter 9.3.4 for further details.

12.5.2. Shear strength

Beside flexural strength, also adequate shear strength should be provided by bolted connection, to avoid shear failure at column-to-column interface.

Maximum shear force for design can be taken from Table 26 and correspond to $V_{Sd}=275\text{kN}$. Friction bolted connection is considered. The single bolt pretension load is estimated as suggested in EN 1993-1-1:2005:

$$F_{P,Rd} = 0.7 \cdot A_{res} \cdot \frac{f_{tu}}{\gamma_{M7}} \quad (167)$$

where A_{res} =bolt's effective area; $\gamma_{M7}=1.10$; f_{tu} =ultimate tensile strength (1000 MPa for 10.9 grade bolt)

For a M24 10.9 bolt, $F_{P,Rd}=288\text{kN}$. A total number of four bolts are considered for the verification. Conservatively a friction coefficient $\mu=0.3$ is taken (non-treated steel surface).

$$F_{s,Rd} = \mu n_b n_s F_{bd} / \gamma_{M3} \quad (168)$$

where μ =friction coefficient ($\mu=0.3$); n_b =bolt's number ($n_b=1$); n_s =considered friction surface ($n_s=1$); $\gamma_{M3}=1.25$

The total shear strength result equal to 276kN, then higher than maximum solicitation (275kN). Furthermore there is a overstrength reserve, that Eurocode and National code do not allow to take explicitly under consideration. It is related to the shear strength mobilized by friction vertical steel plate should start sliding one over the other. The shear force considered for design is associated to an axial load equal to 2000kN (Table 26). These means than an amount of $2000 \times 0.3 = 600\text{kN}$ are also available to withstand shear force coming from seismic input.

12.6. Core-joint M-N domain strength

Estimation of core-joint strength domain for design is reported in chapter 7.3. It always results wider than the reference HSC column domain. Thus no weak behaviour should be expected by this component.

12.7. Core-joint shear strength

In general a typical beam-column joint is subjected to high shear forces while the adjacent beams develop their maximum flexural strength. In fact the joint strength capacity should not be lower than the demand of the plastic hinges in the adjacent beams. In order to control the global displacements and to prevent any global or local collapse, the columns should remain elastic both above and below the joint. Then the attention can be focused on the shear transmission mechanisms and on the prevention of brittle failure.

12.7.1. Design for shear

During a seismic action, the internal solicitations of a joint consist of a couple of bending moment and axial force transmitted by the columns which is counterbalanced by another couple of bending moment transmitted by the beams. The end faces of each element transmit shear forces that converge two at a time in the opposite corners of the joint.

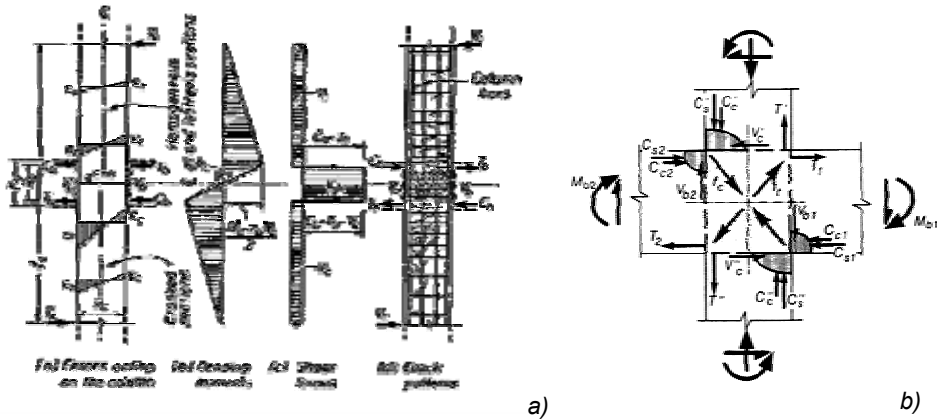


Fig. 339: a) Force distribution along columns in RC frames; b) force identification inside joint

Let's consider a portion of an interior column (Fig. 339a), delimited by two points of contraflexure (approximately at half-story heights) can be isolated as a free body, as show The beam actions transmitted to the column are represented by the internal horizontal beam tension T_b , compression C_b and the vertical shear V_b forces. The equilibrium of the free body requires

$$V_{jh} = C_b + T_b - V_c \tag{169}$$

where V_{jh} =horizontal shear force acting inside joints

Looking at Fig. 339a, expression 170 can be written as:

$$V_{jh} = C_{sb} + C_{cb} + T_1 - V_c = T_1 + T_2 - V_c \tag{170}$$

where T_1 and T_2 are the tensile forces provided respectively by upper and lower beam reinforcement

Following expression is reported by EN 1998_1:2005 for interior joint,

$$V_{jh} = \gamma_{Rd} (A_{s1} + A_{s2}) f_{yd} - V_c \quad (171)$$

where A_{s1} and A_{s2} is the area of upper and lower beam reinforcement; $\gamma_{Rd}=1.2$

and exterior joints

$$V_{jh} = \gamma_{Rd} A_{s1} f_{yd} - V_c \quad (172)$$

Similarly, consideration of equilibrium of vertical forces at the joint should lead to expressions for the vertical joint shear force, V_{jv} . However, because of the multilayered arrangement of common RC column reinforcement, the derivation of vertical stress resultant is more cumbersome. For common design situations, it is generally considered sufficiently accurate to estimate vertical joint shear force in proportion to horizontal shear force. This can be expressed as

$$V_{jv} = V_{jh} \cdot h_b / h_c \quad (173)$$

where V_{jh} =vertical shear force acting inside joints; h_c =column depth; h_b =beam depth

Regard the joint shear resisting mechanisms, the recent literature seems to confirm the effectiveness of the theory formulated by Paulay, 1989. The joint behaviour is described in terms of admissible mechanisms capable of transmitting shear forces starting from equilibrium criteria.

The model proposed considers that the total shear within the joint core is carried partly by a diagonal concrete strut and partly by a shear panel mechanism provided by idealized trusses, consisting of horizontal hoops, intermediate column bars and inclined concrete struts between diagonal cracks (diagonal compression field)

The strut mechanism is associated with a diagonal force, D_c within the concrete strut, developed by major diagonal concrete compression forces formed at the corners of the joint. A substantial portion of the total joint shear, horizontal and vertical, can be resisted by this mechanism. However, the strength of the strut mechanism is reduced by tensile strains perpendicular to the direction of the strut. In such situations, confinement of the joint core would help improving the strength of the strut.

The second mechanism is mainly governed by steel forces transferred through bonding and introduced into concrete at the four boundaries of the joint core, forming a compression field with diagonal cracks in the joint as shown in Fig. 5.8b. These forces being in equilibrium generate a total diagonal compression force D_s coming from all the concrete bars between the diagonal cracks. The mechanism associated is also called truss mechanism and is supported by well distributed transverse reinforcement within the joint.

The sum of the horizontal components of D_c and D_s from both mechanisms gives an estimate of the shear resistance in horizontal direction. Similarly, the sum of the vertical components gives the shear resistance in vertical direction.

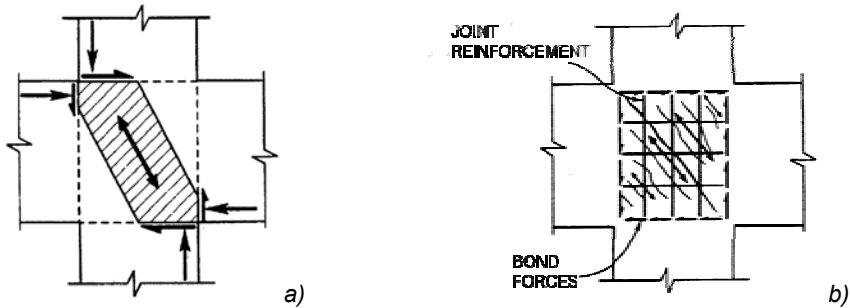


Fig. 340: a) Joint strut mechanism; b) joint shear panel mechanism (compression field)

From the Code Provisions point of view, the two mechanisms are not explicitly evaluated, but several prescriptions are imposed to withstand the two above mentioned strength mechanisms.

To account for the strut mechanism, nominal shear capacity is usually expressed as a function of concrete strength irrespective of the amount of shear reinforcement. Firstly the reference joint width should be defined. EN 1998:1:2005 provides following formulations:

$$b_j = \min(b_c; b_b + 0.5h_c) \quad \text{if } b_c > b_b$$

$$b_j = \min(b_b; b_c + 0.5h_c) \quad \text{if } b_b > b_c \quad 174)$$

where b_b =beam's width; b_c =column's width

The nominal shear stress level can be then expressed as:

$$v_{jh} = V_{jh} / (b_j \cdot b_c)$$

$$v_{jv} \approx v_{jh} \cdot h_b / h_c \quad 175)$$

where h_c =column depth; h_b =beam depth;

Paulay & Priestley, 1992 suggest a simple formulation, limiting shear concrete stress v_{jh} to $0.25f_{cd}$.

However the nominal shear capacity is influenced even by the confinement provided by the adjoining members. A beam member that frames into face is considered to provide confinement to the joint if the framing member covers at least three-quarter of the joint face.

ACI 318-08 sets the nominal shear strength of the joint as a function of concrete strength, which in turn depends upon the degree of confinement, offered by the members and is given as $1.7\sqrt{f_c}$ if confined on four faces, $1.25\sqrt{f_c}$ if confined on three faces and $1.0\sqrt{f_c}$ for the other cases. Apart from this fact, the code requires a minimum amount of transverse reinforcement in the joint as shear reinforcement to provide for confinement of the core concrete.

EN 1998-1:2003 (and NTC2008) limit the nominal shear stress v_{jh} to be less than the stress value given by the expression, which account for interior (confined) and exterior (unconfined) joints:

$$v_{jh} = \eta f_{cd,jnt} \sqrt{1 - \frac{v_d}{\eta}} \quad (176)$$

$$\eta = \alpha \left(1 - \frac{f_{ck,jnt}}{250} \right) \quad v_d = N / (A_c f_{ck,col})$$

where η =reduction factor on concrete compressive strength due to tensile strains in transverse direction; A_c = concrete column area; $\alpha=0.48$ for exterior joints and 0.6 for interior ones

Expression 176 appears to be more limiting than equivalent formulations proposed by ACI 318-08 and Paulay and Priestley (1992).

For what concern the truss mechanism (compression field mechanism) minimum amounts of shear reinforcements in horizontal and vertical directions are required. Usually, the horizontal shear V_{jh} is supported by stirrups and hoops placed in the horizontal direction while the vertical shear V_{jv} is taken care adequately by intermediate column bars

ACI 318-08 impose the following limitations for horizontal reinforcement in rectangular columns:

$$\rho_{st} > 0.3 \cdot (A_g / A_{conf} - 1) \cdot f_{ck} / f_{ywk} \quad (177)$$

$$\rho_{st} > 0.09 \cdot f_{ck} / f_{ywk}$$

where is the specified yield strength of the spiral reinforcement but not greater than 420 MPa; A_g =gross sectional area; A_c =area of confined core concrete; f_{ywk} =yielding stress of lateral reinforcement

EN 1998-1:2005 and NTC2008 give expressions for adequate confinement to be provided to limit the maximum diagonal tensile stress in the concrete core. The minimum amount of reinforcement required for adequate confinement and for limitation of diagonal tensile concrete stresses is given as

$$\frac{A_{jh} \cdot f_{ywd}}{b_j \cdot h_{jw}} \geq \frac{[V_{jh} / (b_j \cdot h_{jw})]^2}{f_{ctd} + v_d \cdot f_{cd}} - f_{ctd} \quad 178)$$

where b_j =reference joint width (eq. 174); f_{ywd} = design yielding stress of lateral reinforcement; f_{yd} = design yielding stress of longitudinal reinforcement; v_d =normalized axial force (eq. 176)

Alternatively following expression should be used for interior joints

$$A_{jh} \cdot f_{ywd} \geq \gamma_{Rd} \cdot (A_1 + A_2) \cdot f_{yd} \cdot (1 - 0.8v_d) \quad 179)$$

where A_{s1} and A_{s2} is the area of upper and lower beam reinforcement; $\gamma_{Rd}=1.2$; f_{ywd} = design yielding stress of lateral reinforcement; f_{yd} = design yielding stress of longitudinal reinforcement; v_d =normalized axial force (eq. 176)

and for exterior joints:

$$A_{jh} \cdot f_{ywd} \geq \gamma_{Rd} \cdot (A_1) \cdot f_{yd} \cdot (1 - 0.8v_d) \quad 180)$$

Finally, vertical shear reinforcements sustain basically the truss mechanism. Besides, the vertical reinforcements resist vertical shear V_{jv} , and are provided in the form of intermediate column bars.

The EN 1998-1:2005 suggests the following expression:

$$A_{jv} = \frac{2}{3} A_{jh} \cdot \frac{h_b}{h_c} \quad 181)$$

where h_c =column depth; h_b =beam depth;

Above reported formulations are adopted to check adequacy of proposed joint.

First the shear force acting inside the joint is estimated. Considering $\phi 28$ longitudinal rebars provided by lattice girder across the core-joint and adopting equation 171 following value is estimated for V_{jh} .

$$V_{jh} = 1.2 \left(\frac{28^2 \pi}{4} \cdot 8 \right) \cdot \frac{355}{1.05} \approx 2000 kN \quad 182)$$

The vertical shear component can be estimated adopting equation 173:

$$V_{jv} = 2000 \cdot 380 / 330 = 2300 kN \quad 183)$$

It should be noticed that into equation 182, the shear contribute provided by upper column (see Table 26) is conservatively disregarded. Besides, $\phi 28$ diameter is assumed for longitudinal reinforcement, which is an upper limit for the possible diameter range.

For determining the reference shear strength provided by the strut mechanism inside the core joint, the mere concrete confined by vertical steel plate is considered. For this reason expression 175 is conservatively replaced by the span among vertical steel plate ($\approx 180\text{mm}$).

Considering a concrete strength $f_{ck}=30$ MPa, and an axial force level equal to 4000 and 2000 kN for interior and exterior joint respectively, equation 176 provides following reference shear stress limit:

$$v_{jh,INT} = 0.6 \cdot \left(\frac{0.85 \cdot 30}{1.5} \right) \sqrt{1 - \frac{0.5}{0.53}} = 2.4 \text{ MPa}$$

$$v_{jh,EXT} = 0.48 \cdot \left(\frac{0.85 \cdot 30}{1.5} \right) \sqrt{1 - \frac{0.25}{0.43}} = 5.2 \text{ MPa} \quad 184)$$

It should be noticed as EN 1998-1:2005 formulation provides higher values for exterior joints, due to a more favourable axial load condition. Assuming the lower value computed in equation 184, the reference shear strength given by truss mechanism is at least equal to:

$$V_{jh}^R = 2.4 \cdot 180 \cdot 330 = 140 \text{ kN} \quad 185)$$

This means that just a limited part of the acting shear force is withstood by concrete strut mechanism.

Furthermore no compression field mechanism can develop, being a total absence of confining stirrups.

Nevertheless the proposed joint layout is characterized by vertical steel plate, that result effective not only in bearing axial loading, but also to support joint shear force.

Lets' consider an axial load level equal to 4000kN. Based on stiffness estimation 3/4 of such a load act directly on vertical steel plate. Considering also the shear forces reported in 182 and 183, the equivalent Von Mises stress can be calculated:

$$\sigma_{eq} = \left(\left(\frac{3/4 \cdot 4000 \cdot 1000}{2 \cdot 40 \cdot 210} \right)^2 + 3 \left(\frac{2000 \cdot 1000}{2 \cdot 40 \cdot 210} \right)^2 + 3 \left(\frac{2300 \cdot 1000}{2 \cdot 40 \cdot 380} \right)^2 \right)^{0.5} = 300 \text{ MPa} \quad 186)$$

Such a stress level is considerably lower than the level to attain the yielding limit (345 MPa). This result suggest that the considered joint is able to withstand the seismic induced core shear force, with a different mechanism than the ones usually considered for RC frame (equations 177 to 181).

12.7.2. Design for confinement

Beside adequate shear strength, reinforcement limitations required by codes aim to provide adequate concrete confinement to avoid brittle failure due to sudden concrete splitting. This aspect is particularly important for exterior joint, where passive confinement provided by flooring system and beams is limited.

Referring to the considered joint prototype, effective confinement capabilities of the joint are still an open issue. Surely a certain confinement level is provided by the vertical steel plates, at least to the concrete located among them

Nonetheless, experimental static tests evidenced a brittle failure of the core concrete as axial force level equal to 6000kN was attained.

This suggests that, even if not required for shear strength, a certain number of stirrups should be place at core-joint level to provide adequate confinement.

Reference is first made to equation 180. An exterior joint is considered ($V_{jh}=1000\text{kN}$ and $v_d \approx 0.25$).

$$A_{jh}^{TOT} \geq 1000 \cdot (1 - 0.8 \cdot 0.25) = 800 \text{mm}^2 \quad 187)$$

In NTC 2008 a further limitation is then imposed, with reference to confinement to be provided only for exterior joints, independently from adopted ductility class. Such an expression recalls equation 177 reported by ACI 318-08:

$$\rho_{jh}^{TOT} \geq 0.05 \cdot f_{ck} / f_{yw} = 0.05 \cdot 0.85 \cdot 0.875 / 450 = 0.0062 \quad 188)$$

$$A_{jh}^{TOT} = \rho_{jh}^{TOT} \cdot b_j \cdot h_j = 0.0062 \cdot 500 \cdot 380 = 1178 \text{mm}^2 \quad 189)$$

Lateral reinforcement determined by equation 189 is nearly 3 times the amount required by equations 187.

To provide adequate confinement $\phi 12$ stirrups with spacing 70 mm should be introduced, at least for exterior joints.

To fulfill this requirement and contemporary keep adequate assembling ease of the proposed joint, a proposal is made to improve current layout (see par. 12.8).

12.8. Improved layout for exterior joints

To conclude the study of the proposed precast system, an update of present joint layout is proposed. Aim is the fulfilling of Codes' provisions for adoption of the proposed precast system in high-seismicity region, without renouncing to some of its main advantages, namely mounting ease and speed and reduced tolerance problem.

Both bending and shear strength provided by different components of the assembly comply with Codes' requirements (see par. 12.2, 12.4, 12.5, 12.6), hence suggesting that the general layout of the system is effective as it is and should not be furtherly modified. Unattended prescriptions deal with confinement and minimum amount of confining reinforcement, in particular at base column at ground floor, where plastic hinging is expected during seismic event, and at core-joint level where lateral stirrups are required (par. 12.7.2). The first aspect is studied in chapter 11.4.2 and an improved solution for base column is reported in Fig. 287.

Latter aspect deals with the effective capacity of joint to withstand large inelastic deformations without undergo splitting failure or rapid stiffness degradation. Both experimental cyclic testing and numerical cyclic simulation evidenced adequate performance. On the other hand, experimental static tests suggest that brittle splitting failure of core-joint concrete could be expected under high axial load level, if not adequate confinement is provided. To improve this aspect light modifications are introduced on the precast system, starting from the layout of the CSTC beam (Fig. 341). The steel trusses' shape is arranged in order to create a central tunnel, where the lattice girder should be placed and made slide through the core-joint, to its final position. The presence of the lateral CSCT beam's trusses and the vertical steel plates provided by steel-core-joint should assure a considerable improvement in term of confinement and thus still higher ductility performance of the precast system during beams' plastic hinging. In the case an exterior-corner-joint is considered, additional steel plates are welded at the end of the lattice girder, to assure adequate interaction with surrounding concrete and increase girder's anchorage length, despite joint limited depth.

Finally, the major improvement is constituted by the confinement reinforcement for the core-joint, to fulfil Codes' requirements. A modular element is defined, constituted by C shaped stirrups welded on vertical rebars, in turn welded on L shaped steel plate (Fig. 342). This component can be assembled directly off-site. Besides, L-shaped flanges can act as a scaffolding during concrete casting in the arc-shaped part of the column.

After positioning of this modular element, fixed through a bolt screwed down on the bottom steel plate, C-shaped rebars are adopted to complete the lateral confinement's layout. An overlapping at least 20 diameter long should assure continuity for the confining stirrups. As it can be observed in Fig. 344, this solution is not suitable only for exterior-corner joints, but also for lateral-exterior joints or interior ones. It keep main advantages of the original layout, with enhanced reinforcement details.

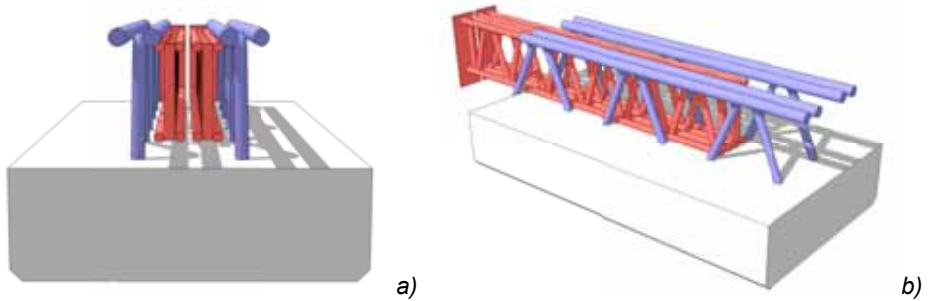


Fig. 341: Updated CSTC beam layout and lattice girder for exterior corner joints

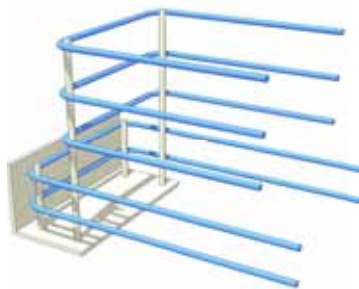
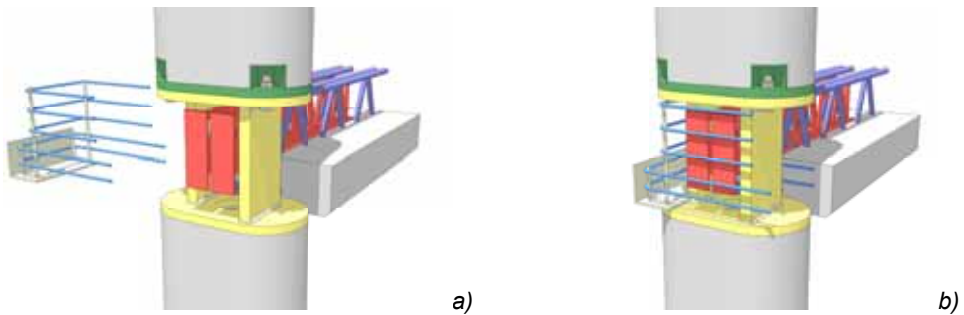


Fig. 342: Modular reinforcement cage component constituted by C-shaped stirrups



Analysis and development of an innovative prefabricated beam-to-column joint

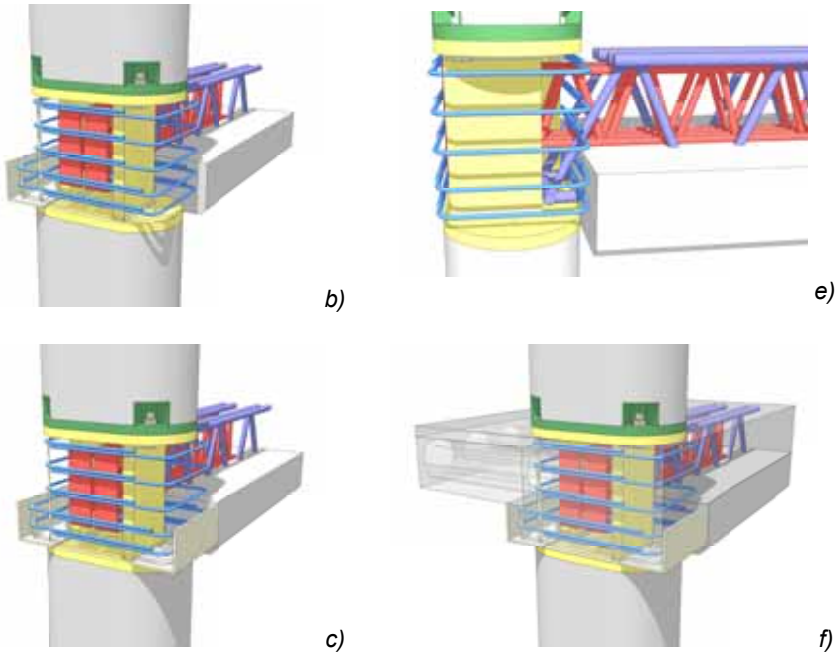


Fig. 343: Mounting operations for an exterior corner joint

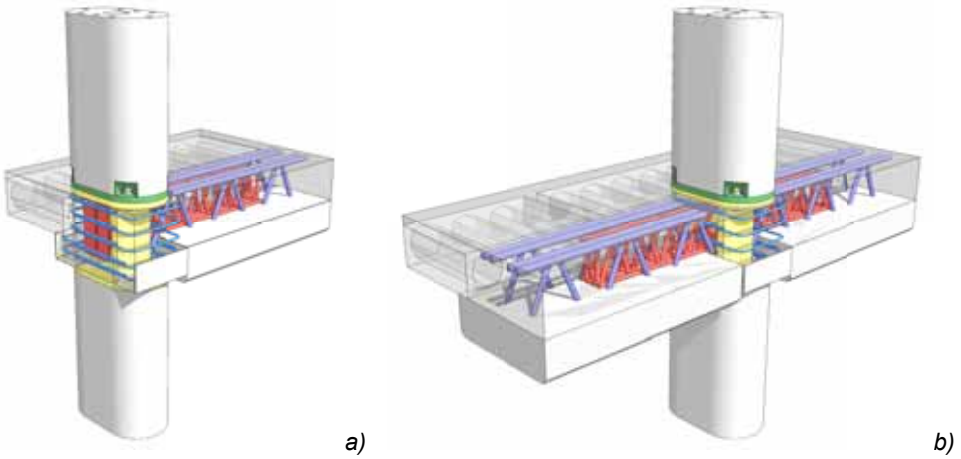


Fig. 344: a) exterior corner joint layout; b) exterior lateral joint layout

13. REAL CASE-STUDY APPLICATION

Beneath the development study phase, the proposed precast system has been already employed in several real-case applications. Among the others, an example is reported consisting in a 5 storey parking garage structure built in Milan in 2010. This project allows to appreciate the high bearing capacity of the system, with bays spans 5.5 to 8.5-meters-long, despite high live load adopted for structural design (Fig. 345). In Fig. 346 are reported some images relative to mounting phase of lower storeys.

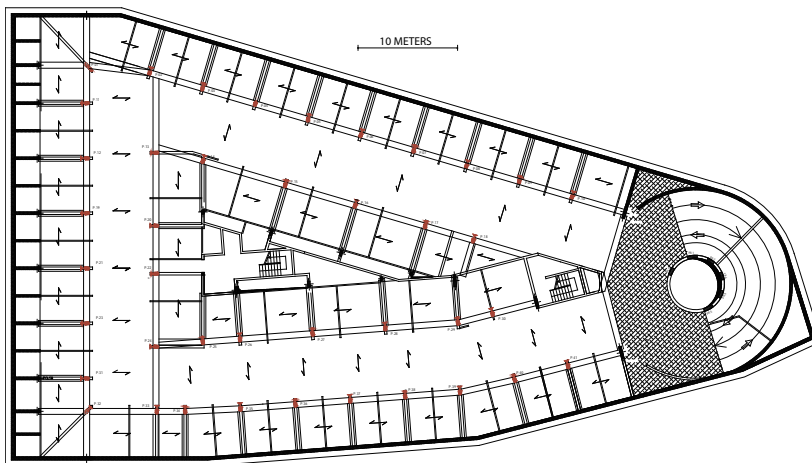


Fig. 345: Plant view of a parking garage structure in Milan



Fig. 346: Mounting phases of a parking garage structure in Milan

CONCLUSIONS

Great interest has been devoted in Italy in the last decade to the development of precast systems able to deal with the seismic issue and suitable for a wider application field than bare industrial/commercial one.

The research activity presented in this thesis aims to provide a positive contribute to this topic though the proposal of an innovative high-performance precast beam-to-column joint for multi-storey framed structure (cf. ch.2).

The horizontal structural element of the joint is constituted by a Steel Truss Composite Concrete (CSCT) beam with concrete base, a precast system developed by Salvatore Leone during the '60s, nowadays widely adopted over the National territory and spreading rapidly even outside the Italian Borders. Among the benefits provided by this solution some are recalled: high bearing capacity, high mounting speed thanks to unpropped erection, limited costs owing to high prefabrication level, good fire-strength. Vertical elements of the joint consist in monolithic precast columns, easy to transport and manage, with ovoid section and outer dimensions 330 by 550 millimetres, made by centrifuged High Strength Concrete (HSC). This material provides high bearing capacity to columns albeit limited section, allowing the maximization of sealable spaces, while keeping a limited cost thanks to the highly automated manufacturing process. Components' coupling is realized through a specifically designed steel-core-joints acting to ensure mounting ease and speed, together with complete self-supporting capacity of the system in temporary phase, before the completion casting. Column-to-column structural continuity is fully restored by a bolted connection, thus reducing drastically scheduling conflicts between construction phases, with reduced construction time and with favorable economical impact on construction costs.

To check on effectiveness of proposed precast technology, the research activity consists of two complementary approaches. An experimental phase, aiming to improve knowledge on mechanics and resisting mechanisms of the joint, owing to innovative layout and lack of analogous reference experiences from literature. Afterwards an analytical and numerical study phase, that starting from previously collected data, further expands the horizon of analysis to shed light on the following aspects:

- evaluation of components' strength domains, useful for everyday design;

- optimization of structural components;
- appraise about seismic applicability and performance of proposed technology.

Experimental campaign was conducted at State Key Laboratory for Disaster Reduction in Civil Engineering (SLDRCE) in Tongji University in January 2010 and consisted in both static and cyclic lab tests (cf. ch.3). The firsts focused on axial load bearing capacity of the composite-column, and investigate the influence of steel-core-joint geometry on static performances through 6 different samples. For all tests, failure is achieved as a consequence of core-joint buckling after concrete splitting, thus providing reference limit strength to be used for design of temporary phase, equal to almost 6000kN. Tests highlight the issue about adequate confinement to be guarantee at core-joint level, in particular at high axial load levels for outer column, where flooring confining effect is limited. Furthermore they suggest that considerable material saving could be attained by limiting steel's plate thickness without affecting static performances, at least in temporary phase. Cyclic tests investigate the performance of the joint under lateral loading and the capability of beams to develop plastic hinging at column interface. Despite brittle lower-column's failure characterized sample "D2", due to unexpected boundary conditions different from those supposed during preliminary test planning, for all remaining samples, FRP strengthening promoted a ductile behaviour. This allows to clarify the resistant mechanism in the plastic hinge zone and the role played by CSTC beam's truss and lattice girder, the latter implemented in the precast joint to restore beams' through-joint structural continuity, providing useful information for design. CSTC beams' truss performed nearly elastically during the whole tests, confirming the limited strength contribute provided by this component, similarly to experimental results reported by Amato et al., 2010. On the contrary, longitudinal bars belonging to lattice girder experienced consistent plastic straining, confirming their active role for plastic hinging development. Beside adequate strength contribute, strain data analysis suggests that limited slipping occurred between concrete and lattice, despite plain rebars were adopted.

After experimental testing, the subsequent study phase required for two preliminary investigations.

Firstly the identification of a reference constitutive model for concrete, in particular for the compressive behaviour, reported in chapter 4. This step is required considering the wide range of concrete strength classes adopted for proposed precast system and the importance of correct accounting of brittle response typical of HSC. Among several models considered for a comparative analysis using third-party experimental tests as a reference (Sharma et al., 2005), the Legeron model

and subsequent improvement by Cusson resulted the most proper. National and International Code provisions are also accounted for definition of input unconfined plain concrete's properties.

Secondly the identification of suitable numerical tools, able to deal with non-linear concrete mechanics, characterized by softening behaviour and mesh dependency issue. The choice has been addresses towards two robust and well-known Finite Element softwares, namely Ansys V.11 (ANSYS Inc., 2007) and Abaqus V.6.10 Simulia, 2010. The first takes advantage of native scripting tool (Ansys Parametric Design Language), which allows for a parametric modelling. The latter offers the advantages of a straightforward modeling of complex tridimensional RC samples, a wide library of materials' constitutive laws and an improved solution-convergence capability during iterative numerical solving process.

Given the structural complexity of the proposed precast system and the non-trivial precast members' interaction, the first part of study phase focuses on base structural components taken as separate, namely lattice girder and composite-column, in turn constituted by HSC column, core-joint and column to column and column to core-joint coupling system.

Investigation on lattice girder's performance is reported in chapter 5. Compared to alternative approaches adopting straight longitudinal rebars to provide beams' through joint structural continuity, this solution have evidenced better performance in term of strength, ductility and cyclic stiffness in several experimental tests (Scotta & Tesser, 2011). However there is still an open issue about force transfer mechanisms among lattice and concrete, which relies on web truss capability to bear against concrete. To deepen this topic some numerical pull-out tests are presented, different from those currently available from literature and conceptually analogous to classical experimental pull-out tests commonly adopted to study straight rebars' bond phenomena (Pochanart & Harmon, 1989; Mazzarolo et al., 2012). Lattice girder get solid modelled as embedded inside a concrete block; an axial pull-out force is subsequently applied on lattice's ends, while the reaction force is exerted on the concrete block. The numerical model is built in Ansys and a parametric analysis is conducted varying the longitudinal bars diameters, the web truss diameters and total girder's length (number of lattice-spans). Excessive slenderness of web truss, insufficient anchorage length or a combination of both, may lead to a premature pull-out failure due to concrete crushing or web trusses' yielding. On the basis of those results some proposal are made about correct lattice geometry to be adopted for proper design of this reinforcing element (cf. eq. 71).

Concerning the investigation of composite-column and its base components, a preliminary activity consists in the development of a reference numerical model,

reported in chapter 6. Experimental survey over static performance of composite-column is adopted to this purpose, since the column's geometry is rather simple and collected data provide a comprehensive picture about samples' response during testing. Global and local quantities provided by experimental campaign are compared to those retrieved by a detailed tridimensional samples' model implemented in Abaqus. Global quantities expressed in terms of force vs. displacement relationships show a satisfactory agreement. Realistic simulation of second order effects relative to buckling phenomena of vertical steel plates, is a further proof about the robustness of the adopted numerical approach. Also local quantities show a rather good correspondence, in particular those referring to concrete strains, despite the mesh dependency issue related to numerical modeling of concrete material, confirming numerical tool's ability to deal with highly non-linear problems.

Based on the validated numerical model, both HSC column (cf. ch.7.2) and core-joint (cf. ch.7.3) are separately modeled to provide an estimation about their respective strength domains. These analyses allows to classify core-joint as a strong component of the assembly, able to withstand higher axial-bending solicitations before failure, as long as adequate confinement to concrete core-joint is provided. This information results particularly important for seismic design consideration, since it allows to exclude the development of undesired bending failure mechanism at joint level. Referring to static performance, maximum pure axial bearing capacity of the column attains almost 15000 kN, a significant limit considering the limited column's section dimensions. Based on defined strength domain an analytical procedure is developed to fit the numerical response. To this purpose the strength's reduction factor for analytical modeling of HSC is explicitly accounted. Among several formulations suggested by Codes and literature (cf. ch.9.2), the one reported by Eurocode leads to the best fit with numerical evidences (cf. ch.9.3.2 and 9.3.3). Thank to satisfactory validation process, analytical approach represents a viable alternative to time-costing numerical analyses and allows to get an effective strength domain estimation for everyday design (cf. ch.9.4).

On the basis of this reference strength domain, the static performances of regular frames adopting proposed precast technology are evaluated though a static non-linear analyses also considering second order effect due to possible column vertical misalignment (cf. ch.11.5.1). The limit storey number for regular frames is estimated in 10 and 8, for beams' span equal to 6 and 8 meters, respectively. Considering the large amount of live load accounted for this evaluation, the identified static performance should be taken as a reference lower limit for this kind of technology.

To complete the study about single components' structural performance, core-joint to column and column to column connection system is investigated. This analysis considered two different steps. Firstly a parametric numerical investigation is conducted on composite-column numerical models implemented in Abaqus, varying the thicknesses of flanges at connections (cf. ch.7.4, 7.5, 7.6). This procedure aims to identify the optimum layout, able to provide adequate stiffness and strength to the assembly, with the minimum amount of required steel, in order to make the proposed precast system still more competitive from the manufacturing costs point of view. In the case of single flange welded connection, the best solution corresponds to a flange thickness equal to 40 mm. In bolted connection the best solution is identified in 30 mm thick flanges. Second step deals with estimation of equivalent rotational spring stiffness, provided by connections (cf. ch.8). Two formulations are presented based on components-approach. Both of them provide similar results and this is taken as a proof of approaches' validity. To give a classification about rotational stiffness value of connections, the end-fixity factor is introduced. This parameter confirms as single flange welded connection should be considered as fully rigid, even when limited axial loading is provided. Conversely, bolted connections result less stiff compared to adjoining members and should be classified as semi-rigid, a fundamental information for proper modeling of framed structures.

Final part of study phase deals with the evaluation of seismic performance of proposed precast technology.

In chapter 10, beam to column joint's cyclic performance under lateral loading condition are estimated through an accurate tridimensional numerical model of the joint implemented in Abaqus. Goodness of the model is evaluated reproducing experimental cyclic tests on sample "D2". It allows to capture main evidences provided by this testing, in particular the brittle failure mode of lower column and the input lateral force level at stake. Based on the same model a further numerical simulation is conducted, imposing boundary conditions representative of the joint behaviour inside a framed structure subjected to lateral loading, this latter characterized by contraflexure point of the bending diagram located at members mid-span. Numerical response is encouraging. Failure is attained at 3% storey drift due to rebars fracture and equivalent viscous damping ranges between 20 to 30% as storey drift exceeds 0.5%, thus suggesting both high deformation and high dissipation capability of the joint, comparable to those of an equivalent RC cast-in-place joint,. The credit for this performance is mainly related to composite-column correct overdesign and to lattice girders, able to restore beam through-joint continuity and high deformation capability in the plastic hinge zone.

Besides evaluation of joint's local seismic response, a fundamental issue for completing the study of the proposed technology is the evaluation of its real applicability for moment resisting frames in seismic areas. In chapter 11 current survey get mainly oriented to National territory, being the Italian market the expected main reference for the proposed solution. To this purpose, an innovative approach is adopted. The evaluation of the seismic performance is based on maximum allowable ground accelerations, introducing a seismic vulnerability parameter expressed as a direct function of Italian territory ratio, where the proposed precast technology can be used depending on real seismic action and ground category. This approach complies with current Italian Seismic Code, which refers to a grid of 10751 points, each of them characterized by specific input seismic action expressed in terms of both, ground acceleration and shape acceleration spectra. Different frames' layout are taken into account, varying beams' span, reinforcement arrangement and total number of storeys. This latter ranges between 3 to 10 and 3 to 8 for frames with beam-span 6 and 8 meter-long, respectively, on the basis of limitations imposed by static considerations expressed above.

Towards this aim, an iterative fully automated verification algorithm is implemented in MATLAB, based on results provided by non linear pushover analyses, these latter conducted on regular plain frames FE models built in SAP2000 V.11.0 (Computer and Structures, 2010). Specific formulations are defined to model frame members' properties, accounting for the different behaviour of the proposed precast framing system compared to an equivalent RC cast-in-place framed structure. In particular, the interaction between precast elements and connections' deformability (cf. ch.8) are explicitly considered.

Based on pushover curves, equivalent ductility factors for Force Based seismic design are also investigated, suggesting a more conservative estimation compared to Code's provisions.

Nevertheless, results provided by iterative analysis looking at seismic vulnerability parameters are unquestionably encouraging. Based on a suitable choice of the longitudinal beams' reinforcement, the proposed precast system results applicable on most part of the National territory for all considered ground site classes, without requiring additional seismic resistant elements such as bracing systems, dissipative devices or shear walls to withstand the earthquake action. This lead to undoubted benefits, as the possibility to create wide openings without interferences, sensibly improving the architectural freedom about final building layout and living space's arrangement. Moreover, a consistent economical saving, being the same skeleton structure able to withstand both vertical and horizontal forces.

At the end of this developing process following key point may be associated new precast frame technology:

- smart layout, suitable not only for industrial/commercial but also, social and residential application
- improved erection sequence compared to alternative solutions
- optimized structural layout for both static and cyclic loading
- high static performance, comparable to an equivalent steel framed structure
- Adequate seismic performance for most part of the National territory

To conclude the study of the proposed precast system, an updated joint layout is proposed (cf. ch.12.8). The final goal is the fulfilment of all Codes' provisions for the adoption of this technology in high-seismicity region, without renouncing to some of its main advantages, namely mounting ease and speed and reduced tolerances problems. Unattended prescriptions deal with confinement and minimum amount of confining reinforcement. In particular, for the base columns at ground floor, where plastic hinging can potentially form during a seismic event (cf. ch.12.4.3) and at core-joint level where lateral stirrups are required (cf. ch.12.7.2). The first aspect is studied in chapter 11.4.2 and an upgraded solution for base column is reported in Fig. 287. The latter aspect deals with the effective capacity of the joint to withstand large inelastic deformations without undergo splitting failure of the core-joint and consequently rapid stiffness degradation. To improve this aspect, outer joints, where flooring confining action is generally limited, are investigated. Slight modifications are introduced on the precast system, starting from the layout of the CSTC beam and lattice girder (Fig. 341), this latter upgraded by end-bearing plates to comply with anchorage length. A modular element constituted by a specifically design reinforcement cage for core-joint is also introduced to provide adequate confinement (Fig. 342, Fig. 343).

Further research should be addressed in order to investigate the effectiveness of the proposed modified layout though laboratory testing, investigating in particular its performance under lateral loading. A deeper revision is also required to update the proposed precast system in order to withstand seismic action on both orthogonal directions.

BYBLOGRAPHY

ACI Committee 318, (2008), *Building Code Requirements for Structural Concrete (ACI 318-08) and Commentary*, ACI 318-08, American Concrete Institute, Farmington Hills, MI.

Aiello M.A., (2008), *Analisi sperimentale della connessione acciaio-calcestruzzo nelle travi reticolari miste*. VII Workshop Italiano sulle Strutture Composte, Benevento.

Aiello M.A., La Mendola L. and Tullini N., (2009), *Prove sperimentali di push-out su travi reticolari miste*. AICAP. Pisa (Italy).

Alcocer S.M., Carranza R., Perez-Navarrete D. and Martinez R., (2002), *Seismic tests of beam-to-column connections in a precast concrete frame*, PCI journal, 47, 3, 70-89.

Amato G., Badalamenti V., Colajanni P. and La Mendola L., (2010), *Comportamento ciclico delle connessioni tra travi prefabbricate reticolari miste e pilastri in c. a.* 18° Congresso C.T.E., Brescia.

ANSYS Inc., (2007), *Release 11.0 Documentation for ANSYS SAS IP, Inc.*

Attard M. and Setunge S., (1996), *Stress-strain relationship of confined and unconfined concrete*, ACI Materials Journal, 93, 5.

Azizinamini A., Kuska S.S.B., Brungardt P. and Hatfield E., (1994), *Seismic behavior of square high-strength concrete columns*, ACI Structural Journal, 91, 3.

Badalamenti V., La Mendola L. and Scibilia N., (2008), *Prove di push-out su travi reticolari miste*. XVII Congresso CTE. Roma.

Bellotti D., Bolognini D. and Nascimbene R., (2008), *Seismic behaviour of reinforced concrete precast traditional italian frames and subassemblies*. International Association for Earthquake Engineering.

Borri A. and Grazini A., (2007), *Analisi del comportamento di travi tralicciate in c.a. per il miglioramento della risposta sismica degli edifici*. Anidis Pisa.

Briseghella B., (2005), *Cyclic behaviour of a non conventional composite steel and concrete joint*, Thesis: University of Trento, Trento.

Analysis and development of an innovative prefabricated beam-to-column joint

Briseghella L., (1988), *Behaviour and analysis of R.C. structures under alternate actions including inelastic response*, Rome.

British Steel, (1998), *Recommendations from Y/T working group for SINTAP procedure*", SINTAP BS/23-1998.

Brzev S. and Perez G.T., (1990), *Precast Concrete Construction*.

CEB-FIP, (2003), *Bulletin 27: Seismic Design of Reinforced and Precast Concrete Buildings*, John Wiley & Sons Inc.

Chang B., Hutchinson T.C. and Robert E.E., (2008), *Experimental Seismic Performance Evaluation of Innovative Beam-Column Subassemblies*, University of California, San Diego (CA).

Cheok G. and Lew H., (1991), *Performance of precast concrete beam-to-column connections subject to cyclic loading*, PCI journal, 36, 3, 56-67.

Cheok G. and Lew H., (1993), *Model precast concrete beam-to-column connections subject to cyclic loading*, PCI journal, 38, 4, 80-92.

Cheok G. and Stone W., (1993), *Performance of 1/3-Scale Model Precast Concrete Beam-Column Connections Subjected to Cyclic Inelastic Loads - Report No. 3*, Gaithersburg.

China Traffic Ministry, (2005), *Highway engineering cement and cement concrete experiment regulations*, JTG E30-2005

Colajanni P., La Mendola L. and Monaco A., (2011), *Modelli per l'interpretazione dei risultati di prove di push-out su travi reticolari miste*. ANIDIS, Bari.

Collins M.P., Mitchell D. and MacGregor J.G., (1993), *Structural design considerations for high strength concrete*, Concrete International: Design and Construction, 15, 5, 27-34.

Colombo A., Negro P., Zhao B. and Lu X., (2008), *Recent collaborative research activities between europe and china on the seismic behaviour of precast structures*. 14th WCEE, Beijing, China, International Association for Earthquake Engineering.

Computer and Structures I., (2010), *SAP2000 release 14.0 - Analysis Reference*, Berkeley, CA.

Consiglio Superiore dei Lavori Pubblici, (2009), *Linee guida per l'utilizzo di travi traliciate in acciaio conglobate nel getto di calcestruzzo collaborante e procedure per il rilascio dell'autorizzazione all'impiego (in Italian)*.

CSA Standard, (2010), *Design of concrete structures*, CAN/CSA-A23.3-04 R2010, Canadian Standards Association Mississauga, Ontario, Canada.

Cui C. and Sheikh S., (2010), *Analytical Model for Circular Normal-and High-Strength Concrete Columns Confined with FRP*, Journal of Composites for Construction, 14, 5, 562-572.

Cusson D., (1994), *High Strength Concrete Columns Confined by Rectangular Ties*, Journal of Structural Engineering, 120, 783.

Cusson D. and Paultre P., (1995), *Stress-strain model for confined high-strength concrete*, Journal of Structural Engineering, 121, 3, 468-477.

Cusson D. and Paultre P., (2008), *Prediction of effective confinement pressure in high-strength concrete columns*. Annual conference of the Canadian Society for Civil Engineering, Quebec City, Canada.

Day S., (1999), *Cyclic load testing of precast hybrid frame moment-resisting connections*, Thesis: University of Washington, Washington.

Di Marco R., (1995), *Sperimentazione su travi continue REP con traliccio tipo TR (Experimental tests on hyperstatic REP beams with TR truss type)*, Internal Report University IUAV of Venice.

Eligehausen R., Popov E.P. and Bertero V.V., (1983), *Local bond stress-slip relationships of deformed bars under generalized excitations: Experimental results and analytical model*, University of California.

Elliott K.S., Ferreira M.A. and El Debs M.K., (2004), *Strength-stiffness requirement approach for semi-rigid connections in precast concrete structures*. International Conference On Concrete Engineering and Technology, Malaya, 1-8.

Englekirk R.E., (1995), *Development and Testing of a Ductile Connector for Assembling Precast Concrete Beams and Columns*, PCI journal, 40, 2, 36-51.

Englekirk R.E., (2002), *Design-construction of The Paramount: a 39-story precast prestressed concrete apartment building*, PCI journal, 47, 4, 56-71.

Englekirk R.E. and Wang J., (2008), *Design Procedures for Innovative Beam Column Subassemblies to be Used in Regions of Moderate and High Seismicity*, University of California, San Diego (CA).

European Committee for Standardization, (1993), *Eurocode 2 - Design of Concrete Structures - Part 1-1: General Rules and Rules for Buildings*, EN 1992-1-1:1993;.

European Committee for Standardization, (1995), *Hot rolled products of non - alloys structural steel. Technical delivery conditions*, EN 10025.

European Committee for Standardization, (2005a), *Eurocode 2 - Design of Concrete Structures - Part 1-1: General Rules and Rules for Buildings*, EN 1992-1-1:2005;.

Analysis and development of an innovative prefabricated beam-to-column joint

European Committee for Standardization, (2005b), *Eurocode 3 - Design of Steel Structures - Part 1-1: General Rules and Rules for Buildings*, EN 1993-1-1:2005.

European Committee for Standardization, (2005c), *Eurocode 4 - Design of Composite Steel and Concrete Structures - Part 1-1: General Rules and Rules for Buildings*, EN 1994-1-1:2005;

European Committee for Standardization, (2005d), *Eurocode 8 - Design of Structures for Earthquake Resistance - Part 3: Assessment and Retrofitting of Buildings*, EN 1998-3.

Fafitis A. and Shah S.P., (1985), *Prediction of Ultimate Behaviour of Confined Column Subjected to Large Deformations*, ACI Journal, 82, 4, 423-433.

Fajfar P., (1996), *Design spectra for the new generation of codes*. 11 WCEE, Acapulco, Mexico, Sociedad Mexicana de Ingeniería Sísmica, 23-28.

Fajfar P. and Gašperšič P., (1996), *The N2 method for the seismic damage analysis of RC buildings*, Earthquake engineering & structural dynamics, 25, 1, 31-46.

Federal Emergency Management Agency (FEMA), (2000), *Prestandard and commentary for the seismic rehabilitation of buildings*, FEMA 356, American Society of Civil Engineers (ASCE), Reston, Virginia.

Ferreira S.H.M.A., Elliott K.S., S. and Hasan, (2011), *A theoretical investigation on the moment continuity of precast concrete beam-column connections under gravity loads*. Fib Symposium. Prague.

Fintel M., (1986), *Performance of Precast and Prestressed Concrete in Mexico Earthquake*, PCI journal, 31, 1, 18-42.

Ghosh S.K., Nakaki S.D. and Krishnan K., (1997), *Precast Structures in Regions of High Seismicity: 1997 UBC Design Provisions*, PCI journal, 42, 6, 76-91.

Giordano G., Ombres L. and Spadea G., (1987), *Modellazione teorica e controllo sperimentale del comportamento a rottura di travi inflesse di tipo REP (Theoretical modelling and experimental verification of the collapse behaviour of REP type bended beams)*, L'Industria Italiana del Cemento, 617.

Giordano G., Ombres L. and Spadea G., (1988), *Problemi di aderenza nelle travi miste prefabbricate tipo REP (Bond issue in composite precast REP beam)*. Atti del Congresso CTE, Venezia, 4-6.

Giordano G. and Spadea G., (1983), *Stato ultimo di flessione di travi in cemento armato con doppia armatura tipo REP: ricerca sperimentale (Ultimate limit state of double R.C. beam using REP type reinforcement)*, University of Calabria, Calabria.

Griffis L., (1992), *Composite frame construction*, Elsevier Applied Science, New York.

Hawkins N.M. and Ghosh S., (2004), *Requirements for the use of PRESSS moment-resisting frame systems*, PCI journal, 49, 2, 98-103.

Hordijk D., Cornelissen H. and Reinhardt H., (1986), *Experimental determination of crack softening characteristics of normalweight and lightweight concrete*, Heron, 31, 2, 45-56.

Husem M. and Pul S., (2007), *Investigation of stress-strain models for confined high strength concrete*, Sadhana, 32, 3, 243-252.

Internation Federation for Structural Concrete (FIB), (1993), *CEB-FIP Model Code 90 - Design of Concrete Structures*, Thomas Telford.

Internation Federation for Structural Concrete (FIB), (2010), *CEB-FIP Model Code 2010 - Design of Concrete Structures*, Thomas Telford.

International Standard, (1999), *Mechanical properties of fasteners made of carbon steel and alloy steel - Part 1: Bolts, screws and studs*, ISO 898-1:1999, International Organization for Standardization, Geneve, Switzerland.

Itakura Y. and Yagenji A., (1992), *Compressive test on high-strength R/C columns and their analysis based on energy concept*. Proc., 10th Word Conf. on Earthquake Engrg, Balkema, Rotterdam, The Netherlands, 2599,2602.

Kim J., (2000), *Final report on testing of hybrid frame corner beam-column subassembly with continuous post-tensioning steel*, Thesis: University of Washington, Washington.

Kramar M., Isakovic T. and Fischinger M., (2008), *Seismic collapse safety of RC columns in precast industrial buildings*. 14th WCEE, Beijing, China, International Association for Earthquake Engineering.

Kurose Y., Nagami K. and Saito Y., (1991), *Beam-Column Joints in Precast Concrete Construction in Japan*, Special Publication, 123, 493-514.

Lee L.H., Kim S.H. and Moon J.H., (2004), *An Experimental Study of the Structural Behavior on the Precast Concrete Beam-Column Interior Joint with Splice Type Reinforcing Bars*, Journal of Architectural Institute of Korea, 20, 10, 53-61.

Legeron F. and Paultre P., (2000), *Behavior of high-strength concrete columns under cyclic flexure and constant axial load*, ACI Structural Journal, 97, 4.

Légeron F. and Paultre P., (2003), *Uniaxial confinement model for normal-and high-strength concrete columns*, Journal of Structural Engineering, 129, 241.

Analysis and development of an innovative prefabricated beam-to-column joint

Li B., Park R. and Tanaka H., (1991), *Effect of confinement on the behaviour of high strength concrete columns under seismic loading*. Pacific Conference of Earthquake Engineering, New Zealand, 67-78.

Li B., Park R. and Tanaka H., (1994), *Strength and ductility of RC members and frames constructed using high strength concrete*, University of Canterbury, Christchurch New Zealand.

Lignola G.P., Di Ludovico M., Prota A. and G.; M., (2010), *Experimental performance of cast-in-place connections in seismic resistant precast reinforced concrete frames*. 14ECEC. Ohrid.

Lundgren K., (1999), *Three-dimensional modelling of bond in reinforced concrete*, Thesis: Chalmers University of Technology, Göteborg.

Mander J.B. and Priestley M., (1988), *Theoretical Stress Strain Model for Confined Concrete*, Journal of Structural Engineering, 114, 1804.

Mander J.B., Priestley M.J.N. and Park R., (1984), *Seismic Design of Bridge Piers* Univ. of Canterbury, Dept. of Civil Engineering, Christchurch, New Zealand.

Marinini L., Spatti P., Riva P. and Nascimbene R., (2011), *Strutture prefabbricate: moderni sistemi di protezione antisismica (in italian)*, Protezione sismica, 3, 23-44.

Markeset G., (1993), *Failure of concrete under compressive strain gradients*, Thesis: The Norwegian Institute of Technology, Trondheim.

MathWorks Inc., (2011), *MATLAB R2011a - Product Documentation*, Natick, Massachusetts, USA. <http://www.mathworks.com/help/techdoc/>

Mazzarolo E., He J., Zordan T., Chen A., Briseghella B., Ma R. and Ruan X., (2010), *Cyclic Behaviour of Prefabricated High-Strength Concrete Composite Beam-to-Column Joints*. IABSE Venice, International Association for Bridge and Structural Engineering, 59-67.

Mazzarolo E., Scotta R., Saetta A. and Berto L., (2012), *Long anchorage bond-slip formulation for modeling of r.c. elements and joints*, Engineering Structures, 34, 1, 330-341.

Mazzotti C., Vincenzi L. and Ferrari M., (2011), *Studio sperimentale-numerico di nodi trave-pilastro di sistemi a telaio prefabbricati*. ANIIDIS 2011. Bari.

Mele M., Ciampoli M. and Menegatti E., (1993), *Nuovi sistemi strutturali composti di acciaio e calcestruzzo: prime analisi sperimentali del comportamento sotto azioni cicliche dei nodi travi-pilastro*. 1° Workshop Italiano nelle Strutture Composte, Trento, 85-98.

Mele M. and Sassone M., (2002), *Sistemi strutturali composti ad armatura: indagine sperimentale sul comportamento di nodi travi-pilastro soggetti a carichi ciclici*. V° Workshop Italiano nelle Strutture Composte, Fisciano, 191-200.

Metelli G. and Riva P., (2008), *Behaviour of a Beam to Column "Dry" Joint for Precast Concrete Elements*. 14 WCEE, Beijing, China, International Association for Earthquake Engineering.

Ministero delle Infrastrutture, (2008), *Nuove Norme Tecniche per le Costruzioni (DM 14/01/2008)*, NTC 2008, Rome.

Monforton G. and Wu T.S., (1963), *Matrix analysis of semi-rigidly connected frames*, Journal of the Structural Division, ASCE, 89, 13-42.

Morgen B.G. and Kurama Y.C., (2004), *A friction damper for post-tensioned precast concrete moment frames*, PCI journal, 49, 4, 112-133.

Mpampatsikos V., Nascimbene R. and Petrini L., (2008), *A critical review of the RC frame existing building assessment procedure according to Eurocode 8 and Italian seismic code*, Journal of Earthquake Engineering, 12, S1, 52-82.

Nagashima T., Sugano S., Kimura H. and Ichikawa A., (1992), *Monotonic axial compression test on ultra high strength concrete tied columns*. 2983-2988.

New Zealand Standard, (2006), *Concrete Structures Standard - Part1 - The Design of Concrete Structures*, NZS 3101:2006.

Palmieri L., (1996), *Evaluation of ductile connections for precast frame systems*, Thesis: University of Minnesota.

Palmieri L., Saqan E., French C. and Kreger M., (1996), *Ductile connections for precast concrete frame systems*, ACI Special Publication, 162, 313-356.

Pampanin S., (2005), *Emerging solutions for high seismic performance of precast/prestressed concrete buildings*, Journal of Advanced Concrete Technology, 3, 2, 207-223.

Panagiotakos T.B. and Fardis M.N., (2001), *Deformations of reinforced concrete members at yielding and ultimate*, ACI Structural Journal, 98, 2.

Park H., Im H., Eom T. and Kang S., (2008), *An experimental study on beam-column connections with precast concrete u-shaped beam shells*. 14 WCEE, Beijing (China), International Association for Earthquake Engineering.

Park R., (2002), *Seismic design and construction of precast concrete buildings in New Zealand*, PCI journal, 47, 5, 60-75.

Park R. and Blakeley R.W.G., (1971), *Seismic resistance of prestressed concrete beam-column assemblies*. ACI.

Analysis and development of an innovative prefabricated beam-to-column joint

Park R. and Bull D.K., (1986), *Seismic Resistance of Frames Incorporating Precast Prestressed Concrete Beam Shells*, PCI journal, 31, 4, 54-93.

Paulay T., (1989), *Equilibrium criteria for reinforced concrete beam-column joints*, ACI Structural Journal, 86, 6, 635-643.

Paulay T. and Priestley M.J.N., (1992), *Seismic design of reinforced concrete and masonry buildings*, Wiley Online Library.

Paultre P. and Légeron F., (2008), *Confinement reinforcement design for reinforced concrete columns*, Journal of Structural Engineering, 134, 5, 738-749.

Petrovich F., (2009), *Un nuovo sistema strutturale per edifici multipiano in zona sismica*, Thesis: University of Trieste, Trieste.

Pique J. and Burgos M., (2008), *Effective rigidity of reinforced concrete elements in seismic analysis and design*. 14th WCEE, Beijing, International Association for Earthquake Engineering.

Pochanart S. and Harmon T., (1989), *Bond-slip model for generalized excitations including fatigue*, ACI Materials Journal, 86, 5.

Popovics S., (1973), *A numerical approach to the complete stress-strain curve of concrete*, Cement and Concrete Research, 3, 5, 583-599.

Precast Concrete Industry (PCI), (2007), *PCI Design Handbook 6th Edition (Precast and Prestressed Concrete)*, Chicago.

Priestley M.J.N., (1996), *The PRESSS Program—Current Status and Proposed Plans for Phase*, PCI journal, 44, 2, 26-39.

Priestley M.J.N. and MacRae G., (1996), *Seismic tests of precast beam-to-column joint subassemblages with unbonded tendons*, PCI journal, 41, 1, 64-81.

Priestley M.J.N. and Tao J.R., (1993), *Seismic response of precast prestressed concrete frames with partially debonded tendons*, PCI journal, 38, 1, 58-69.

Puhali R. and Smotlack I., (1980), *Relazione sulle prove di push-out atte a determinare le leggi carico-scorrimento delle travi in sistema composto tipo REP*, Università di Trieste, Trieste.

Rahman A., Baharuddin A., Ghazali A.R. and Hamid A., (2008), *Comparative study of monolithic and precast concrete beam-to-column connections*, Malaysian Construction Research Journal, 2, 1, 42-55.

Razvi S. and Saatcioglu M., (1996), *Tests of high strength concrete columns under concentric loading*, Carleton Earthquake Engineering Research Centre, Ottawa.

- Razvi S. and Saatcioglu M., (1999), *Confinement model for high-strength concrete*, Journal of Structural Engineering, 125, 281.
- Restrepo J., Park R. and Buchanan A., (1989), *Seismic load tests on connections between precast concrete elements*. Silver Jubilee Conference, Wairakei, Taupo, New Zealand.
- Restrepo J.I., Park R. and Buchanan A.H., (1995a), *Design of connections of earthquake resisting precast reinforced concrete perimeter frames*, PCI journal, 40, 5, 68-77.
- Restrepo J.I., Park R. and Buchanan A.H., (1995b), *Tests on Connections of Earthquake Resisting Precast Reinforced Concrete Perimeter Frames of Buildings*, PCI journal, 40, 4, 44-61.
- Richart F.E. and Brandtzaeg A., (1928), *A study of the failure of concrete under combined compressive stresses*, University of Illinois, Urbana.
- Rodriguez M.E. and Blandon J.J., (2005), *Tests on a half-scale two-story seismic-resisting precast concrete building*, PCI journal, 50, 1, 94-114.
- Roeder C. and Hawkins N., (1981), *Connections between steel frames and concrete walls*, AISC Engineering Journal, 18, 1, 22-29.
- Saatcioglu M. and Razvi S.R., (1992), *Strength and ductility of confined concrete*, Journal of Structural Engineering, 118, 6, 1590-1607.
- Sanpaolesi L., Croci P. and Viviani M., (1988), *Influenza del confinamento del calcestruzzo sul comportamento a fatica oligociclica di nodi trave-pilastro prefabbricati: indagine sperimentale*, Atti del Convegno CTE, 67-70.
- Sagan E.I., (1995), *Evaluation of ductile beam-column connections for use in seismic-resistant precast frames*, Thesis: University of Texas at Austin.
- Sargin M., (1971), *Stress-strain relationship for concrete and the analysis of structural concrete sections*, Solid Mechanics Div., University of Waterloo, Waterloo (Canada).
- Sassone M. and Bigaran D., (2007), *Il comportamento ciclico delle travi reticolari composte parzialmente prefabbricate. XII Convegno "L'Ingegneria Sismica in Italia"*. Pisa.
- Scotta R. and Tesser L., (2011), *Prove sperimentali di rottura ciclica di nodi trave-pilastro realizzati con struttura reticolare mista*. ANIDIS. Bari.
- Sharma U.K., Bhargava P. and Kaushik S., (2005), *Behavior of confined high strength concrete columns under axial compression*, Journal of Advanced Concrete Technology, 3, 2, 267-281.

Analysis and development of an innovative prefabricated beam-to-column joint

Sheikh S.A. and Toklucu M.T., (1993), *Reinforced concrete columns confined by circular spirals and hoops*, ACI Structural Journal, 90, 542-542.

Sheikh S.A. and Uzumeri S., (1982), *Analytical model for concrete confinement in tied columns*, Journal of the structural division, 108, 12, 2703-2722.

Sheikh S.A. and Uzumeri S.M., (1980), *Strength and ductility of tied concrete columns*, Journal of the structural division, 106, 5, 1079-1102.

Simulia, (2010), *ABAQUS V. 6.10 Theory Reference Manual*.

Sorgon S., (2009), *Analisi di un sistema ibrido sismo-resistente costituito da elementi tralicciati in acciaio inglobati nel calcestruzzo*, Thesis: University of Trieste, Trieste.

Sritharan S., Priestley M.J.N., Seible F. and Igarashi A., (2000), *A five-story precast concrete test building for seismic conditions-an overview*. 12WCEE, Auckland, N.Z.

Stanton J., Stone W.C. and Cheok G.S., (1997), *A hybrid reinforced precast frame for seismic regions*, PCI journal, 42, 2, 20-32.

Stone W.C., Cheok G.S. and Stanton J.F., (1995), *Performance of hybrid moment-resisting precast beam-column concrete connections subjected to cyclic loading*, ACI Structural Journal, 92, 2.

Tesser L., (2009), *Composite Steel Truss and Concrete Beams and Beam-Column Joints for Sismic Resistant Frames*, Thesis: University of Padova, Padova.

Tesser L. and Scotta R., (2008), *Sperimentazione su travi tralicciate miste REP® – NOR (Experimental tests on composite truss beams REP® – NOR)*. VII Italian Workshop on Composite Structures, Benevento.

Tullini N., Reato P. and Cappellozza M., (2006), *Indagini sperimentali su travi miste acciaio-calcestruzzo con connessione a traliccio*. XVI Congresso CTE, Parma.

Vidic T., Fajfar P. and Fischinger M., (1994), *Consistent inelastic design spectra: strength and displacement*, Earthquake engineering & structural dynamics, 23, 5, 507-521.

Yong Y.K., Nour M.G. and E.G. N., (1988), *Behavior of Laterally Confined High Strength Concrete under Axial Loads*, Journal of Structural Engineering, 114, 2, 332-351.

Zanchettin A., Briseghella B., Zordan T. and Xue J., (2011), *Behaviour of a Moment Resisting Composite Steel and Concrete Joint Under Alternate Loading*, Construction Technology, 40, 11.

Zordan T., (2004), *Analysis of the response of a non conventional composite steel and concrete joint*, Thesis: University of Trento, Trento.